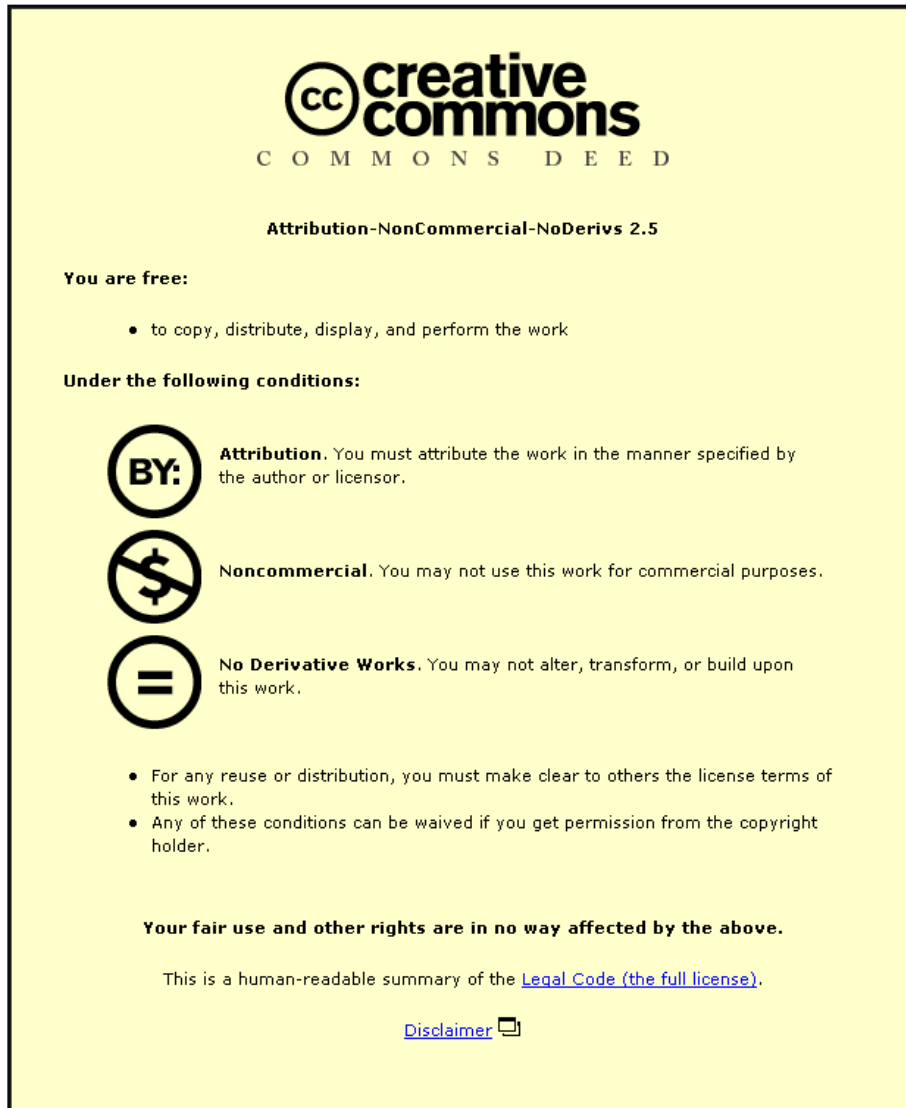


This item was submitted to Loughborough's Institutional Repository (<https://dspace.lboro.ac.uk/>) by the author and is made available under the following Creative Commons Licence conditions.



CC creative commons
COMMONS DEED

Attribution-NonCommercial-NoDerivs 2.5

You are free:

- to copy, distribute, display, and perform the work

Under the following conditions:

BY: **Attribution.** You must attribute the work in the manner specified by the author or licensor.

Noncommercial. You may not use this work for commercial purposes.

No Derivative Works. You may not alter, transform, or build upon this work.

- For any reuse or distribution, you must make clear to others the license terms of this work.
- Any of these conditions can be waived if you get permission from the copyright holder.

Your fair use and other rights are in no way affected by the above.

This is a human-readable summary of the [Legal Code \(the full license\)](#).

[Disclaimer](#) 

For the full text of this licence, please go to:
<http://creativecommons.org/licenses/by-nc-nd/2.5/>



Investigation of the effect of relative humidity on additive manufactured polymers by depth sensing indentation

by

Kazim Altaf

A doctoral thesis submitted in partial fulfilment of the requirements for the award of Doctor of Philosophy of Loughborough University

Wolfson School of Mechanical and Manufacturing Engineering

July 2011

Dedicated to my parents and my lovely wife

Abstract

Additive manufacturing methods have been developed from rapid prototyping techniques and are now being considered as alternatives to conventional techniques of manufacturing. Stereolithography is one of the main additive methods and is considered highly accurate and consistent. Polymers are used as stereolithography materials and exhibit features such as high strength-to-weight ratio, corrosion resistance, ease of manufacturing and good thermal and electrical resistance properties. However, they are sensitive to environmental factors such as temperature, moisture and UV light, with moisture being identified as one of the most important factors that affect their properties. Moisture generally has an adverse effect on the mechanical properties of polymers. Investigation of the effects of moisture on polymers can be carried out using a number of experimental techniques; however, the benefits of the depth sensing indentation method over bulk tests include its ability to characterise various mechanical properties in a single test from only a small volume of material and the investigation of spatial variation in mechanical properties near the surface.

The aim of this research was to investigate the effects of varying relative humidity on the indentation behaviour of stereolithography polymers and to develop a modelling methodology that can predict this behaviour under various humidities. It was achieved by a combination of experimental and numerical methods. Depth sensing indentation experiments were carried out at 33.5 %, 53.8 %, 75.3 % and 84.5 % RH (relative humidity) and 22.5 °C temperature to investigate the effects of varying humidity on the micron scale properties of the stereolithography resin, Accura 60. In order to minimise the effects of creep on the calculated properties, appropriate loading and unloading rates with suitable dwell period were selected and indentation data was analysed using the Oliver and Pharr method (1992). A humidity control unit fitted to the machine was used to condition the samples and regulate humidity during testing. Samples were also preconditioned at 33.5 %, 53.8 %, 75.3 % and 84.5 % RH using saturated salt solutions and were tested at 33.5 % RH using humidity control unit. It was seen that properties such as indentation depth increased and contact

hardness and contact modulus decreased with increasing RH. The samples conditioned and tested using the humidity control unit at high RH showed a greater effect of moisture than the preconditioned samples tested at 33.5 % RH. This was because the samples preconditioned at high RH exhibited surface desorption of moisture when tested at ambient RH, resulting in some recovery of the mechanical properties. In order to investigate these further, tests were performed periodically on saturated samples after drying. Ten days drying of samples conditioned for five days at 84.5 % RH provided significant, though not complete, recovery in the mechanical properties. These tests confirmed that Accura 60 is highly hygroscopic and its mechanical properties are a function of RH and removal of moisture leads to a significant recovery of the original mechanical properties.

Bulk sample tests were performed to characterise the moisture uptake and bulk mechanical properties. The diffusion characteristics at various RH were determined by gravimetric experiments. Non-Fickian moisture absorption was observed at all humidities. To determine the effects of moisture on the mechanical properties of the resin, bulk mechanical tests such as tensile test, compressive test and creep tensile test were performed after conditioning. The experimental results revealed that the tensile and compressive strength of the resin decreased and creep deformation increased with increasing moisture content. The difference in tensile yield and compressive yield also highlighted the hydrostatic stress sensitivity of the resin. Parameters calculated from these bulk tests were used in defining material models for finite element analysis.

2D axisymmetric FE analyses were performed using a sharp conical indenter to represent the Berkovich geometry. A pressure sensitive elastic-plastic material model in conjunction with a rate dependent power law creep model was used to model the indentation behaviour. Transient moisture diffusion analyses were carried out using the analogy between Fourier's law of heat transfer and Fick's law of diffusion. A sequentially coupled hygro-mechanical analysis was carried out to model the indentation behaviour at various RH. The predicted indentation load-depth response using the FE model matched well with experiments. Therefore, the selected FE models were used to characterise indentation hardness at various depths and the results were validated by experiments. On the basis of the results, it is proposed that

the models and procedures employed in this research can be used in predicting the effects of the environment on the performance of SL manufactured components.

For polymeric resins, time dependent deformation is an important characteristic, hence, the measurement of time-dependent parameters using analytical approaches, and not their minimisation, is often desired. Therefore, phenomenological models consisting of rheological elements were used with depth sensing indentation creep data to select a suitable viscoelastic-plastic model and extract material parameters. These parameters were used to find values of hardness, contact hardness and Young's modulus. The results showed that the values of contact hardness and modulus calculated using the analytical modelling approach were close to those calculated using the Oliver and Pharr method after minimising creep effects, however, analytical modelling provided additional properties, which could not be determined using the Oliver and Pharr method. Results confirmed that a more complete description of the time dependent material behaviour is obtained from the application of the elastic-viscous-plastic models.

The experimental and FE modelling methodologies proposed in this work provide a validated and systematic approach for characterising and predicting moisture degradation in additive manufactured components under varying environmental conditions. It is envisaged that the proposed method could be implemented within a general design in which the moisture diffusion of a polymeric material needs to be taken into account in predicting the in-service performance. It is also indicated that humidity control should be used to regulate the environment when instrumented indentation of moisture sensitive materials is carried out. The research work also reinforces the general view that analysis of indentation data using the Oliver and Pharr method works well only for materials that show weak time dependency after the removal of creep, however, it is shown that the parameters derived using this method do have some meaning in the context of a time dependent model of the material. However, the use of a time dependent modelled is still preferred where a full characterisation of the material mechanical response is required.

Keywords: Creep; Depth sensing indentation; Finite Element Analysis; Moisture diffusion; Relative humidity; Stereolithography, Viscoelasticity; Viscoplasticity.

Contents

List of Figures	xi
List of Tables	xvi
Symbols	xvii
Acronyms	xix
Acknowledgement	xx
Publications and Conferences	xxi
Chapter 1 Introduction	1
1.1 Background.....	1
1.2 Aim and Objectives	5
1.3 Research Methodology	6
1.4 Thesis Organisation	7
Chapter 2 Literature Review	10
2.1 Introduction.....	10
2.2 Polymers	11
2.2.1 Structure and Classification	12
2.2.2 Epoxy Resins	13
2.3 Yielding Criteria for Polymers	14
2.3.1 Pressure Insensitive Yield Criteria.....	17
2.3.2 Hydrostatic Pressure Sensitive Yield Criteria.....	19
2.4 Moisture Degradation in Polymers	22
2.4.1 Moisture Diffusion in Epoxy Resins.....	23
2.4.2 Factors Influencing Moisture Diffusion.....	25
2.4.3 Effects of Moisture Diffusion	26
2.4.4 Moisture Diffusion Models.....	27
2.4.4.1 Fickian Model	28
2.4.4.2 Diffusion Relaxation Model.....	30

2.4.4.3	Dual Sorption Model.....	30
2.4.4.4	Dual Fickian Model	31
2.5	Deformation of Polymers.....	32
2.5.1	Mechanical Testing to Investigate Time Dependent Deformation	34
2.5.2	Constitutive Modelling	37
2.6	Depth Sensing Indentation of Polymers	40
2.6.1	Standard Load-Unload Test.....	43
2.6.2	Non-standard Tests	45
2.6.2.1	DSI Creep Test.....	45
2.6.2.2	DSI Using the Strain Rate Method.....	47
2.6.2.3	Dynamic Indentation Testing.....	47
2.6.2.4	Re-indentation Testing.....	49
2.6.2.5	Effect of Indenter Shape	49
2.6.3	Testing under Controlled Humid Environments.....	49
2.6.4	Analysis of DSI Data for Polymers	50
2.6.4.1	Minimisation of Time Dependent Response.....	51
2.6.4.2	Extraction of Time Dependent Model Parameters.....	53
2.7	FE Modelling of DSI of Polymers.....	55
2.8	Summary and Conclusions	57
Chapter 3	Experimental Methods	60
3.1	Introduction.....	60
3.2	Material and Sample Manufacture.....	60
3.2.1	Material.....	60
3.2.2	Stereolithography Process.....	62
3.3	Environmental Conditioning.....	64
3.4	Moisture Diffusion Tests	64
3.5	Bulk Mechanical Characterisation.....	66
3.5.1	Tensile Test.....	66
3.5.2	Compressive Tests	67
3.5.3	Creep Tests	68
3.6	Depth Sensing Indentation.....	69
3.6.1	Important Considerations When Using the DSI System.....	72
3.6.1.1	Safety Precautions during Operation	72

3.6.1.2	Calibrations and Maintenance Checks	73
3.6.1.3	Miscellaneous Factors Influencing Errors	74
3.6.2	DSI Tests	78
3.6.2.1	Investigation of VE/VP Behaviour	78
3.6.2.2	Investigation of the Effects of Relative Humidity	78
3.6.2.3	Effect of Drying on the Properties of Conditioned Samples.....	81
3.7	Summary	81
Chapter 4	Experimental Results.....	83
4.1	Introduction.....	83
4.2	Gravimetric Testing	83
4.2.1	Moisture Absorption at Various Relative Humidities	84
4.2.2	Modelling of Moisture Diffusion.....	86
4.3	Bulk Mechanical Properties.....	91
4.3.1	Tensile Test Properties.....	91
4.3.2	Compressive Test Properties	94
4.3.3	Creep Test Properties	96
4.4	DSI Tests	100
4.4.1	Investigation of Rate Dependent Effects	100
4.4.2	Investigation of Effects of Relative Humidity	105
4.4.2.1	Preconditioned Samples Tested at 33.5%RH.....	105
4.4.2.2	Samples Conditioned & Tested at Various RH.....	109
4.4.3	Investigation of Effects of Drying on Indentation Behaviour.....	113
4.5	Summary	115
Chapter 5	Finite Element Methods.....	118
5.1	Introduction.....	118
5.2	FE modelling of DSI.....	118
5.2.1	Geometry and Boundary Conditions	118
5.2.2	Mesh Design	121
5.2.2.1	Selection of Element Type	122
5.2.2.2	Mesh Sensitivity Analysis.....	124
5.2.3	Selection of Material Model	125
5.2.3.1	Pressure Sensitive Model for EP Deformation	126
5.2.3.2	Time Dependent Effects.....	128

5.2.4	Defining Contact.....	128
5.2.5	Solution Procedure for FE Analysis	132
5.3	Moisture Diffusion Analysis.....	133
5.4	Coupled Diffusion-Stress Analyses Technique	135
5.5	Summary.....	137
Chapter 6 Modelling the Depth Sensing Indentation Response of Polymers by Finite Element Analysis		138
6.1	Introduction.....	138
6.2	Verification of proposed FE model exhibiting DSI response	138
6.3	Transient diffusion modelling.....	141
6.4	Proposed relationship between elastic modulus and moisture concentration	145
6.5	Investigation of RH effects on indentation by FE modelling	149
6.6	Estimation of Hardness	152
6.7	Summary.....	156
Chapter 7 Analysis of Viscoelastic-Plastic Behaviour in Polymers using Depth Sensing Indentation		158
7.1	Introduction.....	158
7.2	Analytical modelling of indentation behaviour	158
7.3	Elastic-viscous-plastic mechanical modelling	160
7.4	Calculation of modulus and hardness from EVP model	171
7.5	Summary.....	175
Chapter 8 Discussion		176
8.1	Introduction.....	176
8.2	Moisture diffusion in SL Resins and its effects	176
8.3	The Indentation response of the SL Resin at various Humidities.....	178
8.4	Modelling the indentation behaviour at various RH.....	181
8.5	Phenomenological modelling of indentation data.....	182
8.6	Summary and Contribution to the Knowledge	183
Chapter 9 Conclusions and Future Work.....		186
9.1	Introduction.....	186
9.2	Conclusions.....	186
9.3	Future Work.....	188
References		190

Appendix-1	207
Appendix-2	211

List of Figures

Figure 1.1 : Schematic of research methodology.....	7
Figure 2.1 Structure of thermoplastic and thermoset polymers.	13
Figure 2.2. Chemical structure of an epoxy resin - DGEBA.....	14
Figure 2.3. True-stress vs. true-strain plot for polymers.....	15
Figure 2.4. Tresca and von Mises yield surfaces.	19
Figure 2.5. Yield envelope of linear Mohr-Coulomb criterion.....	22
Figure 2.6. Water molecules in polymer.....	24
Figure 2.7 Typical creep curve.	35
Figure 2.8: Creep and recovery behaviour in polymers.....	36
Figure 2.9: Mechanical components used in phenomenological models.....	38
Figure 2.10: Arrangement of mechanical components used to give VE phenomenological models.....	39
Figure 2.11: Arrangement of mechanical components used to give VP phenomenological models.....	40
Figure 2.12. Different modes of deformation during the DSI testing of polymers.....	42
Figure 3.1. Schematic of SL process.....	62
Figure 3.2: Build orientation of samples for various types of tests.....	63
Figure 3.3: Geometry details of gravimetric test samples (not on scale).....	65
Figure 3.4. Schematic showing dimensions of tensile test specimen.....	67
Figure 3.5: Geometry details of compression test samples.....	68
Figure 3.6: Geometric details of DSI test samples.....	69
Figure 3.7. Schematic of NanoTest 600 system.....	70
Figure 3.8. Schematic of nano head unit.....	72

Figure 3.9. Pictures of humidity control unit parts.	80
Figure 4.1. Equilibrium moisture uptake by Accura 60 samples at various relative humidities.	85
Figure 4.2: Comparison of moisture uptake in Accura 60 samples at various %RH.....	86
Figure 4.3: Fickian and dual Fickian model fits to experimental data at various environments using Accura 60.	90
Figure 4.4: Moisture dependent tensile stress-strain curves for Accura 60 samples after 720 hours conditioning at various relative humidities.	91
Figure 4.5: Tensile elastic modulus as a function of moisture conditioning time at various RH.	93
Figure 4.6: Tensile yield as a function of moisture conditioning time at various RH.	93
Figure 4.7: Moisture dependent compressive stress-strain curves under compressive load for Accura 60 samples after 720 hours conditioning at various RH.....	94
Figure 4.8: Elastic modulus as a function of moisture conditioning time at various RH under uniaxial compressive testing.	95
Figure 4.9: Compressive yield as a function of moisture conditioning time at various RH. .	96
Figure 4.10. Tensile creep curves for samples preconditioned at 33.5 % RH for 720 hours and tested at 22.5 °C at 35 % RH (± 2 % RH) at various loads.....	97
Figure 4.11. Determination of tensile steady state creep constants of samples preconditioned for 720 hours at 33.5 % RH and tested at 22.5 °C and 35 % RH (± 2 % RH) testing environment.	98
Figure 4.12: Creep curves of Accura 60 samples preconditioned for 720 hours at various RH and tested at 50 MPa at 22.5 °C at 35 % RH (± 2 % RH).....	99
Figure 4.13: Load-depth plots for dry samples tested at 33.5 % RH at various loading rates with no dwell period and unloading rate of 0.5 mN/s.....	101
Figure 4.14. Comparison of indentation hardness and modulus of dry samples with various loading rates, no dwell period, 0.5 mN/sec unloading rate and 20 mN maximum load.	102
Figure 4.15. Load-depth plots for dry samples tested at 33.5 % RH at 0.5 mN/sec loading rate with no dwell period and various unloading rates.	103
Figure 4.16. Load-depth plots for dry samples tested at 33.5%RH at 0.5 mN/sec loading rate with various dwell periods and an unloading rate of 0.5 mN/sec.	104
Figure 4.17. Comparison of indentation hardness and modulus of dry samples with 0.5 mN/sec loading rate, various dwell periods at 20 mN load and 0.5mN/sec unloading rate.	105
Figure 4.18. Load-depth plots of samples preconditioned under various environments for 24 hours and tested at 33.5%RH.....	106

Figure 4.19. Comparison of load-depth plot for samples initially dry with those preconditioned for five days at 84.5 % RH and tested every 24 hours at 33.5%RH.	107
Figure 4.20. Indentation hardness as function of time after pre-conditioning at various relative humidities and testing at 33.5 % RH.....	108
Figure 4.21: Indentation modulus as function of time after pre-conditioning at various relative humidities and testing at 33.5 % RH.....	109
Figure 4.22. Load-depth plots for samples conditioned by HCU for 24 hours under various % RH and tested under the same conditioning environment.	110
Figure 4.23. Indentation hardness as function of time after conditioning and testing under various relative humidities regulated by HCU.....	111
Figure 4.24. Indentation modulus as function of time after conditioning and testing under various relative humidities regulated by HCU.....	111
Figure 4.25: Comparison of indentation hardness of samples conditioned for five days in flask and tested at 33.5 % RH with samples conditioned for five days and tested under various % RH regulated by HCU.....	112
Figure 4.26: Comparison of indentation modulus of samples conditioned for five days in flask and tested at 33.5 % RH with samples conditioned for five days and tested under various % RH regulated by HCU.....	113
Figure 4.27. Comparison of load-depth plot for samples initially dry with those conditioned for five days at 84.5 % RH and tested at 84.5%RH and with samples conditioned for 5 days at 84.5%RH and followed by conditioning at 33.5%RH.	114
Figure 4.28. Recovery in indentation modulus and hardness on drying samples that were conditioned for 5 days under 84.5% RH and retesting periodically at 33.5%RH.....	115
Figure 5.1. Various model boundaries used in far field analysis.	120
Figure 5.2. Details of indenter and specimen geometry.....	121
Figure 5.3. Eight node axisymmetric element.	124
Figure 5.4 : Description of contact condition between the indenter and a specimen.....	129
Figure 5.5: Moisture penetration across the specimen.....	135
Figure 5.6: Flow chart of sequential-coupled diffusion-stress analysis performed in MSC Marc.	136
Figure 6.1: Comparison of load-depth plots from FEA with experiments for samples tested at 33.5%RH at 0.5mN/sec loading and unloading rates and different dwells.....	139
Figure 6.2: Comparison of load-depth plots from FEA with experiments for samples tested at 33.5%RH at various loading rates and 0.5mN/sec unloading rate.....	140
Figure 6.3: Typical finite element mesh for transient diffusion analysis.....	141

Figure 6.4: Normalised moisture concentration profile through 4mm thick samples after 8 hours conditioning under various relative humidity conditions.....	142
Figure 6.5: Normalised moisture concentration profile through 4mm thick samples after 20 hours conditioning under various relative humidity conditions.....	143
Figure 6.6: Logarithmic values of moisture concentration at various %RH for 4mm thick samples against relative humidity.....	144
Figure 6.7: Changes in elastic modulus with moisture over time through 4mm thick samples stored under various relative humidity conditions after 8 hours' time.	147
Figure 6.8: Changes in elastic modulus with moisture over time through 4mm thick samples stored under various relative humidity conditions after 20 hours' time.	147
Figure 6.9: Modulus of elasticity as function of moisture concentration for 4mm thick samples.....	148
Figure 6.10: Comparison of load–depth plots of FEA with experiments of samples conditioned by HCU for a day under various% RH and tested under the same conditioning environments.....	150
Figure 6.11: Comparison of load depth plots of FEA with experiments of samples conditioned by HCU for various days under 84.5 %RH and tested under the same conditioning environment with plot at dry (33.5%RH) taken as reference.	151
Figure 6.12: Comparison of hardness calculated from FEA modelling with experiments after various days of conditioning and testing at 84.5% RH.....	152
Figure 6.13: Comparison of hardness calculated from estimation method applied on single set of load-depth curves of experiment with experiments performed at various depths inside the specimen after 12 h at 84.5% RH.....	154
Figure 6.14: Comparison of hardness estimated at various depths inside the specimen from single load-depth plot of FEA and DSI experiment after 12 h at 84.5% RH.....	155
Figure 7.1: Three step procedure to determine viscoelastic-plastic properties.....	160
Figure 7.2: Elastic-viscous-plastic model-1.....	161
Figure 7.3: Experimental (exp) and predicted (model-1) indentation creep curves for 4mm thick Accura 60 samples tested at 20mN load for 300 sec hold at 33.5%RH at 22.5°C.	164
Figure 7.4: Elastic-viscous-plastic model-2.....	165
Figure 7.5: Experimental (exp) and predicted (model-2) indentation creep curves for 4mm thick Accura 60 samples tested at 20mN load for 300 sec hold at 33.5%RH at 22.5°C.....	166
Figure 7.6: Elastic-viscous-plastic model-3.....	167
Figure 7.7: Experimental (exp) and predicted (model-3) indentation creep curves for 4mm thick Accura 60 samples tested at 20mN load for 300 sec hold at 33.5%RH at 22.5°C.....	168

Figure 7.8 : Experimental and predicted (model-3) indentation creep curves for 4mm thick Accura 60 samples tested at 20mN load for 300 sec hold at various RH after 8 hours of conditioning at 22.5°C. 170

List of Tables

Table 3-1: Typical properties of the SL resin, Accura 60.....	61
Table 3-2: Frequency of calibration and maintenance checks.	74
Table 4-1: Fickian and dual Fickian model constants for 4mm thick Accura 60 samples at various relative humidities.	87
Table 4-2 : Creep power law constants at various %RH after periodic conditioning.	100
Table 5-1 : Element types available for executing axi-symmetric analysis.	122
Table 5-2 : Details of the different meshes used in the mesh convergence analysis.	125
Table 5-3 : Constants for linear Mohr-Coulomb yield criteria after 720 hours conditioning at various environments.	127
Table 5-4 : Details of adaptive stepping.	133
Table 5-5 : Analogy between Fickian moisture diffusion and heat transfer.	134
Table 7-1 : Parameters of EVP models calculated from indentation creep data for 4mm thick Accura 60 samples tested at 20mN load for 300 sec at 33.5%RH and 22.5°C.....	169
Table 7-2 : Parameters of EVP model-3 calculated from indentation creep data for 4mm thick Accura 60 samples tested at 20mN load for 300 sec after 8 hours of conditioning at various RH at 22.5°C.	170
Table 7-3 : Comparison of values of modulus for Accura 60 calculated from different techniques after 8 hours conditioning at various RH.	172
Table 7-4 : Comparison of values of hardness for Accura 60 calculated from EVP model parameters with those calculated using OP method after 8 hours conditioning at various RH.	174

Symbols

A	Power law constant
b	Thickness of specimen
C	Concentration
C_∞	Saturated moisture concentration
$C_{1\infty}, C_{2\infty}$	Fractions of saturated moisture concentration in a dual Fickian model
C_t	Moisture concentration at time t
D	Diffusion coefficient
D_1, D_2	Diffusion coefficients of first and second stage in a dual Fickian model
δ	displacement
ε_{pl}	Plastic strain
$\dot{\varepsilon}_{ss}$	Steady state creep strain rate
E_t	Tensile elastic modulus
E_c	Compressive elastic modulus
E^*	Reduced modulus
E_e	Contact or equilibrium modulus
H	Hardness
H_e	Contact or equilibrium hardness
h	Indentation penetration depth
I_1	First stress invariant
J_2	Second stress invariant
J_3	Third stress invariant
l	Length of the diffusion path
M_∞	Saturated moisture content
$M_{1\infty}, M_{2\infty}$	Fractions of saturated moisture content in a dual Fickian model
M_t	Moisture content at time t

m	Power law constant
n	Number of terms in a series
P	Indentation load
p^*	Hydrostatic stress
p_m	Mean pressure beneath the indenter
S	Stiffness
σ	Stress
σ_v	von Mises equivalent stress
σ_{ult}	Ultimate tensile strength
σ_{ulc}	Ultimate compressive strength
σ_y	Yield stress
σ_{ty}	Tensile yield stress
σ_{cy}	Compressive yield stress
T	Temperature
t	Time
τ	Retardation time

Acronyms

2D	Two Dimensional
3D	Three Dimensional
AM	Additive Manufacturing
EP	Elastic plastic
EVP	Elastic viscous plastic
DN	Doerner and Nix
DSI	Depth Sensing Indentation
FE	Finite Element
FDU	Fused Deposition Modelling
HCU	Humidity Control Unit
OP	Oliver and Pharr
RH	Relative Humidity
RP	Rapid Prototyping
RM	Rapid Manufacturing
SL	Stereolithography
SLS	Selective Laser Sintering
VE	Viscoelastic
VEP	Viscoelastic-plastic
VP	Viscoplastic

Acknowledgement

I am deeply in debt to my supervisors Prof. Dr. I. A. Ashcroft and Prof. Dr. R. Hague for their supervision, recommendations, constructive criticism and encouragement. Their patience and understanding helped me navigate through the hard times. I would also like to thank Prof. Dr. R. Wildman for his inputs during annual assessments of my research.

Special thanks to the staff at Micro Materials, Wrexham, UK, for their technical help on various issues related to nanoindentation machine during the experimentation stage.

I am also thankful to the staff of the Wolfson School of Mechanical and Manufacturing Engineering for their assistance. I appreciate the guidance provided by Mr. Andy Sandaver, Mr. Mark East and Mr. Phil Brindley during the experimentation phases of the research.

I would also like to extend my gratitude to my fellow researchers; Dr. Aamir Mubashar and Dr. Zahid Rizwan Khokhar for their help and friendship throughout the research.

Publications and Conferences

Journal Papers:

1. ALTAF, K., ASHCROFT, I. A. and HAGUE, R., Modelling the effect of moisture on the depth sensing indentation response of a stereolithography polymer. *Computational Materials Science*.
2. ALTAF, K., ASHCROFT, I. A. and HAGUE, R., Investigation of the effect of relative humidity on polymers by depth sensing indentation. *Journal of Materials Science*.
3. ALTAF, K., ASHCROFT, I. A. and HAGUE, R., Review Paper: The mechanical characterisation of polymers by depth sensing indentation. Drafting in progress.
4. ALTAF, K., ASHCROFT, I. A., and HAGUE, R., Analytical modelling of viscoelastic-plastic deformation of polymers at various humidities using berkovich indenter. Drafting in progress.

Conferences:

1. 20th International Workshop on Computational Mechanics of Materials, 8-10 September 2010, Loughborough University, Loughborough, UK.
2. CAMTEC II, Symposium on fine scale mechanical characterisation and behaviour, 29-30 March 2010, The Gordon Laboratory, Department of Materials Science and Metallurgy, Cambridge University, Cambridge, UK.
3. 9th Micromaterials European user meeting, 9-10 November 2009, Institute of Physics at Academy of Sciences, Prague, Czech Republic.

Introduction

1.1 Background

Polymers have a wide range of applications in areas such as; automobiles, packaging, medical, consumer electronics, bodies of various machines, toys, pipes, utensils, bottles, architecture etc. Their broad range of applications is due to their extraordinary features including high strength-to-weight ratio, corrosion resistance, ease in manufacturing and good thermal and electrical resistance properties. Further advances have led to their usage in microelectronics and coatings for corrosion resistance applications (Licari and Hughes 1990; Ward and Sweeney 2004), bio-medical devices and tissue engineering (Grinstaff 2002; Oehr 2003; Wang et al. 2006).

In the last decade, additive methods have been developed from rapid prototyping techniques and are now being considered as alternatives to conventional techniques of manufacturing. This approach enables designers to design complex geometries without the constraints and costs associated with conventional manufacturing techniques. This technique of manufacturing is termed rapid manufacturing (RM) or additive manufacturing (AM) (Rosen 2007). There are many AM processes including stereolithography (SL), fused deposition modelling (FDM), selective laser sintering (SLS) etc. SL is one of the main processes of AM and is considered highly accurate and consistent (Hague et al. 2003). The polymeric materials used in the SL process are thermosetting polymers such as epoxies and acrylates. SL materials are also termed photo-polymers because they are primarily cured using ultra-violet (UV) light sources. Despite recent progress, AM still faces challenges in becoming a widely accepted manufacturing method, in particular the limitations of current materials.

Hence, material development is currently the main focus of study to make AM a reliable manufacturing method (Lev et al. 2003).

Polymers tend to be sensitive to environmental factors such as temperature, moisture and UV light and their long time usage in service may be compromised by environmental ageing. Moisture is considered to be one of the most important factors that affect the properties of polymers. There are hydrophobic polymers that do not absorb significant amounts of moisture; however, polymers exhibiting polarity can absorb a considerable amount of moisture (Bell et al. 2008). This moisture absorption can lead to a wide range of effects, both reversible and irreversible, such as plasticization (Ivanova et al. 2000), de-bonding at filler-matrix interfaces (Kasturiarachchi and Pritchard 1985; Kumazawa et al. 1994; Bowditch 1996), leaching of un-reacted functional groups (Antoon and Koenig 2003), structural damage such as micro-cavities or crazes (Apicella et al. 1979; Diamant et al. 2003), etc. Hence, for successful applications of SL polymers, reliable methods of predicting service life are essential. The development of these methods will help in materials research, leading to confidence in the SL process for making structured parts. The development of methods starts with the physical testing of SL resins. Changes in the mechanical properties of polymeric components due to moisture absorption can be examined by performing mechanical tests after moisture conditioning samples. Generally, characterisation of polymers is performed using bulk sample tests. However, the properties of many materials have been found vary spatially and to be dependent upon scale. Therefore, depth sensing indentation (DSI) is becoming a popular technique to generate the mechanical properties of materials on a micron scale.

DSI (or instrumented indentation) was developed in the 1970s as a quantitative measurement method of the mechanical properties of relatively small volumes of materials by monitoring load and depth during indentation. DSI is also known as nanoindentation because it can potentially be applied to a submicron depth range with sub-nanometer depth resolution. Two important properties that are readily obtained from DSI test data are hardness and elastic modulus (Newey et al. 1982;

Pethica et al. 1983), however, in the last two decades, researchers have also developed procedures to measure additional properties, such as creep (Asif and Pethica 1998; Lucas and Oliver 1999), strain rate sensitivity (Schwaiger et al. 2003), stress-strain relations (Field and Swain 1993; Hochstetter et al. 2003), bond strength (Takahashi et al. 2002), strain hardening (Yang et al. 2006), storage and loss moduli (Asif et al. 1999; Balooch et al. 2004), fracture behaviour (Pharr et al. 1993; Weppelmann and Swain 1996), scratch and wear properties (Burnett and Rickerby 1987; Morel and Jardret 2002). Additional functionality may include; micro-impact (Voevodin et al. 1995), adhesion testing (Burnett and Rickerby 1988), testing in a fluid system using a liquid cell (Ashcroft and Spinks 1996; Hengsberger et al. 2002; Akhtar et al. 2005), testing under various humidity environments by using a humidity control chamber (Altaf et al. 2011a, 2011c), dynamic testing (Park et al. 2004; White et al. 2005), and testing at elevated (Beake and Smith 2002; Yang et al. 2007), as well as sub-zero temperatures (Chen et al. 2010). Applications of DSI with polymers include testing in a fluid environment to understand environmental degradation, nanotribology, measurement of rate dependent properties; such as loss and storage modulus, ultra-low-load testing, elevated temperature testing, nano-impact and nano-fatigue testing.

The benefits of DSI over bulk tests include its ability to characterise various mechanical properties in a single test from only a small volume of material and the investigation of spatial variation in mechanical properties near the surface (Tezcan and Hsiao 2008). However, the DSI technique faces numerous challenges when applied to polymers, owing to their complex structure and time dependent viscoelastic (VE) or viscoplastic (VP) deformation (Fischer-Cripps 2004). Thus, the measured properties are a function of experimental parameters such as loading and unloading rate, dwell period at maximum load, geometry of indenter, maximum load, temperature, humidity etc. Various approaches to investigate polymers using DSI have been carried out; however, additional work is required to establish procedures to understand the rate dependent effects and the effects of varying moisture in the indentation of polymers.

The currently published research using nanoindentation is based on fixed environment humid conditions; ambient or immersed. However, in real applications, polymers are likely to be exposed to changing humidity conditions where moisture will vary during operation. These variable conditions make relative humidity an important factor that needs to be incorporated in the material research and designing phase of the components. Hence, a mechanism of incorporating a moisture uptake model and a numerical model describing indentation behaviour under varying moisture conditions is essential in order to lay the foundation of reliable durability predictions. Once the prediction technique to investigate moisture effects on SL resins is developed, it can be used for other materials as well to predict their performance at varying humidities and their useful life under varying relative humidities.

The research presented in this thesis aims to develop methodologies and models to predict the moisture diffusion and indentation behaviour of SL resin Accura 60 under variable moisture conditions. The complex multi-physics modelling of moisture diffusion and nanoindentation has only become possible during recent years due to the advent of multi-physics commercial software packages and advanced processing machines. These technological advances lay down a framework for successfully tackling the challenging issues of coupled diffusion-stress analysis. The proposed research is timely and industrially applicable in the context of modern developments in nano-materials, nanoindentation and modelling techniques. This is beneficial for all industrial sectors such as electronics, biomedical, automobiles etc. The research also highlights the significance of using a humidity control unit (HCU) to regulate the relative humidity. The research provides experimental methods and numerical modelling techniques that can help designers and engineers in improving the SL process and its epoxy based polymeric materials. This will lead to improved reliability and durability of SL resin products and give manufacturers more confidence in use of SL for making end-use parts. The core study of this research, namely the investigation of the effect of relative humidity on additive manufactured polymers by depth sensing indentation is a novel approach to an area which is, at present, largely ignored.

1.2 Aim and Objectives

The aim of this research is to investigate the effects of varying relative humidity on the indentation behaviour of stereolithography polymers and to develop a modelling methodology that can predict this micron scale behaviour under various humidities.

The following objectives were identified to achieve the aim of the research:

- Characterisation of bulk samples of SL resin to determine the moisture based diffusion and mechanical properties for subsequent use in numerical modelling.
- Investigation of viscoelastic and viscoplastic behaviour under DSI and selection of suitable experimental parameters that can be used for extracting meaningful mechanical properties.
- DSI at various controlled environments in order to investigate the behaviour of SL resin under varying humidities and examine the effectiveness of the HCU for regulating the environment during testing.
- Analysis of moisture diffusion in the SL resin under different moisture conditions and develop a finite element (FE) model for moisture diffusion analysis.
- Model the indentation behaviour of the SL resin using the FE method and verify using the experimental results.
- Development and implementation of a coupled diffusion-stress FE methodology for predicting indentation behaviour under variable moisture conditions.
- Estimation of mechanical properties at various depths under the influence of moisture by FE modelling and verification of results by experiments.
- Use of phenomenological modelling technique to select appropriate VE-P material model, find time dependent material parameters and correlate them with the mechanical properties at various humidities.

1.3 Research Methodology

Figure 1.1 shows a schematic of the overall research methodology. The research consists of both experimental and finite element modelling parts. The SL epoxy resin, Accura 60, was the selected polymeric material because it was in the latest range of SL materials at the initiation of the project. DSI testing was carried out to understand the VE and VP material properties at various relative humidities near the surface. Bulk experiments were carried out to characterise the moisture diffusion and mechanical properties of the polymeric material at various humid environments. These experimental results were used in the development of the predictive models. All the experiments and moisture conditioning were carried out at a fixed temperature of 22.5 °C with ± 1 °C variation in temperature and at 33.5 %, 53.8 %, 75.3 % and 84.5 % relative humidities with ± 1 variation in RH.

For the predictive modelling of the indentation behaviour, a novel methodology was used that is applicable under variable environmental conditions. This methodology consists of a coupled moisture diffusion-stress based FEA contact analysis to determine the indentation response of the material under various environmental conditions. The modelling results were validated by comparison with the DSI experimental data. Modelling was also used to predict hardness at various depths under different humid environments and the results were validated with the experimental results. Additionally, an analytical modelling approach was used to characterise material parameters from DSI creep curves under various relative humidities and use these parameters to find mechanical properties.

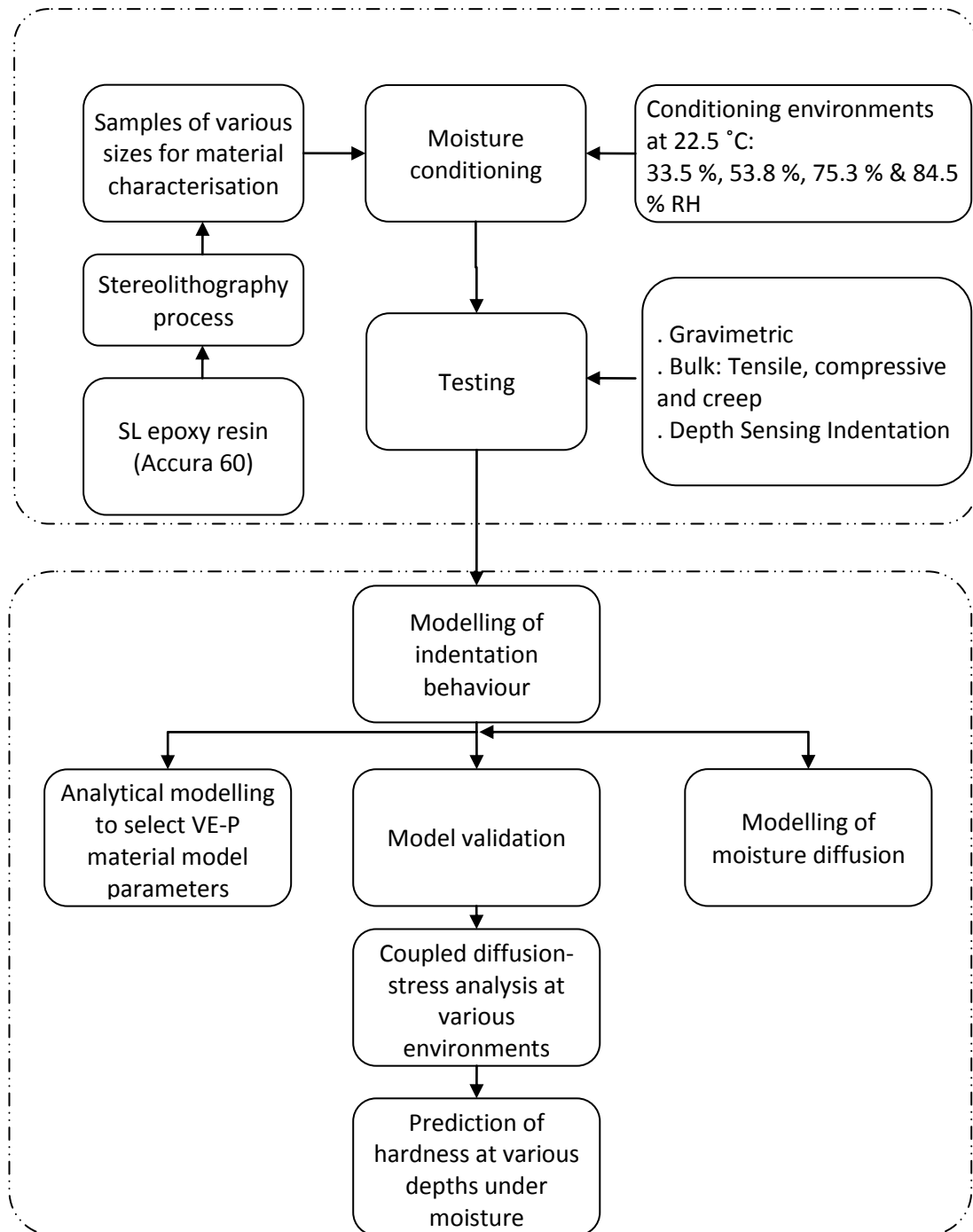


Figure 1.1 : Schematic of research methodology.

1.4 Thesis Organisation

The thesis is comprised of eight further chapters. A brief description of the contents of these remaining chapters is given here.

Chapter 2 Literature Review. This chapter provides a review of the literature to identify the relevant previous research work. The chapter can be divided broadly into

five parts. The first part discusses the structure and classification of polymers and their yielding criteria. The second part discusses moisture degradation, diffusion phenomena and their effects on mechanical properties. The next part describes the deformation in polymers, testing methods and constitutive modelling to investigate and describe time dependent behaviour. There follows a review of the mechanical characterisation of polymeric materials by depth sensing indentation technique. The final part discusses numerical modelling techniques for moisture diffusion and indentation behaviour.

Chapter 3 Experimental Methods. Details of the material, its manufacturing technique and moisture conditioning, experimental methods and procedures for moisture uptake, bulk mechanical tests and DSI are provided in this chapter.

Chapter 4 Experimental Results. Results from the experiments are provided in this chapter. A comparison of moisture diffusion models is carried out in order to select suitable model for later use in the diffusion modelling. Bulk mechanical test results are also shown that are used in defining the material model. Finally, characterisation of the Accura 60 by DSI at various relative humidities is discussed.

Chapter 5 Finite Element Methods. This chapter provides details of the finite element modelling methods used in the research work. The geometry, boundary conditions, mesh design (including element choice and mesh convergence), material model, solution procedure, moisture diffusion analysis and coupled diffusion-stress analysis details are provided.

Chapter 6 Modelling the Depth Sensing Indentation Response of Polymers by Finite Element Analysis. Load-depth plots from FEA are compared with experimental results. Later, the proposed numerical model is used to measure hardness at various depths at different humidities and the results are validated by the experiments.

Chapter 7 Analysis of Viscoelastic-Plastic behaviour in Polymers using Depth Sensing Indentation. This chapter describes analytical modelling techniques to predict the indentation behaviour. Various phenomenological models describing viscoelastic-plastic behaviour are used to predict the indentation behaviour of Accura 60 under loading at various RH environments and find time dependent parameters. Finally these parameters are correlated to various mechanical properties. These

properties, calculated from VEP model parameters, are compared with the properties calculated from bulk compressive tests and those from DSI tests using OP analysis.

Chapter 8 Discussion. This chapter presents a discussion of the experimental results and the modelling methodologies presented in the previous chapters and summarises the outcomes from this research work.

Chapter 9 Conclusions and Future Work. The main conclusions of this research along with recommendations for future work are given in this chapter.

Literature Review

2.1 Introduction

Polymeric components can be manufactured from conventional techniques such as injection moulding, however, additive manufacturing (AM) is increasingly being considered as an alternative manufacturing method. AM processes can be used to develop prototypes, where the process is called rapid prototyping (RP) or end-use products in which case the process is termed rapid manufacturing (RM) or AM. Stereolithography (SL) polymers used in AM are currently sensitive to high levels of relative humidity (RH) and ultraviolet (UV) radiation and one of the areas that needs major development is the environmental stability of AM materials post-build (Hague et al. 2004).

Absorbed moisture affects the mechanical properties of polymers, such as; toughness, strength and the time dependent deformation (Mostovoy and Ripling 1971; Morgan et al. 1980; Shen et al. 1985). The absorbed moisture can also act as a plasticiser and decrease the glass transition temperature (T_g) (St. Lawrence et al. 2001). The degradation in mechanical strength by moisture can be reversible or irreversible. The changes in mechanical properties of polymeric components due to moisture absorption can be examined by performing tensile tests, compressive tests, shear tests, creep tests, depth sensing indentation (DSI) tests etc. after moisture conditioning of the samples. However, the viscoelastic (VE) or viscoplastic (VP) behaviour of polymers will influence the measurements and interpretation of results from these tests. Therefore, the selection of testing parameters is largely dependent upon the type of the material being tested and the information required from the test. Hence, the extracted properties must be related to these experimental parameters as they may vary with them.

This chapter presents a literature review of the effect of moisture on the mechanical properties of polymers and their time dependent deformation behaviour. The chapter starts with the structure and classification of polymers and their yield criteria. There follows a review of the various types of environmental degradation observed in polymers. Factors that influence moisture absorption and their effects on mechanical properties are then discussed and there is a review of testing methods used to characterise polymers. Constitutive modelling techniques to describe rate dependent behaviour are described and lastly numerical modelling techniques and their use in modelling the environmental degradation and time dependent deformation of the polymers are discussed.

2.2 Polymers

The word ‘polymer’, derived from poly (many) and ‘mer’ (units), means many units that are joined several times in a chain like structure by covalent bonds. These are manufactured from small molecules called monomers which are linked together in a chemical reaction by a polymerization process (Ravve 2000). The quantity of these ‘mer’ present in the polymeric material is termed the degree of polymerization. For example $[-CH_2 - CH_2-]_n$ means that linear polyethylene is the repeating unit having ‘n’ degrees of polymerization. If two or more repeating units exist, it is termed a copolymer.

Polymers have a wide range of applications that exceed any other class of materials and have replaced metals in many applications (Kalpakjian and Schmid 2006). Their applications include foam, coatings, adhesives, agriculture, automobiles, biomedical applications, composites, packaging, electronic devices and textiles. This widespread application of polymers can be attributed to their unique mechanical and physical properties such as:

- low density,
- high strength-to-weight ratio, especially when reinforced,
- good resistance to corrosion,

- ease of manufacturing,
- various choices of colours,
- low cost.

2.2.1 Structure and Classification

A fundamental property of bulk polymers is their degree of polymerization but the physical structure of the chain is also important as this determines the macroscopic properties (Anderson 2005). Molecular structure can typically be:

- Linear
- Branched
- Cross-linked
- Network

In polymers two types of bonds exist; primary or covalent bonds hold the atoms together in the molecule while secondary bonds or van der Waals forces hold the group of chains together to form the polymeric material. The properties of polymers are dependent on these bonds and chain length. For example, stronger forces between the chains will make the polymer less flexible and vice versa. Similarly, increase in chain length will increase the strength of the polymer but only after reaching a critical length. Broadly, polymers can be classified as thermoplastics and thermosets. Figure 2.1 shows the structure of thermoplastic and thermoset polymers. Thermoplastics have linear or branched chains with no cross-linking. On heating, the weak forces between the chains can be broken. This means that they can be moulded into the desired shape when their temperature is raised above a glass-transition temperature, ' T_g ' or melting temperature, ' T_m '. T_g is a temperature where a transition from a glassy to a rubber-like state takes place. This process is reversible and on cooling the thermoplastic returns to its original properties (Woodward 1995). Examples of thermoplastics include polyester (PE), polyethylene (PE) and acrylonitrile butadiene styrene (ABS).

Thermosets have their long-chain molecules cross-linked in a three-dimensional arrangement with covalent bonds. This primary bonding prevents relative movement of chains in thermosets. They are hardened by cross-linking the polymer chains by chemical additives, UV radiations or heat and the process is called ‘curing’. The curing reaction is irreversible and, hence, thermosets cannot be reshaped on heating. Examples of thermosets include epoxy resin, vulcanized rubber, melamine and Bakelite. Thermosets do not have a well-defined ‘ T_g ’ and begin to burn or degrade on heating to high temperatures. Thermosets have better mechanical, thermal, chemical and electrical properties and dimensional stability than thermoplastics (Kalpakjian and Schmid 2006).

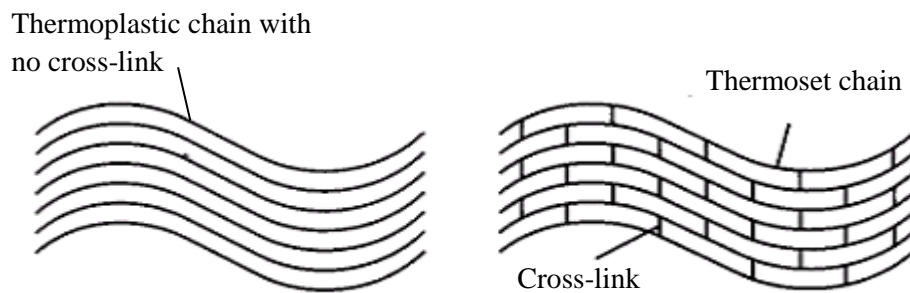


Figure 2.1 Structure of thermoplastic and thermoset polymers.

2.2.2 Epoxy Resins

Epoxy resins are a class of thermosetting copolymers that contain two or more epoxy groups, also called oxirane or ethoxyline groups. They have a wide range of applications, such as; adhesives, fibre reinforced plastic matrices, biomedical, electrical systems and coatings. They are formed from two chemicals; a resin and a hardener (or curing agent) and a catalyst is used to initiate the reaction between the epoxide molecules. The resulting polymer is highly cross-linked. They are known for their excellent chemical resistance, adhesion, electrical insulation and mechanical properties (May 1988). Their properties can be improved by using different types and combinations of resin, hardener and catalyst. Figure 2.2 shows the chemical structure of a typical epoxy resin, diglycidyl ether of bisphenol A (DGEBA) with two unreacted epoxide or epoxy units at the two ends with ‘ n ’ number of polymerised units.

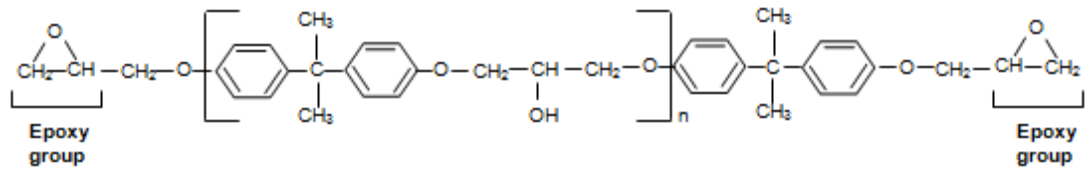


Figure 2.2: Chemical structure of an epoxy resin - DGEBA (Diglycidyl ether of bisphenol A).

In the present research work, an epoxy-based polymeric material Accura 60 is investigated. This material is used in SL processes to manufacture different objects. Details of the material properties, manufacturing process and post-processing technique are explained in section 3.2.

2.3 Yielding Criteria for Polymers

Polymers may yield at high values of stress either by crazing or shear yielding. Crazing occurs in regions that are under the influence of high tensile hydrostatic pressure leading to an increase in volume and the formation of micro voids and fibrils. Shear yielding usually occurs in polymers under deviatoric shear stress, resulting in a decrease in volume. Therefore, a yielding mechanism sensitive to hydrostatic pressure is obtained by crazing while shear yielding is seen with large deviatoric stress components under either tension or compression (Anderson 2005).

Yielding in polymers is also dependent upon environmental effects, such as temperature and moisture, and its intrinsic properties, such as stiffness of chain, critical entanglement, molecular weight and density, nature of monomer unit and degree of crystallinity (Schultz 1974; Kakani and Kakani 2004). Uniaxial tensile and compression tests are carried out to investigate the mechanical properties of polymeric materials (Kitagawa et al. 1992). Since the cross-sectional area and the length of the specimen changes considerably during testing of polymers, the true stress and true strain terms are widely used instead of engineering (or nominal) stress and strain. The true-stress vs. true-strain curve provides information about the elastic modulus, yielding, ultimate strength, fracture toughness and elongation at break.

Figure 2.3 shows a plot of a typical true-stress vs. true-strain curve of a polymer under tensile loading. Elastic modulus can be obtained from the slope of the initial part of the curve where stress is proportional to strain. With further increase in the stress, the curve decreases in slope until it reaches a point, termed as the yield point. After the yield point, the cross-sectional area decreases quickly with the formation of necking. If necking is extensive it is termed cold drawing, during which molecules align parallel to the loading direction. This measures crystallinity, which is why material can support higher true stress in the necking region. Once necking is completed, strain hardening occurs and true stress rises until fracture is reached. A typical ductile polymer yields at 5-10% strain.

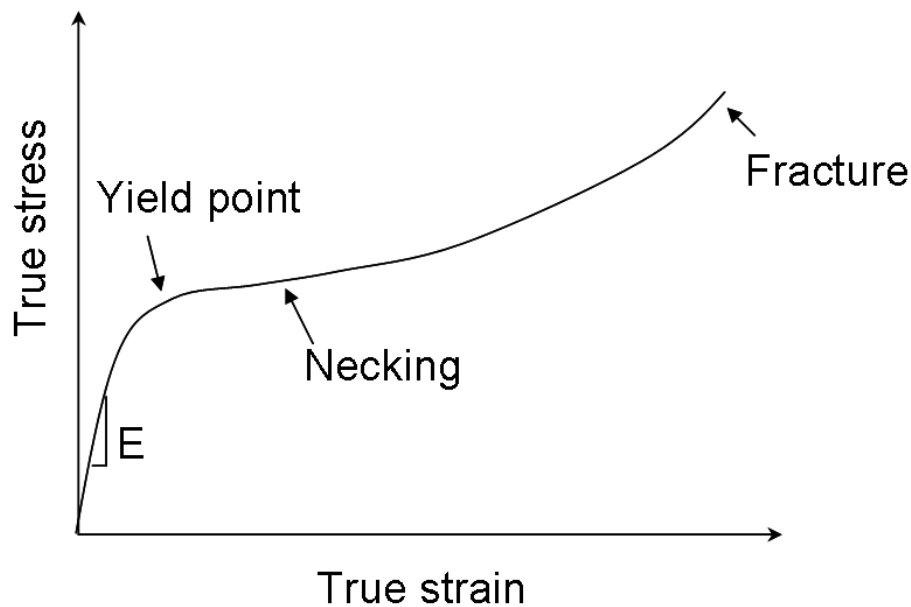


Figure 2.3. True-stress vs. true-strain plot for polymers.

A defined condition under which yield occurs under a stress system is termed a yield criterion. Selection of a suitable yield criterion is imperative for accurately modelling the behaviour of materials under multiaxial loading. The selected yield criteria must be able to account for the effects such as strain rate, hydrostatic pressure and stress relaxation.

Stress in a particular area is not uniformly distributed but varies from one point to another. Therefore, for an isotropic body, the stress at any point is defined by nine components of second order tensor also termed as Cauchy stress tensor as:

$$\sigma_{ij} = \begin{bmatrix} \sigma_{11} & \sigma_{12} & \sigma_{13} \\ \sigma_{21} & \sigma_{22} & \sigma_{23} \\ \sigma_{31} & \sigma_{32} & \sigma_{33} \end{bmatrix} \quad (2.1)$$

The components σ_{11}, σ_{22} and σ_{33} are the normal, or direct, stresses and they act perpendicularly to the plane on which they act. The remaining components are shear stresses and act parallel to the plane. This tensor can be separated broadly into two components; hydrostatic or dilatational (change in volume) and deviatoric stress (change in shape) components as:

$$\begin{bmatrix} \sigma_{11} & \sigma_{12} & \sigma_{13} \\ \sigma_{21} & \sigma_{22} & \sigma_{23} \\ \sigma_{31} & \sigma_{32} & \sigma_{33} \end{bmatrix} = \begin{bmatrix} p & 0 & 0 \\ 0 & p & 0 \\ 0 & 0 & p \end{bmatrix} + \begin{bmatrix} \sigma_{11} - p & \sigma_{12} & \sigma_{13} \\ \sigma_{21} & \sigma_{22} - p & \sigma_{23} \\ \sigma_{31} & \sigma_{32} & \sigma_{33} - p \end{bmatrix} \quad (2.2)$$

where the hydrostatic stress is given by:

$$p = \frac{1}{3}(\sigma_{11} + \sigma_{22} + \sigma_{33}) \quad (2.3)$$

At every point in a stressed body there are planes where there are no shear stress components and the stresses are acting normal to these planes. These planes are called principal planes and stresses acting normal to these planes are called principal stresses. If we choose a coordinate system with axes oriented to the principal

directions, then the direct stress becomes a principal stress and the stress tensor shown in Equation 2.1 can be represented as:

$$\begin{bmatrix} \sigma_1 & 0 & 0 \\ 0 & \sigma_2 & 0 \\ 0 & 0 & \sigma_3 \end{bmatrix} \quad (2.4)$$

where σ_1, σ_2 and σ_3 are the principal stresses. There are stress invariants associated with each tensor that don't depend upon coordinate system. The principal stresses can be combined to give the following three stress invariants:

$$I_1 = \sigma_1 + \sigma_2 + \sigma_3$$

$$J_2 = \sigma_1\sigma_2 + \sigma_2\sigma_3 + \sigma_3\sigma_1$$

$$J_3 = \sigma_1\sigma_2\sigma_3 \quad (2.5)$$

The principal stresses are used in the formulation of the different yield criteria, as described in section 2.3.1.

2.3.1 Pressure Insensitive Yield Criteria

Pressure insensitive yield criteria, or deviatoric stress based criteria, are suitable for materials that are ductile and their yield is independent of the hydrostatic stress component, such as metals. Two popular pressure insensitive criteria are Tresca and von Mises, which are functions of the deviatoric stresses only and predict equal yield stresses under tension and compression.

Tresca yield criterion states that yielding occurs when the maximum shear stress (τ_{\max}) exceeds a critical value (Tresca 1864). In terms of principal stresses, if $\sigma_1 > \sigma_2 > \sigma_3$, the Tresca criterion is:

$$\frac{\sigma_1 - \sigma_3}{2} = \tau_{\max} \quad (2.6)$$

For a uniaxial test σ_3 is zero so:

$$\tau_{\max} = \frac{\sigma_1}{2} = \frac{\sigma_y}{2} \quad (2.7)$$

where σ_y is the yield stress in tension or compression.

Von Mises yield criterion states that yielding occurs when the deviatoric strain energy in the material reaches a critical value (von Mises 1913). In other words, yielding begins when J_2 reaches a critical value, k , i.e.

$$f(I_2) = \sqrt{J_2} - k = 0 \quad (2.8)$$

where J_2 is the second stress invariant and k is the yield stress of the material under pure shear. If σ_y is the yield stress under uniaxial testing:

$$k = \frac{\sigma_y}{\sqrt{3}} \quad (2.9)$$

Putting Equation 2.9 in 2.8, we get:

$$\sigma_y = \sqrt{3J_2} \quad (2.10)$$

When we compare both criteria as shown by Figure 2.4 where Tresca and von Mises yield surfaces are drawn in a deviatoric plane, we find that Tresca predicts plastic

yielding for stress states that are still elastic according to the von Mises criterion. Thus for plastic material behaviour, Tresca's criterion is more conservative.

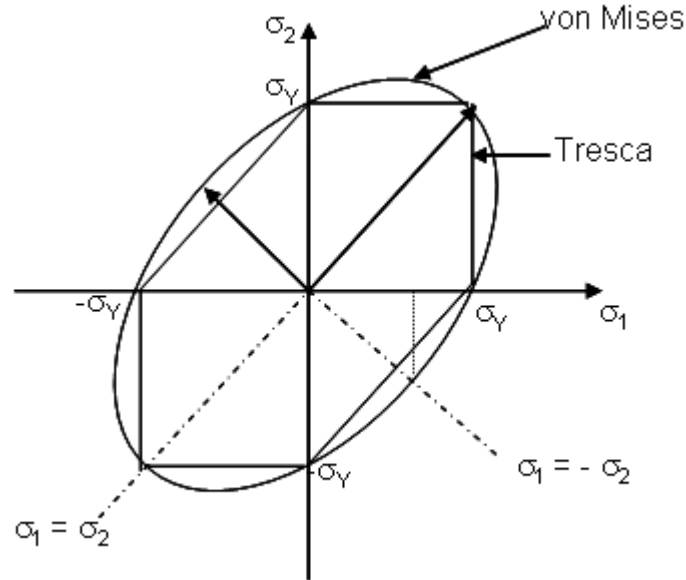


Figure 2.4. Tresca and von Mises yield surfaces.

Since Tresca and von Mises criteria are functions of the deviatoric stresses only and predict equal yield stresses in tension and compression, which is an assumption that is appropriate for metals but not necessarily for polymers. In polymers, the compressive yield stress is usually found to be higher than the tensile yield stress, which indicates hydrostatic stress sensitivity of the polymer, i.e. the hydrostatic component of the applied stress influences the yield process (Young and Lovell 1991). The next section 2.3.2 discusses yield criteria that account for the hydrostatic component in the stress tensor.

2.3.2 Hydrostatic Pressure Sensitive Yield Criteria

The elastic-plastic behaviour of polymers can be explained by assuming a pressure-dependent yield criterion, such as the modified Tresca, modified von Mises, linear Mohr–Coulomb, parabolic Mohr–Coulomb or Drucker–Prager (Caddell et al. 1974).

The modified Tresca criterion is determined by adding a hydrostatic stress term to the Tresca criterion (Whitney and Andrews 1967). This criterion states that the critical value of maximum shear stress is linearly dependent on the hydrostatic stress component, and is written as:

$$\tau_{\max} = \tau^0 + \mu_t p \quad (2.11)$$

where τ^0 is the yield stress in pure shear, μ_t the pressure sensitivity of the polymer under consideration and p is the hydrostatic stress component.

Similarly, a modified von Mises yield criterion has been proposed by adding a hydrostatic component to the von Mises criterion (Sternstein and Ongchin 1969; Bauwens 1970) and its expression is given as:

$$\sigma_m = \tau_m^0 + \mu_m p \quad (2.12)$$

where σ_m denotes the von Mises yield stress, τ_m^0 is the yield stress in pure shear and μ_m represents a yield envelop in the form of a circular cone.

The von Mises yield criterion has an advantage over the Tresca criterion because its surface/envelope (circular cone) does not encounter the discontinuities present in the Tresca yield (hexagonal pyramid). Both these modified criteria; Tresca and the von Mises, can be used for tensile test experimental data, where the hydrostatic stress is positive, but tend to be unconservative when the hydrostatic stress is negative or compressive (Bardia and Narasimhan 2006).

The Mohr-Coulomb criterion has been used to overcome the problems associated with the modified von Mises criterion (Bowden and Jukes 1972). The linear Mohr-Coulomb yield criterion states that failure occurs when the shear stress on any plane in the material reaches a critical value that varies linearly with the stress normal to that plane, and is given by:

$$\tau = c + \tan \phi \sigma_N \quad (2.13)$$

where τ is shear stress, c is cohesion of the material, ϕ is angle of friction and σ_N is the compressive stress on the shear plane.

The deviatoric yield function, f , is assumed to be a linear function of hydrostatic stress, and is given as:

$$f = \alpha I_1 + J_2^{1/2} - \frac{\bar{\sigma}}{\sqrt{3}} = 0. \quad (2.14)$$

Where I_1 and J_2 are the stress invariants while α and $\bar{\sigma}$ are the constants that can be related to c and ϕ as:

$$c = \frac{\bar{\sigma}}{\sqrt{3(1-12\alpha^2)}} \quad , \quad \sin \phi = \frac{3\alpha}{\sqrt{(1-3\alpha^2)}} \quad (2.15)$$

Figure 2.5 shows the yield envelope of the linear Mohr-Coulomb criterion. It can be seen that the model assumes that failure is independent of the intermediate principal stress, σ_2 . The Mohr-Coulomb model is considered to be sufficiently accurate for most polymeric applications where compressive strength exceeds significantly

compared to the tensile strength (MSC Marc 2007). In the current research work, the linear Mohr-Coulomb yield criterion has been used in a numerical model to define the rate independent behaviour. In order to include rate dependency, a creep model has been used in conjunction. Further details on the implementation of the linear Mohr-Coulomb and creep models are given in Chapter 5.

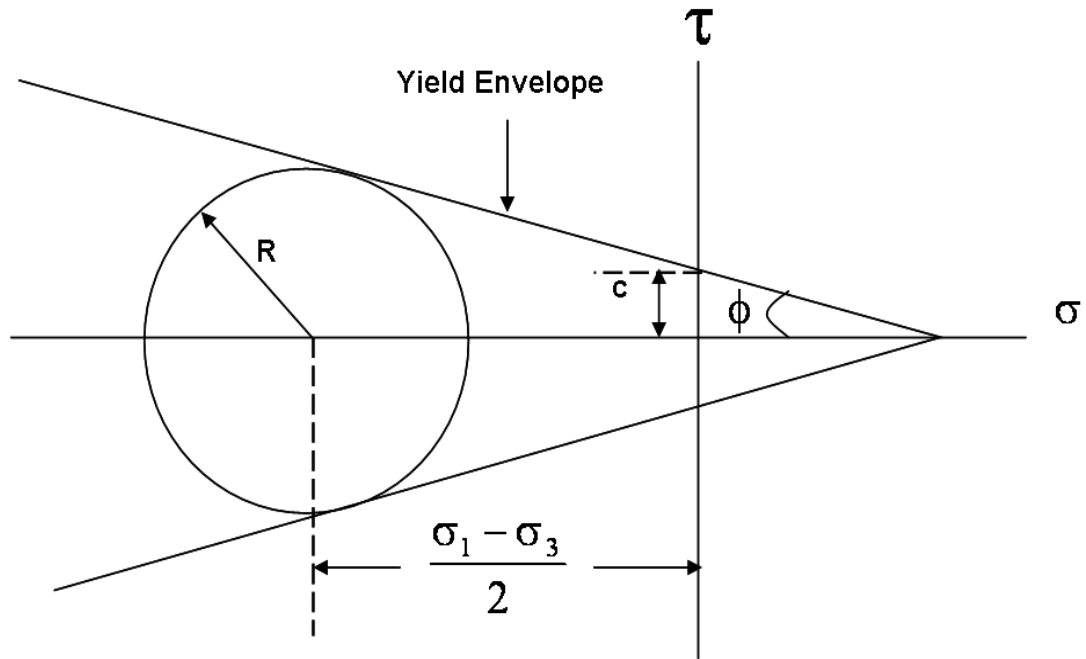


Figure 2.5. Yield envelope of linear Mohr-Coulomb criterion.

The other yield criteria such as parabolic Mohr-Coulomb giving parabolic envelope in case of plane strain and Drucker-Prager plasticity model which is a smooth approximation of yield surface can also model the behaviour of polymers and their historical review and further explanation can be found (Paul 1968).

2.4 Moisture Degradation in Polymers

Degradation can be defined as a reduction in performance owing to exposure to service conditions such as temperature, humidity, UV radiations and chemicals (Zaikov 1995). Hence, the lifetime of a polymeric part is not only dependent upon its molecular structure but also on the surrounding environment. Deteriorative reactions occur during the life of a material when they are subjected to degradation factors.

Therefore, the factors and the mechanisms of degradation must be understood if the technology and application of polymers are to continue to advance. Moisture is considered as one of the main factors of degradation in polymers. In the coming subsections, moisture diffusion in epoxy resins, factors affecting moisture diffusion, the effects of moisture on their properties and various diffusion models are discussed.

2.4.1 Moisture Diffusion in Epoxy Resins

Epoxies have a great tendency to absorb water, owing to presence of hydroxyl groups in their molecular structure, which attracts water molecules and form hydrogen bonds. The ingress of moisture starts by diffusion, which is the concentration gradient based process in which transportation of matter takes place due to random molecular motion.

Epoxy resins consist of both occupied volume and free volume (Adamson 1980). Free volume in polymers exists due to gaps between the polymeric chains and is influenced by density and the physical state of the polymer. Free volume is defined as the difference between the volume at a given temperature and the volume at 0 K. Therefore, the diffusion of moisture is dependent on the availability of free volume present within the polymer. Hence, a large free volume allows for higher moisture ingress in polymers by diffusion as it provides more channels for diffusing particles (Masaro and Zhu 1999). During initial moisture uptake, the moisture enters the free volume of the polymer, but the polymer does not start swelling (Adamson 1980). However, during the later stages, when most of the free volume is occupied, this absorbed moisture distorts the polymer network and causes swelling. When the polymer swells, additional free volume becomes available for the further diffusion of moisture.

The absorbed moisture content in a polymer can exist in free or bound states (Carter and Kibler 1978). Moisture that chemically reacts with the polymer becomes attached to the polymer and is not free to move anymore, whereas, the moisture present in the free volume of the polymer is free to move, as shown in Figure 2.6. A

model has been suggested to predict moisture concentration based on the probability that bound water may release and that free water will become bound (Carter and Kibler 1978).

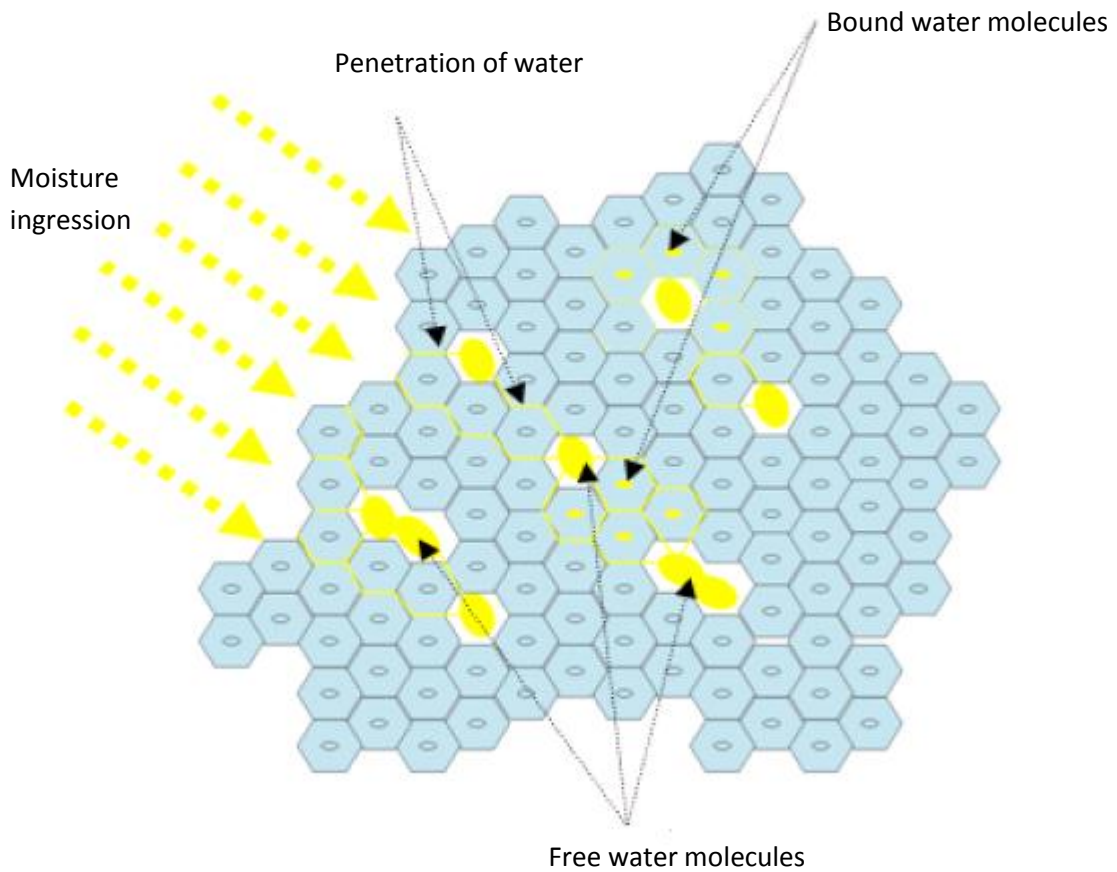


Figure 2.6. Water molecules in polymer.

Moisture diffusion in polymers may be described by Fick's law, which is based on the assumption that the rate of transfer of the diffusing substance through a unit area of a section is proportional to the concentration gradient, as given in Equation 2.16.

$$F = -D \frac{\partial C}{\partial x} \quad (2.16)$$

where F is the diffusion flux, D the diffusion coefficient, C the concentration of diffusing substance and x is the spatial coordinate. The equation has a negative sign that shows that diffusion occurs in the opposite direction to increasing concentration.

The maximum amount of moisture that can be absorbed by a volume is called as the saturated moisture content, M_{∞} . Both diffusion coefficient, D , and saturated moisture content, M_{∞} , are commonly used to define the moisture diffusion characteristics of the polymers. Moisture uptake in epoxy resins can be measured by using different techniques such as gravimetric method, spectroscopy and dielectric measurements. Gravimetric measurement is the most commonly used method in which the changes in mass of the samples subjected to certain moist condition at a fixed temperature is measured (BS EN ISO 62 2008).

2.4.2 Factors Influencing Moisture Diffusion

Moisture diffusion in polymers is influenced by many factors, such as; temperature, relative humidity present in the environment and additives in the polymer. The effect of these factors can be seen in the values of diffusion constant and saturated moisture content, which can vary remarkably.

Increase in temperature during moisture conditioning results in an increase in the rate of diffusion (Gledhill et al. 1980; Wright 1981; Ashcroft et al. 2011), as diffusion is a thermally activated process. The temperature dependence of water uptake in epoxies, at different temperatures, has been studied (Gledhill, Kinloch et al. 1980; Ashcroft et al. 2011). Results showed accelerated ageing in the samples that were subjected to humid environments at high temperatures. The diffusion coefficients measured from the experimental data showed an increase when the conditioning temperature was increased. The dependence of diffusion coefficient on temperature has been found to follow an Arrhenius relationship (Lin and Chen 2005), given as:

$$D = D_0 \exp\left(-\frac{Q}{RT}\right) \quad (2.17)$$

where D_0 is a constant, Q the activation energy for diffusion, R the universal gas constant and T is temperature.

Increase in temperature can also results in an increase in the saturated moisture content. The mobility of molecular chains increases with an increase in temperature, resulting in reduced density owing to thermal expansion. This increases the free volume of the polymer, thus increasing the saturated moisture content (Duncan et al. 2005).

Increase in the RH of the conditioning environment is another major factor affecting moisture diffusion (Wright 1981; Ashcroft et al. 2011). The nature of the polymer is important in considering the effect of environmental humidity e.g. hydrophobic polymers absorb relatively low amounts of water and the diffusion coefficient is generally independent of moisture concentration but hydrophilic polymers usually attract water molecules and tend to have a moisture concentration dependent on the diffusion coefficient. The results of the moisture uptake at 50°C for SL resins at various RH showed an increasing pattern in the diffusion coefficient with an increase in RH (Ashcroft et al. 2011). Increase in the saturated moisture content with increase in environmental humidity was also reported in that work.

The amount of hardener in epoxies also affects the saturated moisture concentration. A study on adhesives showed that an increase in the hardener resulted in an increase in saturated moisture content, which was attributed to introduction of more hydrophilic groups by the hardener in the matrix (Wright 1981).

2.4.3 Effects of Moisture Diffusion

In polymers, moisture absorption can lead to a wide range of effects, both reversible and irreversible, such as plasticization by weakening of the intermolecular

interactions among the functional groups of the chains (Park et al. 1997; Ivanova et al. 2000), de-bonding at filler-matrix interfaces (Kasturiarachchi and Pritchard 1985; Kumazawa et al. 1994; Bowditch 1996), leaching of un-reacted functional groups (Antoon and Koenig 2003), structural damage such as micro-cavities or crazes (Apicella et al. 1979; Diamant et al. 2003), and chemical degradation of the polymer matrix due to hydrolysis and oxidation (Apicella et al. 1979; Hamid 2000; Diamant et al. 2003). It can also involve the generation of free radicals or other reactive species, which may act as plasticizers or reactants (Verdu et al. 1996; Ritter et al. 1998).

Long-term exposure can decrease the molecular weight due to chain scission or the breaking of cross-links in the polymer network (McKague Jr et al. 2003). Absorbed moisture significantly affects the mechanical properties and glass transition temperature (T_g) of polymeric materials (Kumazawa et al. 1994; Bowditch 1996; Park et al. 1997; Butkus et al. 1998; St. Lawrence et al.2001).

The effects of moisture diffusion in polymers may be observed in the form of changes in their mechanical properties. Various studies have shown that mechanical properties, such as elastic modulus and yield strength, of epoxies decrease with an increase in absorbed moisture (Brewis et al. 1980; Loh et al. 2005; Ashcroft et al. 2011).

2.4.4 Moisture Diffusion Models

Moisture diffusion models can be used to predict the moisture concentration in polymers and determining their strength after moisture conditioning. It has been suggested that the kinetics of sorption of moisture in polymers systems is governed by three limiting cases (Crank 1979), as described below.

Case I (Fickian or diffusion controlled), in which moisture transport is a stochastic process driven by the presence of a concentration gradient. This case predominates

in systems where the penetrant has little hygroelastic effect on the polymer or the rate of diffusion is much less than that of relaxation. In Case I, the weight uptake is initially linear with respect to the square root of time, i.e if the amount sorbed at time t is Kt^n , then n is equal to 0.5.

Case II (Non Fickian or relaxation controlled), in which diffusion is more rapid than relaxation. Consequently, there is a discontinuity in concentration between the swollen and unswollen polymer. Initially the discontinuity advances into the polymer with a constant velocity, resulting in linear initial uptake of penetrant with respect to time, i.e if the amount absorbed at time t is Kt^n , then n is equal to 1.

Case III (Anomalous diffusion), in which both the mechanisms described above are present to varying degrees, resulting in anomalous uptake, i.e. n is between 0.5 and 1.

A description of moisture diffusion models based on diffusion type and process is provided in the following sections.

2.4.4.1 Fickian Model

Ficks law was briefly introduced in section 2.4.1. In this model, diffusion can be presented in a quantitative manner by adapting the mathematical equations of heat conduction derived by Fourier in 1822, as shown by Fick in 1855 (Crank 1979). The mathematical theory of diffusion is based on the hypothesis that the rate of transfer of a diffusing substance through a unit area of a section is proportional to the concentration gradient measured normal to the section. This hypothesis is presented mathematically by Equation 2.16, which is usually referred to as Fick's first law.

Considering the total transport of moisture into and out of a two dimensional differential element, the rate of change of moisture with time can be obtained by Fick's second law, which is shown in Equation 2.18 (Crank 1979).

$$\frac{\partial c}{\partial t} = D \frac{\partial^2 c}{\partial x^2} \quad (2.18)$$

The solution to Equation 2.18 for the case of a plane sheet where the region x ($-b < x < b$), C_t the concentration at time t and C_∞ when saturated is given by Equation 2.19 (Crank 1979).

$$\frac{C_t}{C_\infty} = \left[1 - \frac{4}{\pi} \sum_{n=0}^{\infty} \frac{(-1)^n}{2n+1} e^{\left[\frac{-D(2n+1)^2 \pi^2 t}{4b^2} \right]} \cos \frac{(2n+1)\pi x}{2b} \right] \quad (2.19)$$

Equation 2.19 can be integrated with respect to x to determine the total mass of water absorbed at time t . If M_t indicates the mass of the total amount of penetrant absorbed at time t and M_∞ is the mass at saturation, then:

$$\frac{M_t}{M_\infty} = 1 - \sum_{n=0}^{\infty} \frac{8}{(2n+1)^2 \pi^2} e^{\left[\frac{-D(2n+1)^2 \pi^2 t}{4b^2} \right]} \quad (2.20)$$

Fickian diffusion, as described in the equations above, is unable to accurately represent the anomalous uptake behaviour often seen in the sorption of moisture in polymers. Many models for anomalous uptake have been proposed. These can be classified as either “diffusion-relaxation” or “dual-uptake” models as given in the following sections.

2.4.4.2 Diffusion Relaxation Model

These models are concerned with moisture transport when both Case I and Case II mechanisms are present (Berens and Hopfenberg 1979; Joshi and Astarita 1979; De Wilde 1994). Berens and Hopfenberg (1978) assumed that the net penetrant uptake could be empirically separated into two parts, a Fickian diffusion controlled uptake and a polymer relaxation controlled uptake, with the latter being a first order function of the concentration difference. The equation for mass uptake using Berens and Hopfenbergs model is shown below.

$$M_t = M_{D\infty} \left[1 - \sum_{n=0}^{\infty} \frac{8}{(2n+1)^2 \pi^2} e^{\left[\frac{-D(2n+1)^2 \pi^2 t}{4b^2} \right]} \right] + \sum_i M_{R\infty,i} [1 - e^{-\Omega_i t}] \quad (2.21)$$

where, M_t is the total mass at time t , $M_{D\infty}$ is the equilibrium amount of sorption in the un-relaxed polymer. $M_{R\infty,i}$ and Ω_i are the equilibrium sorption owing to the relaxation process and the relaxation rate constant, respectively, for the i^{th} relaxation process. Berens and Hopfenberg (1978) showed that in general only one or two relaxation terms are required to provide a good fit to the experimental data.

2.4.4.3 Dual Sorption Model

Dual-sorption models are based on the premise that whilst some penetrant molecules diffuse normally in the polymer matrix, others will be affected by polymer-penetrant interactions or micro-void filling (Vieth and Sladek 1965; Gurtin and Yatomi 1979). Carter and Kibler (1978) addressed this problem in terms of the probability that a water molecule may react with a polymer molecule. Their model is based on the theory that moisture in a polymer network can be either bound or free. The probability that a free water molecule becomes bound is γ and the probability that a bound water molecule is emitted from the bound site and becomes mobile is β . The local weight fraction reaches equilibrium, M_i , when the number of free molecules per unit volume, n , and the number of bound molecules per unit volume, N , approach values such that Equation 2.22 is satisfied.

$$\gamma n = \beta N \quad (2.22)$$

When γ and β are small compared to K , the moisture uptake is described by Equation 2.23.

$$\frac{M_t}{M_\infty} = 1 - \frac{\gamma}{\gamma + \beta} e^{-\beta t} - \frac{8\beta}{\pi^2(\gamma + \beta)} \sum_0^{\infty} \frac{1}{(2n+1)^2} e^{-K(2n+1)^2 t} \quad (2.23)$$

where $K = \pi^2 D / b^2$.

2.4.4.4 Dual Fickian Model

Loh et al. (2005) proposed a dual-uptake model based on the summation of two Fickian diffusion models. Physically this can be interpreted as two different uptake processes operating in parallel, both of which are adequately described by Fickian diffusion. This model was seen to accurately represent anomalous moisture transport in an epoxy-based material exposed to different levels of humidity. Both of the Fickian diffusion models are based on Equation 2.20, with separate diffusion coefficients (D_1 and D_2) and saturation levels ($M_{1\infty}$ and $M_{2\infty}$), respectively. The equation for mass uptake using the dual Fickian model is hence:

$$M_t = M_{1\infty} \left[1 - \sum_{n=0}^{\infty} \frac{8}{(2n+1)^2 \pi^2} e^{\left[\frac{-D_1(2n+1)^2 \pi^2 t}{4b^2} \right]} \right] + M_{2\infty} \left[1 - \sum_{n=0}^{\infty} \frac{8}{(2n+1)^2 \pi^2} e^{\left[\frac{-D_2(2n+1)^2 \pi^2 t}{4b^2} \right]} \right] \quad (2.24)$$

Similarly Equation 2.19 will convert as:

$$C_t = \left[1 - \frac{4}{\pi} \sum_{n=0}^{\infty} \frac{(-1)^n}{2n+1} e^{\left[\frac{-D_1(2n+1)^2 \pi^2 t}{4b^2} \right]} \cos \frac{(2n+1)\pi x}{2b} \right] C_{1\infty} + \left[1 - \frac{4}{\pi} \sum_{n=0}^{\infty} \frac{(-1)^n}{2n+1} e^{\left[\frac{-D_2(2n+1)^2 \pi^2 t}{4b^2} \right]} \cos \frac{(2n+1)\pi x}{2b} \right] C_{2\infty} \quad (2.25)$$

where $C_{1\infty}$ and $C_{2\infty}$ are the fractions of saturated concentration C_{∞} , D_1 and D_2 are the diffusion coefficients and $2b$ is the length of the diffusion path.

In addition to the above mentioned moisture prediction models, various other models are also available that can predict moisture with varying degrees of success (Gupta and Pawar 2005; Tsai et al. 2007). In recent research work on various similar SL epoxy resins, it was found that the dual Fickian model better predicted the moisture diffusion, better than the Fickian model, (Altaf et al. 2011b), and hence, the dual Fickian model has been implemented in the current studies. Further details on the application of this model are described in Chapter 4.

2.5 Deformation of Polymers

In polymers, deformation can be both time independent and time dependent. The time independent deformation of polymers can be classified as either elastic or plastic. Elastic deformation corresponds to bond lengthening and straightening. Plastic deformation in polymers is different from metals as polymers do not contain crystallographic planes, grain boundaries and dislocations. In polymers, plastic deformation is dependent on the van der Waals forces (or secondary bonds) between molecular segments and is initiated by overcoming these forces (Anderson 2005).

Similarly, the time dependent deformation of polymers can be classified as either VE or VP. Viscoelasticity denotes that deformation is a combination of both viscous and elastic mechanisms. When stress is applied to polymers, molecules will tend to change their position. The segmental movement of the polymers will be dependent upon the extent to which branching and cross-linking is present in the structure as well as on value of T_g compared with the ambient temperature. The applied stress will result in creep and the creation of a back stress (Royle 2001). When the back stress becomes equal to the applied stress, creep is arrested. Due to accumulated back stress, on the removal of the applied stress, deformation will be recovered fully in the case of VE solid polymers and partially for VE fluid polymers. In the case of VE deformation, stress-strain curves show energy dissipation in the form of hysteresis, which is not present in pure elastic materials.

VP deformation in polymers is defined as rate dependent plastic or unrecoverable deformation (Fischer-Cripps 2004). The main difference between VP deformation and time independent plastic deformation lies in the fact that the former not only results in permanent deformation on the application of load but continues to creep afterwards under the influence of the load (Perzyna 1966). Since, this time-dependent phenomenon in polymers is common, they are often called VE or viscoelastic-plastic (VE-P) materials.

Creep in polymers is the time dependent deformation under constant load or stress resulting from VE/VP flow. The load and the time under that load affect the creep behaviour of a polymer. In polymers, creep and plastic deformation should be treated carefully because creep deformation can result from any of the VE or VP mechanisms present in the material. If the deformation rate is high compared to the relaxation rate, stresses can exceed the yield strength resulting in VP deformation. Hence, creep can occur under any value of stress but plasticity cannot. Polymers also exhibit stress relaxation behaviour. Stress relaxation in polymers is the relief of stress at constant strain. Hence, non-linear behaviour in polymers can be described by creep and stress relaxation phenomenon.

Factors such as strain rate, moisture, temperature and molecular structure also influence the deformation behaviour in polymers (Ferry 1980). For example, at high strain rate, or low temperature relative to T_g , polymers exhibit brittle deformation. However, at high temperatures, where the polymer is in a rubbery state, molecular movement becomes segmental, resulting in more deformation. Moisture causes a decrease in T_g and, hence, has a similar effect to increasing temperature (Ashcroft and Briskham 2010), provided other effects, such as chemical decomposition and micro cracks, don't occur.

Time dependent deformation in polymers can be investigated by mechanical tests and this is discussed in Section 2.5.1 while constitutive modelling techniques can be used to describe that deformation behaviour, as discussed in Section 2.5.2.

2.5.1 Mechanical Testing to Investigate Time Dependent Deformation

In order to investigate the mechanical behaviour and derive constitutive relationships for polymers, various types of mechanical tests are performed including, creep and recovery tests, relaxation tests, uniaxial tensile and compressive tests at various strain rates and dynamic mechanical analysis (DMA).

Normally, a creep test for a polymer involves testing in constant environment by applying an instantaneous constant load and monitoring deformation as a function of time. The resulting strain-time curve gives us instantaneous elastic or EP strain followed by primary creep (transient), secondary creep (steady state) and tertiary creep regions (Ashcroft and Briskham 2010). If we ignore the tertiary creep region, the total strain can be empirically described by:

$$\varepsilon = \varepsilon_0 + A\sigma^m t + B\sigma^{\alpha(1-e^{-\beta t})} \quad (2.26)$$

where ε and σ denote strain and stress respectively while A, B, m, α and β are the empirical constants obtained by curve fitting of experimental data. In Equation 2.26, the first term ε_0 represents the instantaneous strain that can be elastic or EP dependent on the magnitude of stress. The second term represents steady state creep while the third term represents the transient creep strain. Figure 2.7 shows a typical creep curve for polymeric materials under constant applied load with primary, secondary and tertiary stages.

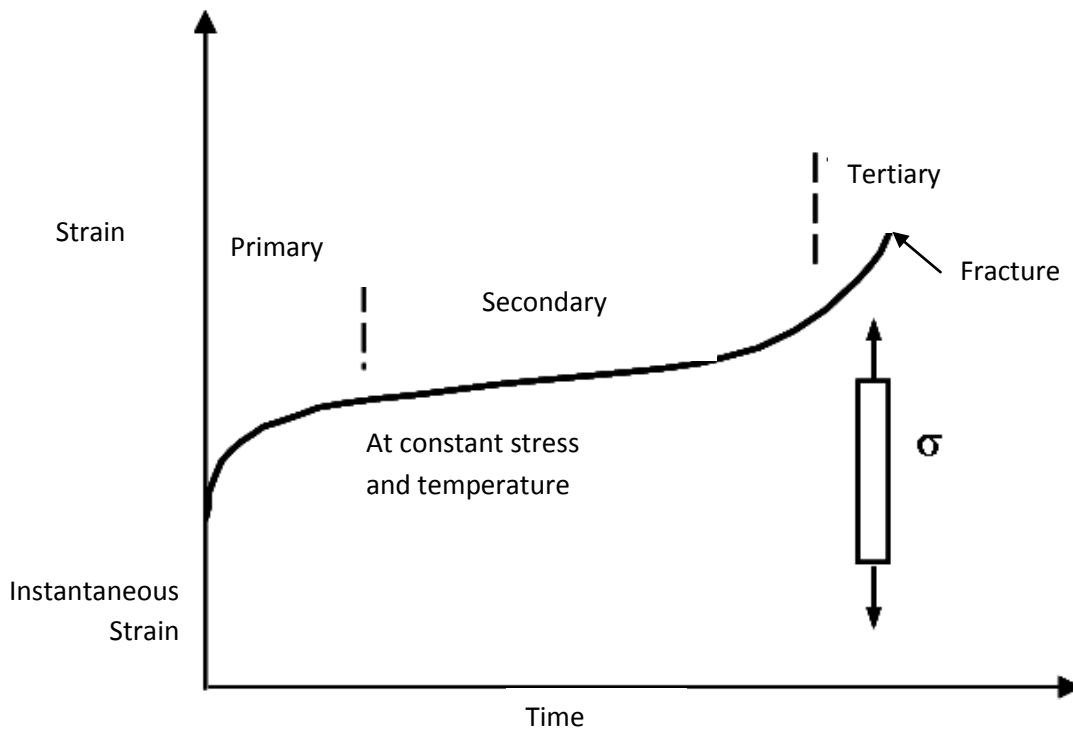


Figure 2.7 Typical creep curve.

Creep behaviour in polymers is affected by changes in environment, such as changes in temperature and humidity. Therefore, calculated creep deformation should be related to the testing conditions. If the load is removed instantaneously during the secondary creep stage and strain is monitored further, the time dependent strain recovery can be monitored. Figure 2.8 shows a typical creep and recovery behaviour shown by most polymers. After conducting creep tests at various loads, stress-strain plots at a given time can be used to investigate whether the VE is linear or nonlinear.

These plots are called isochronous stress-strain curves, the gradient of the curves being the creep modulus. In the linear range, the creep compliance is independent of the value of applied stress i.e. creep compliance is constant (Ashcroft and Briskham 2010).

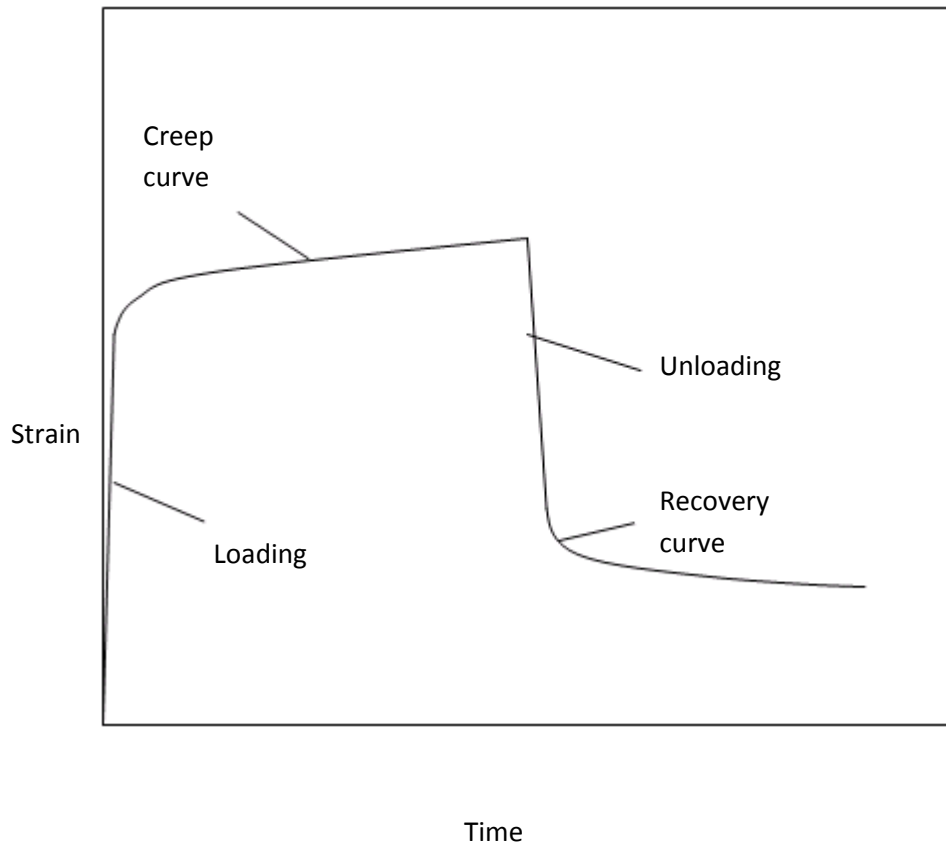


Figure 2.8: Creep and recovery behaviour in polymers.

Both creep and recovery strains are dependent on the polymer network. A highly cross-linked polymer exhibits less creep strain under a given applied stress and a greater proportion of recovery is observed on the removal of stress (Dillard 2010).

In some cases, where the transient creep strain is very small, we can ignore the third term in Equation 2.26 and then by differentiating strain with respect to time obtain a power law relationship between the strain rate ($\dot{\epsilon}$) and applied stress (σ) (Ashcroft and Briskham 2010).

$$\dot{\epsilon} = A\sigma^m \quad (2.27)$$

The empirical constants, A and m , can be calculated by plotting $\log(\dot{\epsilon})$ against $\log(\sigma)$. In the present study, creep tensile experiments have been carried at various environments to investigate the VE/VP behaviour of Accura 60 and to calculate the empirical constants for subsequent use in numerical modelling. Details on these experiments are given in Section 3.5.3, while method of calculation of the constants is discussed in Chapter 4.

Another method of measuring rate dependent behaviour is the relaxation test. Relaxation describes the decrease in stress over time under constant applied strain. The initial applied strain results in stress, but with the progress of time, entangled chains and sub chains in polymers re-arrange themselves, resulting in a decrease in the overall stress. As with creep, the stress-relaxation of polymeric materials is also dependent on the loading rate, magnitude of initial loading, temperature and moisture (Findley et al. 1989).

2.5.2 Constitutive Modelling

The time dependent properties of polymers are often described using rheological models. The development of these constitutive models has gained interest in both academia and industry, resulting in the development of various models constructed from physical or phenomenological aspects. In the phenomenological approach, the mechanical behaviour is represented by an arrangement of spring, dashpot and friction element (Shames and Cozzarelli 1992). Depending upon the stress-strain relationship being linear or nonlinear, we can use mechanical components as shown in Figure 2.9.

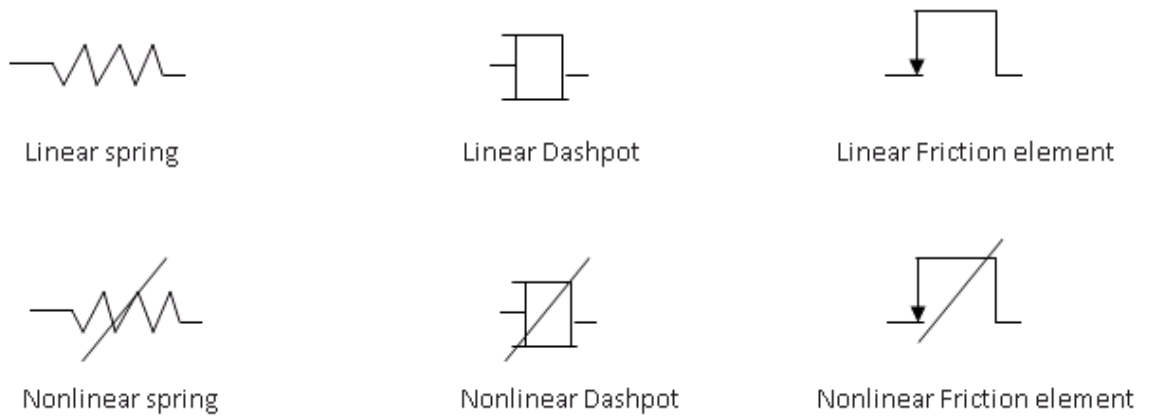


Figure 2.9: Mechanical components used in phenomenological models.

The mechanical components showed in Figure 2.9 can be used in different combinations to represent various types of response seen in polymeric materials as shown in Figure 2.10. For linear VE behaviour, a combination of two elements (spring and dashpot) in series gives the Maxwell model that can describe relaxation, and their combination in parallel gives the Kelvin-Voigt (KV) model, that can describe creep behaviour. Three elements, comprising a spring in parallel to a Maxwell model gives a Zener model and the combination of a spring in series with a KV model gives a standard linear solid (SLS). Four elements constituting Maxwell and KV models in series is called a Burgers fluid. The use of an arbitrary number of Maxwell elements in parallel with a spring is a Maxwell-Wiechart model, which is also called a Generalized Maxwell model, and can be used to describe relaxation behaviour with a Prony series. Similarly, a series of KV model in parallel with a spring can be used to describe creep. Further details on these models and their equations can be found elsewhere (Shames and Cozzarelli 1992; Ward and Sweeney 2004).

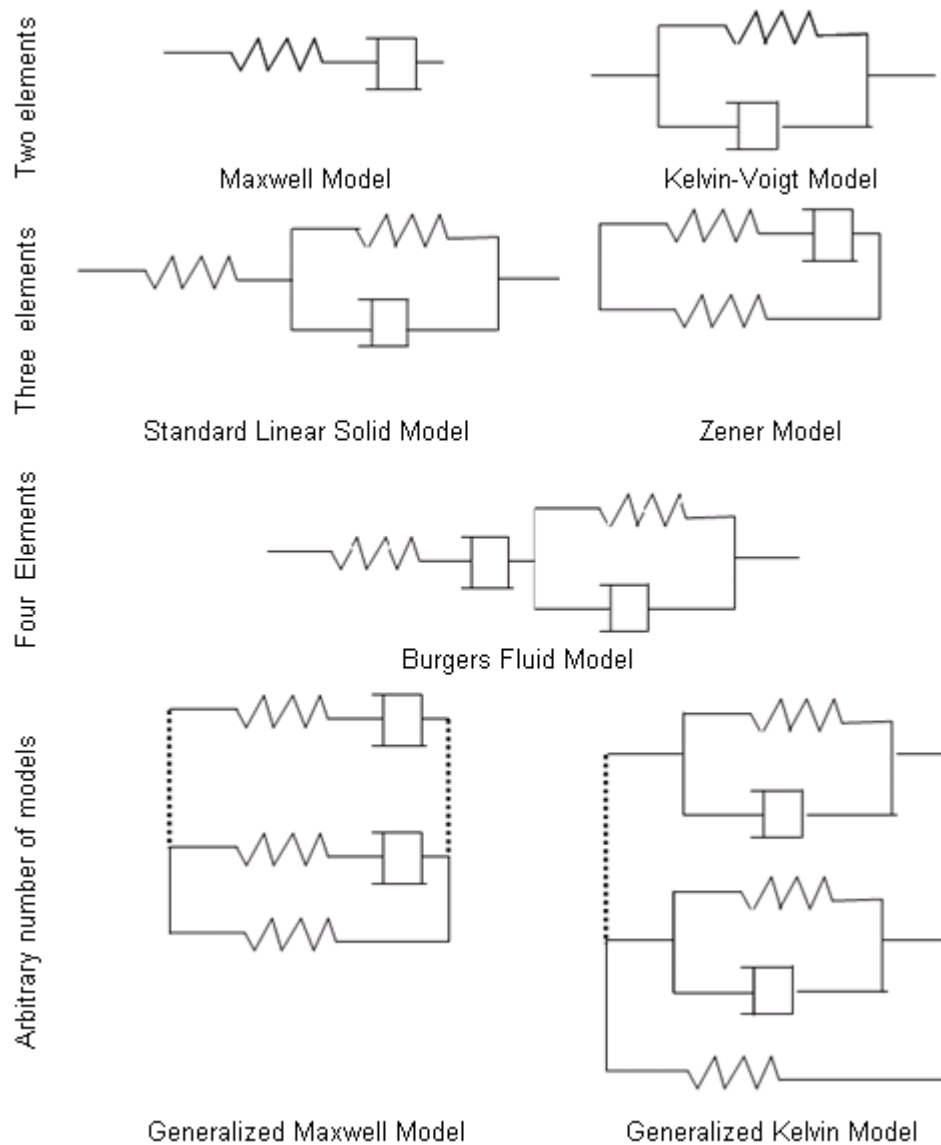


Figure 2.10: Arrangement of mechanical components used to give VE phenomenological models.

In the case of elastic-plastic (EP) or VP deformation, a friction element is combined with elastic and/or viscous elements to indicate plasticity. Figure 2.11 shows an elasto-viscoplastic (E-VP) solid and a viscoelastic-plastic (VE-P) solid. The E-VP model shows that the material will act elastically below the yield stress and VE after yield. The VE-P model behaves like a SLS model until yield and then will behave like a Burger's fluid. Hence, the friction element can be included to describe a transition between different material behaviours. The simple superposition model for VP behaviour combines creep strain with plastic strain. In contrast, over stress or

unified constitutive models give rate dependent plastic strain without differentiating between plastic and creep strain, which can be advantageous in cases where the differentiation of plastic and creep strain is not possible. Two terms; back-stress and over-stress are usually used with these models where-back stress defines the stress state that tends to make equilibrium state when material creeps while the difference between applied stress and back stress gives the over stress.

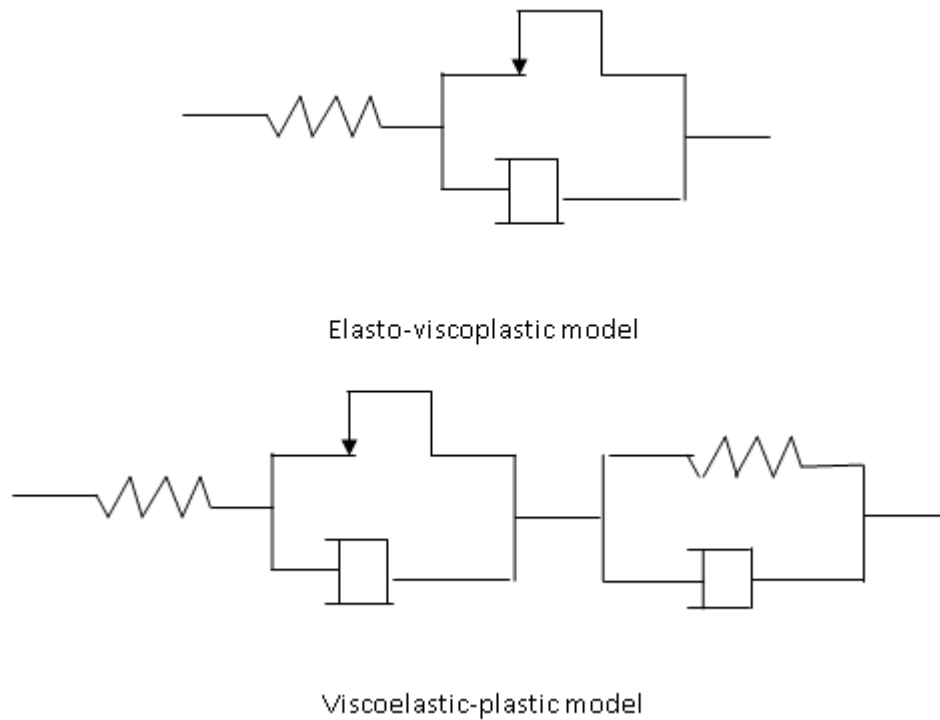


Figure 2.11: Arrangement of mechanical components used to give VP phenomenological models.

The use of phenomenological models to describe VE and VP behaviour in polymers using bulk mechanical test data has been established. In recent years, simplified phenomenological models have been used with indentation data and details are given in section 2.6.4.

2.6 Depth Sensing Indentation of Polymers

DSI is a quantitative measurement of the mechanical properties of relatively small volumes of materials by monitoring load and depth during indentation. Owing to the use of small volumes, the spatial variation of surface mechanical properties can be

evaluated through this method (Tezcan and Hsiao 2008). DSI is also known as nanoindentation because it can potentially be applied to a submicron depth range with nanometer depth resolution. DSI is different from macro and micro indentation techniques as it is based on calculating projected area from indentation depth rather than the residual area of indentation.

In DSI, penetration of the indenter tip into the sample is usually controlled by employing either a constant loading rate or a constant displacement rate (Doerner and Nix 1986; Oliver and Pharr 1992; Corcoran et al. 1997). Two important properties that are readily obtained from DSI test data are hardness and elastic modulus (Newey et al. 1982; Pethica et al. 1983), however, researchers have also developed procedures to measure additional properties, such as creep (Asif and Pethica 1998; Lucas and Oliver 1999). A strain rate sensitivity (Schwaiger et al. 2003), stress-strain relations (Field and Swain 1993; Hochstetter et al. 2003), bond strength (Takahashi 2002), strain hardening (Yang et al. 2006), storage and loss moduli (Asif et al. 1999; Balooch et al. 2004), fracture behaviour (Pharr et al. 1993; Weppelmann and Swain 1996), scratch and wear properties (Burnett and Rickerby 1987; Morel and Jardret 2002). Applications of DSI with polymers include testing in a fluid environment to understand environmental degradation, nanotribology, measurement of VE properties; such as loss and storage modulus, ultra low-load testing, elevated temperature testing, nano-impact and nano-fatigue testing. Commercially available DSI systems have been developed by Hysitron Inc. (USA) (Bhushan et al. 1996), Micro Materials Ltd. (UK) (Newey and Wilkins 1982), CSIRO (Australia) (Bell et al. 1991), CSM Instruments (Switzerland) (Randall, Consiglio 2000), and MTS Systems Corporation (USA) (Oliver, Pharr 1992).

The DSI technique faces numerous challenges when applied to polymers, owing to their complex structure and nature of deformation. Polymers can exhibit both time independent EP and time dependent VE or VP deformation during indentation. The DSI tests give us load-depth plots that can help in identifying these different deformation mechanisms. The modes of deformation during the DSI testing of polymers are summarized in Figure 2.12. If the maximum load produces a stress that

is below the yield point, such that material stays in the elastic state, and there is no time dependency of the mechanical response, then on removal of the load, deformation will be fully recovered and both loading and unloading plots will follow the same path, as described by curve ABCBA in Figure 2.12. However, for materials showing time dependency, if the load remains below the yield point, then when the load is removed the unload curve follows a different path to the loading curve, resulting in hysteresis. This hysteresis characterizes the VE solid and is represented by curve ABCDA. Curves ABCBA and ABCDA are usually only obtained when a blunt indenter, such as a flat or spherical indenter, is used for the indentation of polymers. An elastic response will usually only occur if the temperature is low and indentation time is small, while the VE response will prevail at higher temperatures when the indentation time increases. Curve ABCE, if time independent, demonstrates EP behaviour, whereas if curve ABCE is time dependent then it represents VE-P deformation. Both EP and VE-P deformation can be obtained by using a sharp indenter; such as the Berkovich indenter.

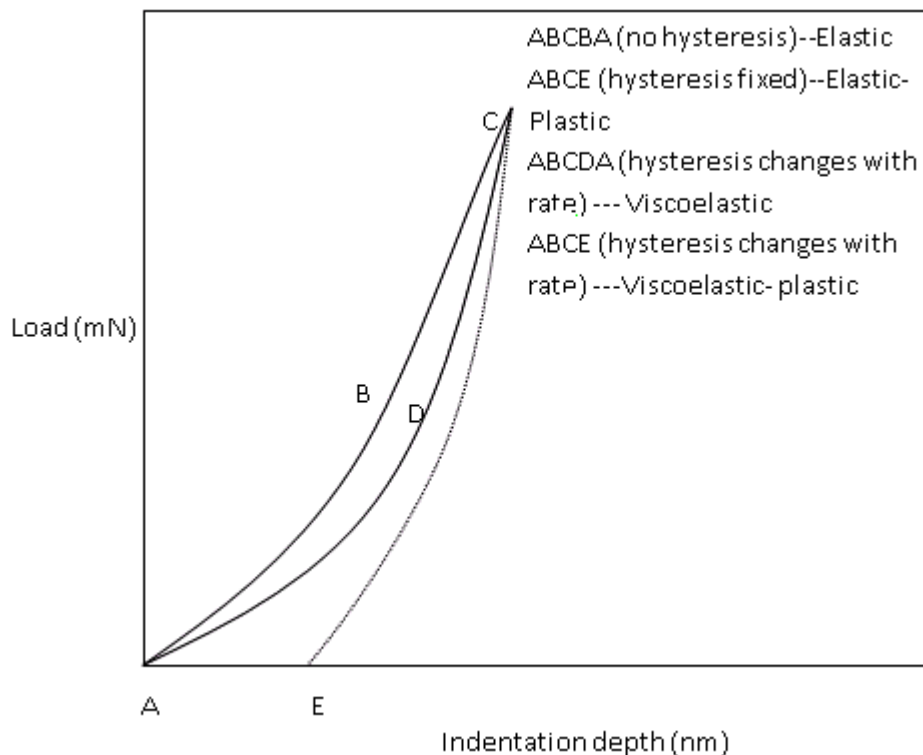


Figure 2.12. Different modes of deformation during the DSI testing of polymers.

Two main approaches are used to account for time dependent deformation in polymers. The first approach is most suitable for polymers with only mildly time dependent behaviour. In this approach, an attempt is made to eliminate time dependent effects by using a long enough dwell period at maximum load to obtain pseudo-elastic behaviour on unloading. In the second approach, the time dependent indentation behaviour is experimentally investigated and used to formulate a time dependent material model, such as one of the rheological models consisting of springs and dashpots.

This section discusses DSI experimental techniques when used on polymers. It is subdivided into four parts. The first part discusses the techniques to extract pseudo time-independent mechanical properties, such as hardness and elastic modulus, where time dependency has been minimized during unloading, from standard load-unload tests. The second section discusses testing techniques used to characterise the time dependent deformation while the third section investigates the polymer properties in controlled environments. The fourth section discusses techniques for analysing DSI test data of polymers.

2.6.1 Standard Load-Unload Test

When performing a standard load-unload test on polymers, a common source of error in analysing the test results is the assumption that unloading can be considered as elastic. The time dependent deformation of polymers can lead to errors in conventional calculations of hardness and modulus from the initial part of unloading in load-depth curve. In DSI tests on polymers, many researchers have found a bulge or “nose” effect during the initial portion of unloading as a result of creep. Creep during unloading can lead to errors in the calculation of contact stiffness (Briscoe et al. 1998; Ngan and Tang 2002; Cheng and Cheng 2005; Lu et al. 2009). This creep leads to an increase in depth in the early stage of unloading. The “nose” indicates that the material is deforming due to the presence of creep at a rate greater than elastic recovery (Chudoba and Richter 2001). This invalidates the assumption of fully elastic unloading and leads to errors in calculating contact depth and area and

influences the measured indentation hardness and modulus. Three important parameters in a standard load-unload test are loading rate, unloading rate and dwell period.

Loading rate selection is important in the DSI testing of polymers as this parameter contributes towards VE/VP effects. The maximum indentation depth increases as loading rate decreases and the nose effect becomes less pronounced. This is because the fast rate of loading means the polymer has less time to reach an equilibrium, hence, the back-stress is higher and the rate of deformation in the unloading segment higher. The creep behaviour seen on unloading, including the 'bowing effect', is when unloaded at lower rates. It has been proposed that the effect of delayed deformation on the unloading may be neglected if the creep velocity is reduced to a penetration depth growth of less than 1% per minute (Sardar et al. 1968). The influence of creep on unloading curve, and hence on stiffness and contact depth calculation can be decreased if the contact depth is calculated using the effective contact stiffness method (Feng and Ngan 2002). However, the disadvantage is that the indenter depth at the start of unloading is larger than at the end of loading, which results in a larger contact area and thus lower value of hardness (Mencík et al. 2009). To cater for this changing indenter depth, relatively fast unloading is recommended. In order to reduce the time dependent effects during the initial part of unloading, a dwell/holding time is usually introduced between the loading and unloading phases (Chudoba and Richter 2001). However, an excessive dwell time can result in inconsistent loading and unloading curves as a result of machine stability issues due to thermal drift. Hence, by the careful selection of loading, unloading rate and dwell, time dependence can be removed in many cases (Pharr and Rho 1999; Vanleene et al. 2006; Tang et al. 2007). However, the calculated indentation modulus and hardness are related to the selected experimental parameters, i.e. dependent on contact conditions and may vary with them. In the present research, various loading and unloading rates and dwell periods were used to select optimum experimental parameters to obtain pseudo-elastic initial part of unloading and are detailed in Chapter 3 while the results are shown in Chapter 4. This method can be useful in comparative studies with weakly time dependent materials; however, with many

polymers the time dependent deformation behaviour is of interest and should be investigated rather than minimized. This is discussed in the following section.

2.6.2 Non-standard Tests

Apart from the standard load-unload test, other DSI techniques can be used to quantify the VE and VP properties of polymers. One method is to use DSI creep tests to generate data that can be fitted to an appropriate mechanical model. Other techniques include testing at controlled strain rates, dynamic indentation testing, where a small oscillatory force or displacement is introduced, and miscellaneous techniques such as re-indenting and indenting with a blunt punch. These techniques are discussed in this section.

2.6.2.1 DSI Creep Test

DSI can be used in a similar fashion to the bulk creep tests discussed in section 2.5.1 to experimentally determine indentation creep. The DSI creep test can be used to calculate the localized creep parameters. The method can be used to calculate indentation creep parameters for multi-phase materials, thin films etc. for which bulk testing is not possible.

A typical DSI creep test provides indentation depth vs. time data. The constants of Equation 2.27 for an indentation creep power law can be calculated from this data in a similar way to that discussed earlier for bulk test results. For the case of DSI, Equation 2.28, proposed by Mayo and Nix (1988) who generalized the equation given by Pollock et al. for a pyramid indenter, can be used to calculate the indentation creep strain rate ($\dot{\epsilon}_I$) from the change in indentation depth with respect to time (dh/dt) as:

$$\dot{\epsilon}_I = k \frac{\left(\frac{dh}{dt}\right)}{h_p} \quad (2.28)$$

where ‘k’ is a dimensionless constant ($\cong 1$) and ‘h_p’ is the plastic depth of penetration. The indentation stress is commonly defined as the mean pressure (P_m) under the indenter, which is given by the load (P) over the projected contact area, which for Berkovich indenter is:

$$P_m = \frac{P}{24.5h_p^2} \quad (2.29)$$

The creep constants can then be calculated from $\log(\dot{\epsilon}_I)$ vs. $\log(P_m)$ plots.

DSI creep tests have been used to study rate dependent deformation and measure creep parameters for various materials (Lucas and Oliver 1999; Li and Ngan 2004; Alkorta et al. 2008; Wang et al. 2009). In one recent study, DSI creep tests were carried out at room temperature on various materials, for which the creep parameters were well established through bulk tests, to measure and compare creep parameters (Goodall and Clyne 2006). However, the results varied and no correlation was found. In another work, uniaxial and DSI creep tests were conducted on nano-crystalline nickel and the stress exponents were found to be almost the same from both tests (Wang et al. 2010). However, the strain rate from the DSI creep tests was 100 times greater than in the uniaxial creep tests.

When comparing bulk creep parameters with DSI creep parameters, we should remember the difference between the two types of experiments. In the case of DSI, there is a complex stress distribution that varies with load. The strain rate will also vary spatially and temporarily in an indentation test. This can be compared with the simple, uniform stress state in standard creep tests. Also, standard creep tests are mainly concerned with secondary (steady-state) creep at modest loads, whereas primary creep at high stress and strain rates is more usual in DSI tests.

Keeping in view the arguments from the literature where the DSI creep constants of some materials varied significantly from uniaxial creep constants, it can be concluded that the DSI creep method is still unreliable and needs further investigation. Therefore, in this research work, bulk creep tests are preferred for calculating the creep constants at various RH environments for subsequent use in numerical models.

2.6.2.2 DSI Using the Strain Rate Method

DSI using a strain rate control method involve proportional loading followed by holding at constant load while monitoring displacement of indenter as function of time and then unloading at an appropriate rate. In case the experiments are carried out by controlling displacement than testing is usually considered to follow proportional displacement. The strain rate method can be used to calculate not only hardness and modulus but also strain rate sensitivity (Lucas and Oliver 1999). It has been shown that hardness approaches a constant value when the strain rate is held constant (Cheng and Cheng 2000). This can usually be obtained by keeping the ratio of loading rate to imposing load or displacement rate to displacement, constant (Briscoe et al. 1998). This is illustrated by the following equation.

$$\dot{\varepsilon} = k \frac{\dot{P}}{P} = k \frac{\dot{h}}{h} \quad (2.30)$$

The effects of the strain rate method on DSI results are associated with creep and it is still not clear that employing a constant strain rate method corresponds meaningfully to steady-state creep conditions (Goodall and Clyne 2006). The method has been used on some soft materials; however, it faces various challenges before making acceptance as a successful technique for time dependent materials.

2.6.2.3 Dynamic Indentation Testing

Dynamic indentation has some advantages over quasi-static testing as it offers a significantly decreased testing time for assessing a material's time dependent response (Menčík 2007). Because of the short testing time, the effects of thermal

drift on the measured mechanical properties are negligible. The method is used to determine the storage and loss moduli of the material over a range of frequencies and amplitudes.

The Continuous Stiffness Measurement (CSM) technique is the most commonly used technique for dynamic indentation. The excitation is provided through a force transducer during the loading process using a low magnitude oscillation superimposed onto the overall quasi-static force signal. The resultant phase lag is measured at the same frequency as the applied oscillating force and is related to the contact stiffness and damping.

An alternate method of dynamic indentation testing was proposed by Fischer–Cripps (2004), in which storage and loss modulus determined using a multi-frequency dynamic oscillatory motion mode of deformation. The applied load was modulated by a pseudo-random force signal comprising multiple frequencies. Fourier transforms were then used to deconvolute the response into single frequency components. This method allows for cancellation of the instrument dynamic response by equalization with a spectrum response obtained on a standard specimen of known elasticity and thus avoids the need for an expensive frequency- specific lock-in amplifier.

Singh et. al. (2005) demonstrated a new displacement modulation based technique, Continuous Contact Compliance (CCC), to determine the storage and loss moduli of an epoxy as a function of excitation frequency. The CCC technique allows the control of amplitude and frequency of excitation independently from the electromagnetic loading coil and thus makes available a wider range of amplitude and frequencies of excitation.

2.6.2.4 Re-indentation Testing

Finding the parameters for a constitutive VE model from DSI data where elastic, viscous and plastic material behavior may exist is a potential problem (Shimizu et al. 1999; Sakai et al. 2002; Zhang et al. 2005; Oyen-Tiesma 2009). In order to account for the presence of plastic deformation, a multiple indentation technique can be utilized (Zhang et al. 2005; Jäger and Lackner 2009), where the first indentation introduces plastic deformation while the subsequent indentation only exhibits VE deformation. A five step loading scheme has also been proposed that can be used to study elastic-viscoelastic and plastic deformation separately (Zhang et al. 2006). The multiple-indentation technique is helpful to isolate time-independent plastic deformation from VE/VP deformation.

2.6.2.5 Effect of Indenter Shape

Sharp indenters, such as the Berkovich indenter, have been in use for decades and cause plastic deformation almost instantly due to their sharp points. They can provide hardness and modulus values successfully (Oliver and Pharr 2004), however, due to the sharpness of the Berkovich indenter, any pre-yielding behaviour is lost. A way to avoid instant plastic deformation, and hence investigate the transition from elastic or VE to plastic or VE-P deformation, is by using a blunt indenter such as a flat or spherical indenter. Also, by using an appropriate load one can avoid plastic deformation and stay in the pure elastic or VE region (Oyen and Cook 2009). Hence, by selection of appropriate indenter geometry, desired modes of deformation can be investigated.

2.6.3 Testing under Controlled Humid Environments

The mechanical properties of polymers can vary significantly with the amount of absorbed moisture. In order to investigate the effect of absorbed moisture by DSI, we can use either a fluid cell or a humidity control unit (HCU). A fluid cell allows the testing of samples under fully immersed conditions by immersing both sample and indenter tip in a liquid bath. This technique has been used successfully with biological and polymeric samples (Ashcroft and Spinks 1996; Hengsberger et al. 2002; Akhtar et al. 2005, Bell et al. 2008). A HCU is used to control the humidity in

the DSI cabinet and can be used to perform tests from approximately 20-95% relative humidity (RH). A HCU is typically comprised of a humidifier, a dehydrating unit, a hygrometer and a control circuit. The literature review revealed that there is currently no published work where DSI testing has been carried out at varying relative humidities using a HCU.

In the current research work, HCU was used to condition Accura 60 samples by regulating the DSI chamber to 33.5 %, 53.8 %, 75.3 % and 84.5 % RH. Further details on use of the HCU and the results from the tests are described in Chapter 3 and 4 respectively.

2.6.4 Analysis of DSI Data for Polymers

The analysis of load-penetration depth plots obtained through DSI experiments is mostly based on the work of Doerner & Nix (DN) (1986), and Oliver & Pharr (OP) (1992), that was developed for elastic-plastic materials using a theoretical relationship developed by Sneddon (1965), for the contact between an elastic half space and a rigid punch. The method is questionable, however, for VE or VE-plastic materials such as polymers and biological tissues (Sneddon 1965; Oyen and Cook 2004; Zhang et al. 2006; Liu et al. 2006; Mencík, et al. 2009). The DN method calculates hardness from the loading curve and modulus from the unloading curve, assuming the unloading curve to be linear and the contact area to remain constant when the indenter is initially unloaded. The OP method assumes a power law approximation for the initial unloading. The DN method is suitable for only flat punch applications while the OP method has been successful with polymers having high T_g compared with ambient temperature. Cheng and Cheng (1998) have also described the relationship between modulus, contact area and slope of the initial part of unloading by dimensional analysis and FEA of nanoindentation data. They derived a method to estimate hardness and modulus for solids, indented with conical or pyramid indenters by taking a ratio of irreversible work to total work during indentation and relating this with the ratio of hardness and modulus. However, this method needs further improvement as deviations up to 15% have been reported in calculating mechanical properties from the method.

The next section discusses the methods whereby minimizing the time dependent effects the OP method can be used for weakly VE materials. This method is reasonable for materials that have a high value of T_g compared to ambient. Time dependent constitutive models can also be used with load, depth and time data to extract the parameters and this method is detailed in section 2.6.4.2.

2.6.4.1 Minimisation of Time Dependent Response

The DSI testing of polymers is challenging due to their time dependent response to indentation. However, by selecting optimal parameters, such as loading and unloading rate and dwell period, the VE/VP effects can be minimised, as discussed in section 2.6.1 and then the OP approach can be used to analyse the data (Oliver and Pharr 2004). In this approach the initial unloading curve is approximated by a power law, as given in Equation 2.31.

$$P = \alpha(h - h_r)^m \quad (2.31)$$

where α and m are curve fitting constants, 'h' is penetration depth and 'h_r' is the final unloading depth. The derivative of Equation 2.31 at maximum load is the contact stiffness (S) as shown in Equation 2.32.

$$S = \frac{dP}{dh}(h = h_{\max}) = m\alpha(h_{\max} - h_r)^{m-1} \quad (2.32)$$

The plastic contact depth at maximum load is then calculated from:

$$h_p = h_{\max} - \epsilon \frac{P_{\max}}{S} \quad (2.33)$$

where ϵ is a constant that depends on the geometry of the indenter, which is 0.75 for the Berkovich indenter. The projected area ‘A’ is calculated from ‘ h_p ’ and then used to find hardness ‘H’ as shown in Equation 2.34.

$$H = \frac{P_{\max}}{A} = \frac{P_{\max}}{24.5h_p^2} \quad (2.34)$$

The effective modulus can be calculated from stiffness ‘S’ using:

$$S = \beta \cdot \frac{2}{\sqrt{\pi}} E_{\text{eff}} \sqrt{A} \quad (2.35)$$

where β is a correction factor that depends on the type of indenter used and its value is 1.05 for the Berkovich indenter. We can calculate the modulus, E, of the tested material by using Equation 2.36:

$$\frac{1}{E_{\text{eff}}} = \frac{1-\nu^2}{E} + \frac{1-\nu_i^2}{E_i} \quad (2.36)$$

where subscript ‘i’ represents values for the indenter. The OP method has been found to work well for some polymers (Cheng and Cheng 1997). However, the use of this method for analyzing highly VE/VP polymers, other than in a comparative fashion, is inappropriate (Tranchida and Piccarolo 2005; Tranchida et al. 2007). These observations have been confirmed by other researchers who also suggested the inability of this method under a broad range of conditions (Lim and Chaudhri 2003).

2.6.4.2 Extraction of Time Dependent Model Parameters

Investigation rather than minimisation of time dependent response is of interest in the case of many polymers and biological tissues. Hence, instead of minimising the time dependency, constitutive equations need to be developed that can describe the time dependent behaviour shown by the polymer being tested. Various techniques have been employed to deal with the time dependent response present in polymers. However, the need for taking VE/VP behaviour into account in contact modelling faces noticeable mathematical difficulty related to the complex three-dimensional stress and strain fields.

A method has been used where the time variable in constitutive equations was replaced by a Laplace transformation with respect to time to make the problem an elastic analogue and then the solution was used with an inverse Laplace transform to obtain the desired VE solution from the elastic solution (Lee and Radok 1960). This Laplace transformation method is limited as it requires that the relation between stress and strain does not vary with time. Another method involved the use of functional equations where the elastic constant were replaced by VE operators (Radok 1956). The developed equations were used on creep and relaxation test data obtained from the micro and nanoindentation of polymeric coatings. The functional method has been found to be partially successful but it works well only for a monotonically increasing contact area (Vandamme and Ulm 2006). However, this restriction to only monotonically increasing area was finally removed by developing implicit equations (Ting 1966; Galanov 1982). Use of these implicit equations has remained a challenge due to the involvement of differentiation and repeated integration. Most recently, the problem of decrease in contact area was solved by Greenwood after some minor modifications in Ting's approach (Greenwood 2010). In another recent work, a closed form solution was derived from functional formulations of viscoelasticity to solving the problem for conical indentations (Vandamme and Ulm 2006). Thus Lee and Radock's method of functional equations is still attractive today and is considered the base for deriving formulae for the characterisation of time dependent response.

In recent years, simplified phenomenological models based on the mechanical element analogy, analytical treatments and numerical simulations have also been used with indentation data but it is still not clear that the fitting parameters are representative of bulk measurable values and have physical significance (Oyen and Cook 2009). In case of phenomenological approach, when a polymer is indented, the deformation can be VE or VE-P. VE models combine elastic and viscous elements. Their combination can be either in series, giving a Maxwell element or in parallel giving a Kelvin Voigt (KV) element. For complex cases, VE models usually combine these elements. For example a spring in series with a KV element, the SLS model, has been fitted to nanoindentation data from polymer coatings and the results matched well with the results by fitting this model to bulk test data (Strojny and Gerberich 1998).

In one case, a VE model was used on indentation data where the plastic depth was subtracted from the total penetration depth in order to keep the analysis of deformation viscoelastic (Yang et al. 2004). The plastic depth h_p was calculated using the OP method discussed in section 2.6.4.1. The authors used a Burger's fluid to model the indentation creep of selected polymers and proposed a method to find the elastic modulus from this VE model (Yang et al. 2004). The elastic modulus calculated using this method is independent of dwell and unloading parts and the results match closely with the values calculated from bulk tests (Yang et al. 2004).

In order to model the VE-P behaviour that often results from the indentation of polymers by sharp indenters, a plastic element can be added to represent the instantaneous plastic deformation, which is characterised by the yield strength. VE-P model, combining elastic, viscous and plastic elements has been applied to tooth enamel (Mencík et al. 2009).

Oyen and Cook's mechanical analogy of indentation with VE-P elements (a spring, a linear dashpot, a quadratic dashpot for elastic, viscous, and plastic responses respectively) for a one dimensional case can be considered successful when fitted to the curves of PC, PMMA, PE and PU polymers (Oyen and Cook 2009). Although the resultant fits did capture the nanoindentation load-displacement curves, the resulting fitting parameters were not consistent with those from bulk tests. Cheng and Cheng (2005) demonstrated a way to measure the modulus from the initial unloading slope, however, the measured modulus varied significantly from the bulk one (Tranchida et al. 2007).

Despite the cases where VE and VE-P elements have been fit to nanoindentation data, more work is still required to characterise the complex time dependent stress and strain fields beneath the indenter in polymeric materials. Moreover, the phenomenological constitutive model approach needs further validation under various environments and with different materials. In the present research, VE and VEP models are used analytically on indentation data to derive material parameters at various relative humidities. Further details are given in Chapter 7.

2.7 FE Modelling of DSI of Polymers

The FE modelling technique has been used to analyse nanoindentation behaviour of materials such as metals (Bhattacharya and Nix 1988; Pelletier et al. 2000), ceramics (Fischer-Cripps 1997), films and coatings (Pharr et al. 1998; Li et al. 2008; Pelegri and Huang 2008), polymers (Fang and Chang 2004; Anand and Ames 2006) and biological materials (Spilker et al. 1992; Warner et al. 2001). Most of the studies have been carried using 2D simulation approach while 3D simulations remained limited in numbers. FE studies of DSI have covered many aspects such as: understanding the deformation regimes around indenter (Mata et al. 2002), measurement of plastic properties of bulk materials (Xu and Rowcliffe 2002), comparison of spherical and Berkovich indentations (Fischer-Cripps 2001), role of friction on sharp indentation (Mata and Alcalá 2004), investigation of unloading behaviour of sharp indentation (Marx and Balke 1997), characterisation of heterogeneous materials (Shen and Guo 2001), and comparison of 2D (conical) and

3D (Berkovich) modelling to identify the effect of indenter geometry and its associated results (Swaddiwudhipong et al. 2006; Shim et al. 2007; Xu and Li 2008).

Selection of appropriate material model is important while FE modelling the indentation behaviour of polymers. The classical plasticity models that are insensitive to hydrostatic stress are inappropriate when analysing hydrostatic stress sensitive materials such as polymers. Commercial FE software packages usually have a number of in-built rate dependent models, while additional models can be implemented via user subroutines. The indentation behaviour of glassy polymers has been modelled using a subroutine in the commercial software package Abaqus (SIMULIA, Providence, RI, USA) (Swaddiwudhipong et al. 2005). However, that model demanded high computational resources and was unable to account for the relaxation behaviour during the final portion of the unloading. In another work, a generalised Kelvin-Voigt model was used to model the non-linear VE behaviour of PMMA (poly methyl methacrylate) (Anand and Ames 2006). However, the model was only able to simulate the load-displacement plots over a very narrow range of strain rates at room temperature. A 3D VE-P user defined constitutive model was also used to model mechanical response of polymers with varying success (Ovaert et al. 2003).

From the literature review, it can be concluded that limited attempts have been undertaken to date to model the indentation behaviour of polymers using the FE technique. It is known that when polymers are indented using a Berkovich indenter, the deformation is a combination of both EP and VE/VP deformation. Hence both time independent and time dependent elements of deformation should be taken into account. In this research, the commercial FEA code, MSC Marc 2007, a nonlinear FEA program, by MSC Software Corporation (Santa Ana, CA, USA) is used where the EP deformation, with hydrostatic stress dependence, is modelled using a linear Mohr-Coulomb model and is coupled to a rate dependent creep power law to model the indentation behaviour of the SL resin; Accura 60. Further details on the FE modelling of indentation in this work are given in Chapter 5.

No published data has been found on the use of FE to model the indentation behaviour of polymers under the influence of varying moisture levels. However, various studies have been used to assess environmental degradation in polymers and adhesive joints (Liljedahl et al. 2005; Crocombe et al. 2006; Ashcroft et al. 2011). These studies carried coupled hygro-mechanical analysis in FEA codes to determine the effects of moisture on strength while moisture diffusion inside the material was determined from transient FE analysis.

In this work, in order to generate simulated load-depth plots of indentation under various RH, coupled stress-diffusion finite element analyses were performed. In MSC Marc 2007, there is no direct option for moisture transport analysis, however, moisture diffusion can be analysed by adapting the mathematical equations of heat conduction, derived by Fourier, as described by Crank (1979). Therefore, heat transfer analyses in conjunction with stress analyses were used to carry out coupled analyses. Further details on the hygro-mechanical indentation analyses are provided in Chapter 5 while FE results and comparison with experimental data are presented in Chapter 6.

2.8 Summary and Conclusions

The deformation behaviour of polymers is highly time dependent in nature and their deformation mechanisms are totally different from metals and ceramics. Yield criterion based on pressure insensitive behaviour are not appropriate and hence material models describing hydrostatic stress sensitivity should be selected to describe the behaviour of polymers.

The mechanical properties of polymers are significantly affected by environmental factors, such as moisture, elevated temperature and UV radiation. Moisture is considered to be one of the main factors that can lead to reversible and irreversible effects in polymeric materials.

The DSI technique faces various challenges when applied to polymers owing to their complex structure and nature of deformation. Mostly, two approaches have been employed in the characterization of polymers by DSI. The first is to select test parameters to minimize VE/VP effects in order to obtain time independent results. This is appropriate for polymers showing only weak time dependent behaviour and the mechanical properties extracted using DSI should be related to the experimental parameters such as load, loading/unloading rate, dwell etc. as their variation will affect the results. The second approach is to use DSI results to determine the parameters for a time dependent material model. However, this is complicated by the complex stress state beneath the indenter. The selection of indenters is important e.g. sharp indenters can provide a VE-P response while blunt indenter can be used to investigate a VE response. DN and OP methods for data analysis have been successful for EP materials but are not satisfactory for most polymeric applications. Hence, VE/VP constitutive models need to be incorporated into data analysis.

The DSI technique can be used to investigate environmental effects on polymers such as elevated temperatures and varying relative humidities. Additionally, the method has been successful in extracting spatially varying properties and describing near surface behaviour. However, the properties measured from nano tests vary in most cases when compared with results taken from bulk mechanical tests. Hence more work is required to develop means for extracting general material behaviour from DSI tests.

In the last 25 years, the DSI testing technique has made remarkable progress. The technique has been used successfully in material research on a range of materials, such as metals, ceramics, polymers, bones and tissues and thin coatings. However, no one has worked on investigation of varying moisture effects on polymers using DSI. In real applications, polymers are likely to be exposed to changing humidity conditions where moisture will vary according to the ambient and operational conditions. These variable conditions make relative humidity an important factor that needs to be incorporated in the material research and designing phase of the components. Additionally, a mechanism of incorporating suitable moisture uptake

and indentation models is required to describe the indentation behaviour of polymers under varying moisture conditions. In order to address, the present study involves DSI testing at various relative humidities to understand the effects of moisture on mechanical properties of SL resins at micron scale. Coupled diffusion-stress FE modelling is then used to predict the moisture diffusion and indentation behaviour of SL resin Accura 60 under variable moisture conditions.

|Experimental Methods

3.1 Introduction

This chapter describes the methods, equipment and procedures used in the experimental phase of this research. The first section describes the material and the process used to manufacture the samples. There follows a description of the conditioning method. The experimental programme consists of two types of experiments. The first stage consisted of moisture diffusion and bulk mechanical experiments. Moisture diffusion analysis involved gravimetric testing, where the absorbed moisture content as a function of time at various RH was calculated and used to characterise the type of diffusion and determine the diffusion constants. Bulk mechanical experiments consisted of tensile tests, compressive tests and creep tensile tests. The material properties extracted from the diffusion and mechanical experiments were later used in numerical modelling of depth sensing indentation (DSI) at various relative humidities. The second stage of experiments involved DSI testing. These experiments were carried using various experimental parameters to investigate the rate dependent behaviour. Tests were undertaken at various RH environments to investigate the effect of moisture on the near-surface mechanical properties. These tests provided an insight into the spatial variation in properties of Accura 60 at various RH.

3.2 Material and Sample Manufacture

3.2.1 Material

The polymeric material investigated in this study was an epoxy based resin, Accura 60, manufactured by 3D Systems (Rock Hill, SC, USA). Accura 60 was chosen because it was in the latest range of stereolithography (SL) resins at the

commencement of the research. It is stiff, durable and transparent with a low viscosity formulation. Some of its applications include:

- Prototypes
- Consumer electronics e.g. mobile phones
- Automotive design components
- Medical instruments and devices
- Transparent models

Also, due to its transparency, Accura 60 is used in lenses by the automobile industry and for fluid flow visualisation models in various applications. Typical properties of Accura 60 provided by the manufacturer are given in **Table 3-1**.

Property	Value
Elastic modulus (E)	2690 to 3100 MPa
Poisson's ratio (ν)	0.35 to 0.40
Ultimate tensile strength (σ_{ult})	58 to 68 MPa
Glass transition temperature (T_g)	58°C
Elongation at break (%)	5 to 13 %
Appearance	Clear

Table 3-1: Typical properties of the SL resin, Accura 60.

According to the material manufacturer, above mentioned characteristics make Accura 60 a good choice for the development of prototypes for concept design and marketing purposes as well as for some applications as an end-use product. Manufacturer also claims that material has ability to resist humidity and maintain dimensional accuracy that makes it a good choice for patterns for investment casting.

3.2.2 Stereolithography Process

SL is one of the main processes of additive manufacturing (AM) and is considered highly accurate and consistent (Hague et al. 2003). Like other AM techniques, the SL process produces objects directly from 3D CAD models without requiring tools. This helps in reducing total production time. The applications of the process include the development of models, medical products, visualisation models etc.

The SL process consists of a combination of a CAD system with a SL machine to perform the layer-by-layer fabrication of the part under the control of computer. Figure 3.1 shows a schematic of the SL process. Firstly, a 3D CAD model is converted in an STL file format. These files are then converted into 2D cross-sections in rapid prototyping (RP) software. After assignment of a layer thickness, typically between 0.1 to 0.25 mm, cross-sections are created. When a layer has been formed, the platform lowers the part so that the next layer can similarly be formed. The coating blade, moves across the surfaces to recoat the next layer of the resin. This process continues until the whole part is completed. Finally, the platform is raised and the part is removed for post processing treatments.

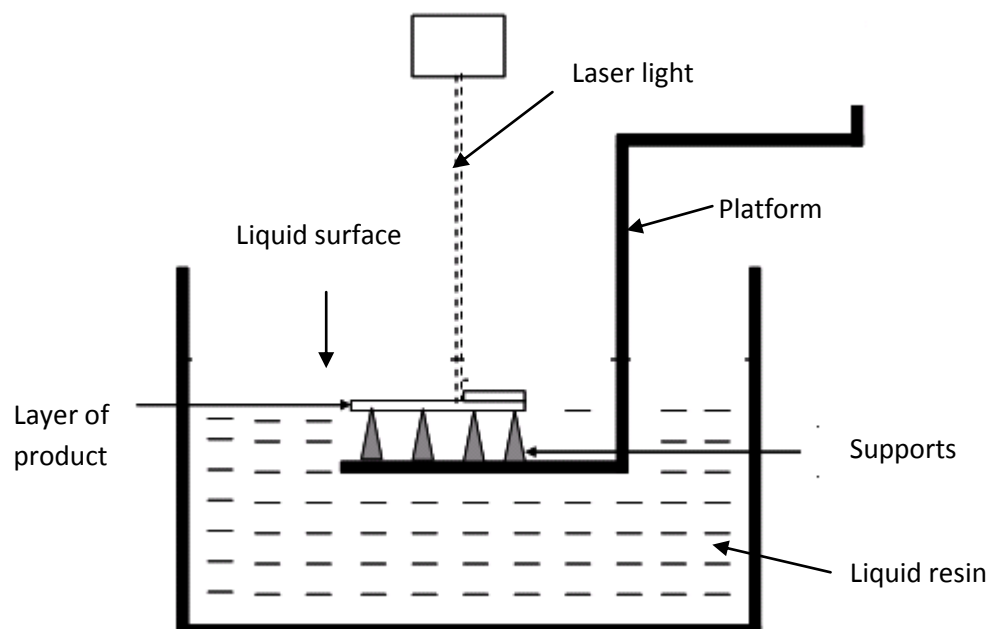


Figure 3.1. Schematic of SL process.

The polymer investigated in this study was an epoxy based resin, Accura 60, manufactured by 3D Systems (Rock Hill, SC, USA). The samples were manufactured in ‘YZ’ orientation as shown in Figure 3.2, using an SLA7000 SL machine, also manufactured by 3D Systems. The maximum build envelope of the machine is 508 x 508 x 584 mm. Supports, used to stabilize the part during building, were generated using the computer software MAGICS (Materialise, Belgium). The parts were built in a vat of resin at a temperature between 20-24 °C, which cured on exposure to UV laser radiation. After completion of the manufacturing process, the finished samples were removed for post-processing treatments.

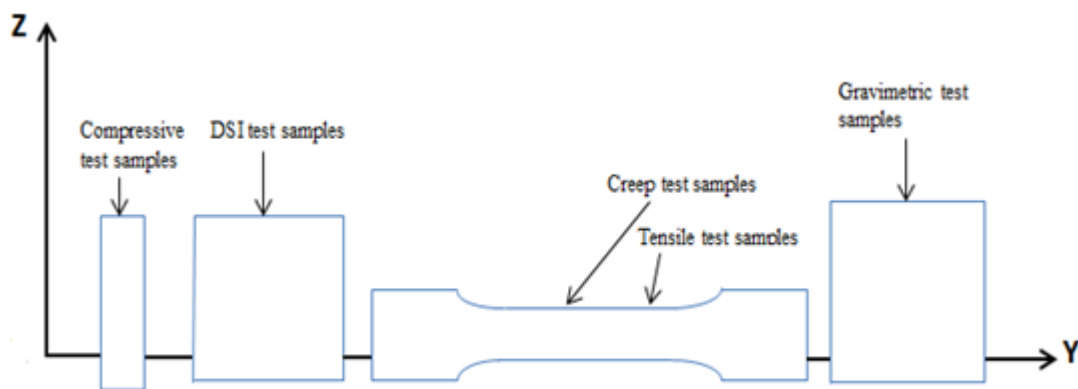


Figure 3.2: Build orientation of samples for various types of tests.

Post-processing involved cleaning and post-curing the manufactured parts. Cleaning is important as it helps to remove excess resin from the parts. The samples were washed in Tri-Propylene Glycol Monomethyl Ether (TPM). TPM is usually the preferred cleaning solvent as it has low volatility and little odour (Ullett et al. 2000). After cleaning, SL parts are usually post-cured either by a thermal or UV post-curing technique. This treatment helps to improve the mechanical properties of SL materials (Ullett et al. 2000), e.g. it increases the strength and stiffness but may also reduce ductility and the elongation at failure. The decision to select a thermal or UV treatment is dependent upon the type of material. Thermal curing can lead to ageing in some materials and thus UV treatment is usually preferred in most cases (Vora et al. 2007). In this study, the Accura 60 samples were UV post-cured, both large sides for 45 minutes each.

After the above mentioned post manufacturing treatments, the samples were stored in darkness in a desiccator. As recommended by 3D Systems, the samples were kept for 8 weeks prior to any testing in order to provide further curing and stability. Afterwards, all types of testing were completed between 8 to 40 weeks. The next sections describe the moisture conditioning, moisture diffusion tests, bulk mechanical and DSI testing methods used in this research work.

3.3 Environmental Conditioning

In this research work, the effect of moisture on the mechanical performance of a SL resin was investigated. Most polymeric components face varying humidity environments during their life ranging typically from 30 to 80 % RH. Therefore, the selected conditioning environments in this study were 33.5 %, 53.8 %, 75.3 % and 84.5 % RH. As moisture absorption can be accelerated by an increase in temperature, the temperature was kept constant at 22.5 °C with ± 1 °C variation for both conditioning and testing.

Samples for gravimetric and bulk mechanical testing were preconditioned inside glass flasks using saturated salt solutions. These salts were; magnesium chloride, magnesium nitrate, sodium chloride and potassium chloride to provide relative humidities of 33.5 %, 53.8 %, 75.3 % and 84.5 % RH respectively, with ± 1 variation. The samples for DSI tests were conditioned by two methods. In the first method, samples were pre-conditioned at 33.5 %, 53.8 %, 75.3 % and 84.5 % RH using saturated salt solutions as described above. In the second method, samples were conditioned at 33.5 %, 53.8 %, 75.3 %, 84.5 % RH by regulating humidity in the DSI system using the HCU. Further details on conditioning and periodic testing after moisture absorption at various RH are described in sections 3.4, 3.5 and 3.6.

3.4 Moisture Diffusion Tests

The moisture diffusion properties of the Accura 60 were determined by a gravimetric testing method. The procedures and guidelines for gravimetric moisture uptake

measurements of bulk samples in British Standard BS EN ISO 62 (2008), were followed. The samples were manufactured with dimensions of 60x60 mm with 4 mm thickness as shown in Figure 3.3. Samples were taken out from the desiccator after 8 weeks of manufacturing and dried by placing in an oven at 35 °C in an oven until a constant weight was recorded. It took approximately 4 days in an oven to dry all the samples. A digital scale (Mettler Toledo Incorporation, Columbus, OH, USA), with an accuracy of 0.1 mg was used to weigh the samples.

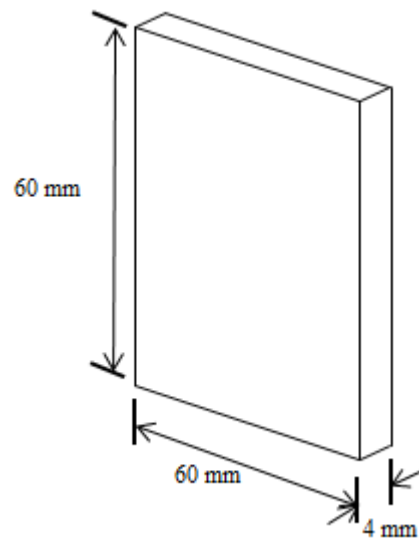


Figure 3.3: Geometry details of gravimetric test samples (not on scale).

Once dried, the samples were conditioned in glass containers at various RH environments at a constant temperature (22.5 °C, ± 1 °C). Five samples were used to obtain an average value for each environment. Specimens were extracted at 4, 8, 12, 20, 32, 44, 68 and 92 hrs and then at time intervals of 24 hrs. On extraction of conditioned samples, surface moisture was removed with a clean, dry cloth, and each sample was weighed to the nearest 0.1 mg. This was completed within 1 minute of removal from the conditioning environment. The conditioning process was continued for 720 hours. The moisture uptake at time, 't' denoted by M_t , was calculated using the following equation:

$$M_t = M_2 - M_1 \quad (3.1)$$

where M_1 is the mass of the specimen after drying but before conditioning and M_2 is the mass of the specimen at a specified time interval during conditioning. The moisture uptake data was used to find the diffusion constants, as detailed in section 4.2.

3.5 Bulk Mechanical Characterisation

In order to characterise the bulk material behaviour, bulk mechanical tests were performed. These tests included uniaxial tensile and compressive tests. Stress-strain relations, yield stress and modulus values extracted from these experiments were used in defining the elastic-plastic material model for FEA. Additionally, creep tests were also carried out to extract rate dependent material constants for use in the FE model. The details of these experiments are provided in sections 3.5.1, 3.5.2 and 3.5.3 respectively.

3.5.1 Tensile Test

The ability of a material to resist breaking under tensile stress is a widely measured property that is used in various structural applications. In a tensile test, the specimen is extended along its longitudinal axis at a constant speed until the specimen ruptures. During testing, the load sustained by the specimen and the elongation are measured. Additional measurements include tensile strength (at yield and at break), elastic modulus, stress, strain, elongation etc. ASTM D638 (2008) is a standardized method for tensile testing of polymers, which is technically equivalent to BS EN ISO 527 (2009). In the current work specimen preparation and testing methods were according to ASTM D638 (2008). The samples were manufactured as per the dimensions shown in the Figure 3.4. The specimens were built in an ‘YZ’ orientation using the SL machine, as described in section 3.2.2. Samples were preconditioned using the techniques described in section 3.3.

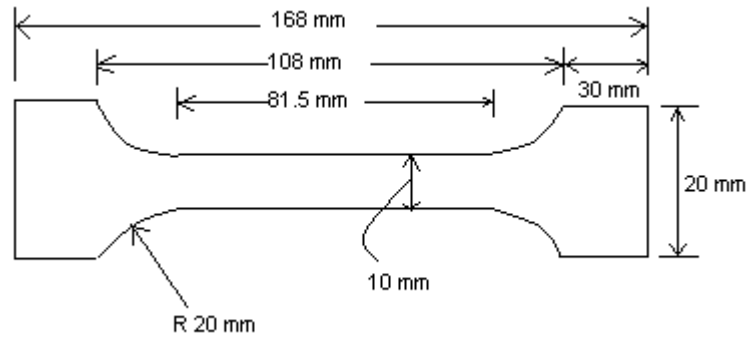


Figure 3.4. Schematic showing dimensions of tensile test specimen.

The tests were carried out at 0.1 mm/min at 22.5 °C (± 1 °C variation) and 35 % RH (± 2 variation). In order to investigate moisture effects, samples were preconditioned at 33.5 %, 53.8 %, 75.3 % and 84.5 % RH. Specimens were extracted at 4, 8, 12, 20, 32, 44, 68 and 92 hrs and then at time intervals of 24 hrs prior to testing. Tests were carried out on samples that were conditioned up to 720 hours. Tensile testing was started after 16 weeks of samples manufacturing and completed in the next 30 days using a universal testing machine (Instron 3366, Instron Corporation, Norwood, MA, USA) with a maximum load capacity of 10 kN. Five repeat tests were performed to obtain an average value. Results from the tensile tests are described in Chapter 4.

3.5.2 Compressive Tests

The compression test is used to characterize the mechanical behaviour of material under a compressive load. In this test, the specimen is compressed along its longitudinal axis at a constant rate until the specimen fractures. Both the load and displacement are measured during the procedure. The test is used to determine properties such as stress-strain relation, elastic modulus, yield point and yield strength. ASTM D695 (2008) and BS EN ISO 604 (2002) are the two available standards for compressive testing of polymers. In the current work, testing was carried out according to the ASTM D695 (2008) standard as per the geometry shown in Figure 3.5. The samples were built in an ‘YZ’ orientation using the SL machine.

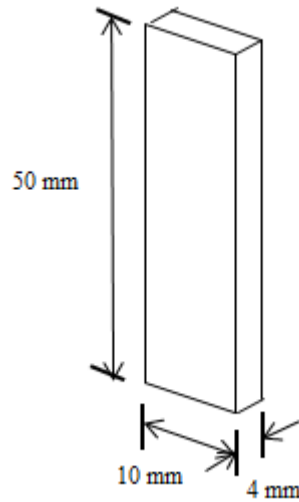


Figure 3.5: Geometry details of compression test samples.

Samples were preconditioned using the techniques described in section 3.2.2. The tests were carried out at 0.1 mm/min at 22.5°C (± 1 °C variation) and 35 % RH (± 2 variation) with samples preconditioned at 33.5 %, 53.8 %, 75.3 % and 84.5 % RH. Specimens were extracted at 4, 8, 12, 20, 32, 44, 68 and 92 hrs and then at time intervals of 24 hrs up to 720 hours. Compression testing was started after 23 weeks of samples manufacturing and completed in the next 30 days using the Instron 3366 universal testing machine described previously. Five repeat tests were performed to obtain an average value. Results from the tests are described in Chapter 4.

3.5.3 Creep Tests

Creep tests can be used to investigate the viscoelastic (VE) and viscoplastic (VP) behaviour of materials using different modes of loading such as tensile, compressive, flexural and torsional. In this research, creep tensile tests were carried on the SL resin in order to determine material parameters for subsequent use in the FE model to introduce rate dependent effects.

A standard creep tensile test consists of measuring extension as a function of time under a constant tensile load at a specific environmental condition. ASTM D2990 (2009) and BS EN ISO 899 (2003) are the standards for tensile creep measurements.

In the present work testing was according to ASTM D2990 (2009) as per the geometry details shown in Figure 3.4. Tests were performed at 22.5 °C (± 1 °C variation) and 35 % RH (± 2 variation) on samples that were preconditioned at 33.5 %, 53.8 %, 75.3 % and 84.5 % RH. These tests were carried out on samples conditioned for up to 720 hours. Specimens were extracted at 4, 8, 12, 24 hrs and then time intervals of 24 hrs. Creep testing was started after 30 weeks of samples manufacturing and completed in the next 30 days using the Instron 3366 universal testing machine. The tests started with instantaneous loading followed by a constant load for 2500 sec. Testing was at five different stress levels; 26 MPa, 32 MPa, 38 MPa, 44 MPa and 50 MPa. Data from these experiments was analysed using a creep power law relationship, as given by equation 2.27. Results from the tests are described in Chapter 4.

3.6 Depth Sensing Indentation

In order to investigate VE, VP and moisture effects on a micron scale in the SL resin, the DSI testing technique was used. The samples for DSI testing were 50x50 mm with 4mm thickness (Figure 3.6) and were built in an ‘YZ’ orientation using the SL machine. Total testing time for DSI tests was between 12 to 40 weeks after manufacturing of samples.

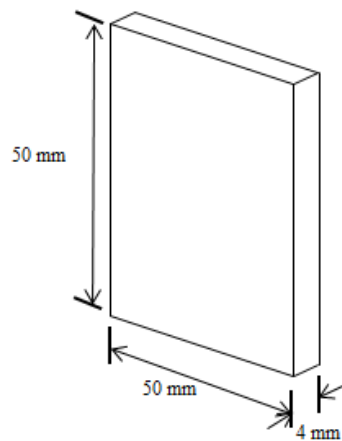


Figure 3.6: Geometric details of DSI test samples.

A Berkovich indenter with face angle of 65.3°, giving the same projected area to depth ratio as the Vickers indenter, was used to produce indents. The NanoTest 600,

manufactured by Micro Materials (Wrexham, UK), was used for the DSI experiments. Figure 3.7 shows a schematic aerial view of the NanoTest 600 showing the high resolution microscopes, the sample stage that can move in x, y and z (perpendicular) directions and the nano head unit.

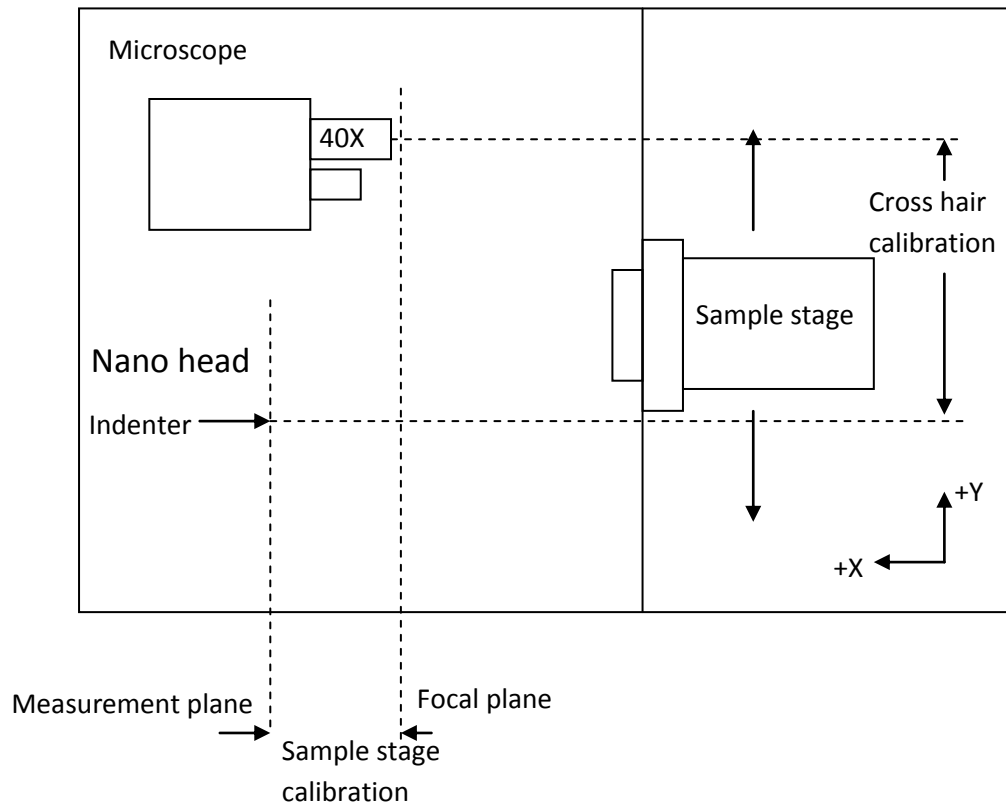


Figure 3.7. Schematic of NanoTest 600 system.

Figure 3.8 shows schematic of the nano head unit that consists of a pendulum with an indenter having a load range of 0.1-500 mN and resolution of 0.1 μ N. The pendulum can rotate on a friction-less pivot and is designed to be lightweight. The solid shaft of the pendulum is made of a ceramic stiff enough to withstand the maximum load with negligible deflection. The pivot is comprised of four stainless steel leaf springs,

which are very compliant in rotation, but can be easily damaged if care is not taken when handling the pendulum e.g. during the change of an indenter.

A coil is mounted at the top of the pendulum and when the coil current is applied, the coil is attracted towards a permanent magnet, producing motion of the indenter towards the sample and into the sample surface. The parallel plate capacitor measures the displacement of the indenter as one of the plates is attached to the indenter holder. Thus, when load is applied and as the indenter is displaced into the sample, the capacitance changes and the displacement is measured by means of a capacitance bridge. To minimize or reduce unwanted capacitance effects, the capacitance bridge unit is located close to the measuring capacitor. The two circular discs are 0.3 to 0.5 mm apart when the system is at full sensitivity. The maximum measurement depth of the system is approximately 15-20 μm . Below the capacitance plates, there is a counter-balance weight necessary to counter the mass of the coil and the indenter that is inserted into the diamond holder.

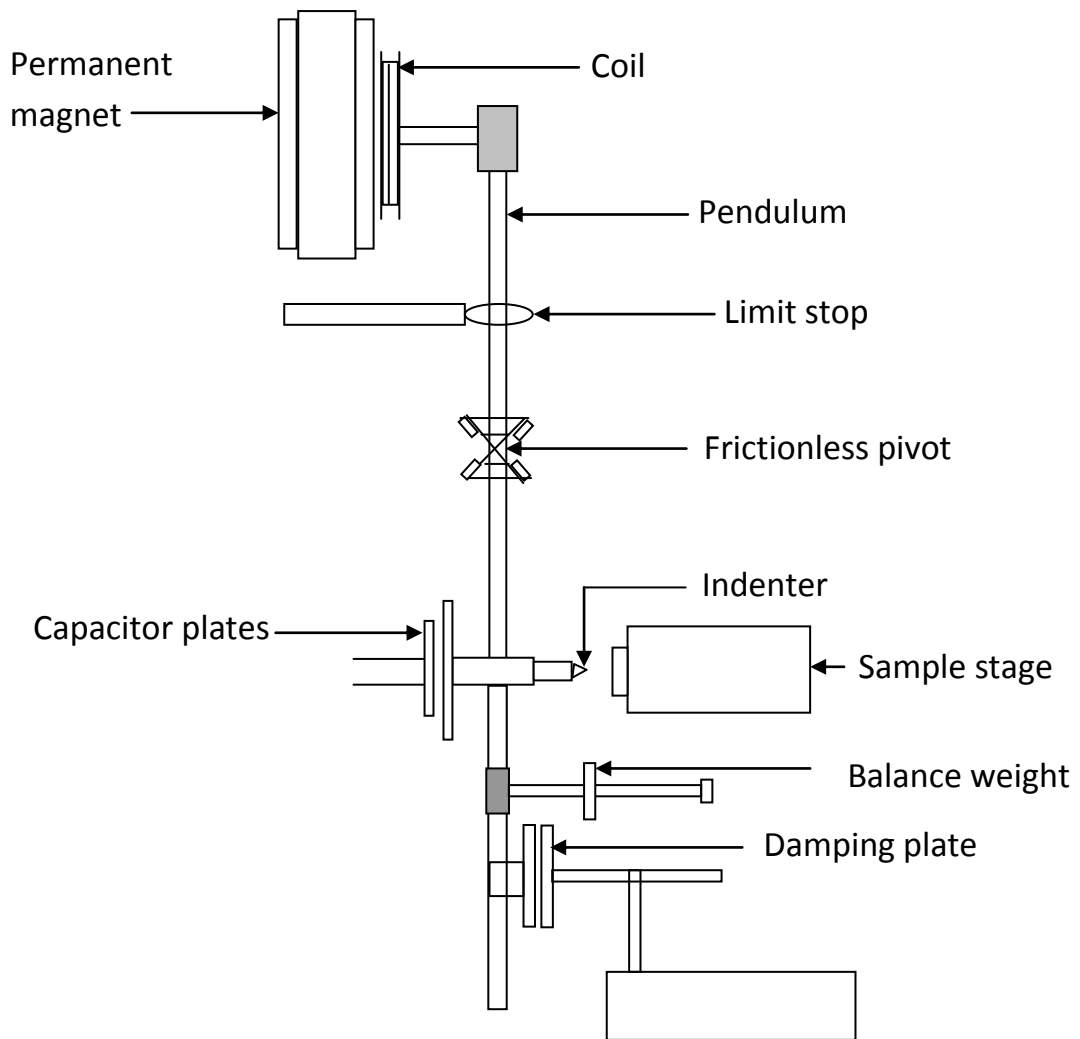


Figure 3.8. Schematic of nano head unit.

In order to operate the DSI system smoothly and obtain results free of errors, certain considerations are required. These are discussed in section 3.6.1.

3.6.1 Important Considerations When Using the DSI System

3.6.1.1 Safety Precautions during Operation

When carrying out DSI tests or calibrations, there are certain measures that are required to keep the equipment safe. Following are the common safety measures that were taken during machine operation:

- a. Before moving the sample stage from the front of the nano head to the focal plane for focussing, the sample stage was moved sufficiently in the positive X-direction so that the sample stage did not collide with the microscopes.

- b. During sample stage calibration and just before contact between the indenter and specimen (at around 2 mm distance apart), the rate of movement of the sample stage in the negative X-direction was reduced to a safe contact speed of 3.8 $\mu\text{m}/\text{sec}$. Otherwise, contact with the sample could damage the indenter tip or the pendulum.

- c. It was ensured that the sample stage was in the focal plane and in-front of the nano head before performing any experiments as it could damage the pendulum or microscopes if the sample stage was in the sample plane in front of the nano head or focal plane but in front of microscope.

- d. Whenever the indenter was changed, care was taken in order to keep indenter tip, pendulum and four stainless steel leaf springs inside the pivot of the pendulum safe.

3.6.1.2 Calibrations and Maintenance Checks

Errors in measurements can arise due to improper calibrations. These errors can produce incorrect results. These calibration and maintenance checks include; load and depth calibration, frame compliance, diamond area function determination, cross-hair calibration, bridge box adjustment, pendulum test, sample stage calibration and noise level tests. These were performed periodically as per the instructions in the user manual of the machine. The periodic calibration and maintenance checks are provided in Table 3.2.

Calibrations/Checks	Frequency
Bridge box calibration and Pendulum test	Each time when started
Zero load calibration	Between 1 to 3 for each measurement
Cross-hair calibration	Every 2 months
Load calibration	Every 3 months
Depth calibration	Every week or when indenter changed
Frame compliance	Every 3 months or when stage components dismantled
Diamond area function	Every 3 months or if indenter renewed
Noise level/signal display	As required

Table 3-2: Frequency of calibration and maintenance checks.

3.6.1.3 Miscellaneous Factors Influencing Errors

In addition to the calibrations and maintenance checks, there are additional influencing factors that can lead to misleading results. These factors are discussed below.

(a) Thermal drift

Thermal drift results from changes in the dimensions of the instrument due to thermal expansion or contraction of the apparatus. Thermal drift becomes important for small indentations made over long periods of time at varying temperatures and this effect appears in the data as an apparent displacement of the specimen. For example when an indenter tip is brought into contact with a specimen at a different temperature, a thermal drift effect can occur. If there is a slow decrease in temperature of the specimen, the measured depth will gradually increase causing a decrease in the contact hardness. The contact elastic modulus will also decrease due to an increase in depth if the temperature falls during the loading period, only however, if temperature decreases during the unloading part as well, the withdrawal

of the indenter will be slower resulting in a higher contact modulus (Mencik and Swain 1995).

Thermal stability is important when performing nanoindentation tests on polymers as variations can affect the extracted properties. In this study, although the temperature inside the room and cabinet were controlled and experiments were performed at constant temperature, there was still the possibility of thermal drift as the experiments were performed for long periods of dwell time. Therefore, the DSI machine was tested for thermal drift. Experiments were carried out with a 20 mN maximum load and 0.5 mN/sec loading and unloading rates by making multiple (three) indentations to 20 mN load and unloading to 2 mN followed by loading to 20 mN and holding for 300 sec and then to 90 % unloading and holding for 90 sec to investigate thermal drift. The average value of drift rate for all experiments remained insignificant. Also, for Nano Test 600, thermal drift was only available to be calculated at 90 % unloading and not during loading and dwell periods and as the material under investigation was polymer that shows creep under loading and remarkable recovery during unloading so factor of thermal drift effect was ignored for all the subsequent experiments.

(b) Surface Roughness

The current SL polymers are limited in surface roughness by the layer thickness and type of resin used. Other factors such as laser profile, laser overcure depth, and build profile, also affect the surface roughness. It is widely acknowledged that the smoothest surface finish is on the top layer while side surface is affected by the layer steps and the bottom surface by the supports. Typical values of roughness, R_a , range between 0.325 to 1.83 μm for top side, 2.68 to 4.25 μm for bottom side and 2.25 to 8.5 μm for the side surface, however, these values are just a guideline as they may vary with layer thickness, type of resin and build parameters. Post-manufacture processing techniques such as sanding and polishing are widely used to reduce the surface roughness effects in the SL manufactured parts.

This roughness of the surfaces can cause errors in determining the area of contact between the indenter and the specimen. This effect becomes more pronounced for small loads and shallow depths where the effective contact area will be smaller. Attempts to reduce surface roughness effects include the use of an imaging technique such as AFM to characterise surface roughness by measuring asperity height and its spatial distribution across the surface and then to introduce a correction in depth (Lai and Bakker 1995). The surfaces can be polished to reduce the surface roughness effects. However, caution should be taken with polishing as it can modify the surface properties. In this research, polishing technique was not considered as it could affect the moisture diffusion ability of the material leading to influence the results of effect of moisture on mechanical properties of specimen near the surface at various moisture levels. The selected testing parameters for DSI tests in this research gave approximately 4.3 μm maximum depth at 33.5 % RH that increased to 10.8 μm at 84.5 % RH at 20 mN maximum load. The DSI tests were performed on the side surface that could lead to surface roughness effects on the calculation of properties, however, measurements from the tests showed repeatability in the results and thus the factor of surface roughness was not considered in this research work.

(c) Initial Penetration Depth

The indentation experiment starts with the indenter making initial contact with the specimen surface. This initial contact is vital because the contact point determines the datum for the displacement measurement. Although, initial contact is made using the smallest obtainable force (P_i) of the instrument, there is always some small amount of indenter penetration (h_i). Hence, this initial penetration depth should be added, especially for low load indentations, to all subsequent depth readings, i.e.

$$h' = h + h_i \quad (3.2)$$

where 'h' is the recorded depth, h_i the initial penetration depth and 'h'' is the corrected value of the penetration depth. For a moderately hard and stiff material and

for maximum loads over 10mN, the initial penetration correction will make only a few percent differences to the measured indentation hardness and modulus and thus can be neglected (Fischer-Cripps 2006).

In the present work, P_i was kept constant at 0.05 mN for all experiments which corresponded to negligible values of h_i . Since this value of h_i was insignificant (3 to 5 nm) compared to the measured contact depth (4.3 μm), the effect of initial penetration depth could be safely ignored.

(d) Effect of the Shape of the Impression

When contact involves plastic deformation, the material may either sink in, or pile up around the indenter, leading to a decrease or increase in the actual area, respectively. This effect of shape of impression can cause a significant effect on the calculated values of contact modulus and contact hardness. In most studies, this effect has been studied using a microscope or profilometer (Mencik and Swain 1995). However, methods of analysing of pile-up/sink-in behaviour that do not require physical measurement of the contact area have also been investigated (Cheng and Cheng 1998; Taljat et al. 1998; Cheng and Cheng 2000).

To date the OP method remains the most popular procedure for analysing indentation data. However, this method does not account for pile up. Hence, the imaging technique is a popular method to determine the pile up, which can then be used to modify the hardness and modulus values. In a recent study of the SL resin; SL7580 (Vora et al. 2007), it was found that for loads of 50 mN and less, with the Berkovich indenter, the piling-up effect was insignificant. In this study, AFM was used to measure the pile area and the subsequently corrected contact area was used to calculate values of indentation hardness and modulus. However, these corrections changed hardness by 2.79 % and modulus by 2.47 % only when compared to these values calculated using the OP method. Since, the current investigated material; Accura 60, is quite similar to SL 7580 the piling-up factor was not taken into account in the data analysis.

3.6.2 DSI Tests

3.6.2.1 Investigation of VE/VP Behaviour

When performing a standard load-unload test on polymers, a common source of error in analyzing the test results is the assumption that unloading can be considered as elastic. The time dependent deformation of polymers can lead to errors in conventional calculations of hardness and modulus from the initial part of unloading in load-depth curve. Hence, a series of experiments were performed on Accura 60 to investigate the VE/VP behaviour and to minimise the time dependency during the initial part of unloading in order to use the OP method for data analysis. These experiments were performed on dry samples taken from desiccator using different combinations of loading rates, unloading rates, dwell periods at 20 mN maximum loads. Each parameter was varied in turn while keeping the others constant. These experiments were carried out with the chamber controlled at 22.5 °C and 33.5 % RH. Five indentations, at 150 µm spacing, were performed to obtain average values for hardness and modulus using the OP method discussed in section 2.6.4.1. Results from these experiments are shown in Chapter 4.

3.6.2.2 Investigation of the Effects of Relative Humidity

In order to investigate the effects of various relative humidities on the mechanical properties of Accura 60 samples, and their comparison with tests at ambient, the same experimental parameters were used that were reduced creep effects during the study of VE/VP effects as discussed earlier in section 3.6.2.1. Prior to use of the HCU for testing the Accura 60 samples, it was necessary first to check the correct functioning of the DSI system under the range of humidity under investigation. This was done by carrying out DSI tests on fused silica samples at 33.5 % RH and 84.5 % RH at 1 mN, 20 mN and 50 mN loads. The results showed that the measured mechanical properties were not significantly altered (maximum change less than 3.5 %) on exposure to a humid environment, confirming that data are not significantly affected by the use of HCU.

Tests were carried on two types of conditioned samples as discussed below.

(a) Preconditioned Samples

Samples stored at 33.5 %, 53.8 %, 75.3 % and 84.5 % RH in flasks, were tested at 33.5 % RH inside the chamber every 24 hours for five days. To maintain uniformity in the experiments, each sample was tested within half an hour of removal from the flask. Five indentations, at 150 μm spacing, were performed to obtain average values for hardness and modulus using the OP method. These tests were carried out at 0.5 mN/sec loading and unloading rates with 300 sec dwell at 20 mN maximum load. Results from these experiments are shown in Chapter 4.

(b) Samples Conditioned by the HCU

The conditioning of samples inside the DSI chamber can be carried out by regulating the RH to any value between 20 and 95 % RH using the HCU. Figure 3.5 shows the various elements of the HCU unit. The HCU consists of an ultrasonic humidifier, a dehydration unit and a control box with humidity sensors. The control box has two humidity indicators mounted on it. Auxiliary components like probes and fans are connected to it through electrical cables. Required values for RH can be set through it. The ultrasonic humidifier consists of a humidifier and circulating fan. When the RH in the chamber falls below the set value, a relay is activated that switches on the humidifier and circulating fan and brings back the RH to the desired level inside the chamber. Once this level is reached, the fan and humidifier turn off automatically. The dehydration unit consists of a polycarbonate box containing several layers of desiccant and a circulating fan. When the RH in the chamber goes above the desired level, the humidity control unit activates the fan, thus circulating moist air over the desiccant. The dried air is then returned to the machine cabinet.

In this research, the HCU was used for conditioning of samples and maintaining the desired RH while testing. Dry samples, stored in a desiccator, were conditioned for five days in the DSI chamber at 33.5 %, 53.8 %, 75.3 %, and 84.5 % RH and tested

every 24 hours. For comparison with the samples preconditioned in flasks, the testing parameters were kept the same. Five indentations, at 150 μm spacing, were performed to obtain the average values for hardness and modulus using the OP method. Results from these experiments are shown in Chapter 4.



(a) Humidifier



(b) Dehydration unit



(c) Nozzle that introduces moisture inside the chamber

Figure 3.9. Pictures of humidity control unit parts.

3.6.2.3 Effect of Drying on the Properties of Conditioned Samples

In polymers, moisture absorption can lead to a wide range of effects, both reversible and irreversible. In order to check the reversibility of the effects of moisture on the mechanical properties of Accura 60, samples conditioned at 84.5 % RH for five days were kept at 33.5 % RH inside the DSI chamber for ten days and tested periodically to investigate any recovery in the mechanical properties. The five indentations, at 150 μm spacing, were performed to obtain the average values for hardness and modulus using the OP method. Results from these experiments are shown in Chapter 4.

3.7 Summary

Moisture diffusion and mechanical properties of SL resin Accura 60 have been experimentally determined. The behaviour was studied at 33.5 %, 53.8 %, 75.3 % and 84.5 % RH. A fixed temperature of 22.5 °C was used for all the experiments. Two sets of experiments were performed. Bulk tests were carried to obtain material constants for subsequent numerical modelling while DSI tests were carried out to investigate the micron scale mechanical properties.

Gravimetric experiments were carried out to find moisture diffusion behaviour. Samples were conditioned in glass flasks using saturated salt solutions. Bulk mechanical properties were also carried out at same environments by performing tensile, compressive and creep tensile tests. Results from these bulk tests were used to define material model parameters for FE analysis of indentation behaviour.

The main advantage of DSI over standard mechanical testing methods is that only a small amount of material is required and, hence, properties can be spatially resolved. In order to correctly operate the DSI system, necessary maintenance and calibration

checks are required. Additionally, there are other influencing factors, such as thermal drift, surface roughness, shape of indent, that can lead to misleading results and need appropriate attention. In the current research, the DSI technique was used to investigate the rate dependent indentation behaviour of a SL resin at the micron scale. The technique was also employed to understand the effects of the level of moisture in the environment on the mechanical properties of a polymer. Samples for DSI tests were conditioned using two methods. One set of samples was preconditioned in flasks using saturated salt solutions and tested periodically at ambient environment while the other set of samples was conditioned in the DSI chamber using the HCU and tested periodically under a HCU controlled environment. Finally, in order to investigate the recovery of properties, preconditioned samples were stored at 33.5 % RH for 10 days and periodically tested. Results from these experiments are shown in Chapter 4, while the use of the material parameters extracted from the bulk tests for FE modelling is discussed in Chapter 5.

|Experimental Results

4.1 Introduction

Results from the experiments described in Chapter 3 are presented in this chapter. The experiments consisted of two types; bulk testing and depth sensing indentation (DSI) testing. Bulk testing consisted of moisture diffusion tests and mechanical characterisation tests. The results of the moisture uptake experiments are given in section 4.2, together with the analytical models used to characterise the diffusion of moisture in the stereolithography (SL) resin. The selected analytical model was incorporated into a finite element (FE) model for moisture prediction. Moisture dependent mechanical characterisation was carried out in order to determine the effect of moisture on the mechanical properties. These tests included uniaxial tensile, compressive and creep tensile tests and their results are given in section 4.3. Results from these bulk mechanical tests are used in defining the moisture dependent material model used in the FE analysis. The second type of testing involved DSI to investigate the viscoelastic (VE) and viscoplastic (VP) deformation of the resin at a micron scale. Experiments were carried out at various relative humidities in order to understand the effects of moisture on the near surface mechanical properties. The results are presented in section 4.4. Finally, results showing the effects of drying the moisture saturated samples and the subsequent recovery in the mechanical properties are presented.

4.2 Gravimetric Testing

Results from the gravimetric moisture uptake tests and diffusion modelling are discussed in this section.

4.2.1 Moisture Absorption at Various Relative Humidities

Moisture absorption in SL resins can be characterised by the equilibrium moisture content, M_{∞} , at various relative humidities. Moisture absorbed at time 't', M_t , can be calculated as:

$$M_t(\text{wt}\%) = \frac{W_{wet} - W_{dry}}{W_{dry}} \times 100 \quad (4.1)$$

where W_{wet} is the weight of a moist sample and W_{dry} is its dry weight. Equation 4.1 is used to calculate the moisture uptake at specific measurement periods, up to 720 hours. In the current study, the equilibrium moisture uptake, M_{∞} , is defined when negligible changes in the sample weight are recorded.

Figure 4.1 shows the plot of equilibrium moisture uptake as a function of relative humidity (RH). Data from five samples for each environment was used to get the average readings. The variation of data remained below $\pm 1\%$. The data shows an initial linear trend (dashed trend line) during low % RH that deviates at higher % RH. However, dotted trend line better describes the relation with initial linear trend changing to the asymptotic (logarithmic decrease) trend at higher % RH between equilibrium moisture and the relative humidity.

A comparison of moisture uptake in the SL resin samples at four different RH can be seen in Figure 4.2, which plots the relation between (M_t , wt %) and (\sqrt{t}/b), where M_t is the weight percentage of absorbed moisture at time t and b is the specimen thickness. The experimental curves shown are the average of readings from five samples for each environment.

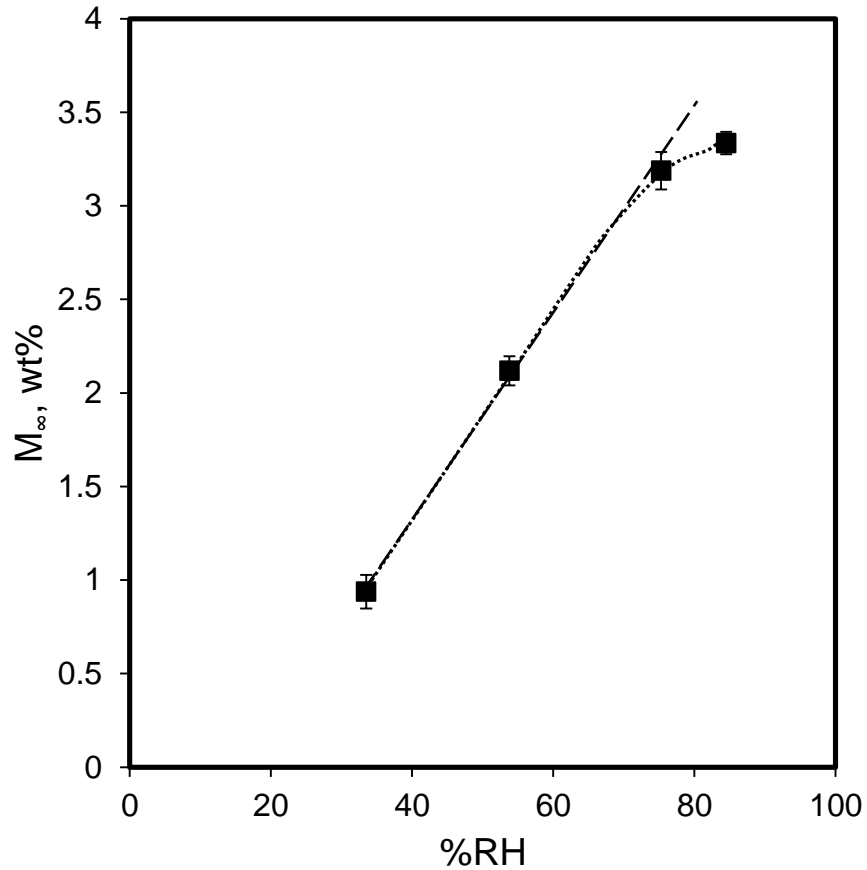


Figure 4.1. Equilibrium moisture uptake by Accura 60 samples at various relative humidities.

The relative humidity has a significant effect on the moisture uptake, as shown in Figure 4.2. It can be seen that samples at higher values of RH absorb more moisture, more quickly. The initial slope of the uptake curves is less steep at low RH and the equilibrium quantity of moisture absorbed is also lower. All the curves show an initially fast absorption rate that slows as equilibrium is reached. Similar trends have been reported in on similar SL materials (Altaf et al. 2011b). This aspect of the investigation has confirmed the extent of the hygroscopy in SL materials.

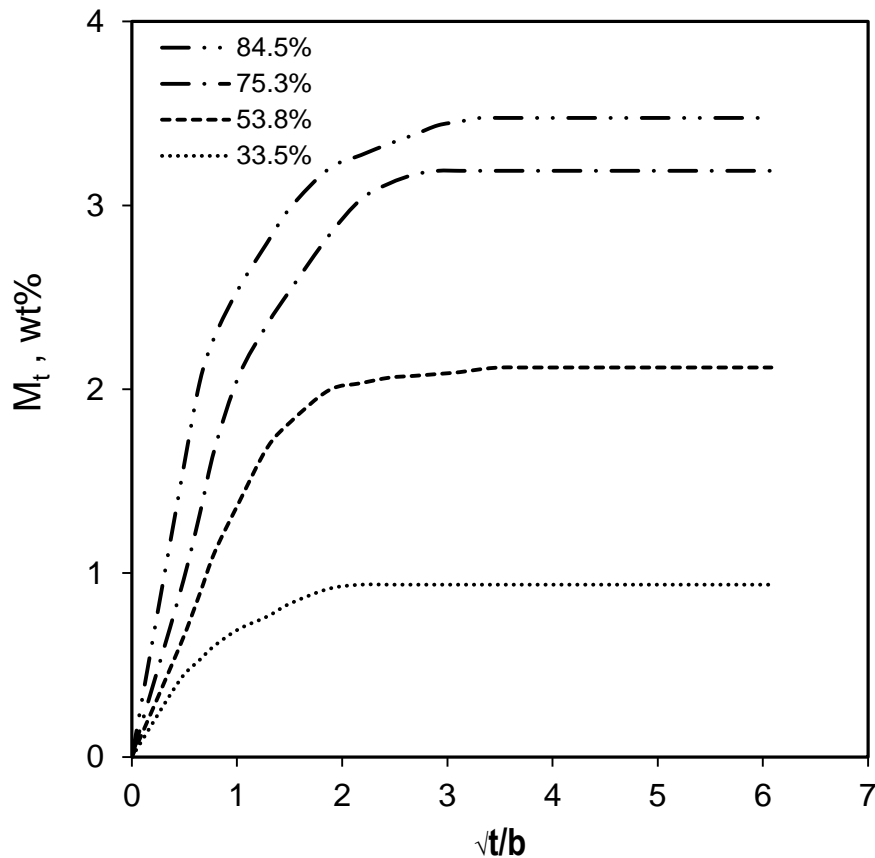


Figure 4.2: Comparison of moisture uptake in Accura 60 samples at various %RH.

4.2.2 Modelling of Moisture Diffusion

In addition to equilibrium moisture content, moisture absorption in SL resins is also characterised by the diffusion coefficient, D , which can be calculated from the plots of moisture uptake against the square root of time. The diffusion coefficient (D) may be determined from the initial slope of an (M_t/M_∞) vs. (\sqrt{t}/b) graph, where ‘ b ’ is sample thickness, and hence it is useful to plot experimental results from moisture diffusion experiments in this form. Equations of various models detailed in section 2.4.4 can be used to characterise moisture diffusion in polymers. However, in a recent study, it was found that SL resins followed Fickian diffusion only during the initial uptake, while a dual Fickian model predicted a better fit to the full experimental data (Altaf et al. 2011b). Therefore, both Fickian and dual Fickian analytical models are applied in this work to predict the experimental moisture

diffusion data and select the most suitable diffusion model for use in the numerical modelling. The parameters of the analytical moisture diffusion models were determined by curve fitting the diffusion models given in equations 2.20 and 2.24 to the experimental data. The curve fitting technique was carried out in MathCAD, (PTC, Needham, MA, USA), using the least square curve fitting technique available in the software. The best fit values of diffusion parameters for the Fickian and dual Fickian models at various RH are given in Table 4-1.

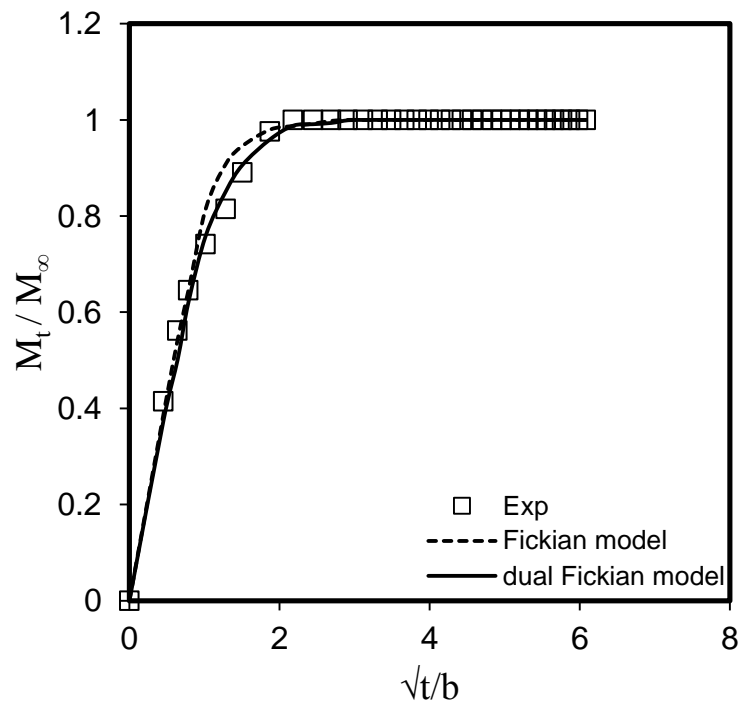
		Relative Humidity			
		33.5 %	53.8 %	75.3 %	84.5 %
Fickian model parameters	M_{∞} (wt.%)	0.937	2.118	3.187	3.335
	D (cm ² /s)	9.772×10^{-8}	8.535×10^{-8}	7.541×10^{-8}	6.937×10^{-8}
Dual Fickian model parameters	$M_{1\infty}$ (wt.%)	0.763	1.467	1.646	1.211
	$M_{2\infty}$ (wt.%)	0.275	0.729	1.437	2.209
	D_1 (cm ² /s)	6.019×10^{-8}	6.725×10^{-8}	7.263×10^{-8}	9.743×10^{-8}
	D_2 (cm ² /s)	3.314×10^{-8}	4.176×10^{-8}	5.682×10^{-8}	6.754×10^{-8}

Table 4-1: Fickian and dual Fickian model constants for 4mm thick Accura 60 samples at various relative humidities.

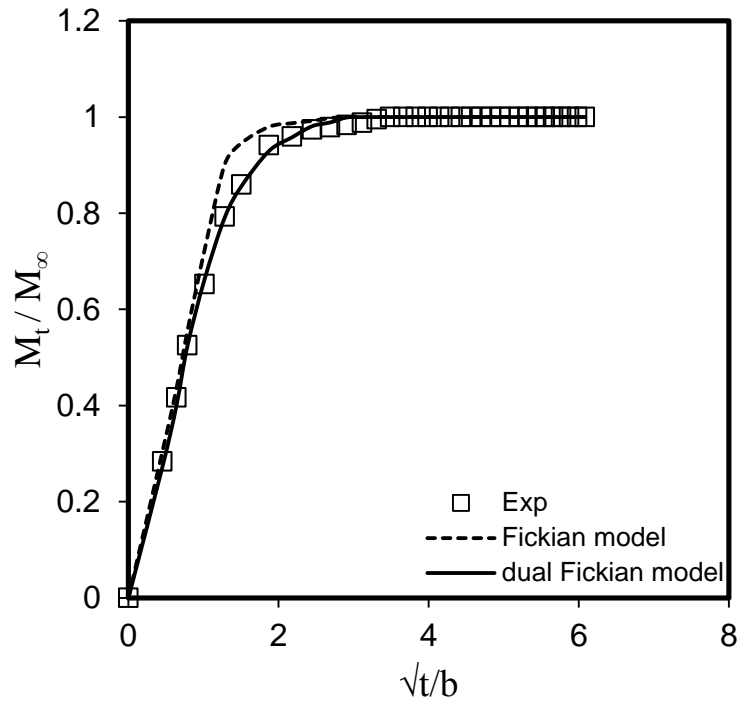
Figure 4.3 [(a) to (d)] shows the comparison of curve fitting the Fickian and dual Fickian diffusion models to the experimental results at various humidities. It is obvious from these figures that, although, the Fickian model adequately fits the early stages of water uptake, it provides a poor fit to the data above 50-70 % of the equilibrium uptake. It can also be seen that the best Fickian fit is for 33.5 %RH, which was the environment under which samples absorbed least moisture. The poor fits can be attributed to the occurrence of second phase of diffusion that is more prominent at higher % RH. This type of moisture uptake, that has a Fickian-like shape but approaches equilibrium more slowly than predicted by the Fickian model, is sometimes termed pseudo-Fickian behaviour (Crank 1979) and is quite common in epoxy resins (Wahab et al. 2001). Therefore, the dual Fickian model was fitted to the

experimental data and provided an excellent fit to the experimental data at all environments, as shown in Figure 4.3 (a) to (d).

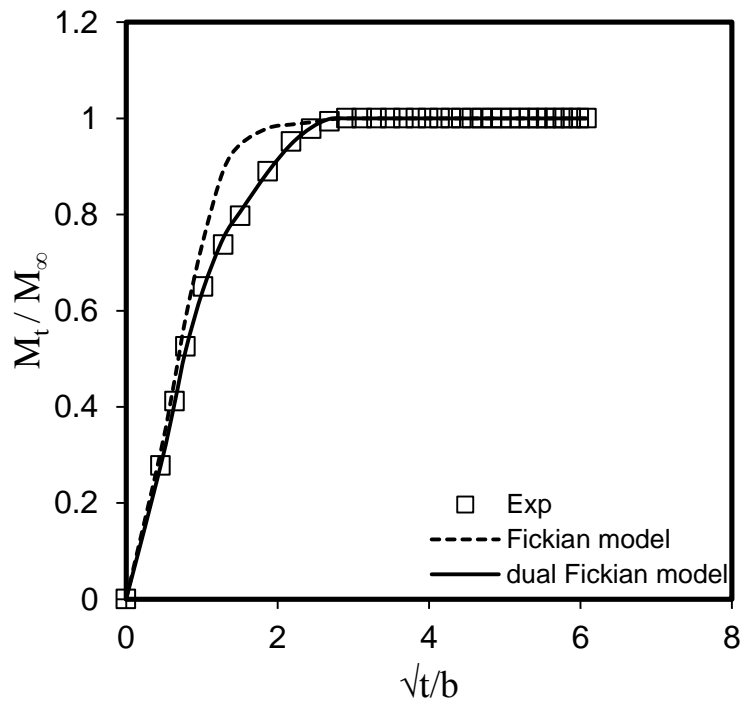
Other models described in section 2.4 can also be fitted to the data, however, the dual-Fickian model is useful as it is quite straightforward to implement in a finite element based coupled stress-diffusion analysis (Loh et al. 2005). Therefore, the dual Fickian model was used in the present work to predict diffusion behaviour numerically using the FE method. This method of analysis enables the ageing behaviour of RM components of virtually any geometry and boundary condition to be accurately modelled.



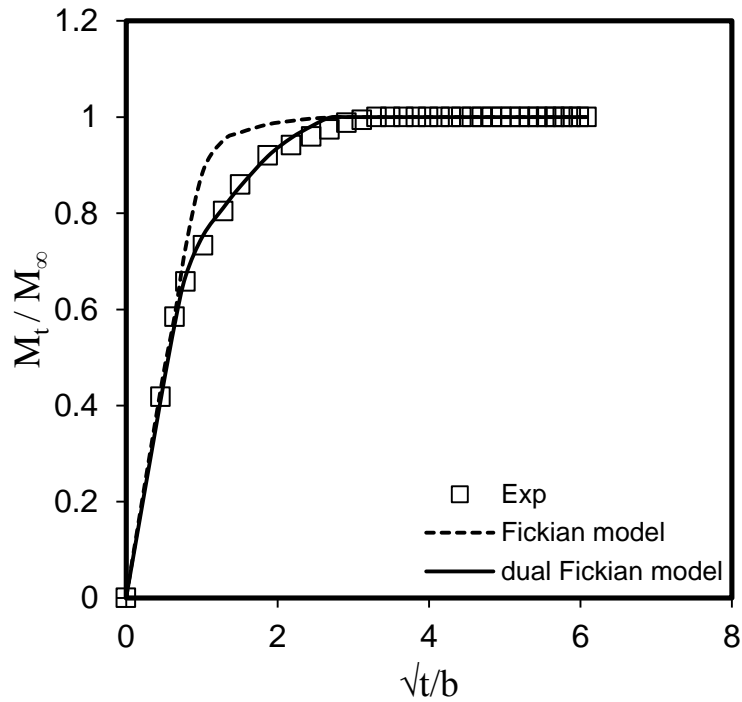
(a) 33.5%RH



(b) 53.8%RH



(c) 75.3%RH



(d) 84.5%RH

Figure 4.3: Fickian and dual Fickian model fits to experimental data at various environments using Accura 60.

To summarise, the experimental moisture uptake data for 4 mm thick bulk samples was fitted to certain diffusion analytical models. The Fickian diffusion model was not able to fully characterise the moisture absorption, however, the dual Fickian model provided a good fit to the data under all conditions. Thus the dual Fickian diffusion model will be used to predict the absorption in the SL resins at various moisture conditions. Further details on implementation of this model in FEA, its predictions and comparison with analytical modelling are provided in Chapters 5 and 6.

4.3 Bulk Mechanical Properties

4.3.1 Tensile Test Properties

Tensile stress vs. strain curves for the Accura 60 samples preconditioned in various environments for 720 hours and tensile tested at 0.1 mm/min at 22.5 °C (± 1 °C) and 35% RH (± 2 variation in RH) are shown in Figure 4.4. Plots are an average of results obtained after repeating five similar tests at each moisture condition with variation less than ± 3 % in the curves along Y-axis and less than ± 2 % along the X-axis. These five stress-strain curves for each % RH environment are shown in the Appendix-1 that highlights good repeatability of measured data. It can be seen in Figure 4.4 that the absorbed moisture has affected the tensile stress-strain behaviour of the samples by decreasing the ultimate tensile strength and increasing the elongation at break. Samples showed relatively brittle behaviour at low % RH while considerable plastic strain is seen at high %RH environments.

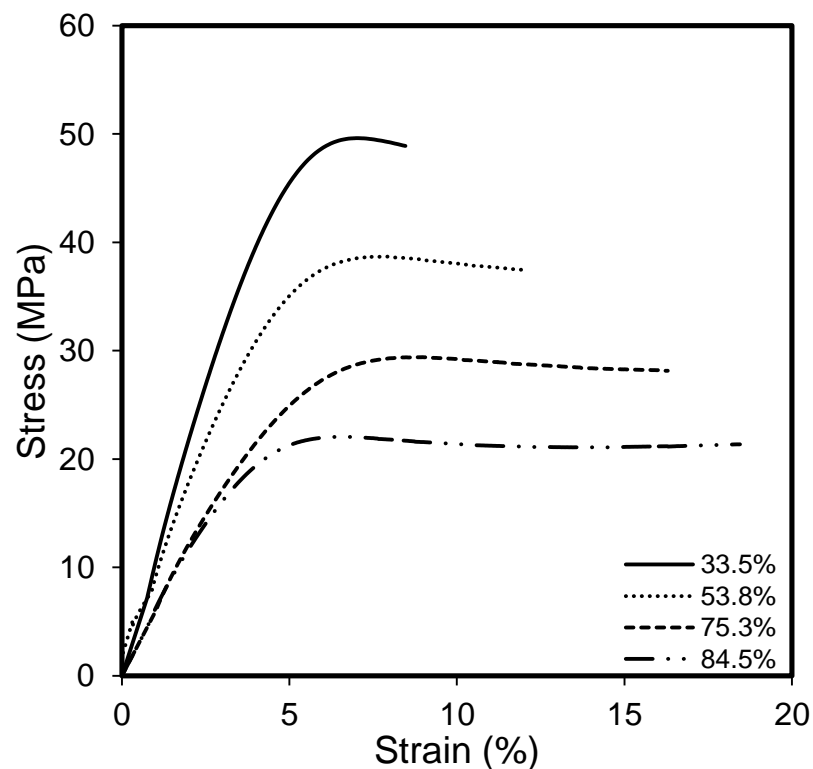


Figure 4.4: Moisture dependent tensile stress-strain curves for Accura 60 samples after 720 hours conditioning at various relative humidities.

The effect of moisture absorption on the tensile elastic modulus (E_t) and tensile yield (σ_{ty}), as determined from the tensile tests, can be seen in Figures 4.5 and 4.6, respectively that plot E_t and σ_{ty} as functions of conditioning time for various environments with $\pm 3\%$ error. A decrease in E_t with increasing moisture absorption is observed.

A similar trend was observed in σ_{ty} , where an increase in moisture content decreased the σ_{ty} . It is interesting to see that values of both E_t and σ_{ty} are relatively insensitive to conditioning time at 33.5 % RH, which indicates that the saturated moisture content at 33.5 % RH at 22.5 °C has negligible effect on the mechanical properties. However, at 75.3 % and 84.5 % RH, the values of E_t and σ_{ty} decrease significantly with conditioning time. This trend highlights an increase in surface moisture concentration with an increase in conditioning time. The rates of change in E_t and σ_{ty} decrease with time as the surface layers reach an equilibrium moisture content.

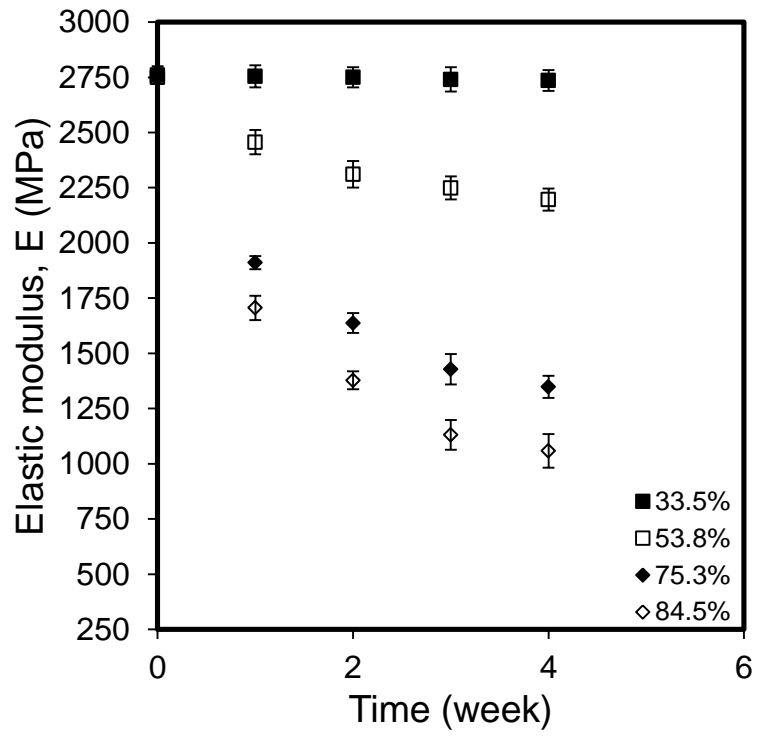


Figure 4.5: Tensile elastic modulus as a function of moisture conditioning time at various RH.

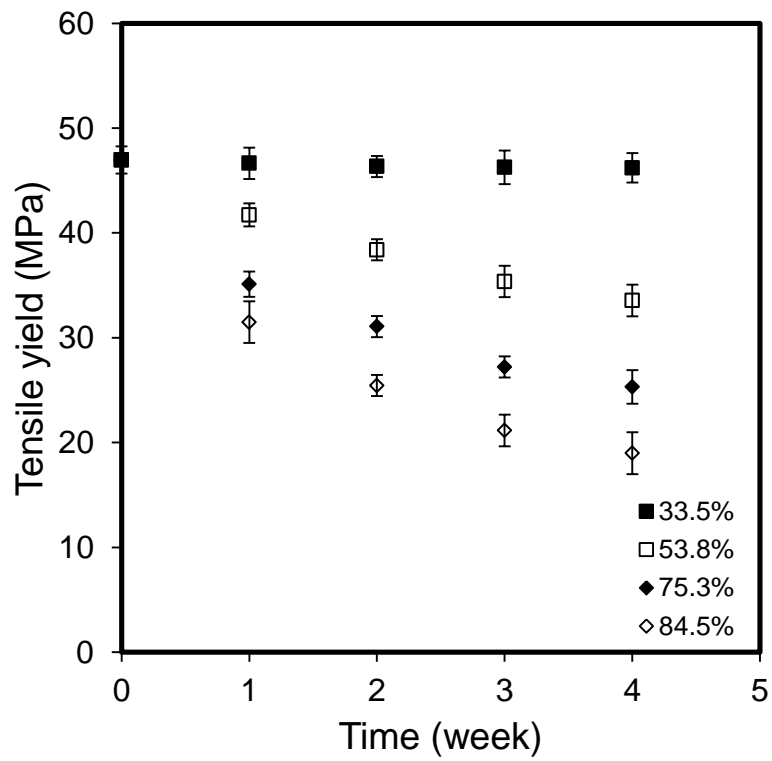


Figure 4.6: Tensile yield as a function of moisture conditioning time at various RH.

The mechanical properties calculated from these tensile tests were used in FE models to define the elastic-plastic properties of the material at various RH. Further details on the use of the tensile test data in numerical modelling are provided in Chapter 5.

4.3.2 Compressive Test Properties

Compressive stress vs. strain curves for Accura 60 samples preconditioned in various environments for 720 hours and tested under a uniaxial compressive load at 0.1 mm/min at 22.5 °C (± 1 °C) and 35% RH (± 2 RH) are shown in Figure 4.7. The plots in Figure 4.7 are an average of results obtained after repeating tests on five specimens at each moisture condition with variation of less than ± 4 % in curves along Y-axis and ± 2 % along X-axis. It can be seen that absorbed moisture has affected the compressive stress-strain behaviour of the samples by decreasing the compression yield and compressive strength and increasing the plastic strain.

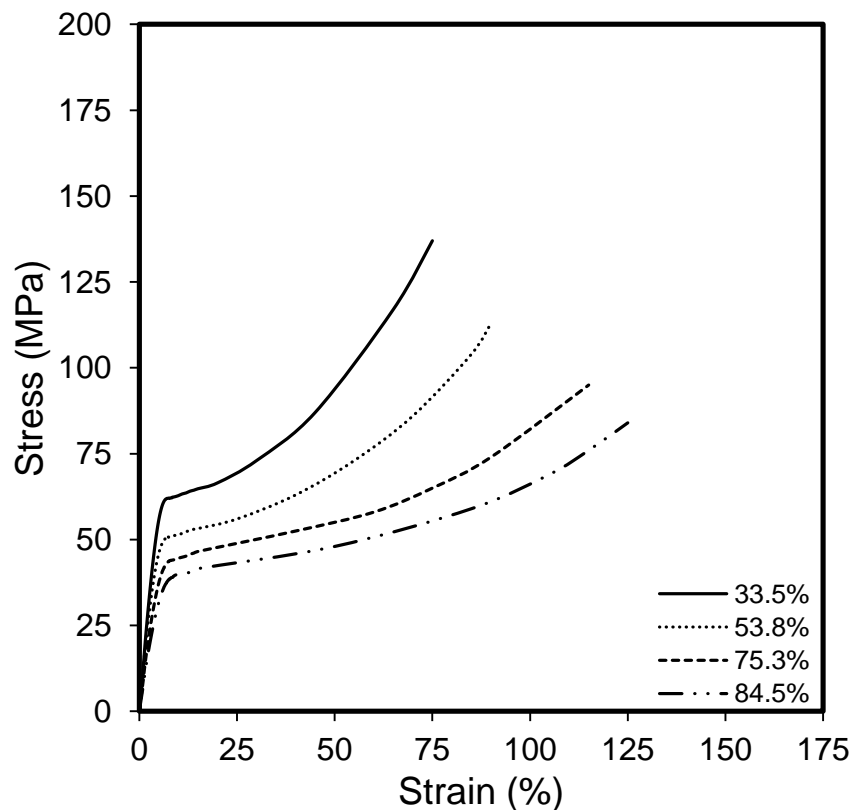


Figure 4.7: Moisture dependent compressive stress-strain curves under compressive load for Accura 60 samples after 720 hours conditioning at various RH.

If we compare stress-strain curves under compression (Figure 4.7) with tension (Figure 4.4), we find a significant difference between the compression yield and tensile yield that can be attributed to hydrostatic stress sensitivity in the material. Also, the plastic strain is increased significantly under compression. This increase in plastic strain under compression may be due to the absence of necking that causes instability under tension. It can be seen that the values of compressive elastic modulus, E_c , and compressive yield, σ_{cy} , are relatively insensitive to conditioning time at 33.5 % RH, which indicates that the saturated moisture content at 33.5 % RH at 22.5 °C has negligible effect on the mechanical properties as shown in Figures 4.8 and 4.9. However, at 75.3 % and 84.5 % RH, the values of E_c and σ_{cy} decrease significantly with conditioning time. This trend highlights an increase in surface moisture concentration with an increase in conditioning time. The rates of change in E_c and σ_{cy} decrease with time as the surface layers reach an equilibrium moisture content. Also, when we compare Figures 4.5 and 4.6 with Figures 4.8 and 4.9 respectively, we find that values of modulus and compressive yield for Accura 60 material at same RH and conditioning time under compression are higher than in tension indicating the hydrostatic stress sensitivity of the Accura 60.

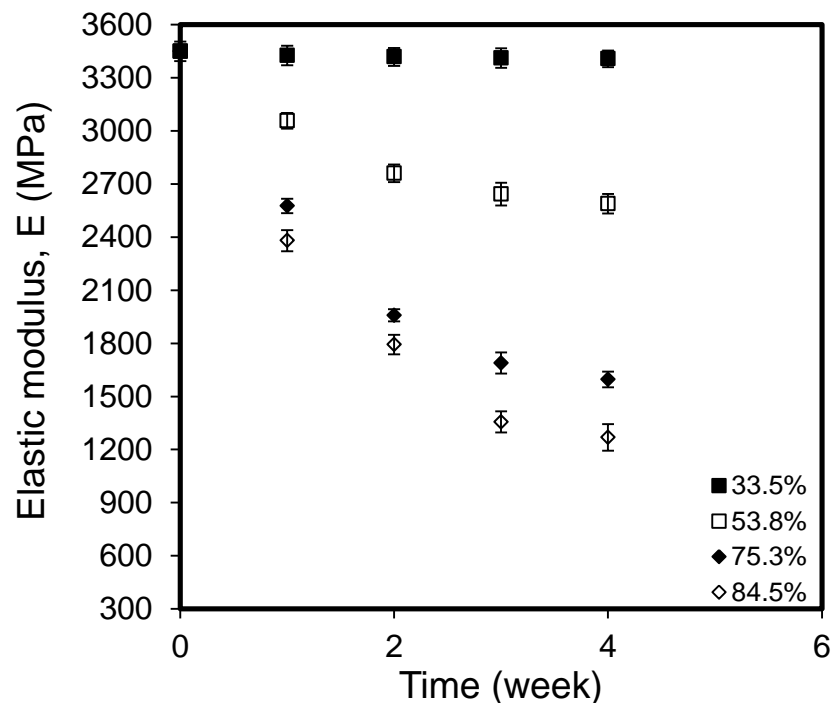


Figure 4.8: Elastic modulus as a function of moisture conditioning time at various RH under uniaxial compressive testing.

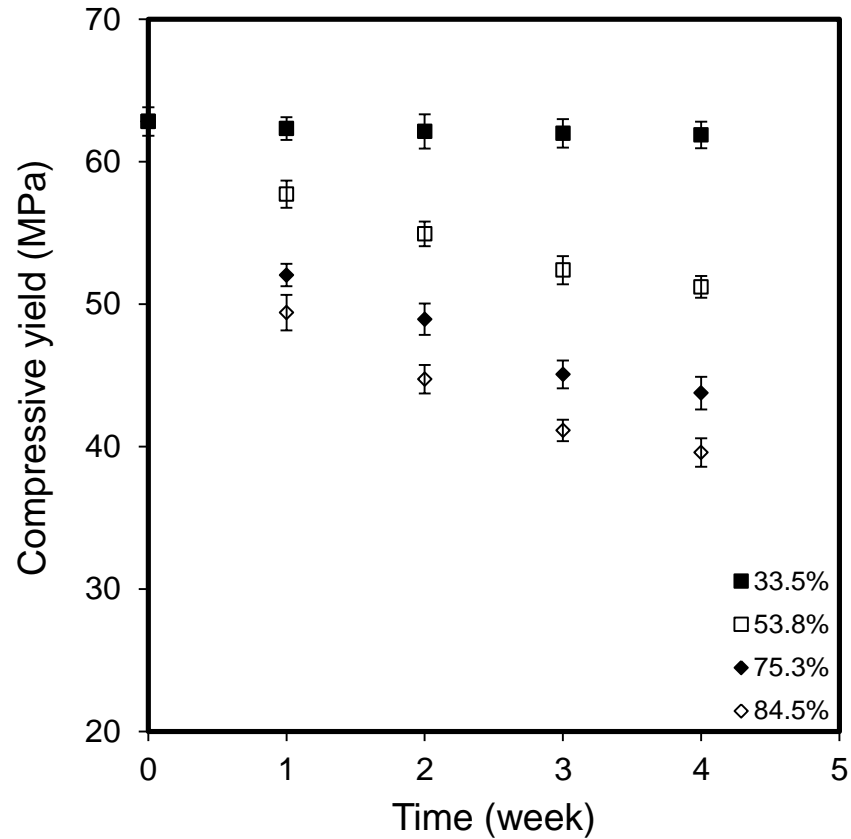


Figure 4.9: Compressive yield as a function of moisture conditioning time at various RH.

The mechanical properties calculated from the compressive tests were used in FE models to define the elastic-plastic properties of the material at various environments. Further details on the use of the test data in the numerical modelling are provided in Chapter 5. In order to investigate rate dependent deformation effects in the material, tensile creep tests were also performed and the results are described in the next section.

4.3.3 Creep Test Properties

Tensile creep test samples preconditioned at 33.5 % RH were tested after 4, 8, 12, 24 hrs conditioning, and then every 24 hours for up to 720 hours conditioning time. Figure 4.10 shows creep curves from the standard creep tensile testing of Accura 60 samples, preconditioned for 720 hours at 33.5 % RH, at various applied loads, with

temperature and moisture held constant at 22.5 °C (± 1 °C) and 35% RH (± 2 RH) respectively. In all cases, the applied load was removed during the secondary creep region after 2500 sec hold time. Each creep curve shows an initial instantaneous strain followed by primary creep, which is characterized by a decreasing strain rate, and secondary creep, which is characterized by a constant strain rate. It can be seen that an increase in applied stress causes an increase in the strain and strain rate. For each level of stress, true strain vs. time was plotted and the steady-state creep rate $\dot{\epsilon}_{ss}$ was calculated from the slope of the best-fit line in the secondary creep region as:

$$\dot{\epsilon}_{ss} = \frac{\Delta\epsilon}{\Delta t} \quad (4.2)$$

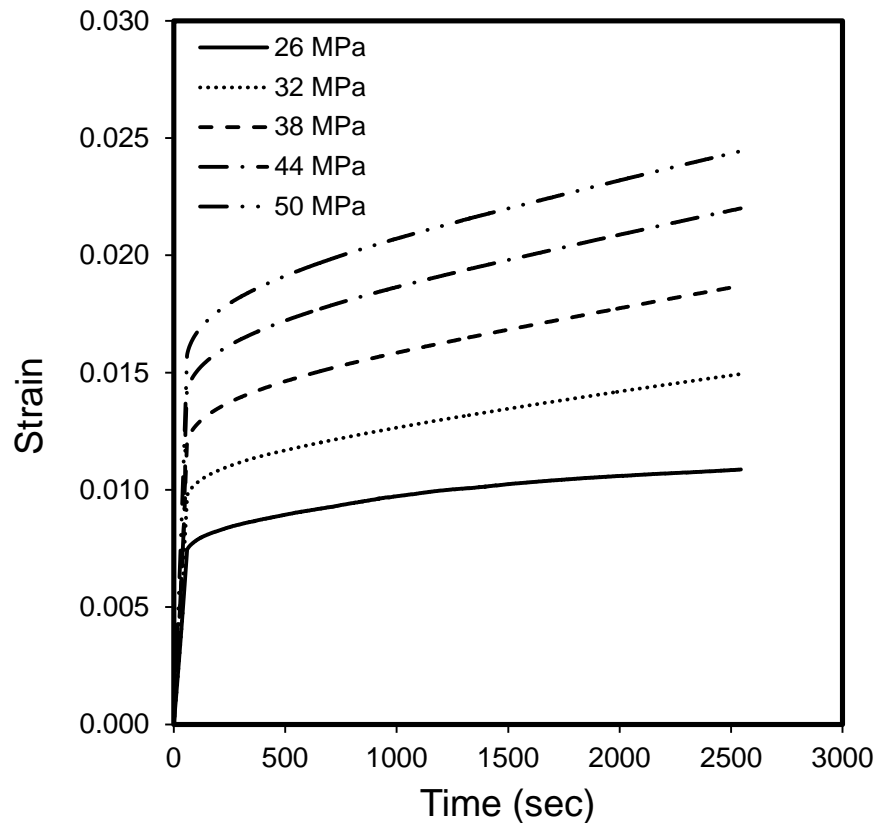


Figure 4.10. Tensile creep curves for samples preconditioned at 33.5 % RH for 720 hours and tested at 22.5 °C at 35 % RH (± 2 % RH) at various loads.

The slope from plot of $\log(\dot{\epsilon}_{ss})$ against $\log(\sigma)$, as shown in Figure 4.11, was used to find the creep power law constants 'm' and 'n' from the following equation:

$$\dot{\epsilon}_{ss} = A\sigma^m \quad (4.3)$$

Curve fitting of the plot gives the creep power law constants, $m = 4.125$ and $A = 1.7 \times 10^{-12}$ in this case.

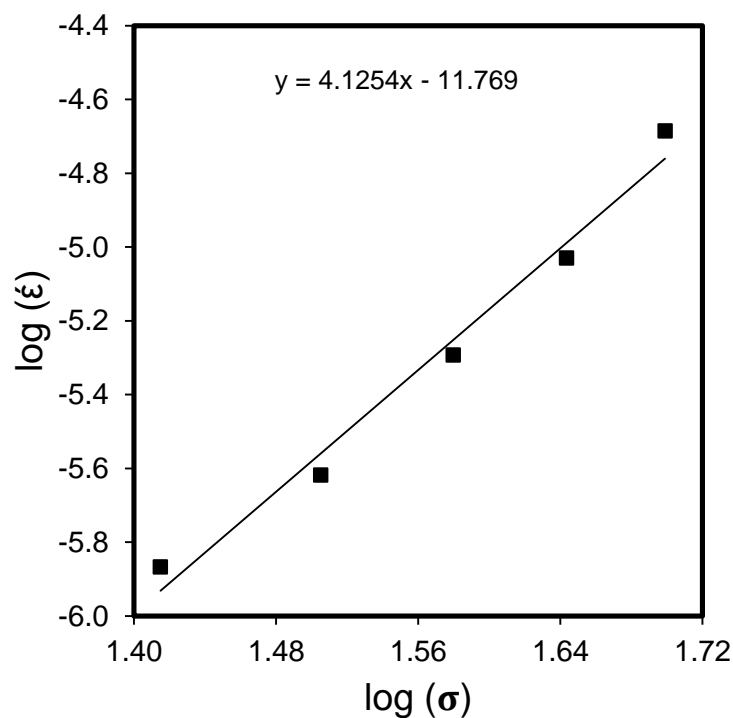


Figure 4.11. Determination of tensile steady state creep constants of samples preconditioned for 720 hours at 33.5 % RH and tested at 22.5 °C and 35 % RH (± 2 % RH) testing environment.

Similarly, creep tests were performed on samples preconditioned for 720 hours at 53.8 %, 75.3 % and 84.5 % RH at the same applied loads. Figure 4.12 shows a comparison of creep curves for samples preconditioned at various RH and tested at 50 MPa after 720 hours conditioning. It can be seen that preconditioning to higher RH has significantly influenced the creep, resulting in an increase in instantaneous

strain, total strain and strain rate. This comparison shows that preconditioning at higher % RH results in higher absorbed moisture content, resulting in a decrease in resistance to the applied load and hence causing an increase in the creep strain.

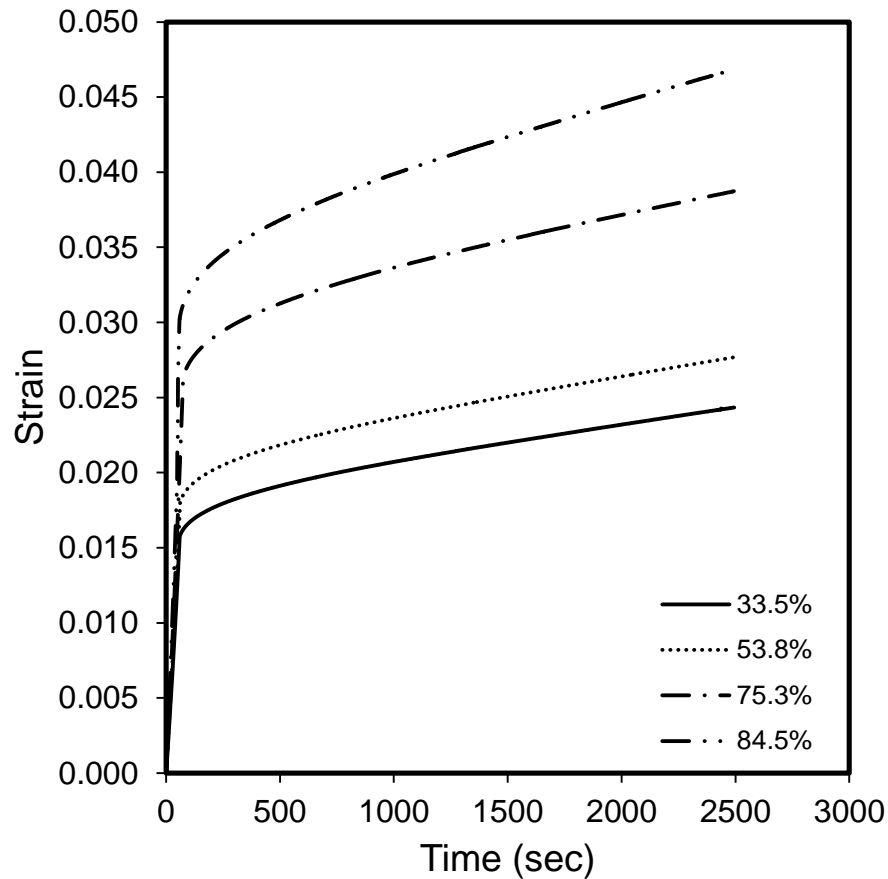


Figure 4.12: Creep curves of Accura 60 samples preconditioned for 720 hours at various RH and tested at 50 MPa at 22.5 °C at 35 % RH (± 2 % RH).

A method similar to the one discussed for the samples preconditioned at 33.5 % RH was used to calculate the creep constants at various RH every 24 hours. Table 4-2 summarizes the values of creep constants at various RH and times. It shows that the empirical constants, 'A' and 'm', of the creep power law stay almost same at 33.5 % RH while they increase with an increase in conditioning time at higher % RH. These constants calculated from the creep tensile tests were used in the FE model to define the rate dependent deformation effects at various RH. Further details are provided in Chapters 5 and 6.

	Relative Humidity							
	33.5 %		53.8 %		75.3 %		84.5 %	
	A	m	A	m	A	m	A	m
240 hrs	1.69e-12	4.143	5.12e-10	4.637	8.975e-6	5.462	5.32e-3	6.214
480 hrs	1.24e-12	4.092	6.701e-8	4.773	6.21e-5	5.759	9.8e-3	6.671
720 hrs	1.7e-12	4.125	7.117e-7	4.848	3.12e-4	5.856	6.04e-2	6.819

Table 4-2 : Creep power law constants at various % RH after periodic conditioning.

4.4 DSI Tests

The DSI technique faces various challenges when employed on polymers due to their time dependent deformation. This section discusses DSI experimental results from experiments when on SL resin Accura 60. It is subdivided into three parts. The first part shows the results of techniques to extract pseudo time-independent mechanical properties, such as hardness and elastic modulus, where time dependency is minimized during unloading. The second section shows the results of experiments carried on preconditioned and HCU conditioned samples. Finally, results from experiments investigating effects of drying on mechanical properties are presented. Analysis of the DSI data to extract time dependent material properties is discussed in Chapter 7.

4.4.1 Investigation of Rate Dependent Effects

Figure 4.13 shows load vs. displacement plots for dry samples tested at 33.5 % RH with a maximum load of 20 mN for different loading rates. The unloading rate was kept constant at 0.5 mN/sec and no dwell period was introduced. It can be seen that the maximum indentation depth increases with decrease in loading rate and that faster loading produces a more pronounced ‘nose’ or ‘bowing’ effect in the initial segment of the unloading curve. This ‘nose’ effect at fast loading rate is because the polymer has less time to reach an equilibrium stress state, and hence, the back stress is higher, resulting in a higher rate of deformation during the start of unloading. This

‘nose’ effect results in an initial negative gradient to the unloading curves, which means that the calculation of elastic modulus and plastic depth using the OP method is meaningless.

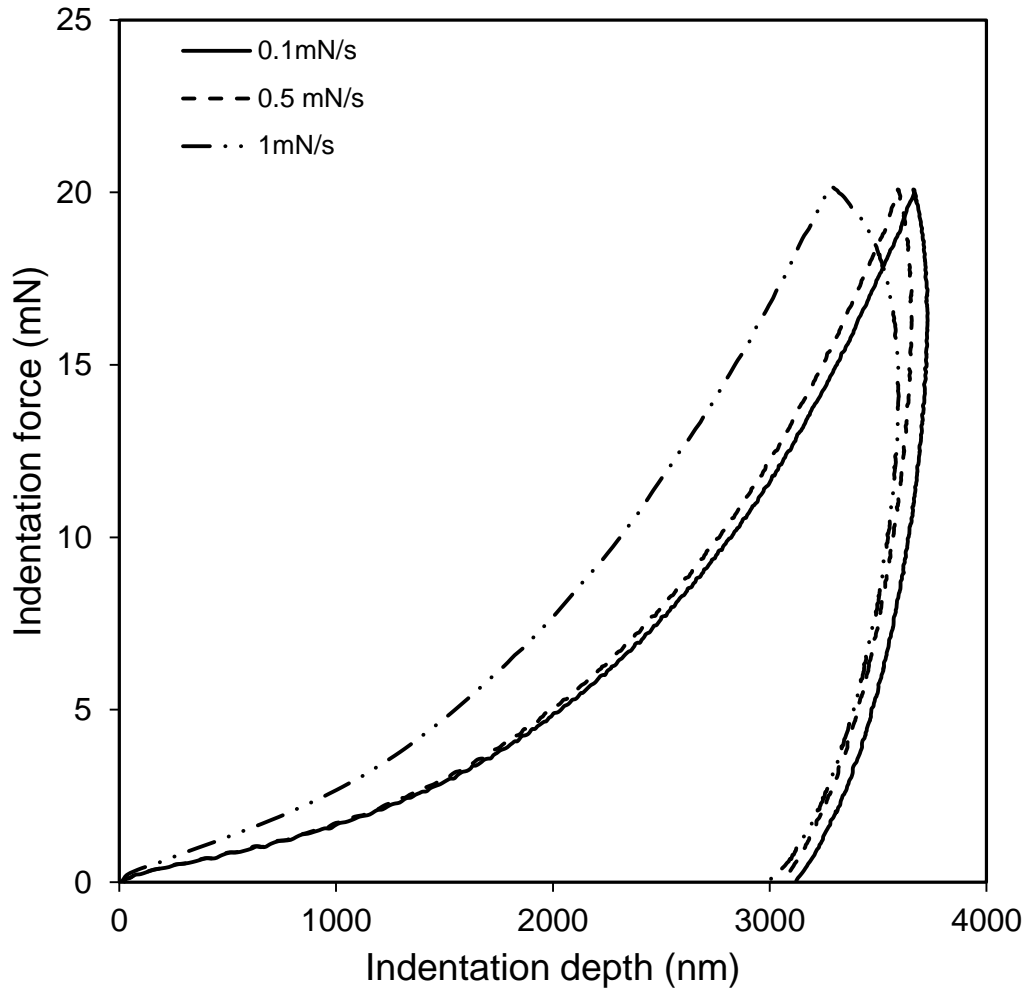


Figure 4.13: Load-depth plots for dry samples tested at 33.5 % RH at various loading rates with no dwell period and unloading rate of 0.5 mN/s.

Figure 4.14 shows the values of indentation hardness and modulus calculated using the OP method with the load-depth plots in Figure 4.13. It can be seen that the values are highly dependent on the loading rate due to the viscoelastic-plastic (VE-P) deformation. Therefore, the assumption that unloading is elastic during the initial portion of the unloading curve is incorrect and this creep behaviour needs to be accounted for before extracting meaningful mechanical characterization parameters.

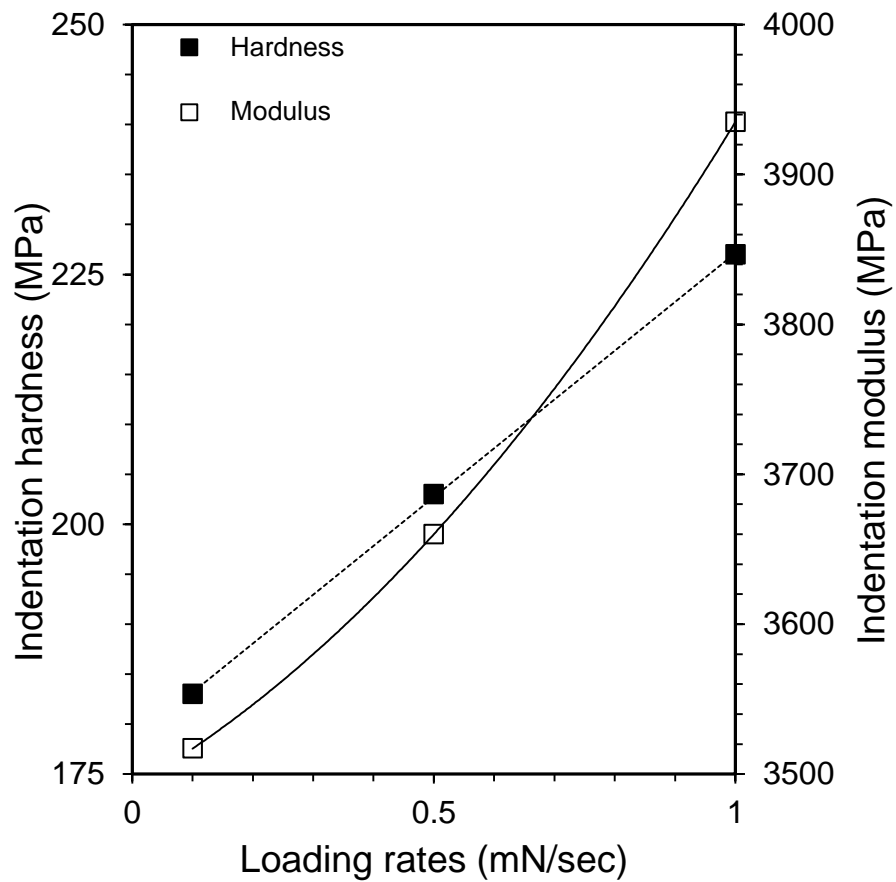


Figure 4.14. Comparison of indentation hardness and modulus of dry samples with various loading rates, no dwell period, 0.5 mN/sec unloading rate and 20 mN maximum load.

Figure 4.15 shows the effect of unloading rate when the loading rate was kept constant at 0.5 mN/sec. It can be seen that the samples demonstrate significant creep behaviour when unloaded at lower rates. Hence, fast unloading is required to minimise the time dependent effect.

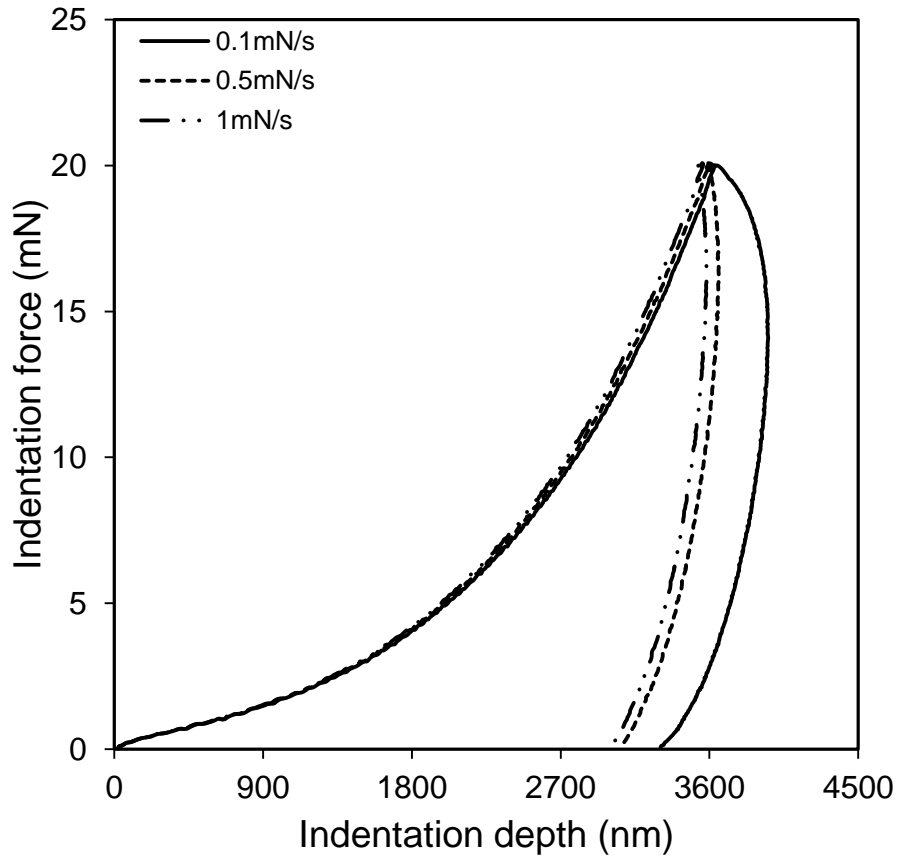


Figure 4.15. Load-depth plots for dry samples tested at 33.5 % RH at 0.5 mN/sec loading rate with no dwell period and various unloading rates.

Figure 4.16 shows load-depth plots for loading and unloading rates of 0.5 mN/sec with 0 sec, 120 sec, 180 sec, 300 sec and 600 sec dwell times at 20 mN maximum load. It can be seen that the bowing effect decreases with an increase in dwell time. The gradient of the initial segment of the unloading curve remains approximately the same with dwell periods greater than 300 sec.

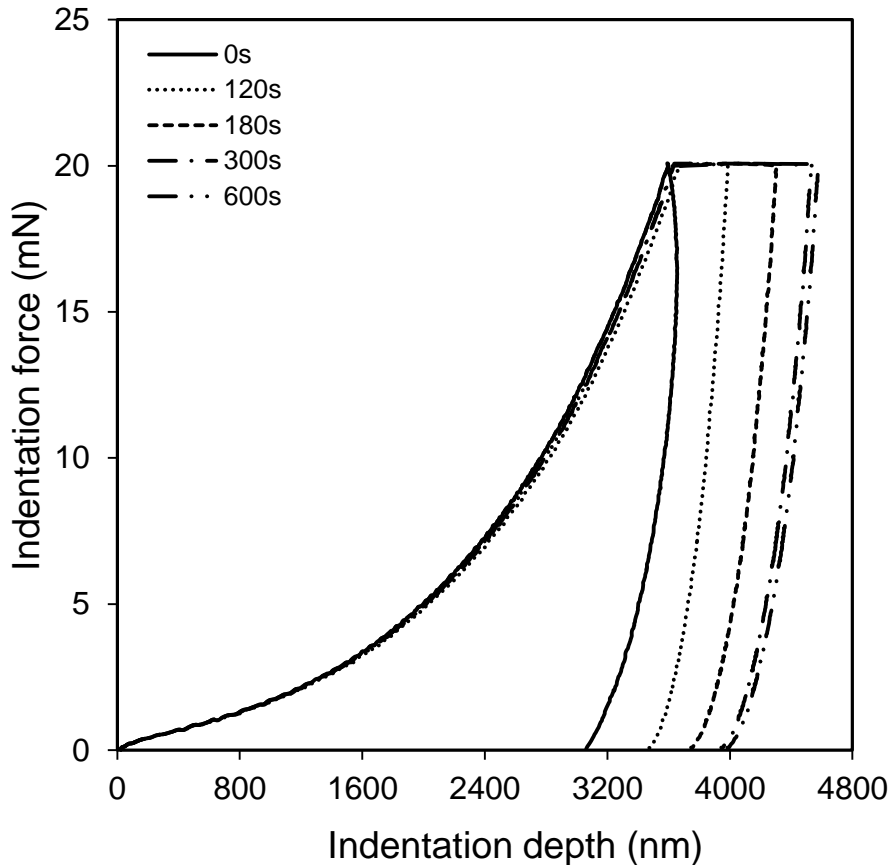


Figure 4.16. Load-depth plots for dry samples tested at 33.5%RH at 0.5 mN/sec loading rate with various dwell periods and an unloading rate of 0.5 mN/sec.

Values of H and E calculated after different hold periods are shown in Figure 4.17. It can be seen that lower hold times result in higher values of indentation modulus and hardness. However by applying a suitable dwell period, the VE-P effects during unloading can be minimized and hence indentation modulus, E_e , can be related to the elastic component of deformation and indentation hardness, H_e , to the mean pressure under the indent at equilibrium deformation, when creep has stopped. Whilst these two values don't fully characterise the complex time dependent mechanical behaviour of the polymers, they do allow meaningful comparisons to be made of the effect of moisture on the mechanical performance of the material, which is the main subject of this research work.

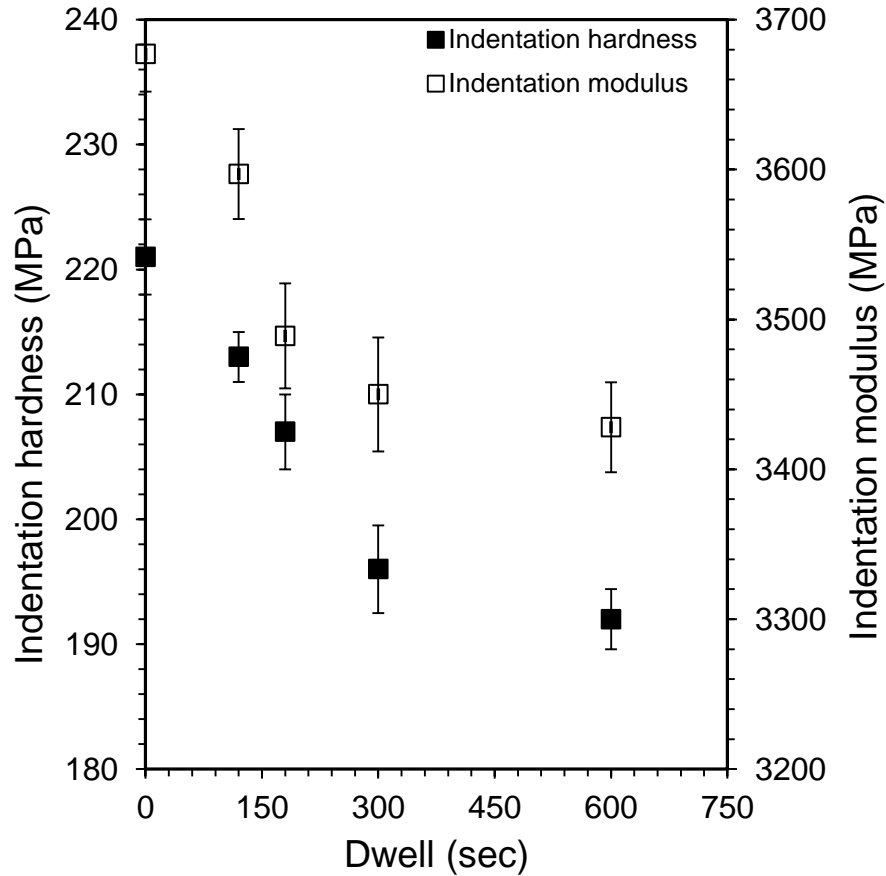


Figure 4.17. Comparison of indentation hardness and modulus of dry samples with 0.5 mN/sec loading rate, various dwell periods at 20 mN load and 0.5mN/sec unloading rate.

Hence, on the basis of the above results related to the investigation of VE/VP effects in Accura 60 when indented, 0.5 mN/sec loading and unloading rates with a 300 sec dwell time and 20 mN maximum load were the selected parameters for the experiments to investigate the effects of moisture at various relative humidities and the results are shown in the next section.

4.4.2 Investigation of Effects of Relative Humidity

4.4.2.1 Preconditioned Samples Tested at 33.5 % RH

Figure 4.18 shows a comparison of load-depth plots for samples preconditioned for 24 hours at different relative humidities and tested at 33.5 % RH in the DSI chamber.

These are the average curves from five repeated tests while five curves for each test at various % RH are shown in Appendix-2 describing excellent trend of data repeatability. It can be seen that maximum indentation depth increases with increasing RH. The increase in penetration depth at higher % RH can be attributed to the absorption of more moisture by the polymer. This absorbed moisture weakens the intermolecular forces in the polymer resulting in a decrease in the glass transition temperature (T_g) and, hence, a decrease in resistance to indentation (Ashcroft and Spinks 1996; Gaofei et al. 2004; Bell and Bielinski 2008).

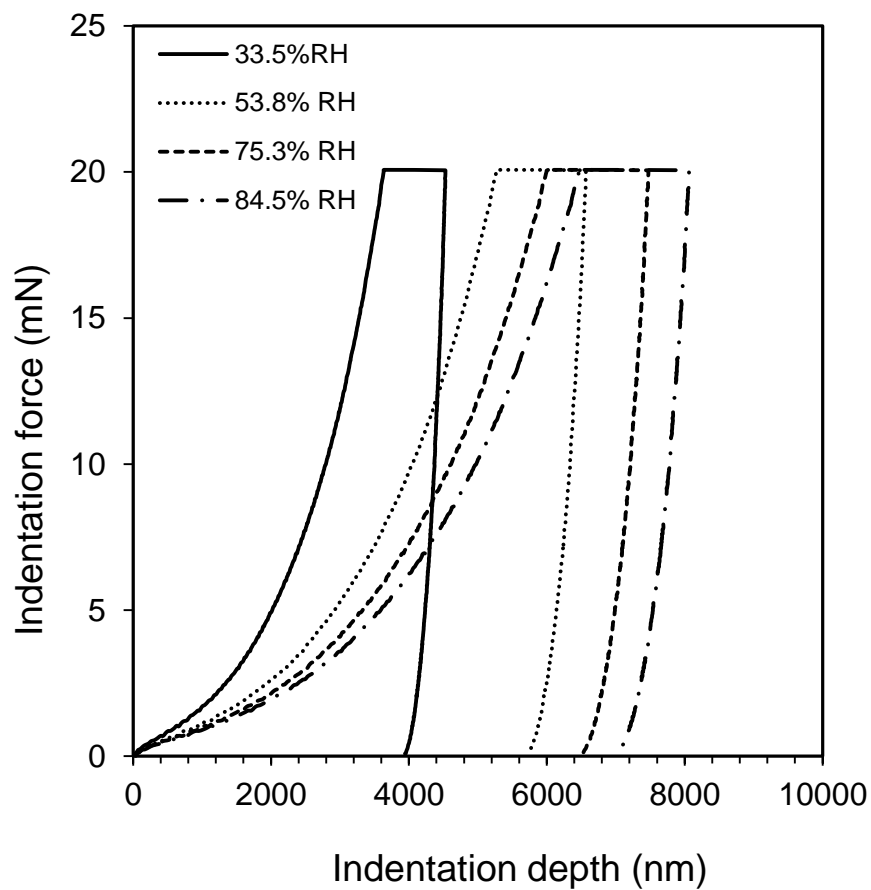


Figure 4.18. Load-depth plots of samples preconditioned under various environments for 24 hours and tested at 33.5%RH.

Figure 4.19 shows the load displacement plots for samples preconditioned at 84.5 % RH for five days and tested every 24 hours in the DSI chamber at 33.5 % RH and 22.5 °C. It can be seen that penetration depth increases with an increase in conditioning time. This trend highlights an increase in surface moisture concentration with an increase in conditioning time. The first 24 hours conditioning gives rapid decrease in the indentation resistance owing to the fast initial absorption due to the high moisture concentration gradient. The rate of increase in penetration depth decreases with time as the surface layers reach equilibrium moisture content.

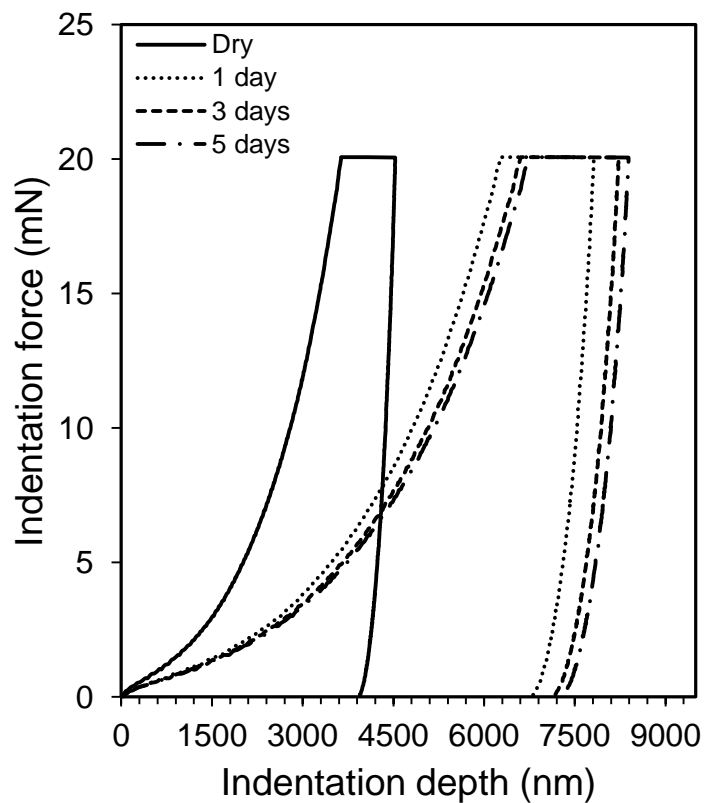


Figure 4.19. Comparison of load-depth plot for samples initially dry with those preconditioned for five days at 84.5 % RH and tested every 24 hours at 33.5%RH.

Figures 4.20 and 4.21 show plots of hardness, H_e , and indentation modulus, E_e , as function of conditioning time for various environments. It is interesting to see that values of both E_e and H_e are relatively insensitive to conditioning time at 33.5 % RH, which indicates that the saturated moisture content at 33.5 % RH at 22.5 °C has only

a modest effect on the mechanical properties. However, at 75.3 % and 84.5 % RH, the values of E_c and H_c decrease significantly with conditioning time. This trend highlights an increase in surface moisture concentration with an increase in conditioning time. The rates of change in both E_c and H_c also decrease with time as the surface layers reach equilibrium content.

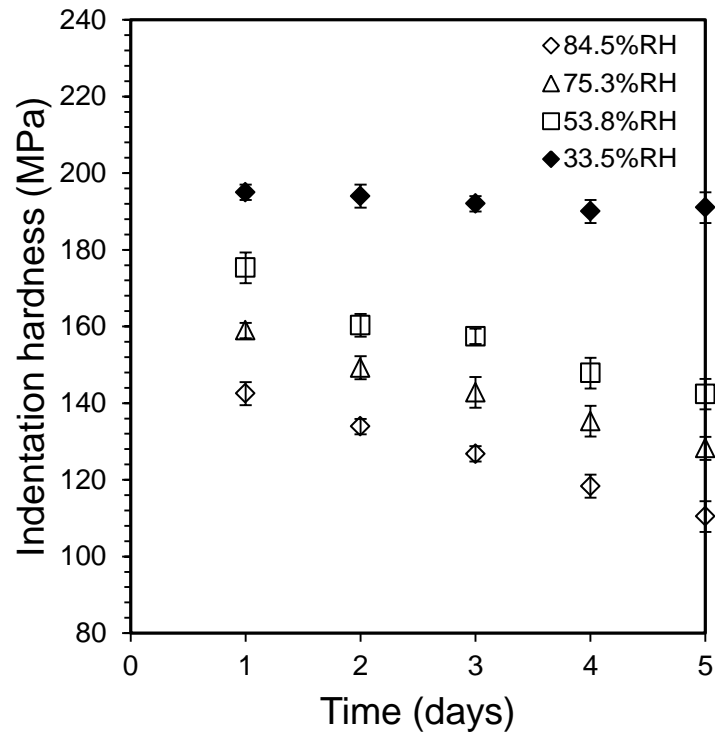


Figure 4.20. Indentation hardness as function of time after pre-conditioning at various relative humidities and testing at 33.5 % RH.

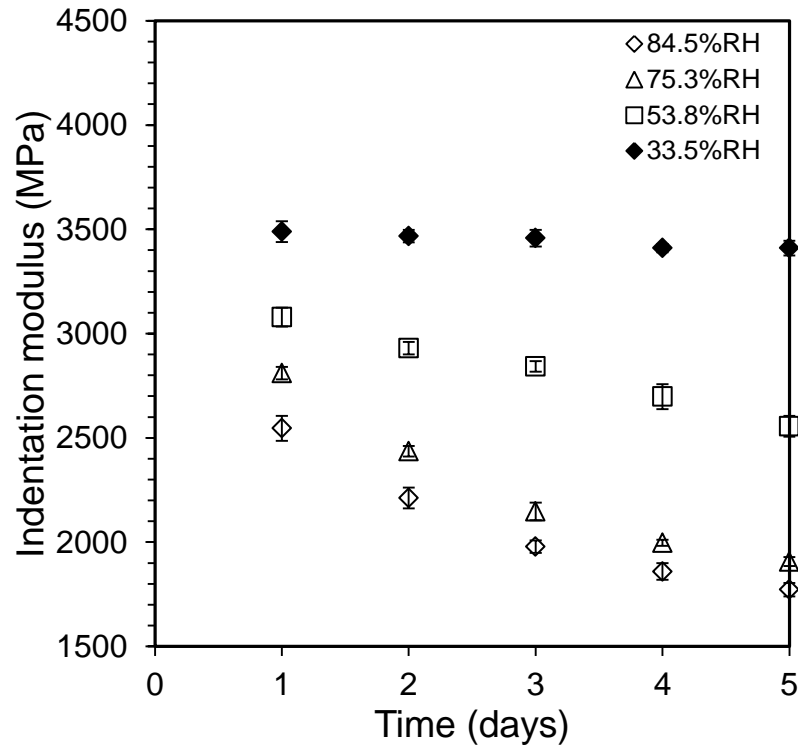


Figure 4.21: Indentation modulus as function of time after pre-conditioning at various relative humidities and testing at 33.5 % RH.

4.4.2.2 Samples Conditioned & Tested at Various RH

Figure 4.22 shows load-depth plots for samples conditioned for 24 hours at various relative humidities by regulating RH using the humidity control unit (HCU) in the DSI chamber and testing at the same controlled RH. It can be seen that the maximum indentation depth increases with an increase in % RH, with samples at 84.5 % RH showing the maximum penetration. The rising RH in the environment increases the absorbed moisture concentration in the sample surface and thus influences the resistance to indentation, as discussed in section 4.4.2.1.

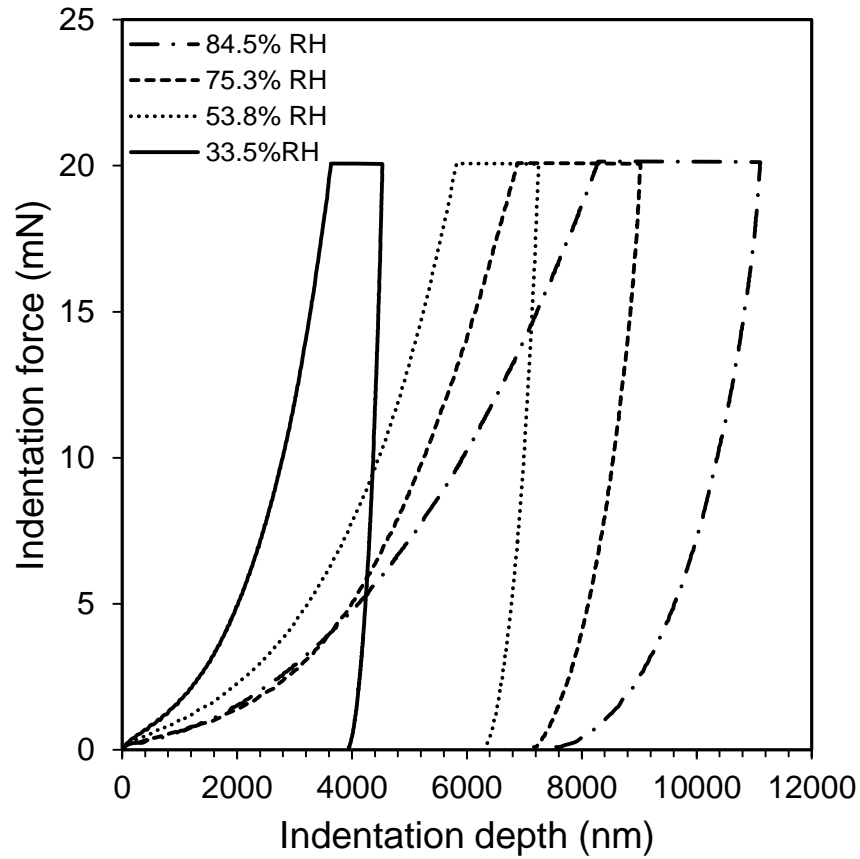


Figure 4.22. Load-depth plots for samples conditioned by HCU for 24 hours under various % RH and tested under the same conditioning environment.

Figures 4.23 and 4.24 show plots of calculated H_e and E_e as functions of conditioning time for various environments. Values of both E_e and H_e are, again, not significantly affected by conditioning time at 33.5 % RH while at 75.3 % and 84.5 % RH, their values decrease significantly with the conditioning time.

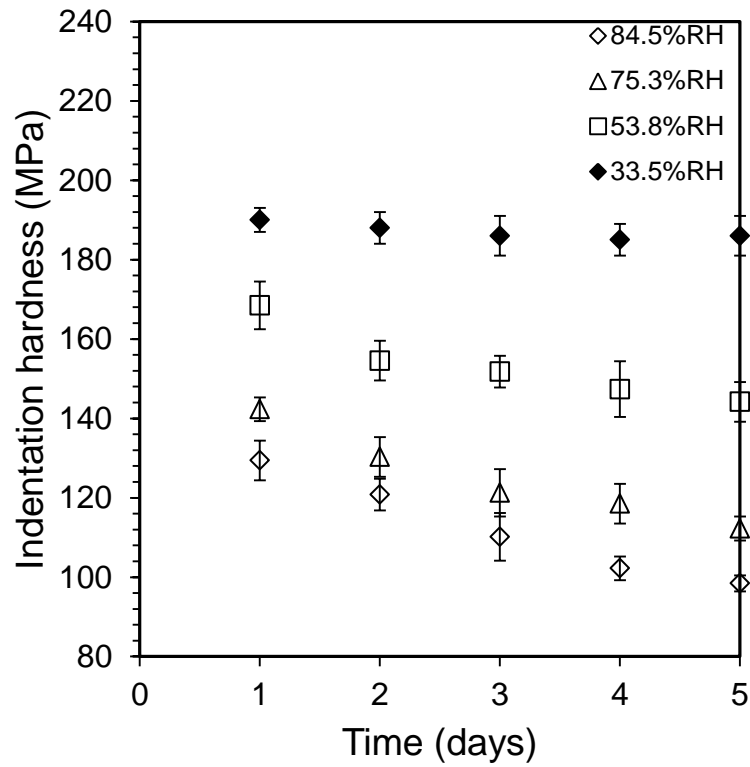


Figure 4.23. Indentation hardness as function of time after conditioning and testing under various relative humidities regulated by HCU.

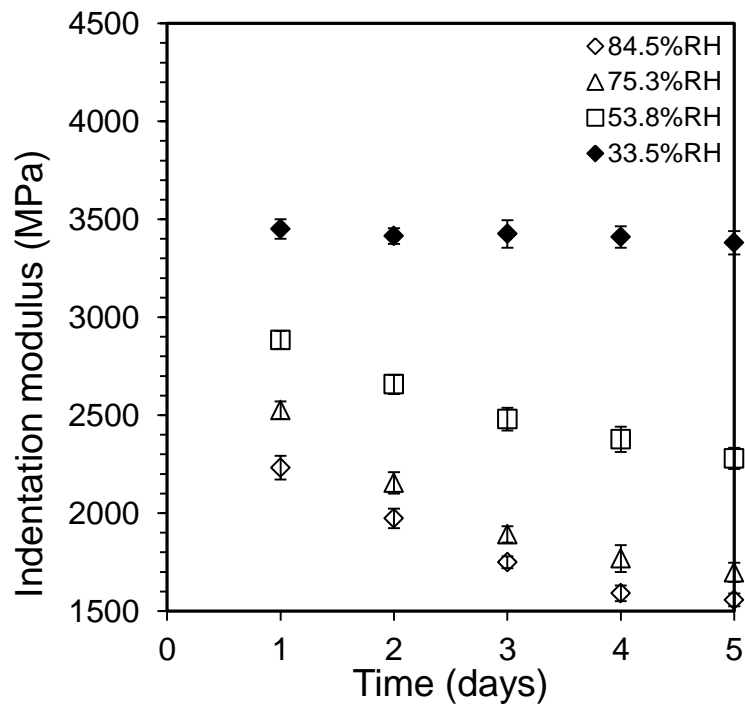


Figure 4.24. Indentation modulus as function of time after conditioning and testing under various relative humidities regulated by HCU.

Comparison of Figures 4.18 and 4.24 shows that penetration depth for a given time and RH is greater for the samples conditioned and tested in the same environment than for the preconditioned samples tested at 33.5 % RH. The exception being the samples conditioned at 33.5 % RH which show similar results for both conditioning methods, as would be expected. This observation can be seen more clearly in Figures 4.25 and 4.26, which shows that the values of H_e and E_e for a given conditioning environment are greater for the preconditioned samples. This is because for the preconditioned samples, tests were at a lower RH than the conditioning environment, resulting in desorption of some of the moisture from the sample surface during the period of the test. Even though the testing was conducted as quickly as possible after removal from the conditioning environment, the effect is quite significant, especially at high RH. This result indicates that at least some of the effect of moisture on indentation resistance is reversible. This is investigated further in the next section.

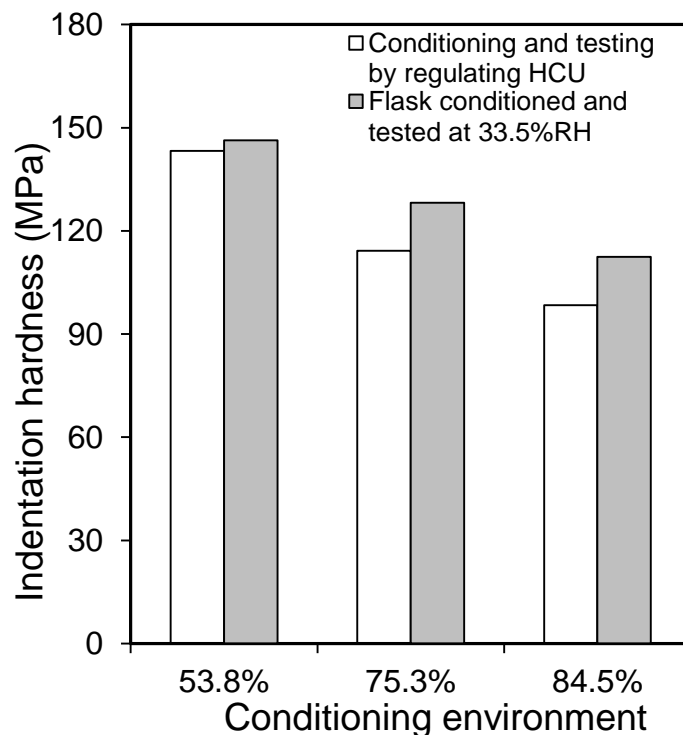


Figure 4.25: Comparison of indentation hardness of samples conditioned for five days in flask and tested at 33.5 % RH with samples conditioned for five days and tested under various % RH regulated by HCU.

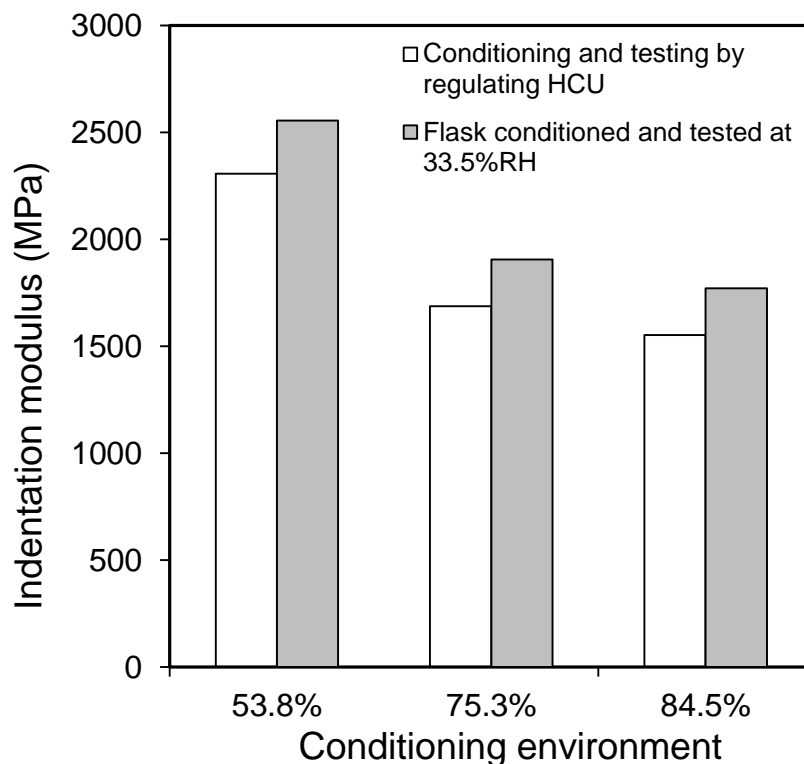


Figure 4.26: Comparison of indentation modulus of samples conditioned for five days in flask and tested at 33.5 % RH with samples conditioned for five days and tested under various % RH regulated by HCU.

4.4.3 Investigation of Effects of Drying on Indentation Behaviour

Figure 4.27 compares load-depth plots for samples that were conditioned at 84.5 % RH for 5 days and tested in the same environment with samples conditioned for 5 days at 84.5 % RH and then conditioned for 10 days at 33.5 % RH inside the chamber and retested periodically. It can be seen that the maximum indentation depth decreases with drying time, indicating a recovery of the polymer properties and reversal of the effects of moisture.

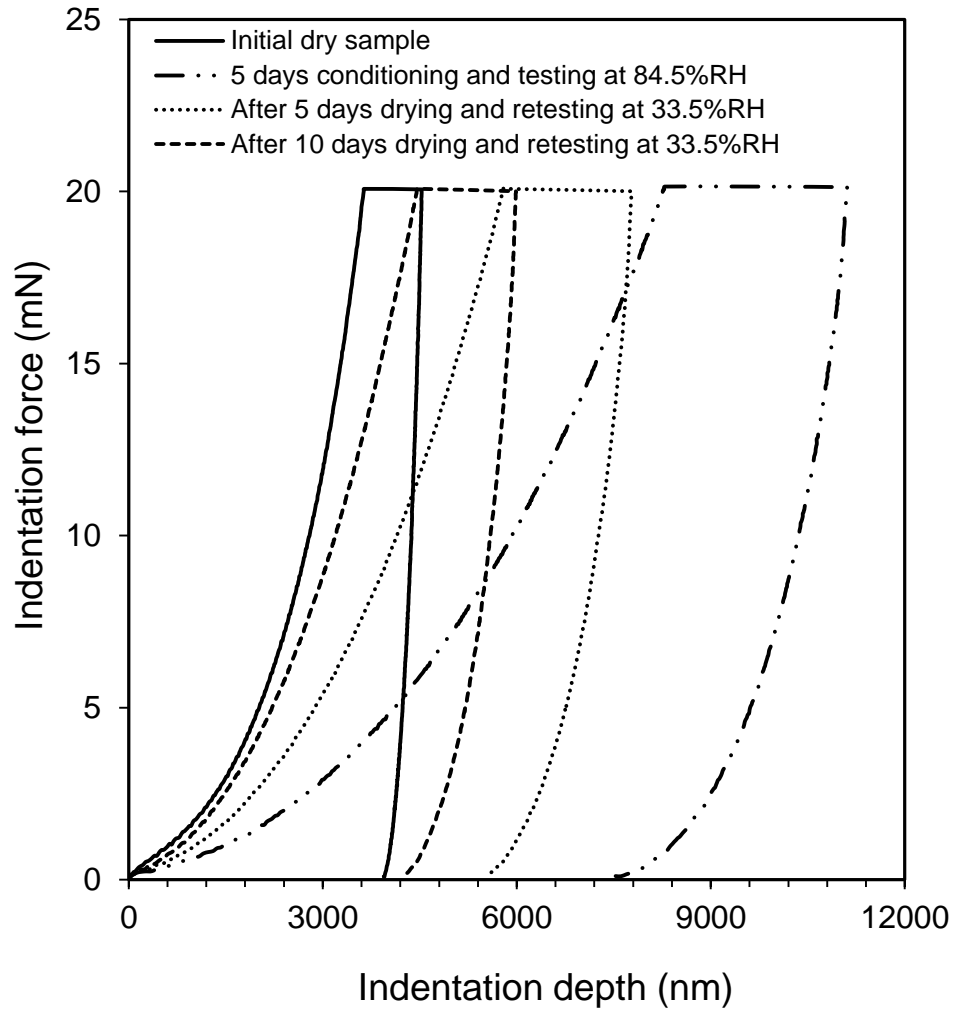


Figure 4.27. Comparison of load-depth plot for samples initially dry with those conditioned for five days at 84.5 % RH and tested at 84.5%RH and with samples conditioned for 5 days at 84.5%RH and followed by conditioning at 33.5%RH.

Figure 4.28 shows a comparison of E_e and H_e values for these samples before and after drying. It is apparent from the plots that the drying process has substantially recovered the mechanical properties of the Accura 60 samples. In the initial period, the recovery is fast, reducing as equilibrium of moisture concentration between the sample surface and the environment is reached. After 10 days storage in ambient, the average recovery in hardness was 68.43 % and in modulus 76.12 %. Recovery of these mechanical properties on drying can be attributed to reversible changes in AM polymers on removal of the moisture, which has been noted previously for epoxy based polymers (Mubashar et al. 2009, 2010).

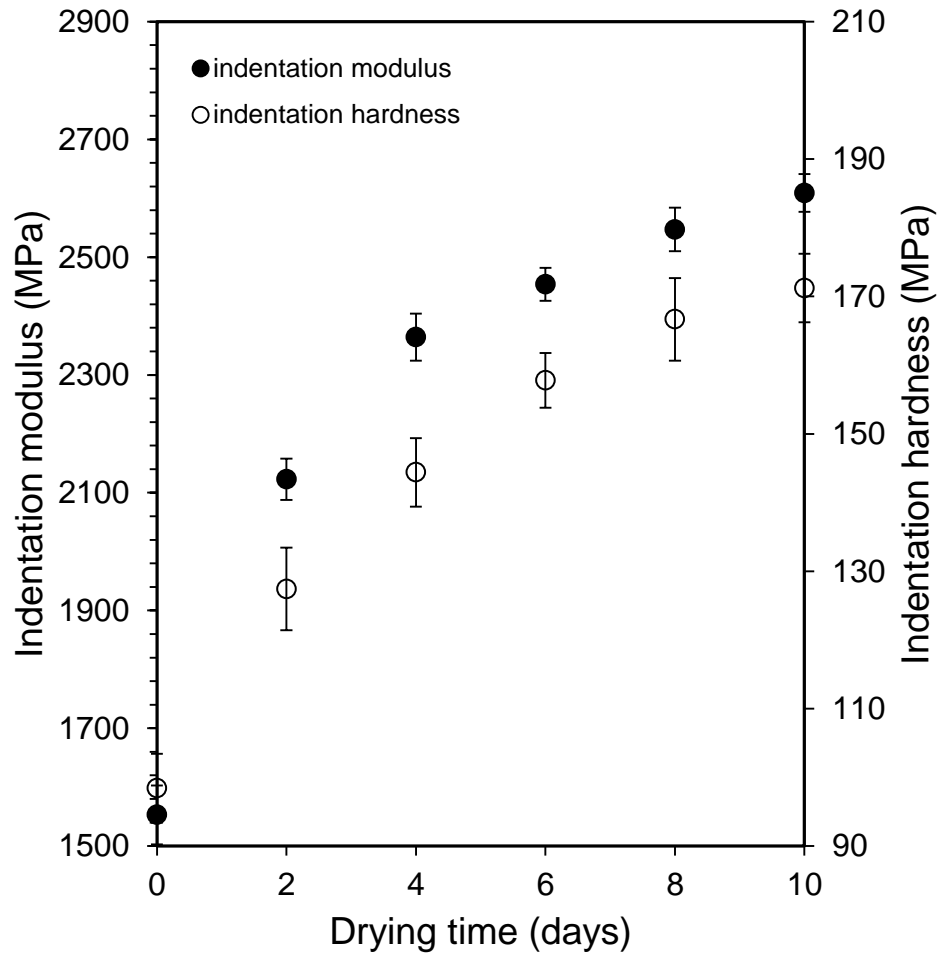


Figure 4.28. Recovery in indentation modulus and hardness on drying samples that were conditioned for 5 days under 84.5% RH and retesting periodically at 33.5%RH.

4.5 Summary

The results of the experimental programme were presented in this chapter. The moisture uptake behaviour of the bulk samples of SL resin under various RH was observed and it showed that both diffusion constant, D , and saturated moisture content, M_{∞} , had a RH dependence, with M_{∞} showing an increase with higher % RH. Both Fickian and dual Fickian analytical moisture diffusion models were used to determine the best fit to the experimental data and to determine values of D and M_{∞} . The dual Fickian model gave the best predictions for moisture uptake in all

environments. Values of D and M_{∞} calculated for the dual Fickian model were used in the FE modelling of moisture diffusion, as detailed in Chapters 5 and 6.

Bulk mechanical testing was carried out that included tensile tests, compressive tests and creep tensile tests at various RH. The tensile testing results showed that E_t and σ_{ult} decreased, while % strain increased, with increasing RH and conditioning time. The compressive test results showed the same trends. Comparison of tensile and compressive tests showed a higher ultimate strength under compression, confirming the hydrostatic stress sensitivity of the SL resin samples. Creep tensile tests were performed to investigate rate dependent effects and to calculate creep power law constants at various RH. Results confirmed that RH influenced the samples, with higher RH resulting in increased instantaneous strain, creep strain and strain rate. The results from the bulk mechanical tests were used in defining the material model for the FE modelling of indentation at various RH.

The DSI technique was used to investigate the indentation behaviour of Accura 60. It was found that the deformation behaviour of the SL resin is highly rate dependent. Changes in loading and unloading rates and dwell periods resulted in variations in penetration depth and the calculated mechanical properties. The application of moderate loading and unloading rates with sufficient hold time can be used to reach an equilibrium indentation depth for the load, resulting in a pseudo-elastic unloading curve. Therefore, by selecting appropriate experimental parameters, time dependent effects were minimized in order to the use OP method for calculating mechanical properties. The effect of the level of moisture in the environment on the mechanical properties of a polymer was also investigated using DSI. The results from this study showed that the mechanical properties of the polymer were highly dependent on the RH of the environment and that a DSI fitted with a HCU was capable of investigating this relationship. Comparison of the results using the HCU with those from the pre-conditioned samples tested at ambient conditions showed that drying of the samples whilst testing can affect the results. Hence, the use of a HCU to control

the environment during testing is needed to accurately determine the effects of moisture on samples at various RH environments. The experiments on samples after drying showed a considerable recovery in the values of E_e and H_e . This recovery in mechanical properties on drying indicates the reversible nature of plasticization in polymers.

|Finite Element Methods

5.1 Introduction

Numerical modelling has been performed using the finite element (FE) method. This chapter provides details of the FE modelling techniques that have been used in modelling DSI and moisture diffusion in the Accura 60. The commercially available FE code MSC Marc 2007, a nonlinear FEA program, by MSC Software Corporation (Santa Ana, CA, USA), was used for the numerical analysis together with the pre and post-processor MSC Mentat, also from MSC Software Corporation. A consistent system of units based on N, mm and sec was used. Modelling details such as: geometry development, mesh size and refinement, element type, defining of contact, boundary conditions and material models are described. In order to generate simulated load-depth plots of indentation under various RH, coupled stress-diffusion finite element analyses were performed and these are also detailed in the chapter.

5.2 FE modelling of DSI

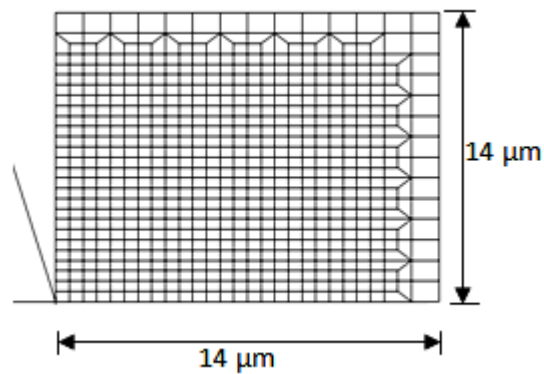
The various modelling considerations are presented in the following subsections that are necessary to model indentation behaviour successfully.

5.2.1 Geometry and Boundary Conditions

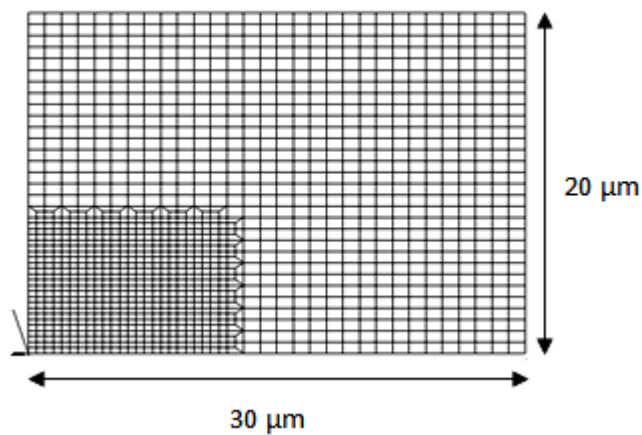
The Berkovich indenter with 65.3° included half angle can be modelled as a cone with 70.3° half angle as this provides the same projected area to depth ratio as the Berkovich indenter (Fischer-Cripps 2004). The comparison of indentation hardness and modulus calculated from the FE modelling of Berkovich indenters of 50nm radius as a conical indenter has been seen to match well for cases where the ratio of maximum indentation depth to indenter radius was greater than 0.07 (Chen et al. 2007). DSI experimental results in Chapter 4 show that the maximum indentation

depth at 20 mN load was always greater than 2500 nm, while the radius of Berkovich indenter was approximately 135nm and thus the ratio was greater than 0.07. Hence, in the present work, a two-dimensional (2D) axisymmetric FE analyses was performed using sharp conical indenter geometry to repeat the Berkovich indenter in a computationally efficient manner.

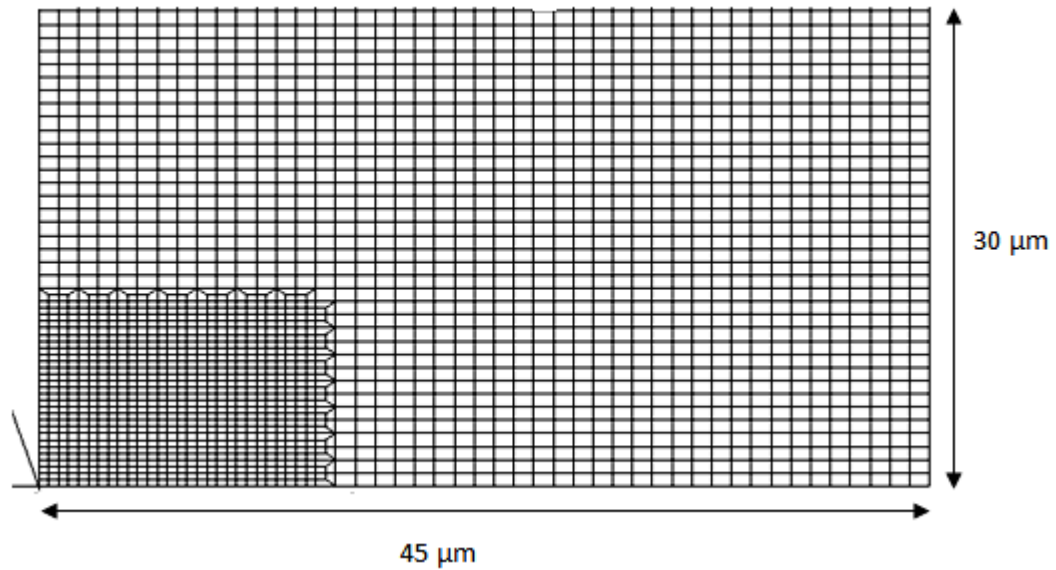
The selection of an appropriate geometry of sample is also important as it can help in saving computational time and cost. In the DSI experiments, the indentation area was small, around $94 \mu\text{m}^2$, compared to the size of sample. Thus sensitivity to far field analyses was carried out to obtain the optimum size of model that provides negligible displacement and stresses at boundaries with the smallest computation time. Hence, various sample sizes, with areas between $150 \mu\text{m}^2$ and $1400 \mu\text{m}^2$, as shown in Figure 5.1, were investigated.



(a) Model boundary area = $196 \mu\text{m}^2$



(b) Model boundary area = $600 \mu\text{m}^2$



(c) Model boundary area = $1350 \mu\text{m}^2$

Figure 5.1. Various model boundaries used in far field analysis.

The selection criterion for geometry size was to have smallest possible sample size with negligible effects on variation in solution results in the contact area and minimal effect of the indentation at boundaries. Results showed that $30 \mu\text{m} \times 20 \mu\text{m}$ (area = $600 \mu\text{m}^2$) was the optimum choice, where the nodes at the boundary showed less than 1 MPa of compressive stresses with around 3.5 nm of displacement. Hence, a $30 \mu\text{m} \times 20 \mu\text{m}$ size model was used in all the FE work.

Figure 5.2 shows the geometry of a conical sharp indenter and the selected size of specimen model. A fine FE mesh was generated for the specimen and its details are given in section 5.3. A maximum point load of 20 mN was applied to the control node of the indenter while the constraint in the y direction at the bottom of Figure 5.2 represents the axis of the axi-symmetry. The specimen was constrained in the x-axis to represent gluing of the sample to the aluminium stub during the experiments. The indenter and the specimen were defined as rigid and deformable bodies respectively and the contact was defined. The indenter was modelled as a rigid body as it is diamond and exhibits negligible deformation when indenting the much softer

materials such as polymeric samples. The details on defining of contact are discussed in section 5.2.4.

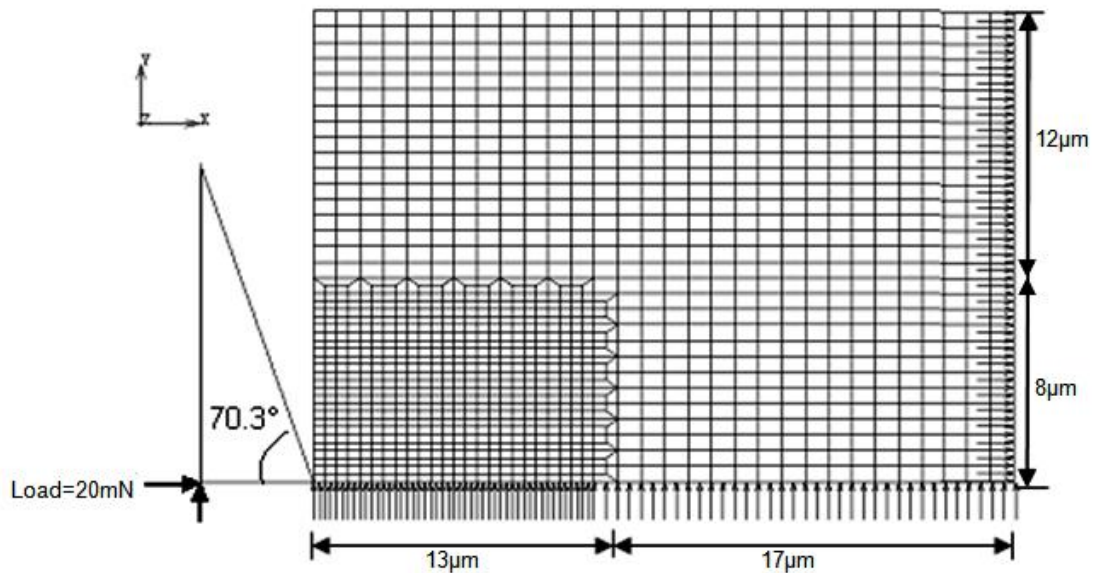


Figure 5.2. Details of indenter and specimen geometry.

5.2.2 Mesh Design

Figure 5.2 shows the meshing details of the sample. Since nanoindentation is a localised process that provides deformation near the contact surface, the primary area of interest is close to the point of contact. Therefore, a continuous mesh was defined with transition from a fine mesh near the contact area to a coarse mesh near the boundaries. The mesh continuity was maintained by sharing nodes between the elements. A fine mesh was used near the contact area in order to provide accuracy in describing the deformation and stresses resulting from contact whilst a coarse mesh at the boundaries helped to reduce computational time.

Since large strains distort the elements, changing contact conditions make a constant finite element mesh inappropriate to capture a full indentation, leading to errors in

calculations. Hence, a local adaptive meshing technique was employed near the contact zone. This enabled the software to automatically re-mesh within time steps of the solution to ensure that the solution converged with accuracy. There are a number of factors to be considered during mesh design, such as selection of an appropriate element type and mesh convergence checks, are discussed in sections 5.2.2.1 and 5.2.2.2 respectively.

5.2.2.1 Selection of Element Type

The selection of an appropriate element is important as it can influence the FE results. The behaviour of an element is usually dependent on the following:

- Number of nodes
- Number of degrees of freedom per node
- Interpolation or shape functions within the element
- Number of integration of points for the calculation of the element stiffness matrix

MSC Marc has an extensive element library that consists of plane stress, plane strain, axisymmetric, plate, beam, shell and three-dimensional solid elements. For axisymmetric analysis (used in this work), there is a wide range of element family, including 3-noded triangle, 4-noded quadrilateral, 6-noded triangle and 8-noded quadrilateral elements (MSC Marc 2007). Further details are shown in Table 5.1.

Element type (number)	Interpolation Function	Availability of updated Lagrange
3 node triangle, (2)	Linear	Yes
4 node quadrilateral, (10)	Linear	Yes
4 node quadrilateral with bending, (95)	Linear	No
6 node triangle, (92)	Quadratic	No
8 node quadrilateral, (28)	Quadratic	Yes
8 node reduced integration quadrilateral, (55)	Quadratic	Yes
8 node quadrilateral with arbitrary loading, (62)	Quadratic	No
8 node quadrilateral with bending, (96)	Quadratic	No

Table 5-1 : Element types available for executing axi-symmetric analysis.

For contact problems that involve large strain problems, two procedures exist in Marc, the total Lagrange and the updated Lagrange formulation. Since, the total Lagrange formulation is not recommended for material behaviour that includes plasticity and large strains (MSC Marc 2007), in the current study, the updated Lagrangian formulation was used for modelling the indentation behaviour. Hence, during the selection of element type it was also considered whether the element could provide support of the updated Lagrange method.

Three-noded isoparametric triangular elements poorly represent shear and bending behaviour as the strains are kept constant throughout the element while the six-noded semi-infinite element was not selected as it is not available with the updated Lagrange formulation.

The four-noded quadrilateral element is an isoparametric that uses bilinear interpolation functions, therefore, strains vary linearly or are constant (depending on direction) through the element which limits the accurate representation of bending and shear behaviour. However, this element type has an advantage as re-meshing can be performed. However, during the analysis, the node in contact with the indenter changes its position (and numbering) during each re-meshing and therefore it is not possible to trace the path of the node in contact with the indenter. Also, a very small size of elements is required to attain convergence resulting in high computational times.

The 8-node axisymmetric element, shown in Figure 5.3, has a higher-order interpolation with a reduced integration scheme that provides a balance of accuracy and low computation time and avoids overestimation of element stiffness. Since, these elements use bi-quadratic interpolation functions, they represent the coordinates and displacements more accurately and strains have a quadratic variation

through the element. It also supports the updated Lagrange formulation and hence has been selected for FE modelling in this work.

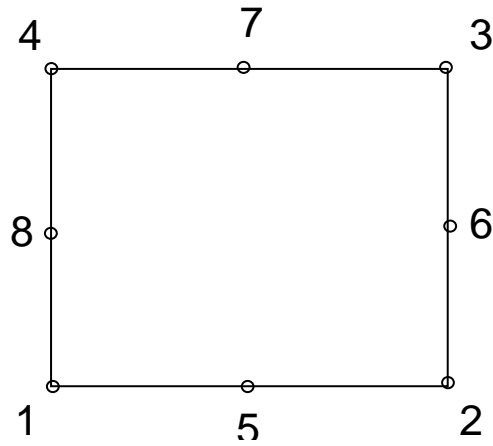


Figure 5.3. Eight node axisymmetric element.

5.2.2.2 Mesh Sensitivity Analysis

After selecting appropriate element type, a mesh convergence study should be carried out. A finer mesh near the contact area results in a more accurate solution, however, as mesh density is increased, computational time increases as well. Hence, in order to balance both accuracy and computational time, a mesh convergence study was performed. Load-displacement plots obtained from the FE were compared with the experimental curves. The following steps were taken for the mesh sensitivity study:

- Start with a mesh using the fewest number of elements with a smallest element size of $1.0 \times 0.6 \mu\text{m}$. In this case convergence was not obtained.
- Recreated the mesh with denser element distribution ($0.5 \times 0.3 \mu\text{m}$) near the contact region and reanalyse the model. This time convergence was obtained and the results were analysed.

- Continue to increase mesh density in contact region until no significant change seen in the obtained results.

The details of mesh convergence study are provided in Table 5.2. The comparison of results from meshes 2, 3 and 4 showed that increasing the mesh density did not significantly affect the prediction of load-depth plots and the results remained in good agreement. However, as seen in Table 5-2, an increase in mesh density increased the computational time. Hence, in order to minimise the computational time, 0.5x0.3 μm was used as the smallest element size for the current study.

Mesh Designation	Smallest element size (μm)	Analysis time (sec)	Total number of elements
M 1	1.0 x 0.6	No convergence	880
M 2	0.5 x 0.3	11455	1360
M 3	0.25 x 0.15	24835	2640
M 4	0.125x0.075	39275	3920

Table 5-2 : Details of the different meshes used in the mesh convergence analysis.

5.2.3 Selection of Material Model

To identify a material model which is suitable to model the indentation behaviour, it is necessary to have some knowledge of the indentation process first. When the Berkovich indenter is used on polymers, we have an initial contact as elastic (although difficult to differentiate) under very small load and there quickly follows non-linear VE deformation. When the stresses beneath the indenter exceed the yield stress, plastic strain starts to accumulate. If the load is held at the maximum load, the material creeps while the stresses under the indenter start to decrease. If the hold or dwell period is sufficient for the material to reach an equilibrium point where the back-stress and applied stress become equal, resulting in zero over-stress, we have an initial part of the unloading that is pseudo elastic followed by recovery. During unloading the contact area and stresses decrease.

Hence, in order to model the indentation behaviour in polymers, a material model is required that should be able to exhibit both time independent and time dependent deformation of polymers. In MSC Marc, we have an option to couple both time independent EP models and rate dependent models together and further details are provided in the next subsections.

5.2.3.1 Pressure Sensitive Model for EP Deformation

The time independent deformation of polymers under the Berkovich indenter is a combination of both elastic and plastic deformation. Since, most polymers also exhibit hydrostatic stress sensitivity, a material model having a hydrostatic stress sensitive yield criterion is required. In MSC Marc Mentat, a pressure sensitive yield criterion, linear Mohr-Coulomb, is available and was used in the current work.

The experimental results from compression tests, at 0.1 mm/min rate at various RH, as described in section 4.3.2, were used to characterise the EP deformation. The elastic property of Accura 60, i.e. Young's modulus, was taken from the bulk compressive tests. Relationship of E with moisture concentration at various RH and its definition in material modelling is detailed in section 6.4. In order to define yielding and the plastic properties, true stress vs. plastic strain relations calculated from bulk compressive test results were used by defining a table. The yield stress and strain hardening behaviour of the material was then estimated from the stress-plastic strain curve with several piece-wise linear segments. In order to define the linear Mohr-Coulomb constants, α and $\bar{\sigma}$, the yield or ultimate stresses determined in tension and compression from the experiments can be used to construct a yield envelope or the following method can be used. Further details on linear Mohr-Coulomb criterion are provided in section 2.3.2.

The following steps were used to calculate the constant, α :

- Calculate ϕ from:

$$\sin \phi = \frac{\sigma_{cy} - \sigma_{ty}}{\sigma_{cy} + \sigma_{ty}} \quad (5.1)$$

- Calculate α from:

$$\sin \phi = \frac{3\alpha}{(1-3\alpha^2)^{1/2}} \quad (5.2)$$

In order to calculate constant, $\bar{\sigma}$, the following steps were taken:

- Calculate 'C' from:

$$C = \frac{\sigma_c (1 - \sin \phi)}{2 \cos \phi} \quad (5.3)$$

- Calculate $\bar{\sigma}$ from:

$$\bar{\sigma} = C[3(1-12\alpha^2)]^{1/2} \quad (5.4)$$

Table 5.3 shows the linear Mohr-Coulomb constants calculated using the above steps from the bulk tensile and compressive tests at various RH after 720 hours of conditioning. These constants were used in the FE model to incorporate the hydrostatic stress sensitivity exhibited by the Accura 60 material at various humidities.

RH	α	$\bar{\sigma}$
33.5%	0.0379	41.527
53.8%	0.0469	29.154
75.3%	0.0654	21.043
84.5%	0.0939	18.046

Table 5-3 : Constants for linear Mohr-Coulomb yield criteria after 720 hours conditioning at various environments.

5.2.3.2 Time Dependent Effects

The time dependent deformation of polymers under the indenter can be described by rate dependent models. In MSC Marc, there are two rate dependent models. The first model is the Maxwell-Wiechart or Generalized Maxwell model, which can be used to describe relaxation behaviour using a Prony series. This model describes linear VE behavior but it does not describe creep and permanent deformation and shows full recovery on unloading.

The second rate dependent model available in the software is the power law creep model. This model shows elastic behavior when stresses are below a defined yield value. However, when stresses are greater than the yield stress, the model describes non-linear VE deformation. Hence, this model can describe both creep and permanent deformation behavior during the loading and is used in the current study. Together with a defined yield, this can be considered to repeat non-linear VP behaviour.

The constants for the creep model were calculated from bulk creep tensile tests. Details of the experimental procedures and results from the creep tests are described in sections 3.5.3 and 4.3.3 respectively. The empirical constants, 'A' and 'm', of the creep power law (Equation 4.3) were calculated using the procedure detailed in section 4.3.3 for various RH and are given in Table 4.4. These constants were used in the creep model in the software to describe the rate dependent deformation of polymeric resin.

5.2.4 Defining Contact

The analysis of contact behaviour is complex as it requires accurate tracking of multiple geometric bodies and their motion due to their interaction during and after contact. This potentially includes friction between the surfaces and heat transfer between the bodies. Different procedures have been developed to treat contact problems such as the augmented Lagrangian method, the penalty method and direct

constraints. Additionally, contact problems require the use of gap elements. However, the easy definition of contact bodies distinguishes MSC Marc from other FEA codes (MSC Marc 2007). Unlike other FEA codes that require manual definition of contacting surfaces, MSC Marc automatically tracks the contacting surfaces and displacement constraint of the contact. It also automatically adjusts the load step to satisfy the contact condition.

Figure 5.4 describes the definition of contact condition between the indenter and the specimen. The specimen in this study was defined as a deformable body containing elements and the indenter as a rigid body. Each node on the exterior and in front of the indenter was defined as a potential contact node and the rigid body was composed of 2D curves. The significant aspect of defining the indenter as a rigid body is that the rigid body does not deform. It was not necessary to completely define the rigid body, however, the contact should not exceed the length of the rigid body and thus the leading edge of the indenter was made sufficiently long.

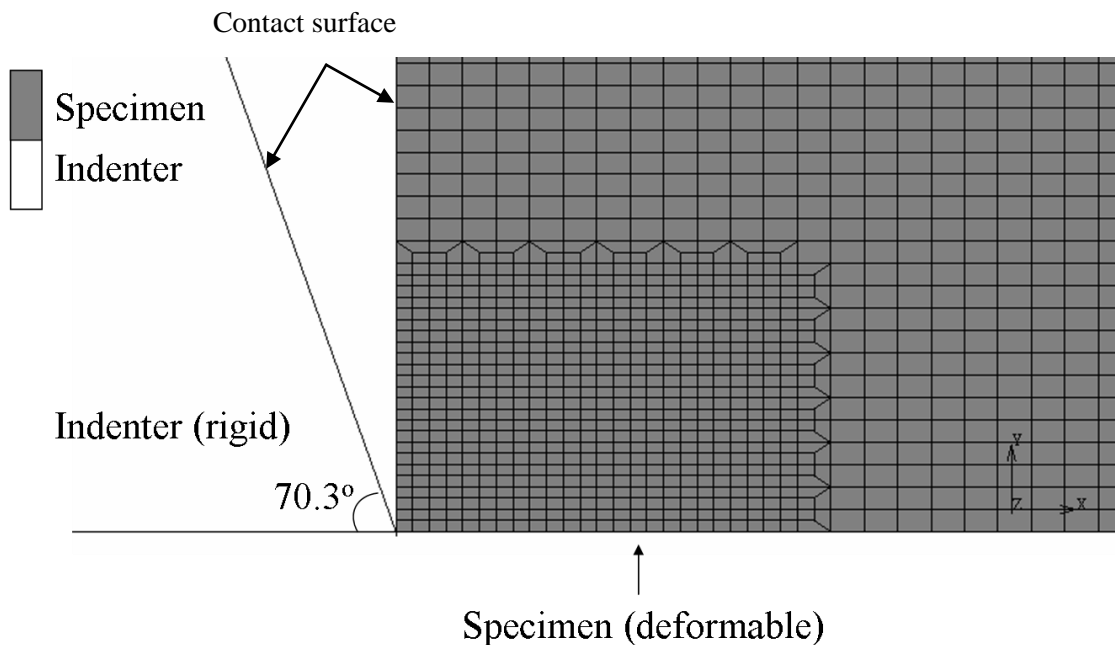


Figure 5.4 : Description of contact condition between the indenter and a specimen.

In MSC Marc and Mentat, the motion of a rigid body can be defined in the following four ways:

- Prescribed velocity
- Prescribed position
- Prescribed load
- Prescribed scaling

Since the experiments involved motion of the indenter under load control, so in FE modelling, the motion of the rigid body was also defined by a prescribed load. When load-controlled rigid body is used, two control nodes can be defined where the first node can have two-translation degree of freedom and the second node, if specified, has one rotational degree of freedom. In this way, both forces and moments can be applied to a body by using the ‘point load’ option for the control nodes. In the current study, only one control node was specified where the point load was applied while the second node was not defined, hence, the rotation of the body was prescribed as zero.

At the beginning of the analysis, bodies can either be separated from each other or in contact. In a DSI experiment, the indenter and the sample are kept in contact for few seconds; hence, similar contact conditions were imposed in the FE model, by keeping the rigid (indenter) and deformable (specimen) body in contact prior to the application of load. In order to avoid any penetration during the initial contact between the bodies, nonzero motion was associated with the rigid body and a contact table was defined to improve the efficiency and computational cost during the analysis. The contact table was also used to separate contact nodes from the rigid body by using a gradual release criterion at the end of iterations.

During the contact process, it is unlikely that a node exactly makes contact with the rigid body; therefore, a contact tolerance can be defined. However, the size of

contact tolerance can have significant impact on the computational cost and solution accuracy. For example, a small contact tolerance can lead to a high computational cost while a large contact tolerance can affect the solution accuracy. As per the recommendations by the software developers, the default error tolerance was selected in this work which is 1/20 of the smallest element size.

In the case of contact between two bodies, phenomenon of friction is also involved, which is a characteristic of factors such as surface roughness, temperature, normal stress and relative velocity. The actual physics of friction and its numerical modelling is complex and continues to be a topic of research. It was found in one study that for cones with included half angle of more than 60° , the friction phenomenon has no significant effect on results (Bucaille et al. 2003). Since, in the present work, the conical indenter modelled has a 70.3° included half angle, the effects of friction were not considered between the rigid and deformable bodies.

During contact simulation, the objective is to deform the specimen and this can result in significant mesh distortion. Also, there is the possibility of the penetration of a node into the rigid body. This problem can be resolved by using a rezoning or adaptive meshing technique. In this study, an adaptive meshing technique was used that generated a greater number of elements and nodes near the contact region by automatically subdividing the elements within the time steps of the solution leading to faster convergence and greater accuracy of the solution.

During contact analysis, a constraint minimisation problem is being solved where the constraint is the 'no penetration' constraint. In Marc, mathematical constraints are applied to the system by using Lagrange multipliers for standard contact problems or by the penalty stiffness method for explicit dynamic problems such as crash simulation. In the current work, the default procedure of constraint, Lagrange multiplier, is used.

5.2.5 Solution Procedure for FE Analysis

The nonlinear iteration procedure can be either full Newton-Raphson or modified Newton-Raphson. The algorithm used by the Newton-Raphson method constitutes an estimation of the displacement for an applied load. Thereafter, the solution is checked for convergence. In the case of non-convergence, the tangent stiffness matrix is evaluated at each iteration and the residual force used to drive the solution to convergence. The modified Newton-Raphson method, though being an inexpensive method as the tangent stiffness matrix is only formed and decomposed once, was not selected because the potential for non-convergence is higher.

A nonlinear analysis usually utilises incremental load (or displacement) steps. At the end of each increment the structure geometry changes and possibly the material is nonlinear or the material has yielded. Each of these things, geometry change or material change, may then need to be considered as the stiffness matrix is updated for the next increment in the analysis. An explicit or implicit incremental procedure can be implemented. An explicit FEM analysis updates the stiffness matrix based on geometry changes/material changes (at the end of each increment). Then a new stiffness matrix is constructed and the next increment of load or displacement is applied to the system. In this type of analysis the hope is that if the increments are small enough the results will be accurate. One problem with this method is that it needs many small increments for good accuracy and thus is time consuming. On the other hand, if the number of increments is not sufficient, the solution tends to drift from the correct solution. Additionally, this method does not enforce equilibrium of the internal structure forces with the externally applied loads. An implicit FEM analysis is the same as the explicit with the addition that after each increment the analysis carries out Newton-Raphson iterations to enforce equilibrium of the internal structure forces with the externally applied loads. The implicit type of analysis tends to be more accurate and can take somewhat bigger increment steps. If carried out correctly the Newton-Raphson iterations have a quadratic rate of convergence which is very desirable. Therefore, the implicit method is used in the current work.

Because of the complexity of non-linear analyses, the solution of most non-linear problems requires an incremental solution schemes and several iterations within each load/time step to achieve convergence. In MSC Marc, an adaptive multi-criteria scheme is available for contact analysis and was used to specify the load step procedure in this work. Table 5-4 describes the adaptive stepping criteria. Automatic time step cut back was used to adjust the increment size as necessary while relative displacement was specified as the criteria for the convergence testing.

Adaptive Stepping criteria	
Initial fraction of loading time	9e-5
Minimum fraction of loading time	9e-5
Maximum fraction of loading time	9e-3
Maximum number of steps	99999

Table 5-4 : Details of adaptive stepping.

Results of the FE modelling of nanoindentation and their comparison with experimental results are detailed in Chapter 6. Moisture diffusion analyses were also incorporated to model indentation behavior at various RH. The details of moisture diffusion and coupled diffusion-stress analyses are provided in sections 5.3 and 5.4 respectively.

5.3 Moisture Diffusion Analysis

Moisture diffusion analysis is carried out by using the analogy between heat transfer and diffusion equations. This analogy is based on the idea that just as a temperature gradient constitutes the driving potential for heat transfer, a concentration gradient provides the driving potential for moisture transfer. Table 5.5 illustrates the analogy between Fickian moisture diffusion and heat transfer by conduction.

Heat Transfer	Moisture diffusion
Fourier's two laws of heat conduction:	Fick's two laws of diffusion:
$F = -k \frac{\partial T}{\partial x}$	$F = -D \frac{\partial C}{\partial x}$
$\frac{\partial T}{\partial t} = \left(\frac{k}{c\rho} \right) \frac{\partial^2 T}{\partial x^2}$	$\frac{\partial C}{\partial t} = D \frac{\partial^2 C}{\partial x^2}$
Where 'k' is thermal conductivity, 'c' specific heat, 'T' temperature, 't' time and 'ρ' density.	Where 'D' is diffusion constant, 'C' moisture concentration, 'F' mass flux and 't' time.
Temperature	Moisture concentration
Heat flux	Mass flux
Thermal conductivity	Diffusion constant

Table 5-5 : Analogy between Fickian moisture diffusion and heat transfer.

MSC Marc can be applied to solve full range of 2D and 3D transient and steady-state moisture diffusion (heat conduction) problems. The software provides heat transfer elements that are compatible with stress elements (MSC Marc 2007). Hence, the same mesh can be used for both the moisture diffusion and stress analyses. Transient heat transfer is an initial-boundary value problem, so proper initial and boundary conditions must be prescribed to the problem in order to obtain a realistic solution.

The FEA method has the ability to analyse the transient moisture diffusion response using the single and dual Fickian models. The dual Fickian model can be implemented by combining the FE nodal moisture concentrations of two separate Fickian diffusion analyses. FEA can be undertaken in terms of the normalised

moisture concentration i.e. with respect to the boundary condition applied to the edges of the model. Figure 5.5 shows a plane sheet case with the introduction of moisture at the edge. The mesh described in section 5.2.4 for the contact analysis was also employed in the diffusion analysis. Eight noded quadrilateral moisture diffusion (heat transfer) elements were used. Values of the coefficient of diffusion and the moisture saturation were taken from Table 4-1 to define the diffusion properties of the material. An automatic time-stepping procedure was used for the transient diffusion analysis. Results from the moisture diffusion analyses are described in Chapter 6.

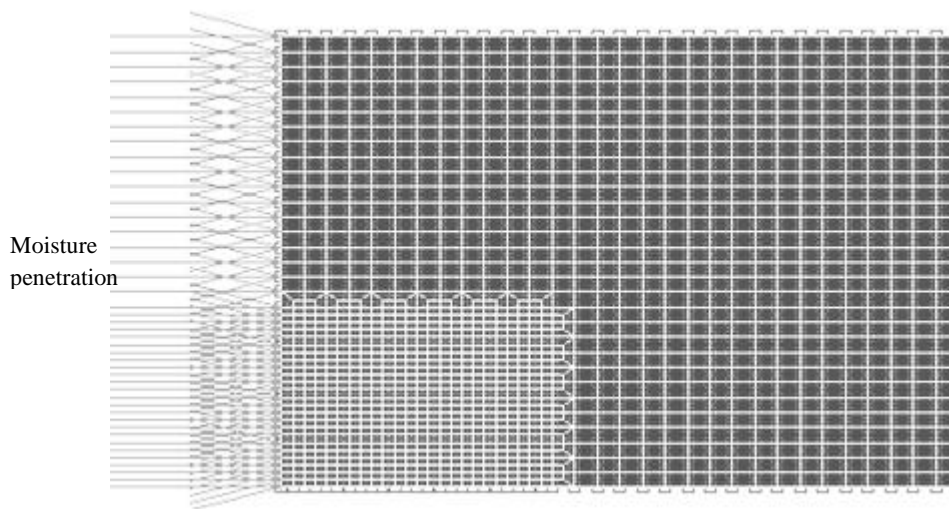


Figure 5.5: Moisture penetration across the specimen.

5.4 Coupled Diffusion-Stress Analyses Technique

A coupled analysis technique available in the MSC Marc software was used to define the multiple physical phenomena. Two types of numerical techniques are available for coupled analysis; direct and sequential. A direct-coupled analysis accumulates all the physics fields in one matrix and solves the whole matrix whereas in sequential coupling, the equation for one field is partially solved and the results are passed as loads to the next field to drive its partial solution and so on until all the steps of iteration are completed (MSC Marc 2007). In the present study, moisture diffusion

and the subsequent effects of diffusion on the indentation behaviour of the Accura 60 samples were carried out using a sequentially coupled hygro-mechanical analysis. Figure 5.6 shows the flow chart of the sequential coupled algorithm. Initially, a transient hygroscopic analysis was carried out to determine the nodal moisture concentrations at time, t_0 . These were then passed to a mechanical model to solve for deformation and stresses under the influence of moisture. The time was incremental but Δt and the procedure repeated until the end time, t_e , was reached.

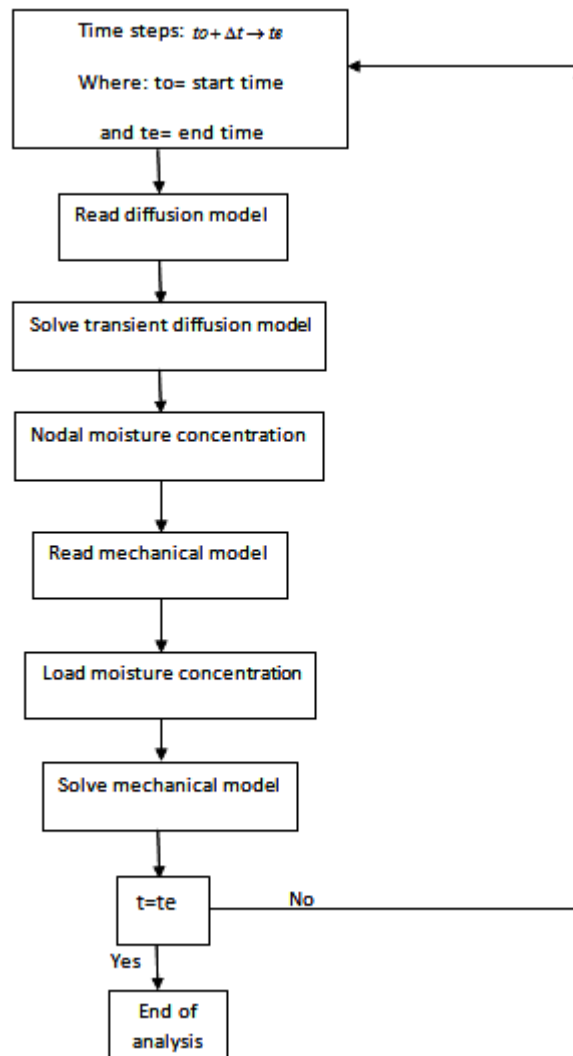


Figure 5.6: Flow chart of sequential-coupled diffusion-stress analysis performed in MSC Marc.

5.5 Summary

The methods employed in the development of the FE models have been discussed in this chapter. 2D axisymmetric FE analyses were performed using a sharp conical indenter to represent the Berkovich geometry. A continuous mesh was used to discretise the geometry, where smaller elements were used near the contact region. The elements were selected based on suitability for contact and far-field analyses were performed to determine an appropriate sample size. Mesh sensitivity analyses were carried out to determine the least number of elements for an accurate solution in order to save computational time. An adaptive meshing technique was used to ensure the mesh remained suitable in the contact region, leading to faster convergence and increased accuracy of the solution. A pressure sensitive EP material model in conjunction with a rate dependent power law creep model was used to model the indentation behaviour. Further details of verifying the FE model and its subsequent use are given in Chapter 6. Transient moisture diffusion analyses were carried out using the analogy between Fourier's law of heat transfer and Fick's law of diffusion. A sequentially coupled hygro-mechanical analysis was carried out to model the indentation behaviour at various RH. Details of the comparison of FE and experimental results to verify the proposed FE model at various environments and the application of the FE model to map hardness at various depths at various RH are described in Chapter 6.

Modelling the Depth Sensing Indentation Response of Polymers by Finite Element Analysis

6.1 Introduction

This chapter describes the depth sensing indentation (DSI) response of the stereolithography (SL) resin at various RH using finite element (FE) modelling and compares the predicted results with the experimental results given in Chapter 4. First the material model used for FE modelling of the DSI response of the SL resin is verified at different loading and unloading rates and dwell periods under ambient conditions (33.5 % RH). There follows the results from the transient diffusion modelling. A FE based approach is used to introduce a methodology for the prediction of moisture concentration distribution under varying moisture conditions as a function of time. The moisture diffusion methodology was implemented in the commercial finite element code MSC Marc using the analogy between conduction heat transfer and moisture diffusion. The implementation was verified by comparing the results of the FEA models with analytical models. The input parameters for the moisture diffusion model were taken from Table 4.1. In order to study the effects of varying moisture on indentation behaviour, a coupled diffusion-stress analysis was carried out and the results compared with the experimental results. Once the model was verified, FE modelling was used to predict the spatial variation in moisture and hardness at various indentation depths and the proposed estimation methodology was compared with the experimental results.

6.2 Verification of proposed FE model exhibiting DSI response

This section compares the FE modelling results with experimental results for various testing parameters in order to justify the selection of the material model

used in the current study. As discussed in Chapter 5, the time dependent deformation behaviour was defined by a power law creep model, which was coupled with a linear Mohr-Coulomb based elastic-plastic model. Figure 6.1 shows a comparison of load–depth curves from the FEA model with experimental curves at 33.5 % RH environment. Loading and unloading rates were fixed at 0.5 mN/sec while various dwell periods were used.

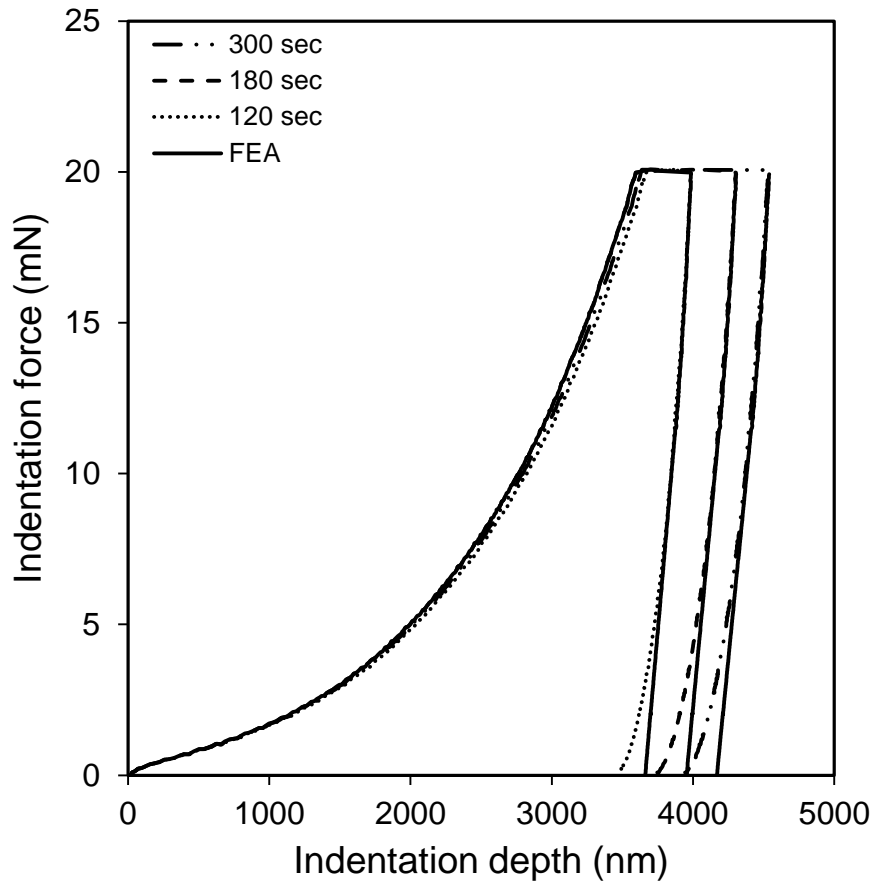


Figure 6.1: Comparison of load-depth plots from FEA with experiments for samples tested at 33.5%RH at 0.5mN/sec loading and unloading rates and different dwells.

It can be seen that there is an excellent match with the experimental curves, except during the last part of unloading. This difference may be attributed to the assumption of frictionless contact and/or the inability of the creep power law to model viscoelastic recovery during last stages of unloading (Altaf et al. 2011a). Another reason for the small differences between the curves could be the difference between the actual tip geometry used in experiments and the ideal conical indenter used in the

modelling. However, all the significant indentation parameters, such as the indentation depth under maximum load, creep in the dwell period and the initial unloading slope, are predicted very accurately by the model (Altaf et al. 2011a).

Figure 6.2 shows comparison of load–depth curves from the FEA model and experiments for samples tested at 33.5 % RH environment at various loading rates with a fixed unloading rate of 0.5 mN/sec and no dwell period. Again, the match of FE and experimental curves is excellent during the loading stage and the initial unloading stages where the model accurately predicts the creep or ‘nose effect’ due to the absence of hold period. Other factors for variation during last parts of unloading are the same as discussed in above paragraph for Figure 6.1.

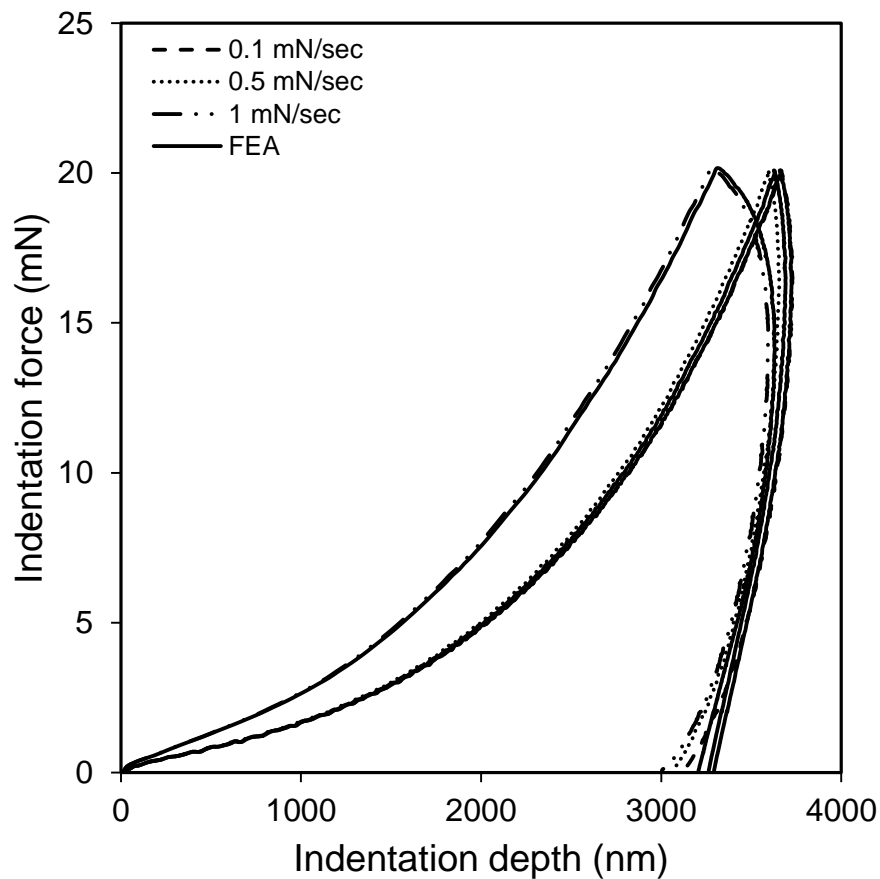


Figure 6.2: Comparison of load-depth plots from FEA with experiments for samples tested at 33.5%RH at various loading rates and 0.5mN/sec unloading rate.

These results from the FEA clearly show that the load–depth response from the DSI of Stereolithography polymers can be predicted with good accuracy by employing a creep power law material model coupled with a linear Mohr-Coulomb yield based elastic-plastic model. Hence, this model is used for modelling the indentation behaviour of the SL resin in the rest of this chapter.

6.3 Transient diffusion modelling

Before performing transient diffusion modelling on the geometry used for contact analysis, both Fickian and dual Fickian FE models were first compared with the analytical models given in equations 2.19 and 2.25 for simple geometries. This comparison was made to establish whether the transient diffusion FE model compares well with the analytical model for bulk test samples before combining with the contact analysis. The geometry used for the analysis is shown in Figure 6.3. Eight noded quadrilateral continuum elements with an average element size of 0.25x0.25 mm were used. The constants for both analytical and FE modelling were taken from Table 4.1.

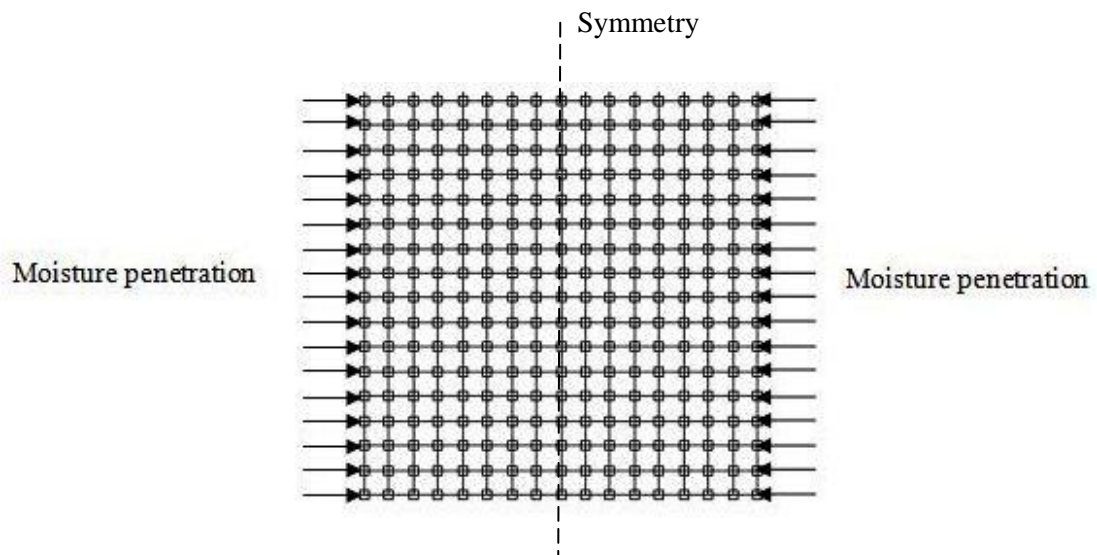


Figure 6.3: Typical finite element mesh for transient diffusion analysis.

Comparisons of normalised moisture concentration from Fickian and dual-Fickian models, using both analytical and FEA techniques are shown in Figures 6.4 & 6.5 for

samples conditioned at various RH for 8 hours and 20 hours respectively. Due to symmetry, only half of the distance through the sample thickness is shown.

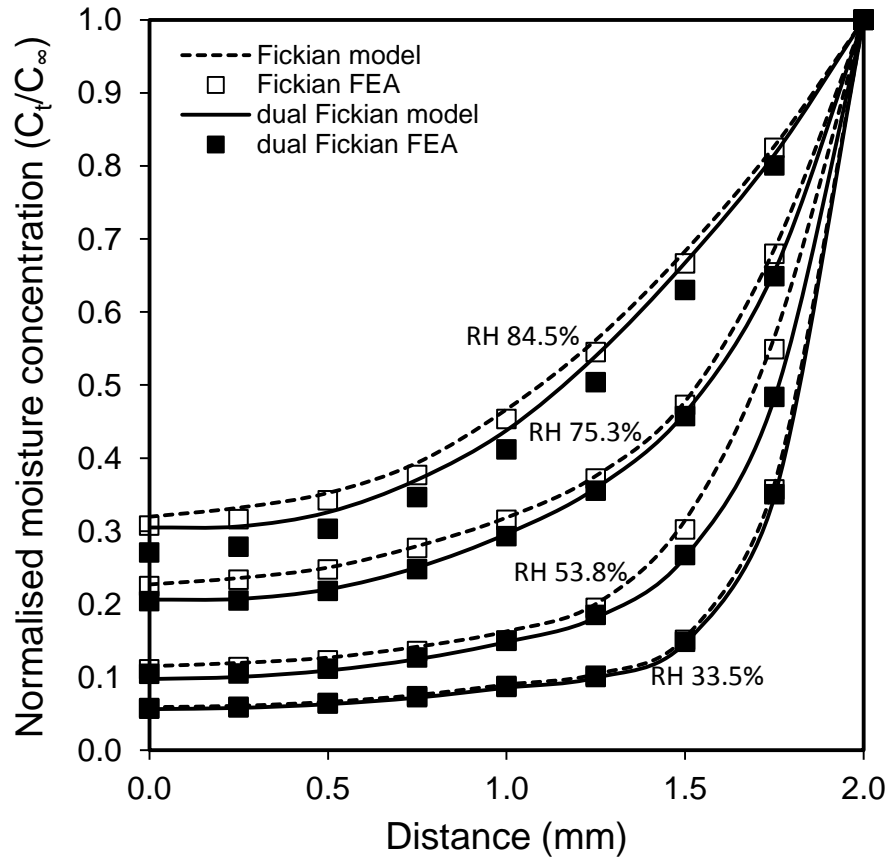


Figure 6.4: Normalised moisture concentration profile through 4mm thick samples after 8 hours conditioning under various relative humidity conditions.

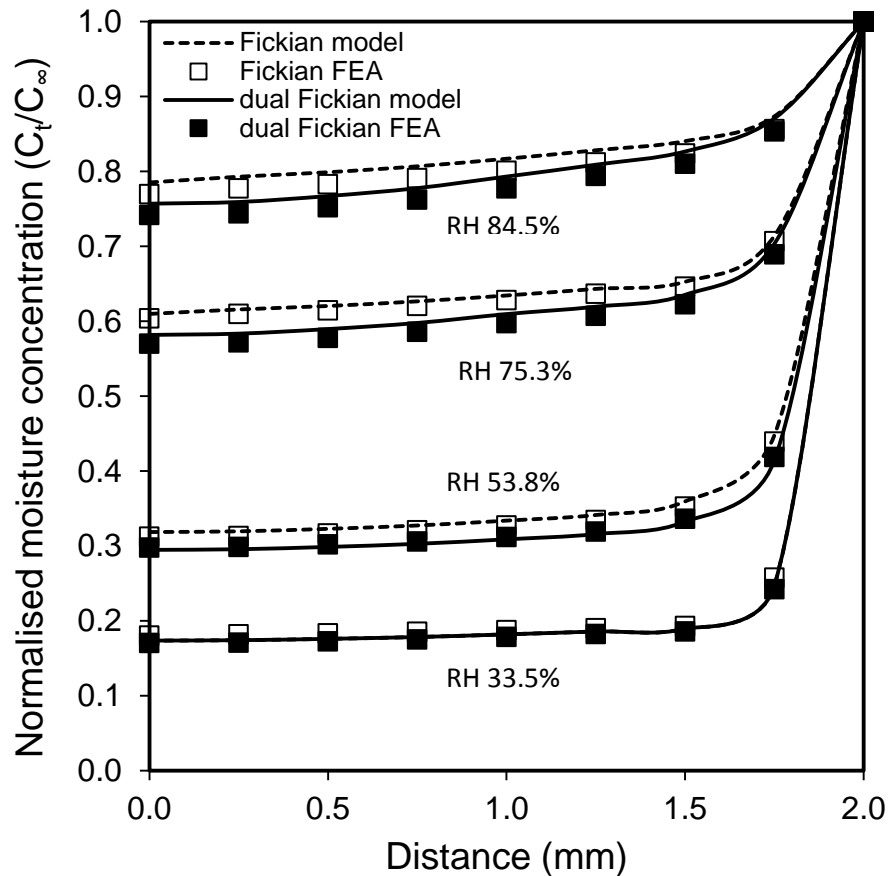


Figure 6.5: Normalised moisture concentration profile through 4mm thick samples after 20 hours conditioning under various relative humidity conditions.

Both plots show that concentration increases with time and varies through the sample thickness. Also, for the same conditioning time, the moisture concentration is higher for samples stored at a higher % RH. It can be seen that there is a good correlation between the analytical and FEA results for both diffusion models, with the FEA predicting slightly lower concentrations. The Fickian and dual-Fickian models result in similar concentration profiles, with the Fickian model predicting higher concentrations, particularly at higher RH and after an increase in conditioning time. This trend can be explained by observing the mass uptake plots shown in Figure 4.3. This shows that the dual-Fickian model correlates very well with the experimental data whilst the Fickian model over-predicts the moisture content, particularly in the time period corresponding to the greatest over-prediction seen in the concentration

profiles. Similar trends were found in our previous work on similar SL resins (Ashcroft et al. 2011).

Figure 6.6 shows a plot of logarithmic values for saturated moisture concentration at various % RH conditions for samples conditioned at different % RH. The trend of the plot supports a logarithmic power relation between saturated concentration and % RH.

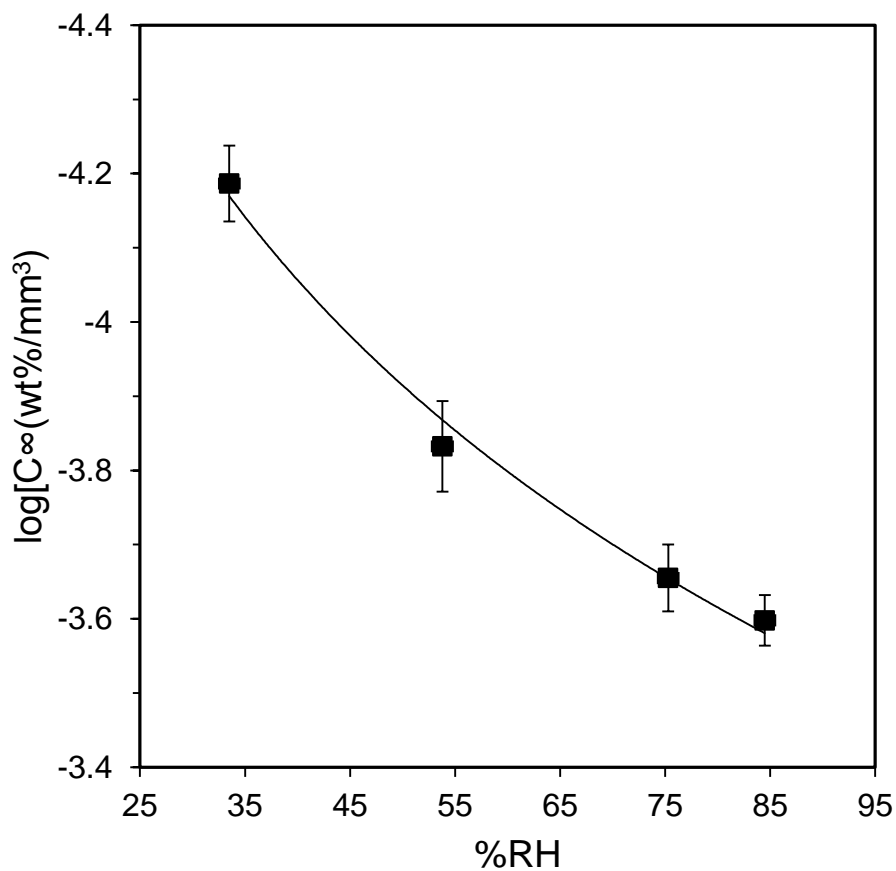


Figure 6.6: Logarithmic values of moisture concentration at various %RH for 4mm thick samples against relative humidity.

It can be seen from the predicted results that the FEA and analytical methods agree well and the difference in results between the Fickian and dual Fickian uptake models illustrate the pseudo-Fickian behaviour of the SL material. Therefore, the

dual Fickian FE model will be used for the diffusion analysis of Accura 60 SL resin. Once this diffusion model is coupled to contact-stress model, we can model indentation behaviour at various RH. However, before implementing the diffusion-stress coupled analysis, it is necessary to develop an analytical model that can predict spatial and temporal changes in elastic modulus, E , due to changes in moisture concentration and this model is developed in the next section.

6.4 Proposed relationship between elastic modulus and moisture concentration

As moisture is absorbed, the concentration at a specific point within the specimen increases with time and this reduces the value of Young's Modulus, E , which gradually varies from the dry modulus, E_d , to the saturated modulus, E_s . It is proposed that Young's Modulus, E , varies with the concentration, C , according to Equation 6.1:

$$E_t = E_d - \left[\frac{C_t}{C_\infty} (E_d - E_s) \right] \quad (6.1)$$

Where E_t is the Young's Modulus at time t . This linear relationship may be rather simplistic but has the advantage of only requiring the values of dry and saturated moduli. For Fickian diffusion, Equation 2.19 can be substituted in Equation 6.1, to yield:

$$E_t = E_d - \left[\left(1 - \frac{4}{\pi} \sum_{n=0}^{\infty} \frac{(-1)^n}{2n+1} e^{\left[\frac{-D(2n+1)^2 \pi^2 t}{4b^2} \right]} \cos \frac{(2n+1)\pi x}{2b} \right) (E_d - E_s) \right] \quad (6.2)$$

Similarly for dual-Fickian uptake, Equation 2.25 can be substituted in Equation 6.1, to yield:

$$E_t = E_d - \left[\left(1 - \frac{4}{\pi} \sum_{n=0}^{\infty} \frac{(-1)^n}{2n+1} e^{\left[\frac{-D_1(2n+1)^2 \pi^2 t}{4b^2} \right]} \cos \frac{(2n+1)\pi x}{2b} \right) \cdot C_{\infty 1} + \left(1 - \frac{4}{\pi} \sum_{n=0}^{\infty} \frac{(-1)^n}{2n+1} e^{\left[\frac{-D_2(2n+1)^2 \pi^2 t}{4b^2} \right]} \cos \frac{(2n+1)\pi x}{2b} \right) \cdot C_{\infty 2} \right] (E_d - E_s) \quad (6.3)$$

As elastic modulus, E, is dependent on moisture concentration, then a variable moisture concentration in the sample, as seen in Figures 6.4, & 6.5, will result in a variation in E of the samples. Equations 6.2 and 6.3 were used to calculate the elastic modulus profiles at various times. The values of E for dry and saturated samples determined from compressive tests were used. Figures 6.7 and 6.8 show the predicted change in E after t = 8 and 20 hours for both Fickian and dual Fickian models for 4mm thick samples conditioned at various humidities. It can be seen that the results obtained for the Fickian and dual Fickian models are quite close to each other, with less than 2.25 % variation. The non-uniform decrease in the value of modulus with conditioning can be attributed to the non-uniform moisture absorption causing plasticisation (Ashcroft et al. 2011). Comparison of both figures shows that an increase in conditioning time has negligible effect on values E for 33.5 % RH environment whilst for higher values of RH there is a significant decrease in modulus with time. As would be expected, modulus is lowest at the exposed edges of the samples and highest in the middle of the sample. However, on saturation, a uniform low value of modulus would be expected.

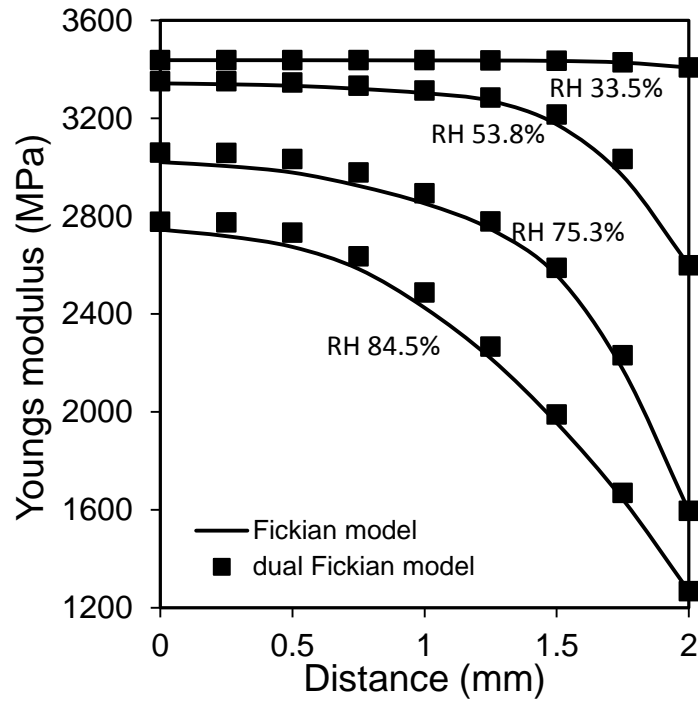


Figure 6.7: Changes in elastic modulus with moisture over time through 4mm thick samples stored under various relative humidity conditions after 8 hours' time.

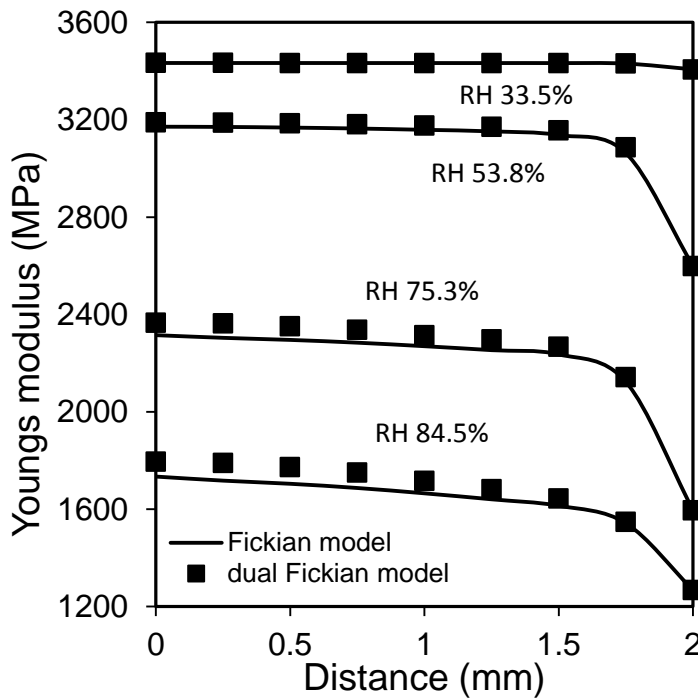


Figure 6.8: Changes in elastic modulus with moisture over time through 4mm thick samples stored under various relative humidity conditions after 20 hours' time.

Figure 6.9 shows an experimental plot of E as a function of moisture concentration. The plot indicates a linear relationship and hence fully supports the linear model proposed in Equation 6.1. A similar linear trend was observed when with other SL resins in our previous work (Ashcroft et al. 2011).

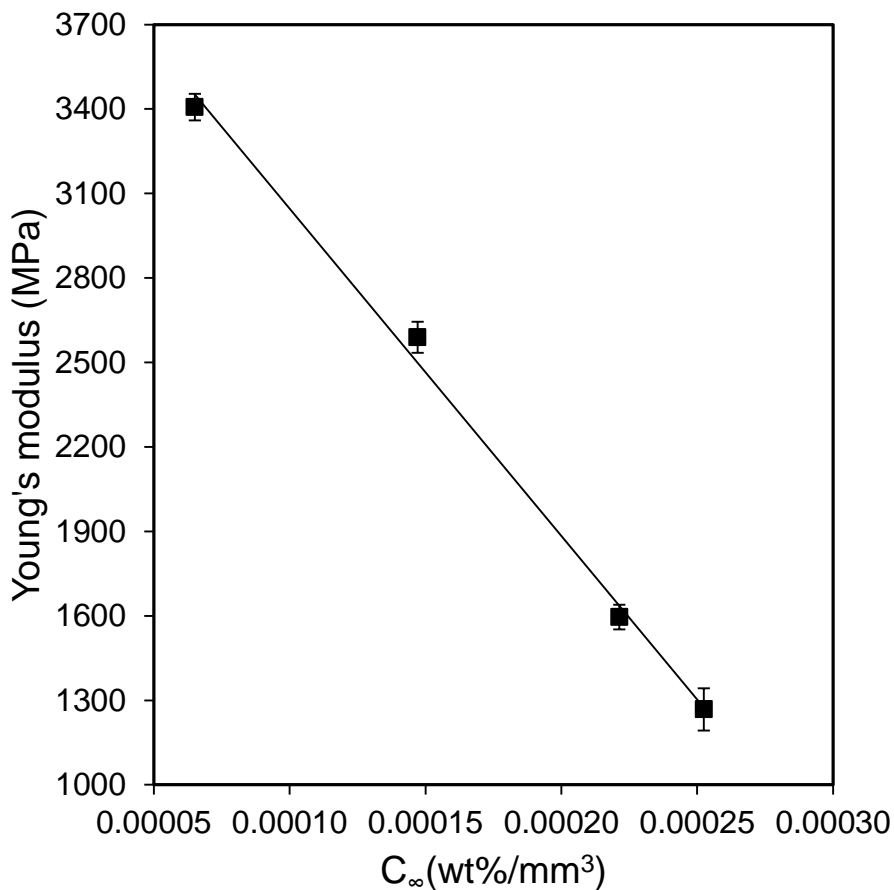


Figure 6.9: Modulus of elasticity as function of moisture concentration for 4mm thick samples.

The relation between E and C needs to be described when defining the material properties in the FE model. Therefore, values of E taken from bulk compressive tests with varying values of moisture concentration were used for this purpose. In the FEA this relationship was used to determine the value of E assigned to each element at different RH environments and conditioning times. Rate dependent material model parameters and elastic-plastic pressure dependent properties at various RH were also

defined as function of moisture concentration to complete the material properties definition step in the FE model. Details are provided in section 5.2.3. The next section compares load-depth plots determined from the FE model with the DSI based experimental curves at various RH in order to investigate the ability of proposed methodology in modelling the indentation behaviour of SL resin at various humidities.

6.5 Investigation of RH effects on indentation by FE modelling

Results from the coupled stress-diffusion FE analyses, performed by incorporating transient moisture diffusion into a contact stress analyses of the indentation process are discussed in this section.

In Figure 6.10, load–depth curves from the FEA model are compared with experimental curves at 33.5 %, 53.8 % and 84.5 % RH environments after the conditioning of samples using the HCU for 24 hours at 22.5 °C and tested in the same environment. It can be seen that penetration depth increases with an increase in RH. This trend highlights the increase in surface moisture concentration with an increase in humidity in the conditioning environment. It can be seen that there is an excellent match between the FEA and experimental curves, except during the last part of unloading. This difference may be attributed to the assumption of frictionless contact and the inability of the creep power law to model viscoelastic recovery during unloading. As with the FE results at ambient, as detailed in section 6.2, all the significant indentation parameters, such as the indentation depth under maximum load, creep in the dwell period and the initial unloading slope, are predicted very accurately by the model for all the RH conditions.

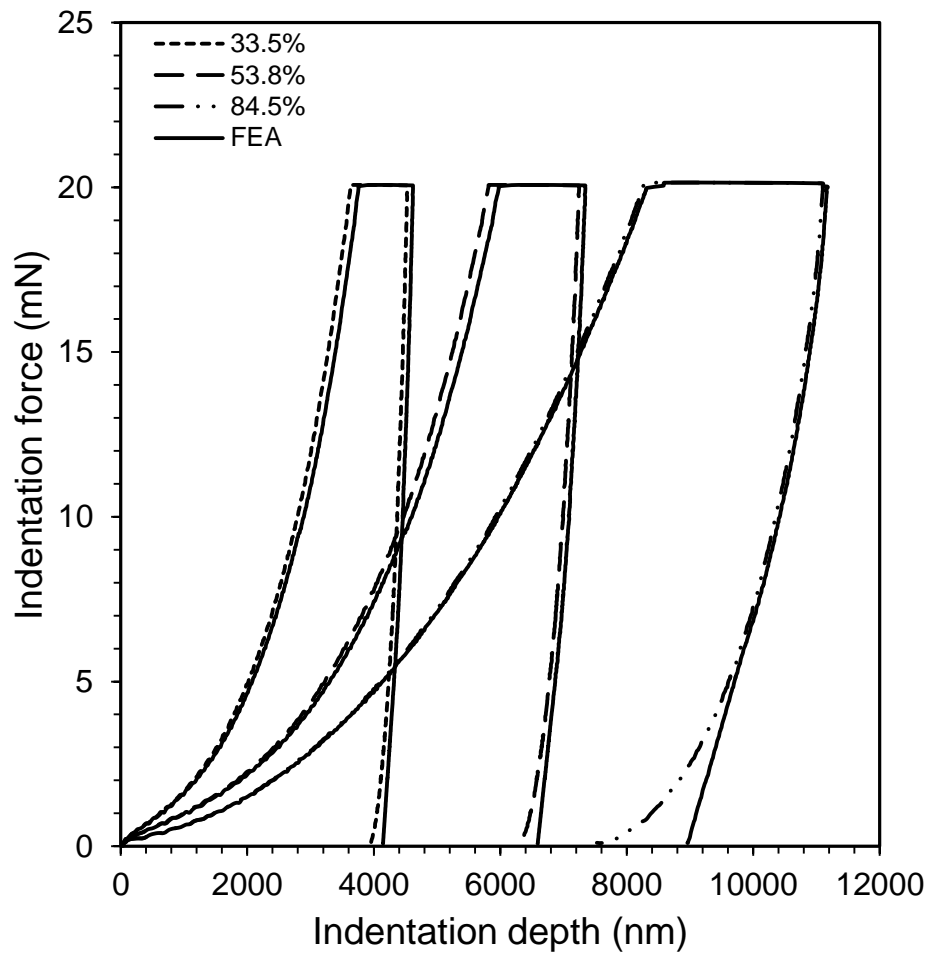


Figure 6.10: Comparison of load–depth plots of FEA with experiments of samples conditioned by HCU for a day under various % RH and tested under the same conditioning environments.

Figure 6.11 compares the load depth plots for the FEA with experiments for samples conditioned for various times at 84.5 % RH and tested under the same conditioning environment. Experimental and FEA curves at 33.5 % RH are also plotted for comparison of the driest environment with the highest % RH conditioning environment. The plots highlight the increase in surface moisture concentration and accompanying reduction in mechanical resistance, with an increase in conditioning time. The first 24 hours conditioning results in a rapid decrease in the mechanical

resistance to indentation owing to the fast initial increase in surface moisture concentration. The rate of increase in penetration depth decreases with time as the surface layers reach equilibrium moisture content. Again, it can be seen that the FE model predicts the experimental curves at various conditioning times to good accuracy.

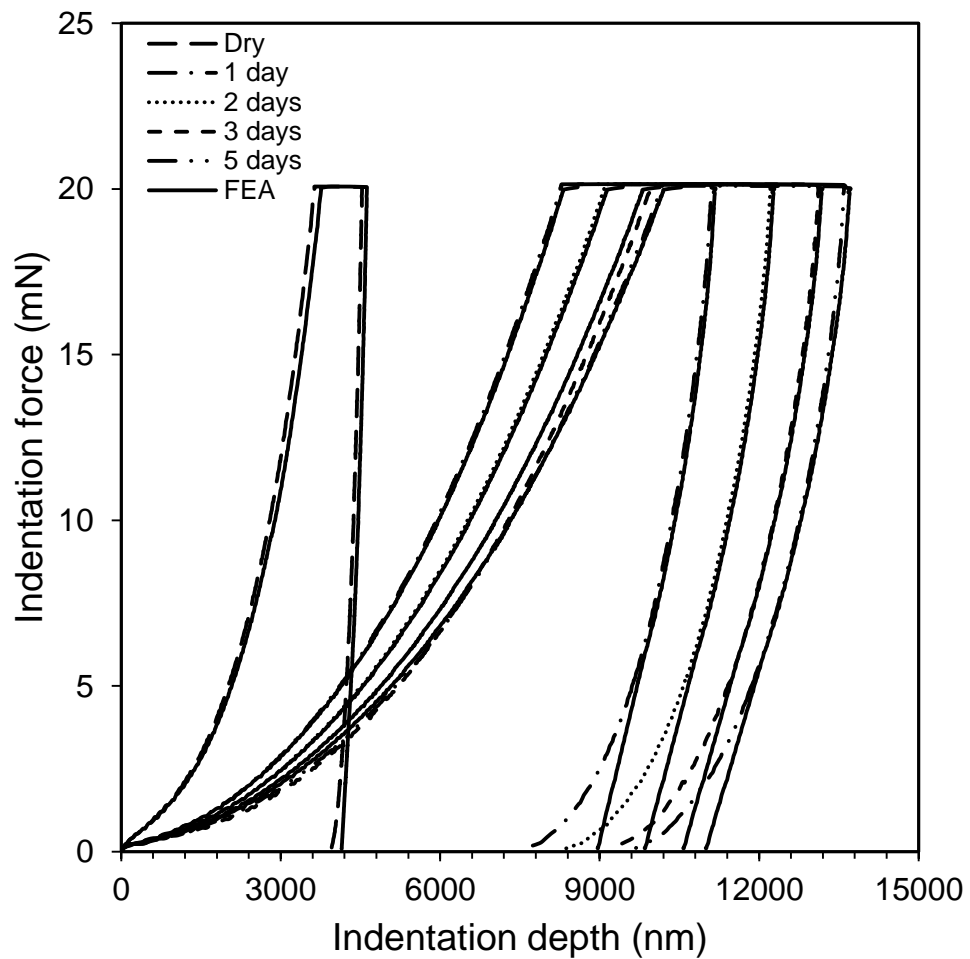


Figure 6.11: Comparison of load depth plots of FEA with experiments of samples conditioned by HCU for various days under 84.5 %RH and tested under the same conditioning environment with plot at dry (33.5%RH) taken as reference.

Results from the FEA modelling show that the load–depth response from the DSI of polymers under varying % RH can be predicted with good accuracy by employing a

coupled stress-diffusion FEA with appropriate moisture and time dependent material and diffusion models. Therefore, it is proposed that indentation hardness can be predicted under various environments and depths using the proposed FE model this is discussed in the next section.

6.6 Estimation of Hardness

Since load-depth plots from FE modelling match closely with the experimental curves, as detailed in the previous section, we can use the OP method on the FE curves to calculate values of H_e . Figure 6.12 shows a comparison of the calculated values of H_e from FEA and the DSI experiments, measured periodically for 5 days under a 84.5 % RH conditioning environment. The normalised mass of absorbed moisture (M_t/M_∞) is also plotted against conditioning time in the figure. The results show a decrease in the value of H_e with time as a result of the increase in moisture content in the surface layers. It can be seen that the prediction from the FEA compares well with the experimental results.

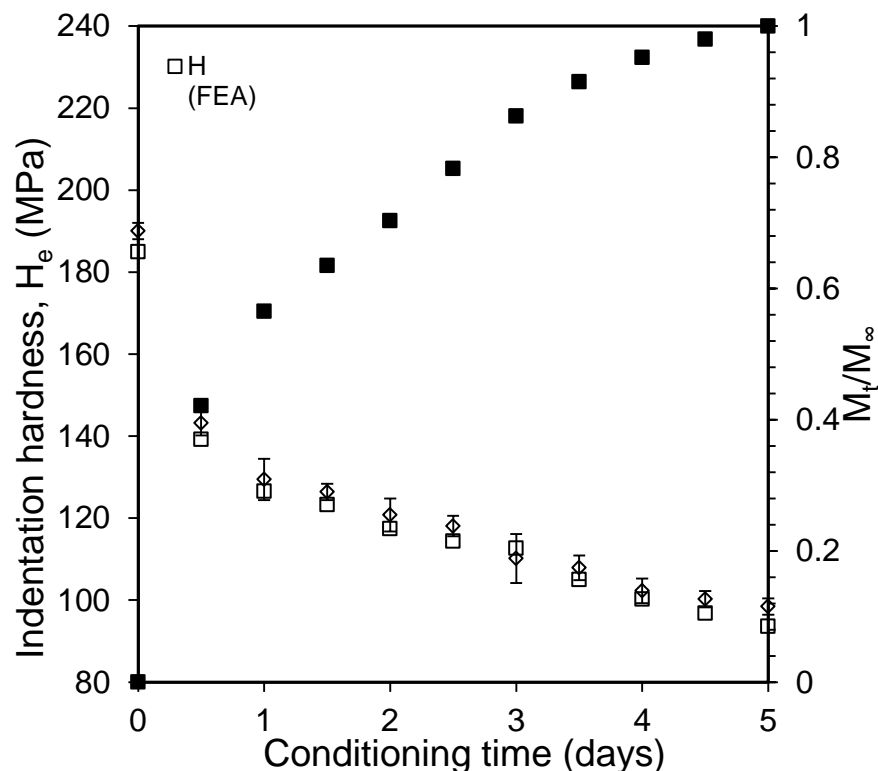


Figure 6.12: Comparison of hardness calculated from FEA modelling with experiments after various days of conditioning and testing at 84.5% RH.

Since the calculated H_e from the FE model matches closely to the experimental results, we can use this model to predict indentation hardness at any conditioning environment and time. Also, indentation hardness can be predicted at various depths at different RH environments by employing the FE model or an inverse method can be used with experimental load-depth curves to predict the distribution of moisture in a sample.

A Berkovich indenter has been used throughout the testing in this research work. With this indenter the slope dP/dh and plastic contact depth, h_p , are used to calculate indentation modulus, E_e , and hardness, H_e . Once the slope dP/dh at maximum load (20 mN) is known for the material at any fixed environment, then it should stay uniform provided we use the same selected parameters during testing i.e. 300 sec dwell, any value of holding load but less than 20 mN and 0.5 mN/sec loading and unloading rates. This assumption can work well above shallow depths where indentation size effects are eliminated and value of modulus (E_e) approaches a constant value. It was reported in the previous work that value of E_e approached a constant value closed to bulk compressive test values for polystyrene samples, when contact depth exceeded 100 nm (Tweedie et al. 2007). In another work on polyethylene-terephthalate (PET) biaxial film, E_e approached constant value after 500 nm contact depth (Beake and Leggett 2002). Therefore, based on the above discussion, contact depths obtained for Accura 60 samples at various RH were sufficient to give uniform unloading slope because E_e was constant at those depth ranges. Thus, H_e may be computed along the loading curve. If 'a' is any point on the loading curve where we want to calculate value of hardness then:

$$h_{p,a} = h_t - P_a \varepsilon \frac{dh}{dP} \quad (6.4)$$

where $h_{p,a}$ and P_a are the plastic depth and load at point 'a' respectively and h_t the total depth at 'a'. Since ε and slope dP/dh are the constant terms whose values are

already known, we can determine the plastic depth from the value of load and total depth at that point. Afterwards, we can calculate hardness at 'a', $H_{e(a)}$, as:

$$H_{e(a)} = \frac{P_a}{24.5h_{p,a}^2} \quad (6.5)$$

Initially, experiments were carried out to measure the values of H_e at various depths and then were compared with the values of H_e calculated using the methodology above with a single experimental curve. The results are shown in Figure 6.13, and it can be seen that the values of H_e calculated from the single load-unload plot match closely with the values of H_e measured directly from the experiments at different loads.

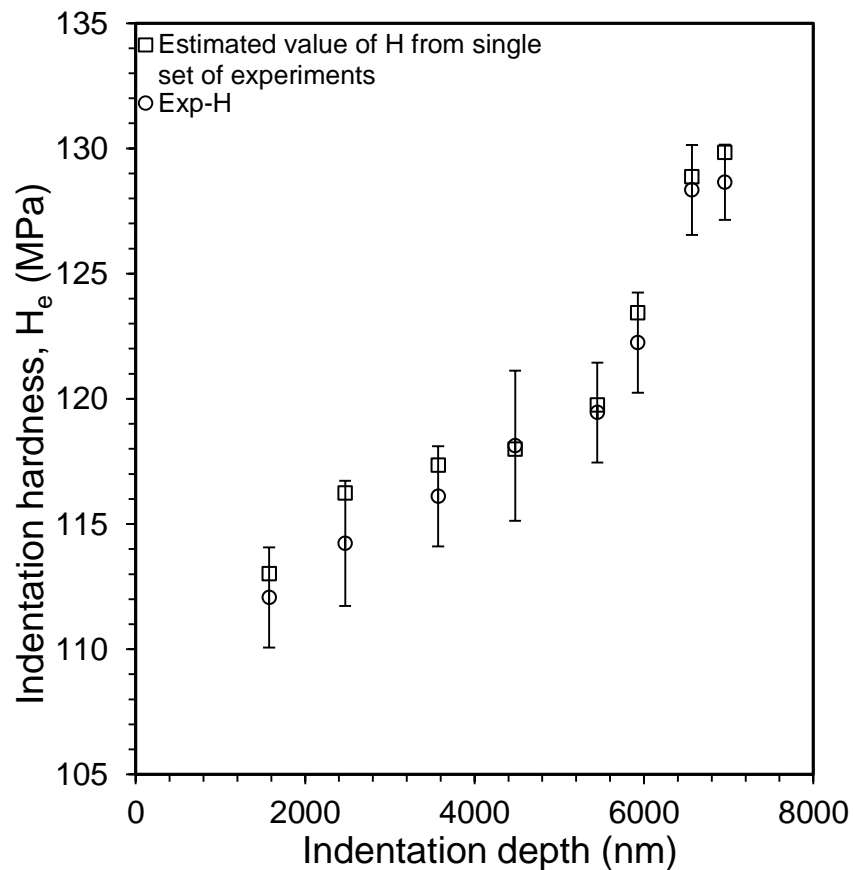


Figure 6.13: Comparison of hardness calculated from estimation method applied on single set of load-depth curves of experiment with experiments performed at various depths inside the specimen after 12 h at 84.5% RH.

Once the methodology was verified, it was used on both FE and experimental curves to calculate hardness as a function of depth. The contact depth h_p at any point was calculated using Equation 6.4. The calculated values were then used in Equation 6.5 to calculate hardness; H_e . Figure 6.14 compares values of H_e at various indentation depths estimated from single load-depth plots of FEA and DSI tests after 12 hours of conditioning at 84.5 % RH. The values of H_e are low at shallow depths due to the influence of the high moisture content; however, they increase at higher depths as the material indented has lower average moisture content. Again, there is an excellent agreement between the FE and experimental results.

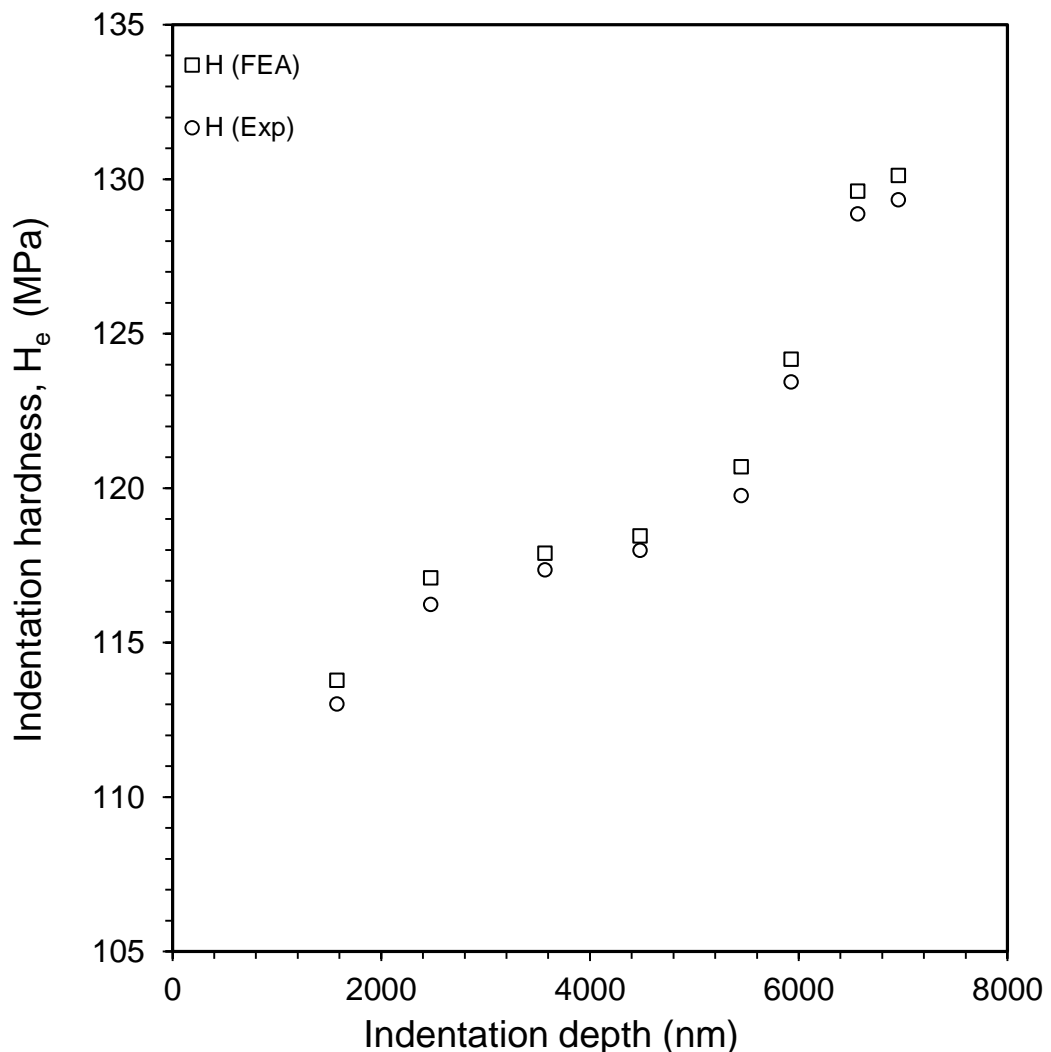


Figure 6.14: Comparison of hardness estimated at various depths inside the specimen from single load-depth plot of FEA and DSI experiment after 12 h at 84.5% RH.

Hence, the proposed method of estimating the value of H_e at various indentation depths from single FE and experimental load-depth curves agree well with each other. Therefore, once moisture has been calibrated as a function of mechanical properties, we can use the FE model to find the spatial variation in the value of hardness and thus the degree of moisture absorbed in a part and its influence on mechanical properties can be investigated using the results from the computational modelling (Altaf et al. 2011a). The FE modelling can also be used to investigate moisture effects on the indentation response at any level of RH and hence save the time required for testing.

6.7 Summary

The effect of moisture, present in the environment, on the mechanical properties of a polymeric SL resin has been investigated using FE modelling. A hydrostatic pressure sensitive Mohr-Coulomb based elastic-plastic model coupled with a creep power law was used as the material model to simulate the depth sensing indentation response of SL resin. With the exception of failing in the last part of unloading, all other significant indentation parameters, such as the indentation depth under maximum load, creep in the dwell period and the initial unloading slope were predicted accurately by the model. In order to model moisture diffusion at various RH environments, a transient diffusion FE technique was used by utilising the analogy between diffusion and heat conduction equations. Comparison of diffusion analysis using both FE and analytic modelling confirmed that the dual Fickian model predicts the moisture distribution with more accuracy than the Fickian model and, hence, this was coupled with the contact-stress analysis. Results from the FEA showed that the load-depth response from the DSI of polymers under varying % RH can be predicted with good accuracy by employing a coupled stress-diffusion FEA with appropriate time and moisture concentration dependent material and diffusion models. It was also demonstrated that the values of indentation hardness could be accurately predicted under various environments and depths using the proposed FEA model. In order to find H_e at various depths, it was proposed that once the slope dP/dh at maximum load is known, then, assuming that E_e remains constant, H_e can be

computed at any point along the loading curve. This method involved calculating plastic contact depth from the simulation results. Values of H_e from the FEA showed a good fit with the experimental data. Hence, this model can be used in predicting the effect of the environment on the performance of SL manufactured components.

|Analysis of Viscoelastic-Plastic Behaviour in Polymers using Depth Sensing Indentation

7.1 Introduction

This chapter describes analysis methods used to determine time dependent material parameters for the SL resin, Accura 60, from depth sensing indentation (DSI) creep data. Rheological models consisting of springs and dashpots are used for the purpose and modelling parameters are calculated from a curve fitting technique. A method is used to calculate both time-independent and dependent mechanical properties from these parameters. These values are compared with the ones calculated using the Oliver and Pharr (OP) method, as detailed in section 4.4, and those calculated from bulk compressive tests, described in section 4.3.2. Comparison with the OP method is used to explore the effectiveness of the use of minimisation of time dependency, and hence use of OP method, in calculating mechanical properties for the SL resin with values calculated from the direct measurement of time-dependent parameters. The comparison of results with bulk tests is used to investigate the effectiveness of the phenomenological modelling approach with DSI data in finding the overall material properties. Finally, analytical modelling is used at various RH to investigate the effects of moisture on the mechanical properties of Accura 60 samples.

7.2 Analytical modelling of indentation behaviour

For materials exhibiting time-dependent behaviour, such as polymers and biomaterials, the use of analysis methods on indentation data, developed for elastic

plastic (EP) materials, can lead to errors. An experimental approach to remove this ambiguity is by introducing sufficient dwell at peak load to minimise the time dependency, as detailed in section 2.6.4, with results in Chapter 4. However, for polymeric resins, the time dependent deformation is an important characteristic, hence, the measurement of time-dependent parameters using analytical approaches, and not their minimisation, is often desired. These approaches include empirical solutions (Oyen and Cook 2003; Yang et al. 2004; Menčík et al. 2009, Menčík et al. 2011) as well as solutions derived from the elastic-viscoelastic correspondence principle (Vandamme and Ulm 2006; Olesiak et al. 2009; Greenwood 2010), which is based on earlier work by Lee and Radok (1960). Further details on the empirical and correspondence methods are given in section 2.6.4.

Simplified phenomenological models based on the mechanical element analogy, analytical treatments and numerical simulations can also be used with indentation data. When a polymer is indented, the deformation can be viscoelastic (VE) or viscoelastic-plastic (VE-P). VE models combine elastic and viscous elements. Their combination can be either in series, giving a Maxwell element or in parallel giving a Kelvin-Voigt (KV) element. For complex cases, VE models usually combine these elements. In order to model the VE-P behaviour that often results from the indentation of polymers by sharp indenters, we have to introduce a plastic element that represents instantaneous plastic deformation, characterised by the yield strength. Hence, a VE-P model combines elastic, viscous and plastic elements in different combinations.

When a sharp tip indenter, such as Berkovich, is used on polymers it provides elastic, viscous and plastic deformations in the material. Therefore, there are two possibilities; either to separate the elastic, plastic and VE deformations and treat them individually or to ignore plasticity and just consider the VE deformation. In the present work, all the indentations were carried out using a Berkovich tip that provided both permanent and recoverable deformations and thus VE-P models were used to determine the material parameters, as described in the next section.

7.3 Elastic-viscous-plastic mechanical modelling

In order to find material parameters characterising the elastic, viscous and plastic properties, a simple five step test can be adopted where the first step involves rapid loading that is followed by a dwell period under the maximum load. The third step involves rapid unloading to a lower value of load while the fourth step involves a dwell period at the lower value of load. The fifth step involves unloading to zero load. In the current research work, a three step procedure, as shown in Figure 7.1, was used that involved fast loading to 20 mN load, holding for 300 sec at that load and finally fast unloading. The reason to not include the hold at low load was due to the non-availability of this feature in the current DSI system. Hence the calculated material parameters are based on creep data while measurements for back-creep to investigate the recovery were not performed.

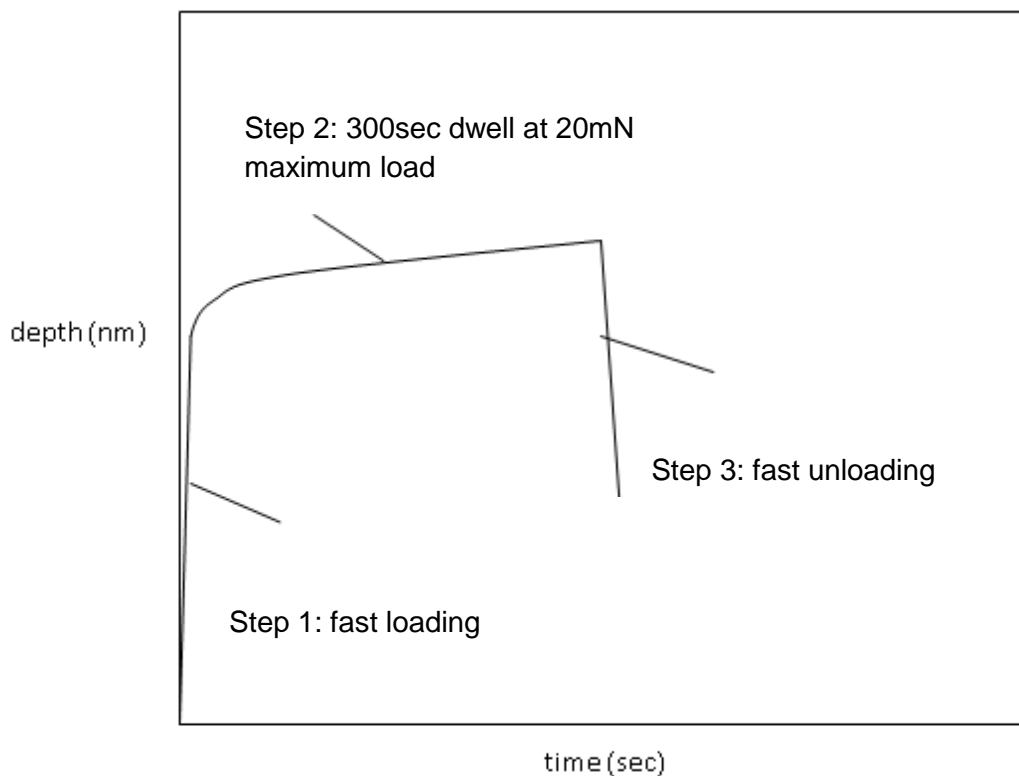


Figure 7.1: Three step procedure to determine viscoelastic-plastic properties.

In the current studies, three combinations of elastic-viscous-plastic mechanical models are used on load displacement curves during dwell. These models consist of springs, dashpots and plastic (or friction) elements.

Figure 7.2 shows an arrangement of an elastic-viscous-plastic (EVP) model-1 consisting of springs, S_1 and S_2 , a dashpot D_1 and a friction element, F_1 . If the load is small enough that stresses beneath the indenter remain below the yield stress, σ_Y , then plastic deformation, h_p , is zero and elastic deformation is represented by spring S_1 . However, in the case of yielding we obtain a deformation that is a combination of the instantaneous elastic-plastic deformation and the viscous deformation represented by springs S_1 and S_2 , and dashpot D_1 respectively.

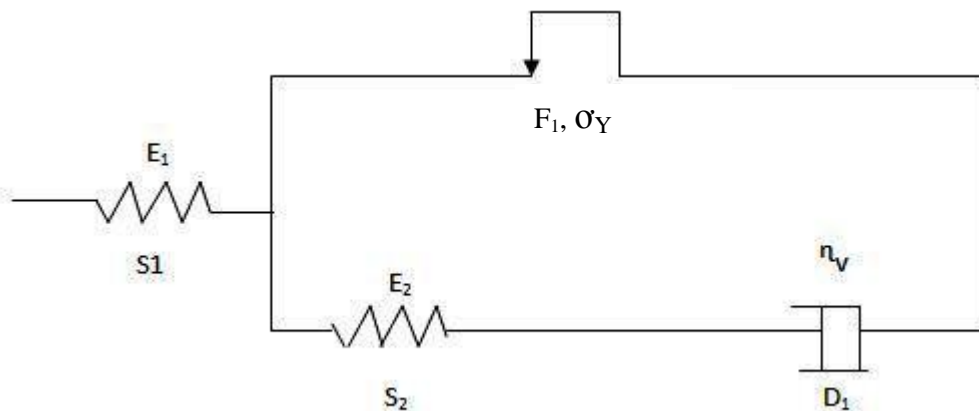


Figure 7.2: Elastic-viscous-plastic model-1.

The following equation shows the relationship between indenter load and depth of penetration for time dependent materials under monotonic loading (Menčík et al. 2009):

$$f(h(t)) = K\psi(P, h, t) \quad (7.1)$$

where 'f' is function, 'h' indentation depth, 't' time and 'K' a constant depending on geometry of indenter and $\psi(P, h, t)$ represents a function that depends on values of load, displacement and time. For the case of a sharp indenter, such as Berkovich (Fischer-Cripps 2004):

$$f(h(t)) = h^2(t) \text{ and } K = \pi/(4 \tan \alpha) \quad (7.2)$$

where α is semi angle of the Berkovich indenter.

For model-1 shown in Figure 7.2, total displacement, h, when stress beneath the indenter exceeds the yield stress, is due to elastic, plastic and viscous deformation given as:

$$h(t) = h_e + h_p + h_v(t) \quad (7.3)$$

$$h(t) = h_{S1} + h_{S2} + h_{D1} \quad (7.4)$$

Since for the Berkovich indenter: $f(h(t)) = h^2(t)$

$$h^2(t) = \frac{P}{E_1} + \frac{(P - P_Y)}{E_2} + (P - P_Y) \frac{t}{\eta_v} \quad (7.5)$$

where P_Y represents the load at yielding. When we use the Berkovich indenter the plastic deformation occurs virtually instantaneously and thus we can assume term P_Y to be so small so that it can be neglected.

$$h^2(t) = P \left[\frac{1}{E_1} + \frac{1}{E_2} + \frac{t}{\eta_v} \right] \quad (7.6)$$

Substituting equations 7.2 and 7.6 in 7.1 gives:

$$h^2(t) = \frac{\pi}{4 \tan \alpha} P \left[\frac{1}{E_1} + \frac{1}{E_2} + \frac{t}{\eta_v} \right] \quad (7.7)$$

The unknown constants in equation 7.7; E_1 , E_2 and η_v were found by minimising the sum of the squared differences between the squares of measured and calculated depths using the solver function in Microsoft Excel 2007. The values of these constants are given in Table 7.1.

Figure 7.3 shows a comparison of the experimental and predicted indentation creep curve for Accura 60 using EVP model-1. The model provides a prediction of the instantaneous indentation depth that contains both elastic and plastic deformations. However, for viscous deformation, the model provides only steady creep deformation and is not able to predict the primary creep, resulting in a poor fit to the experimental indentation creep data. Hence, EVP model-1 needs modification by including a KV unit to enable the prediction of the primary creep.

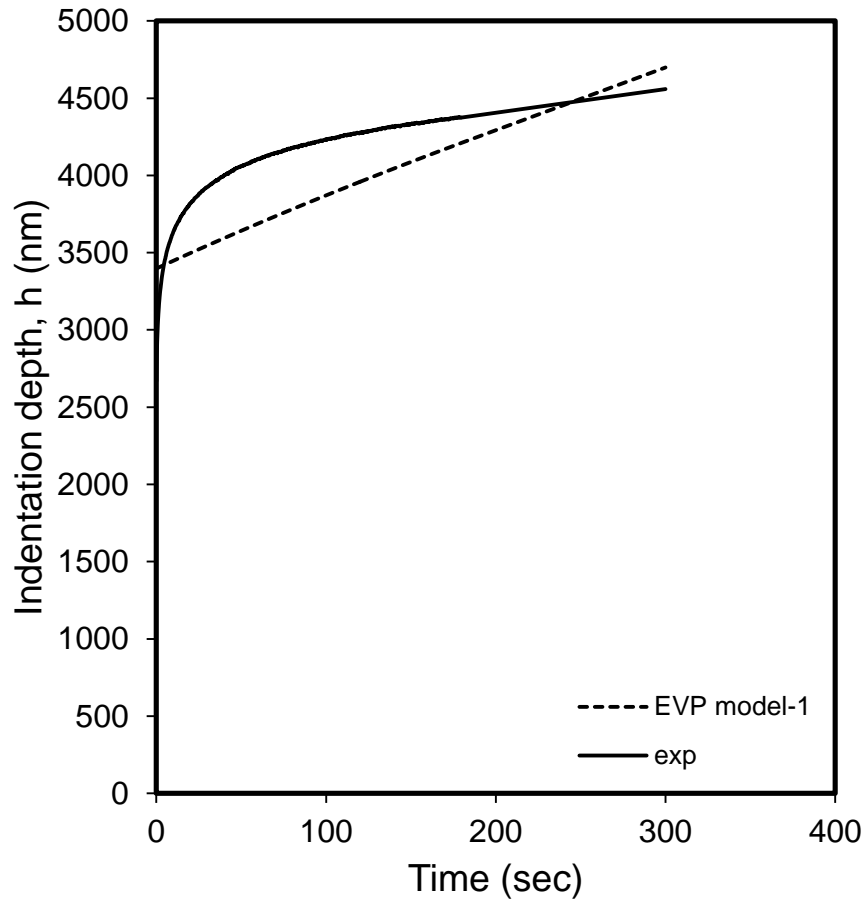


Figure 7.3: Experimental (exp) and predicted (model-1) indentation creep curves for 4mm thick Accura 60 samples tested at 20mN load for 300 sec hold at 33.5%RH at 22.5°C.

Figure 7.4 shows EVP model-2 consisting of springs, S_1 and S_2 , dashpot D_1 , a KV unit and a friction element, F_1 . If the load is small enough that stresses beneath the indenter remain below the yield value than plastic and creep deformation are zero and elastic deformation is represented by spring S_1 . However, in the case of yielding we obtain a deformation that is a combination of instantaneous elastic-plastic deformation and viscous deformation represented by springs S_1 and S_2 , and KV unit and dashpot D_1 . The inclusion of KV unit helps to predict primary creep effectively while dashpot predicts secondary creep.

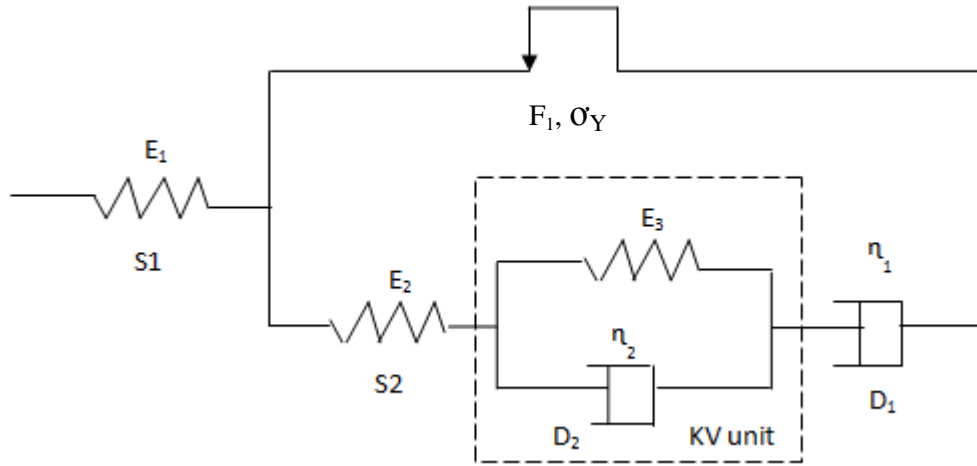


Figure 7.4: Elastic-viscous-plastic model-2.

For EVP model-2, total displacement, h , when stresses beneath the indenter exceed the yield value, is due to elastic, plastic and viscous deformation given as:

$$h(t) = h_e + h_p + h_v(t) \quad (7.8)$$

$$h(t) = h_{S1} + h_{S2} + (h_{KV} + h_{D1}) \quad (7.9)$$

$$h^2(t) = \frac{P}{E_1} + \frac{P}{E_2} + P \frac{t}{\eta_1} + \frac{P}{E_3} (1 - e^{-\frac{E_3 t}{\eta_2}}) \quad (7.10)$$

Substituting $\eta_2/E_3 = \tau$, where τ is a retardation time, gives:

$$h^2(t) = \frac{P}{E_1} + \frac{P}{E_2} + P \frac{t}{\eta_1} + \frac{P}{E_3} (1 - e^{-\frac{t}{\tau}}) \quad (7.11)$$

Substituting equations 7.2 and 7.11 in 7.1 gives:

$$h^2(t) = \frac{\pi}{4 \tan \alpha} P \left[\frac{1}{E_1} + \frac{1}{E_2} + \frac{t}{\eta_1} + \frac{1}{E_3} (1 - e^{-\frac{t}{\tau}}) \right] \quad (7.12)$$

The unknown constants in equation 7.12, E_1 , E_2 , E_3 , τ and η_1 were found by minimising the sum of the squared differences between the squares of measured and calculated depths using the solver function in Microsoft Excel 2007. The values of these constants are given in Table 7.1. Figure 7.5 shows a comparison of experimental and predicted indentation creep curve for Accura 60 sample using equation 7.12 for EVP model-2. The predicted curve fits well to the experimental curve. Model-2 not only provides a good prediction of the instantaneous indentation depth, containing both elastic and plastic deformations, but viscous deformation is also predicted well by including a dashpot and a KV unit.

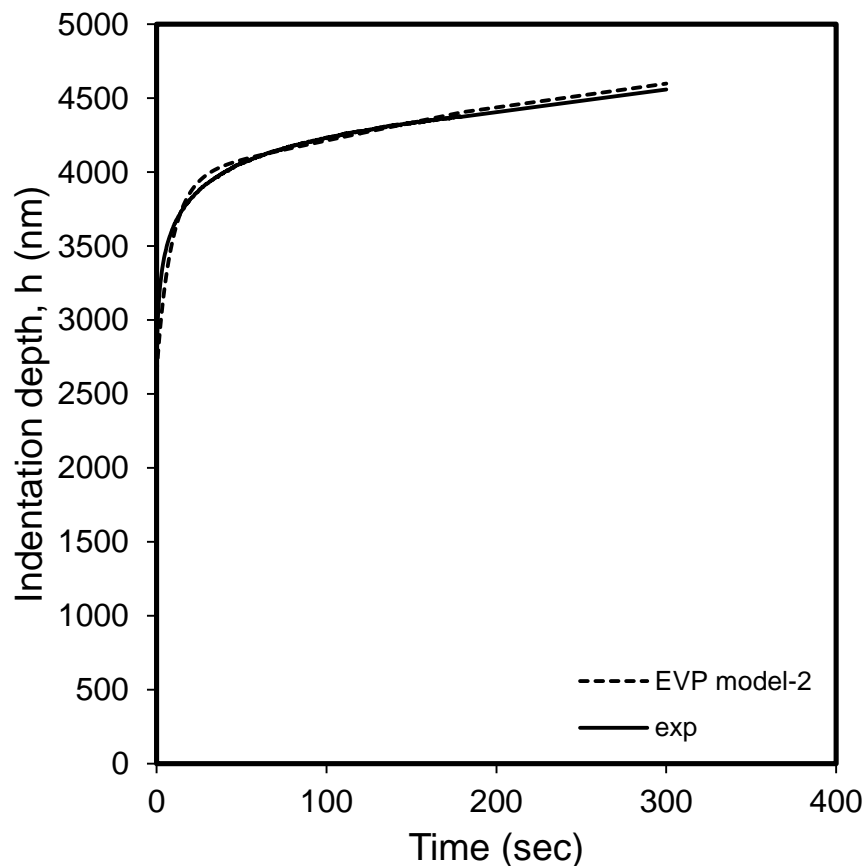


Figure 7.5: Experimental (exp) and predicted (model-2) indentation creep curves for 4mm thick Accura 60 samples tested at 20mN load for 300 sec hold at 33.5%RH at 22.5°C.

Although the prediction using model-2 is quite close to the experimental data, it is proposed that adding an extra KV unit could reduce the error margin further. Therefore, EVP model-3 is included in the study, as shown in Figure 7.6. This model consists of springs, S_1 and S_2 , a dashpot D_1 , two KV units and a friction element, F_1 . If the load is small, such that stresses beneath an indenter remain below the yield value, then plastic deformation, h_p , is zero and elastic deformation is represented by spring S_1 . However, in case of yielding we get h_p , which is a combination of instantaneous plastic deformation and viscous deformation represented by spring S_2 , and two KV units and dashpot D_1 respectively.

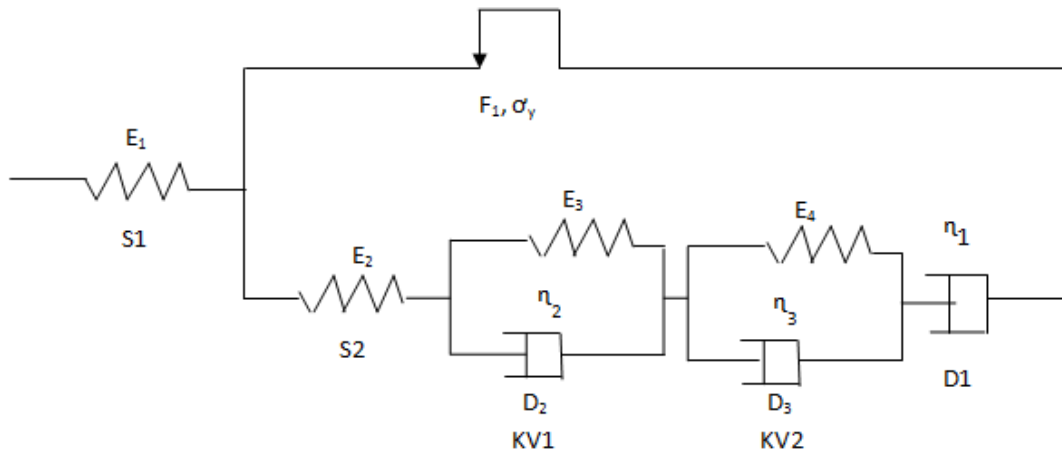


Figure 7.6: Elastic-viscous-plastic model-3.

By including two KV bodies in equation 7.12, we get:

$$h^2(t) = \frac{\pi}{4 \tan \alpha} P \left[\frac{1}{E_1} + \frac{1}{E_2} + \frac{t}{\eta_1} + \frac{1}{E_3} (1 - e^{-\frac{t}{\tau_1}}) + \frac{1}{E_4} (1 - e^{-\frac{t}{\tau_2}}) \right] \quad (7.13)$$

where $\eta_2/E_3 = \tau_1$ and $\eta_3/E_4 = \tau_2$ are the retardation times.

The constants in equation 7.13 were found by minimising the sum of the squared differences between the squares of measured and calculated depths using the solver

function in Microsoft Excel 2007. The values of the parameters of model-3 are given in Table 7.1.

Figure 7.7 shows a comparison between the experimental and predicted indentation creep curve for Accura 60 using equation 7.13 for EVP model-3. It can be seen that the predicted curve fits closely to the experimental curve and the addition of the second KV unit has reduced the error in the primary creep region.

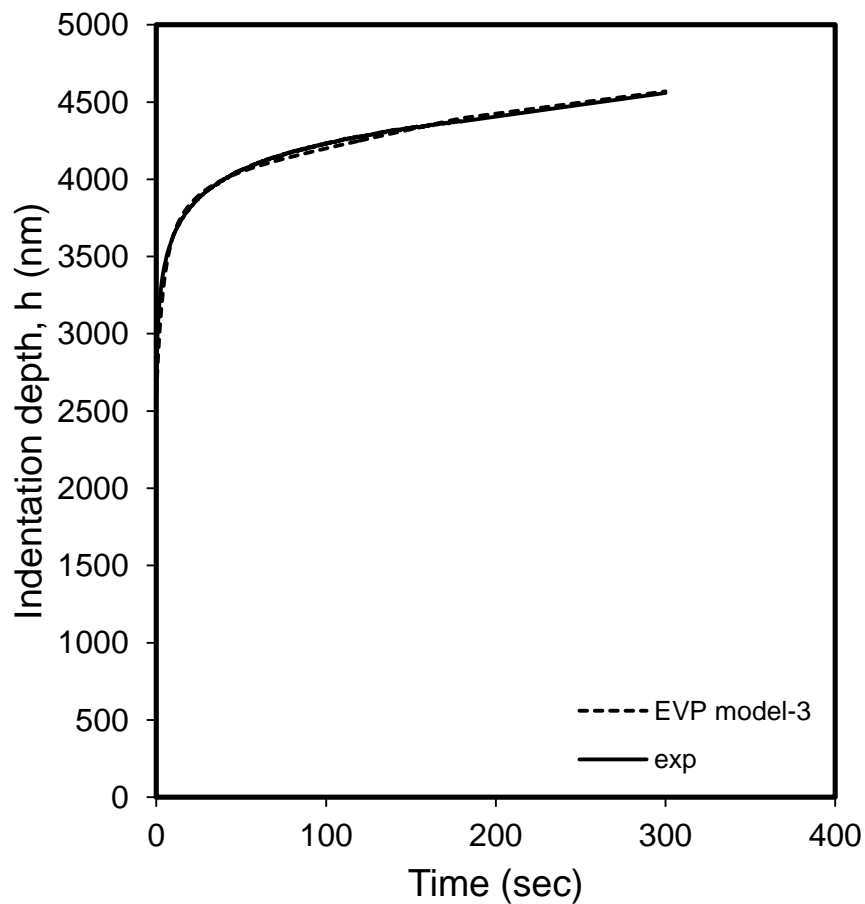


Figure 7.7: Experimental (exp) and predicted (model-3) indentation creep curves for 4mm thick Accura 60 samples tested at 20mN load for 300 sec hold at 33.5%RH at 22.5°C.

EVP models	E₁ (MPa)	E₂ (MPa)	E₃ (MPa)	E₄ (MPa)	η_1 (MPa-sec)	τ (sec)	τ_1 (sec)	τ_2 (sec)
Model-1	3611	1825	-	-	2.41e04	-	-	-
Model-2	3879	2379	1134	-	3.52e05	9.88	-	-
Model-3	3796	2442	1967	1445	4.65e05	-	17.66	4.12

Table 7-1 : Parameters of EVP models calculated from indentation creep data for 4mm thick Accura 60 samples tested at 20mN load for 300 sec at 33.5%RH and 22.5°C.

Since EVP model-3 corresponds well to the indentation behaviour shown by Accura 60 at 33.5 % RH, equation 7.13 was fitted to indentation creep data obtained using a 20mN holding load for 300 sec at 53.8 %, 75.3 % and 84.5 % RH after 8 hours of conditioning. Values of the fitting constants are given in Table 7.2. These values were obtained by minimising the sum of the squared differences between the squares of measured and calculated depths using the solver function in Microsoft Excel 2007.

Figure 7.8 shows a comparison of experimental and predicted indentation creep curves for Accura 60 using equation 7.13 for EVP model-3 at various RH environments. It can be seen that the predicted curves fit quite closely to the experimental curves. Comparison of Figures 7.7 and 7.8 shows that EVP model-3 predicts the experimental data excellently at low values of RH (33.5 % and 53.8 %) while a small deviation is observed at high RH (75.3 % and 84.5 %). The fitting parameters of EVP model-3 at various RH are given in Table 7.2.

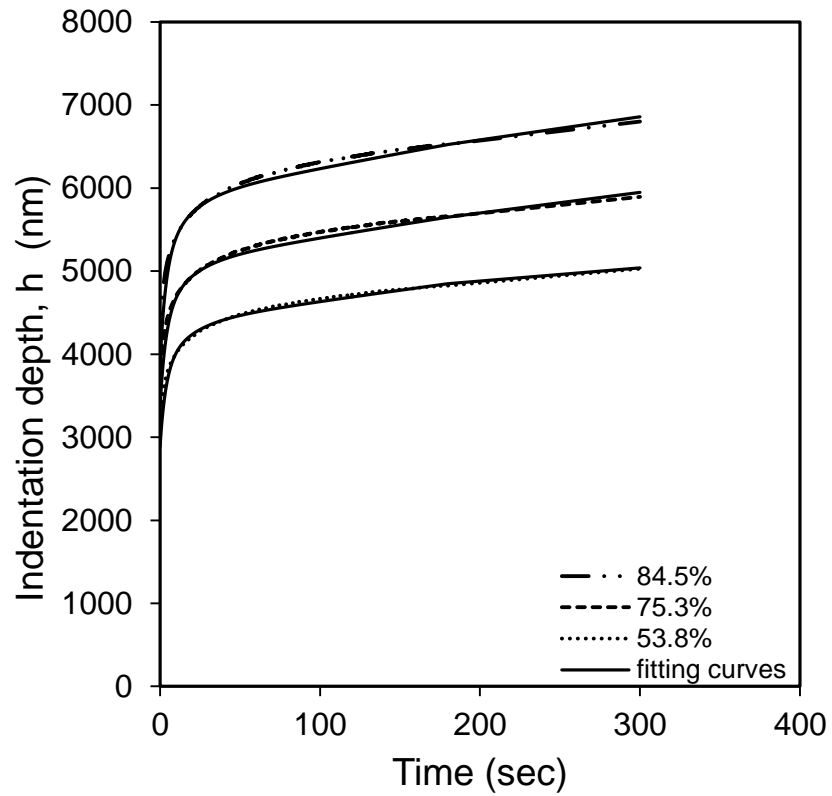


Figure 7.8 : Experimental and predicted (model-3) indentation creep curves for 4mm thick Accura 60 samples tested at 20mN load for 300 sec hold at various RH after 8 hours of conditioning at 22.5°C.

RH	E ₁ (MPa)	E ₂ (MPa)	E ₃ (MPa)	E ₄ (MPa)	η_1 (MPa-sec)	τ_1 (sec)	τ_2 (sec)
33.5%	3796	2442	1967	1445	4.65e05	17.66	4.12
53.8%	3549	2317	1906	1395	3.02e03	14.25	3.31
75.3%	3237	2095	1779	1251	1.14e02	16.31	5.29
84.5%	3053	1916	1654	1225	3.36e01	18.04	4.66

Table 7-2 : Parameters of EVP model-3 calculated from indentation creep data for 4mm thick Accura 60 samples tested at 20mN load for 300 sec after 8 hours of conditioning at various RH at 22.5°C.

Table 7.2 shows that the parameters of model-3 are dependent on RH. Values of E_1 and E_2 decrease with an increase in RH due to the absorption of more moisture at higher % RH. E_3 and E_4 represent the modulus of the KV viscoelastic units and their values are also dependent on the conditioning environment. Finally, η_1 , represents the coefficient of viscoplasticity, which also decreases at higher RH environment. However, the retardation times τ_1 and τ_2 are not found to follow any particular trend with increase in RH.

It is interesting to try to correlate the elements of the VE-P model with the calculated modulus and hardness values and this is discussed in the next section.

7.4 Calculation of modulus and hardness from EVP model

The two most familiar material properties that are commonly calculated from DSI testing are elastic modulus and hardness (or mean pressure beneath indenter, p_m). This section provides details on calculating these values from EVP model parameters. E_1 of spring S_1 is called the plane strain modulus or reduced indentation modulus and is related to Young's modulus, E_{EVP} , and Poisson's ratio, ν , of a specimen material by equation 7.14 (Oyen and Cook 2003; Fischer-Cripps 2004; Oyen and Ko 2007; Mencik et al. 2011).

$$E_1 = \frac{E_{EVP}}{1 - \nu^2} \quad (7.14)$$

where subscript 'EVP' shows that this modulus has been calculated from EVP model parameters. Hence, Young's modulus, E_{EVP} , of Accura 60 was calculated from equation 7.14 using values of E_1 of VEP model-3 and results after 8 hours conditioning at various RH are provided in Table 7.3. Values of Young's modulus calculated using the OP method after providing 300 sec dwell to reach creep

equilibrium, E_e , and those calculated using bulk compressive tests, E_c , at various RH are also provided for the comparison purposes.

Comparison shows that values of E_{EVP} and E_c are quite close to each other with E_{EVP} value found slightly less than E_c at 33.5 % RH while values of E_{EVP} are found slightly higher than E_c at all other conditioning environments, however, the maximum % difference is only 2.93 % found at 33.5 % RH. Thus, the use of VE-P modelling parameters, calculated from DSI creep test data, have provided a close match to uniaxial compressive test results. Comparison of values of E_e with E_{EVP} shows that the values calculated using OP method are slightly higher with maximum % difference of 8.31 % found at 84.5 % RH environment. The table also shows that moisture absorption leads to a decrease in elastic modulus. It can be seen that the OP method can provide a good approximation for the elastic component of deformation for materials, such as for Accura 60, however, the use of appropriate models to characterise all forms of deformation is the best method when applied to time independent materials such as polymers and biomaterials.

RH	Bulk compressive modulus E_c (MPA)	Modulus using EVP model E_{EVP} (MPA)	Modulus using OP method E_e (MPA)	% difference between E_{EVP} and E_c (%)	% difference between E_{EVP} and E_e (%)
33.5%	3429	3330	3489	2.93	4.66
53.8%	3105	3114	3279	0.29	5.16
75.3%	2823	2840	3041	0.60	6.83
84.5%	2651	2679	2911	1.05	8.31

Table 7-3 : Comparison of values of modulus for Accura 60 calculated from different techniques after 8 hours conditioning at various RH.

The next step is to calculate values of hardness from the phenomenological model parameters. Two different hardness values can be calculated from the EVP model parameters. One is value of hardness, H , which is a measure of resistance to plastic deformation and is independent of elastic modulus and viscous deformation. The second value of hardness is contact hardness, H_c , which is equivalent to the hardness value calculated from the OP method and is dependent on the plane strain modulus, E_1 , hardness, H , and viscosity, η_1 (Sakai 1999; Oyen and Cook 2003; Oyen 2006; Oyen and Ko 2007; Olesiak et al. 2010).

In order to calculate hardness, H , the following relation can be used (Oyen and Ko 2007):

$$H = \frac{P}{\bar{\alpha}h_p^2} \quad (7.15)$$

where $\bar{\alpha}$ is a constant that is dependent upon the geometry of indenter used and is taken as 24.5 for the Berkovich indenter while h_p is the instantaneous plastic depth calculated from equation 7.13.

Similarly, contact hardness, H_c , can also be calculated from EVP model parameters for comparison with the contact hardness, H_e , calculated using the OP method. Oyen and Ko (2007) and Olesiak et al. (2010) used equation 7.16 to calculate H_c for various polymers and bones by including viscous deformation in the relation originally developed by Sakai (1999).

$$H_c = \frac{1}{\alpha_1((\alpha_2 E_1)^{-1/2} + (\alpha_1 H)^{-1/2} + 2(t_R/3)(\alpha_3 \eta_1)^{-1/2})^2} \quad (7.16)$$

where t_R is experimental rise time, which is equal to P_{max}/k , k is loading rate and α_1 , α_2 and α_3 are the geometry constants. E_1 is plane strain modulus, H hardness and η_1 indentation viscosity. Values of H and H_c for Accura 60 were calculated from equations 7.15 and 7.16 using the EVP model-3 parameters. Values of H and H_c after 8 hours conditioning at various RH are shown in Table 7.4. Values of contact hardness calculated using the OP method, H_c , are also provided for comparison purposes.

RH	Contact	Hardness	Contact	%Difference	%Difference
	hardness by OP method H_c (MPA)	from EVP model H (MPA)	hardness from EVP model H_c (MPA)	between H_c and H (%)	between H_c and H_c (%)
33.5%	195	354.25	207.85	58.12	6.39
53.8%	190	335.51	196.16	55.54	3.19
75.3%	174	303.92	177.55	54.59	2.03
84.5%	159	277.84	163.21	54.51	2.61

Table 7-4 : Comparison of values of hardness for Accura 60 calculated from EVP model parameters with those calculated using OP method after 8 hours conditioning at various RH.

If we compare values of H , H_c and H_e in Table 7.4, we find that the values of H_c and H_e are quite close to each other while H is significantly higher. The same trend can be seen for all the environments. This is expected as the additional viscous deformation involved in the calculation of contact hardness would increase the contact area and hence decrease the calculated contact hardness. Values of H_c calculated using the EVP model parameters are slightly higher than those calculated from the OP method, however, the maximum % difference at 33.5 % RH is equal to

6.39 % and the difference tends to decrease with increase in RH. It can be seen from the table that an increase in moisture absorption resulted in a decrease in the values of H , H_c and H_e , as would be expected. Similar trends were found for various polymers and bones when values of H , H_c and H_e were compared at ambient environment (Olesiak et al. 2010). Contact hardness is a widely used property reported in the literature and it is demonstrated that VEP model parameters can be used for its calculation. Additionally, the rate independent hardness, H , can also be calculated.

7.5 Summary

The response of viscoelastic-plastic materials under indentation load can be described using rheological models and analysis methods have been discussed in this chapter that can be used to determine time dependent material parameters for the SL resin, Accura 60. These parameters were obtained from DSI creep data at various RH using a 20 mN load and 300 sec dwell period. Three models were investigated and the model which provided the best fit to the experimental data was comprised of elastic, plastic and viscous elements.

An attempt was also made to correlate the parameters from the visco-elastic-plastic model with those calculated from the OP method and bulk tests. Comparison of values of modulus showed that values of E_{EVP} were quite close to E_c and varied slightly from E_e , especially with increase in RH. Similarly, comparison of values of hardness showed that values of H_c and H_e were also close, however, hardness, H , which is independent of elastic modulus and viscous components, was found to be significantly higher. Hence, it can be seen that there is some correlation between the properties obtained through fitting the experimental data to EVP model and those obtained from applying the OP method to data from experiments obtained after reducing time dependent effects. However, a more complete description of the material behaviour is obtained from the application of the EVP model.

|Discussion

8.1 Introduction

This chapter presents a discussion of the experimental results and the numerical and analytical modelling carried out to investigate the effects of varying humidity on the indentation response of the stereolithography (SL) resin, Accura 60. Initially, the effects of moisture on the bulk mechanical properties and possible mechanisms to explain moisture diffusion in the resins are discussed. There follows a discussion on the time dependent indentation response at various humidities and the effects of humidity on the micron-scale mechanical properties of Accura 60. The use of the finite element (FE) method, using a diffusion-mechanical sequential coupled analysis technique, to predict load-depth plots and hardness at various humidities and depths is also discussed. Finally, the phenomenological modelling technique to characterise the viscoelastic-plastic (VE-P) material parameters and determine mechanical properties at different humidities is discussed.

8.2 Moisture diffusion in SL Resins and its effects

SL resins are highly hygroscopic and absorb varying amounts of moisture at different levels of RH. This moisture absorption can lead to a wide range of effects, both reversible and irreversible. In order to generate moisture uptake data for modelling moisture diffusion, gravimetric experiments were performed. Four RH environments; 33.5 %, 53.8 %, 75.3 % and 84.5 % were selected while temperature was maintained at 22.5 °C. Data from these experiments was analysed to identify the type of diffusion. The experimentally determined diffusion profiles gave a poor fit to a Fickian diffusion model and confirmed that the diffusion was non-Fickian. The poor

fit was due to the occurrence of a second phase of diffusion that was more prominent at higher % RH. There is a rapid initial moisture uptake observed during the first phase during which the increase in weight is proportional to the square root of the conditioning time. During this time water content quickly occupies the free volume in the polymeric resin. Once the free volume is occupied further absorption is slower as the rate of absorption is now dictated by the rate of relaxation of the polymer. Water may also become attached to polar groups in the polymer and becomes bound. Therefore, more free volume occurs that results in additional but slower, absorption. Once binding of water to the polymer network and hygroscopic expansion are completed and free volume space is fully occupied, then a true equilibrium is achieved. Thus we can say that the availability of free volume within the polymer dictates the first phase whereas polarity of the resin and the rate of hygroscopic expansion for additional water absorption in the second stage. In order to reduce free volume in polymers, crosslinking must be increased. Increasing the crosslinking can slow down or even stop moisture penetration in polymers. Similarly, epoxies with more polarity tend to absorb more moisture and hence reducing the polarity may slow down or even stop the absorption process during the second phase.

In order to model the two-stage, non-Fickian behaviour described above, various theoretical models such as the dual sorption model and diffusion-relaxation models could be used, however in this work the dual-Fickian model was selected due to the ease with which it can be implemented in the software for FE analysis. Two important modelling constants; equilibrium moisture uptake and diffusion constant were obtained from fitting the model to the experimental data. Results showed that equilibrium moisture uptake was strongly dependent on the relative humidity of the conditioning environment whilst the values of the diffusion constants were relatively insensitive to varying % RH. Higher equilibrium moisture uptake by the resin at higher RH may be expected as there is a higher concentration of moisture in the environment. Absorption of more moisture at higher RH confirms the hygroscopic nature of Accura 60.

In order to investigate the effects of varying humidity on bulk mechanical properties, mechanical testing was carried. Tests included tensile tests, compressive tests and creep tensile tests. Results from the compressive and tensile tests confirmed the hydrostatic stress sensitivity of yielding in the Accura 60. Results also showed that mechanical properties such as Young's modulus and yield stress calculated from both uniaxial tests decreased with an increase in absorbed moisture contents, with significant effects seen at higher values of RH. Samples conditioned at higher RH also showed an increase in ductile behaviour. When moisture is absorbed by the resins, the absorbed content act both as a plasticiser and a reactant. The plasticisation effect contributes to a decrease in the glass transition temperature and reduction of the intermolecular forces in the polymers, which in turn reduces elastic modulus and mechanical strength. This reduction in the cohesive forces between the bonds of polymer chains also results in an increase in the elongation to break. Possible long term effects of moisture include chemical degradation due to hydrolysis or oxidation and chain scission which can lead to the leaching out of small molecules in an immersion environment. Plasticisation also decreases the resistance to the applied load and hence causes an increase in the creep strain. Therefore, creep strain also increased with increase in RH.

Results from bulk testing have confirmed that SL resins are highly hygroscopic, especially when stored/or tested at high values of RH and the mechanical properties of SL materials vary as a function of the RH. Hence, the effect of moisture in the environment needs to be taken into account when designing SL manufactured parts.

8.3 The Indentation response of the SL Resin at various Humidities

A challenge of using DSI on polymers is due to the fact that polymeric materials exhibit both time independent elastic-plastic (EP) and time dependent viscoelastic (VE) and viscoplastic (VP) deformations during indentation and, hence, the traditional analysis techniques such as Oliver and Pharr (OP) method, designed for

EP materials, leads to ambiguities in the interpretation of results. However, while acknowledging the limitations of the widely used OP method in the data analysis of time-dependent materials, we adopted this approach after reducing the time-dependent effects so that the analysis method remained simple and the focus was on the effects of absorbed moisture and ambient humidity on the results of DSI. Various testing parameters were tried at 20 mN maximum load and it was found that a 300 sec dwell period with 0.5 mN/sec loading and unloading rates provided conditions where the effects of creep were minimised and an equilibrium deformation was reached and the initial unloading curve was pseudo-elastic. This equilibrium point occurs when the back-stress resulting from the applied stress has become equal to the applied stress, making the overstress equal to zero, and hence creep has stopped and the polymer has an equilibrium deformation under the applied load. Hence, these testing parameters were used in all DSI experiments to investigate the effects of humidity and the OP method was used to analyse the data. This method, whilst not fully developed, characterising the material provides quantitative parameters that have some meaning. The calculated modulus, E_e , relate to the elastic component of the deformation whilst the calculated hardness, H_e , relates to the equilibrium mean pressure under the indenter following VE-P deformation.

In order to investigate the influence of RH on the indentation behaviour of the SL resin, the samples were conditioned using two methods. In the first method, samples were pre-conditioned at 33.5 %, 53.8 %, 75.3 % and 84.5 % RH using saturated salt solutions. The preconditioned samples were tested at 33.5 % RH, using a humidity control unit (HCU) to control RH in the DSI system. In the second method, samples were conditioned and tested at 33.5 %, 53.8 %, 75.3 % and 84.5 % RH by regulating humidity in the DSI system using the HCU. Temperature was kept constant at 22.5 °C for the conditioning and DSI testing. Results from both methods showed that values of modulus, E_e , and hardness, H_e , were relatively insensitive to conditioning time at 33.5 % RH, as would be expected. However, at high humidity, the values of E_e and H_e decreased significantly with conditioning time. This trend highlights an increase in near-surface moisture concentration with an increase in conditioning time, resulting in an increase in plasticisation of the polymer and, hence, decreases in

the mechanical properties. Comparison of results from both methods confirmed that penetration depth for a given time and RH was greater for the samples conditioned and tested in the same environment than for the preconditioned samples tested at the ambient humidity of 33.5 % RH. This variation in results can be expected because tests in method 1 were performed at a lower RH than the conditioning environment, resulting in desorption of some of the moisture from the sample surface during the period of the test. Even though the testing was conducted as quickly as possible after removal from the conditioning environment, the effect is quite significant, especially at high RH. This indicates that humidity should be controlled when DSI testing hydrophilic polymers if reliable and meaningful results are to be obtained.

To investigate any recovery in mechanical properties on drying; the samples conditioned at 84.5 % RH for five days in the DSI chamber were then conditioned at 33.5 % RH for ten days and retested periodically. Results showed a decrease in the maximum indentation depth and improvement in mechanical properties with increase in drying time. This recovery in mechanical properties indicates that at least some of the effects of moisture, such as plasticisation of the SL resin, are reversible.

The DSI test results at various RH confirm that SL resins are highly hygroscopic on micron scale and the absorbed moisture significantly affects the indentation behaviour of Accura 60. This research work has also highlighted the importance of using HCU to control RH within a DSI chamber during testing of moisture dependent materials. Regulating RH to different values by HCU has also showed its ability to control the range of moisture content that are useful for the DSI testing of polymeric and biomaterial samples. Hence, there is an argument to always using a HCU to control RH within the DSI chamber when testing of moisture dependent materials.

8.4 Modelling the indentation behaviour at various RH

In order to model the indentation behaviour of Accura 60, the commercially available FE code from MSC Software Corporation (Santa Ana, CA, USA) was used for the numerical analysis. Two dimensional (2D) axisymmetric FE analyses were performed using sharp conical indenter geometry. A continuous mesh was used to discretise the geometry, where smaller elements were used near the contact region and relatively larger elements used elsewhere. This approach helps to save computational time. However, it is a major challenge in contact analysis to obtain accuracy and solution convergence with the minimum number of elements. This problem can be solved by using an adaptive meshing technique that results in greater number of elements and nodes being generated near the contact region by automatically subdividing the elements within the time steps of the solution, leading to convergence and accuracy of the solution. In order to include time independent and time dependent deformations during indentation, a hydrostatic stress sensitive Mohr-Coulomb based elastic-plastic model was combined with a rate dependent power law creep model. Results from the FE modelling provided an excellent match with the experimental load-displacement curves, except during the last part of unloading. This difference can be attributed to the assumption of frictionless contact and the inability of the creep power law to model viscoelastic recovery during unloading. Apart from last stages of unloading, all the significant indentation parameters, such as the indentation depth under maximum load, creep in the dwell period and the initial unloading slope are predicted very accurately by the model. This indicates that the selected material model and FE procedure can be used to model indentation behaviour of SL resins accurately.

Sequentially coupled hygro-mechanical analyses were performed to model indentation behaviour at various RH. This technique involves, initially, a transient hygroscopic analysis to determine the nodal moisture concentrations which is then coupled with a contact mechanical model to solve for deformation and stresses under the influence of moisture. Transient moisture diffusion analyses can be carried out in the software by using the analogy between Fourier's law of heat transfer and Fick's

law of diffusion. FE modelling using coupled hygro-mechanical procedure accurately predicted experimental load-displacement curves at various conditioning times. Moisture absorption can lead to surface effects resulting in changes to the value of H_e at various depths due to different moisture concentration. In order to find H_e at various depths, it is proposed that once the slope at maximum load is known, then, assuming that this slope remains constant at all loads below that maximum load, H_e can be computed at any point along the loading curve. This method involves calculating plastic contact depth from the single simulation results. Since, FE modelling provided a good approximation of H_e at various depths, this methodology can be extended to find the spatial variation in mechanical properties and characterisation of moisture at various depths.

Since the proposed FE model and procedure provides a good approximation to the experimental results, it is suggested that the proposed FE model can be used in predicting the effects of the environment on the performance of in-service SL manufactured components. The FE model can also be used to perform inverse FEA and find the properties of various materials for which standard testing techniques cannot be used.

8.5 Phenomenological modelling of indentation data

The response of VE-P materials under indentation load can be described using rheological models. A three step experimental procedure was adopted that involved instantaneous loading, holding at 20 mN maximum load for 300 sec and finally unloading. Experiments were carried at 33.5 %, 53.8 %, 75.3 % and 84.5 % RH at 22.5 °C fixed temperature. Since, indentation using Berkovich indenter provides a combination of instantaneous elastic, plastic and time dependent viscous deformation, elastic-viscous-plastic (EVP) models were investigated. The values of fitting parameters were obtained by minimising the sum of the squared differences between the squares of measured and calculated depths using the solver function in Microsoft Excel 2007. As expected, the values of fitted model parameters E_1 , E_2 , E_3 , E_4 and η_1 were dependent on RH and their values decreased with increased

humidity. This decrease in values of parameters can be attributed to plasticisation effects.

Relating these fitting parameters to various mechanical properties is an important step. Two time-independent properties; Young's modulus, E_{EVP} , and resistance to permanent deformation, H , can be computed from the parameters for springs S_1 and S_2 in the VE-P model. Comparison shows that values of E_{EVP} are quite close to the bulk compressive modulus, E_c . An analytical relation was used to calculate contact hardness, H_c , to compare its values with H_e at various RH. This contact hardness, H_c , is dependent on values of strain modulus, E_1 , hardness, H , and viscosity η_1 . Comparison of values of hardness showed that values of H_c and H_e were quite close, however, hardness, H , which is independent of elastic modulus and viscous components, is totally different from contact hardness values. It can be seen, therefore, that there is a reasonably good correlation between material parameters determined from the VEP model, the OP method and bulk sample testing. Since, use of VEP model provides both time independent and time dependent parameters successfully under all humidities, therefore, it is argued to always use this analytical modelling technique for analysis of indentation data of time dependent materials.

8.6 Summary and Contribution to the Knowledge

Moisture diffusion in Accura 60 samples greatly influenced the mechanical properties. The indentation response of the resin was also affected, especially at high RH. DSI fitted with a HCU was capable of investigating a relationship between mechanical properties and moisture absorption. Experiments on samples after drying showed substantial, though not complete, recovery in the values of E and H . This recovery confirmed the reversible nature of moisture plasticisation. Two approaches were used to analyse the indentation data. In the first approach, the OP method was used on indentation data after eliminating time dependent effects. This method was useful to make a comparison of the effect of absorbed moisture on the mechanical properties when tested at various humidities. In the second approach, phenomenological modelling was used to find a suitable VE-P model that could

characterise the material response to indentation and be used to calculate E and H values at various RH. FE modelling was carried out to investigate the indentation behaviour of Accura 60 numerically at various humidities. The selected material model described both EP and VE deformation well and the FE procedure used to carry out the diffusion-mechanical coupled analysis provided an excellent match to experimental load-depth curves. A method was also proposed to calculate values of H at various depths under the influence of RH and this was verified by comparing the results with experimental values.

Following are the contribution to the knowledge from carrying out this research:

- Results obtained for SL resin, Accura 60, at different humidities can be used as a starting point to understand the behaviour of SL materials under the influence of moisture at a micron scale. This is useful because very limited research has been undertaken to date on SL materials at the micron scale, which is useful as SL material properties tend to vary across a component.
- There has been no previously published work where the effects of varying RH on indentation have investigated using a humidity control unit while testing. This research work has highlighted the importance of using HCU to control RH within DSI chamber during the testing of moisture dependent materials.
- This research presents a significant step in indentation modelling of SL resins at various RH by characterising moisture dependent material properties and presents a methodology to predict mechanical properties at various depths under different moisture conditions. The ability to predict moisture concentration under varying environmental conditions provides increased confidence in the use of SL resins in end-use applications. Therefore, the methodology of characterising and modelling the effect of moisture in the environment may be used during the design stage of polymeric components. Also, by changing the material diffusion properties, the moisture diffusion model may be used to predict moisture concentration of not only

SL resins, but also for other moisture sensitive other polymeric materials and biomaterials. Similarly, by changing the moisture dependent mechanical properties, coupled diffusion-stress analysis can be performed for other moisture sensitive materials to investigate the mechanical response at various humidities.

- Researchers are questioning the effectiveness of the popular Oliver and Pharr method for analysing indentation data of time dependent materials. This research work also demonstrates that the argument to use phenomenological modelling approach to characterise time dependent material parameters and not minimise them is a good choice as it provides a comprehensive picture where both time independent and time dependent properties can be extracted from one set of analysis. Additionally, it is demonstrated that an analytical modelling technique works equally well for polymeric resins at varying moisture environments. Hence, appropriate material models may be used to analyse indentation data from time dependent materials.

|Conclusions and Future Work

9.1 Introduction

The aim and objectives of the research, as laid down in Section 1.2, have been successfully achieved by; (i) the experimental characterisation of moisture dependent material properties and (ii) the development of a methodology that is able to predict moisture diffusion and mechanical properties under variable environmental conditions. The conclusions of the research work and suggestions for future work are presented in this chapter.

9.2 Conclusions

The main conclusions of this research are as follows;

1. Stereolithography (SL) resins are highly hygroscopic, especially when stored/or tested at high values of relative humidity (RH). This absorbed moisture leads to a wide range of effects, both reversible and irreversible, and the mechanical properties of SL materials vary as a function of the RH. Therefore, the effect of moisture in the environment clearly needs to be taken into account when designing SL manufactured parts.
2. Moisture absorption in the Accura 60 resin is non-Fickian, and a dual Fickian model fits well to the experimental moisture uptake data. The saturated moisture content and the strength of the resin are dependent on RH. Neglecting the dependence of saturated moisture content on RH may result in over or under prediction of moisture dependent effects in the polymeric resin.
3. The advantages of depth sensing indentation (DSI) over other testing techniques are the small amount of material required and that the variation of

properties across the depth can be investigated.

4. The DSI technique can be used to investigate environmental effects on polymers such as varying relative humidity environments. A DSI system fitted with a humidity control unit (HCU) is capable of investigating the relationship of mechanical properties as a function of RH. Comparison of the results with the pre-conditioned samples tested at ambient conditions showed that drying of the samples whilst testing can affect the results. Hence, there is an argument to always using a HCU to control RH within the DSI chamber during the testing of moisture dependent materials.

5. Experiments on samples after drying showed substantial, though not complete, recovery in the values of indentation modulus, E_e , and indentation hardness, H_e . This recovery occurs mainly due to the reversible effects such as plasticisation in SL resins.

6. The load-depth response from the DSI of polymers under varying % RH can be predicted with good accuracy by employing coupled stress-diffusion finite element analysis (FEA) with appropriate time dependent material and diffusion models.

7. It is demonstrated that values of indentation hardness, H_e , can be accurately predicted under various environments and depths using the proposed FEA model. This method involves calculating plastic contact depth at various loads from the single simulation results.

8. Analysis of the results from the DSI testing of polymers is challenging because of their complex structure and time dependent deformation. Their deformation mechanisms are totally different from metals and ceramics. Two approaches can usually be employed in the characterization of polymers by DSI. The first is to select test parameters to minimize viscoelastic (VE) and viscoplastic (VP) effects in order to use the OP (Oliver and Pharr) method. However, this is appropriate only in cases when polymers show only weakly time dependent

behaviour. The second approach is to use DSI results to determine the parameters for a time dependent material model.

9. A phenomenological modelling approach, consisting of rheological models using components such as springs, dashpots and friction element, can be used to characterise the VE-P indentation behaviour of polymers. Two independent mechanical properties; hardness, H , and Young's modulus, E_{EVP} , can be calculated while time dependent properties can also be calculated. Hence, VE-P modelling analysis methods must be preferred over widely used DSI data analysis techniques, developed for elastic-plastic materials, when used for polymers and biomaterials.

10. The selection of indenters is also important for material characterisation e.g. sharp indenters can provide a viscoelastic-plastic (VE-P) response while blunt indenter can be used for investigating a VE response or the smooth transformation from VE to plastic deformation.

9.3 Future Work

The proposed variable moisture and strength prediction methodology may be expanded by including the effects of temperature on moisture diffusion in epoxy resins. This would strengthen the currently developed methodology in predicting diffusion and its effects on mechanical properties in polymeric materials under different environmental conditions by including two of the most important environmental degradation factors; temperature and humidity, together.

The FE work may be developed to investigate the effects of pile up, friction, adhesion and surface roughness in the model. Also, 3D modelling of indentation can be performed to compare the conical and Berkovich indenter results in various environments. Further possibilities may be explored to extract material parameters during recovery in the unloading stage.

The FE model can be used with an inverse technique to extract the mechanical properties from the DSI data for complex material models for which standard mechanical test analysis cannot be performed. Additionally, by using built in parametric analysis feature available in most FEA codes or linking the FE model to some other script written in software like MATLAB, material properties can be optimised automatically.

The FE model may also be applied to predict the behaviour of in-service SL components at different environments. This would be beneficial during design stages and provide more confidence in the use of SL manufactured components as end-use products. Due to the ability of the FE method to deal with complex geometries, most types of the epoxy resin configurations may be used with the proposed methodology. Also, by changing the material diffusion properties, the moisture diffusion model may be used to predict moisture concentration of not only SL resins, but also for other moisture sensitive polymeric materials and biomaterials.

DSI testing may be performed to investigate spatial variation in the properties of materials and how these variations are affected by the moisture absorption and to characterise moisture distribution at various locations inside the resin.

In order to extract elastic, viscous and plastic properties effectively, indentation may be carried out using spherical indenters of different radii. Further work may include the extraction of stress-strain curves and developing some relation to find yielding in polymers at various environments from the spherical indentation test data.

Both empirical and correspondence principle approaches to modelling time dependent indentation may be further explored and used on indentation data taken from various types of indenters at different humidities. This would help to formulate a reliable data analysis technique for a range of time dependent materials including both polymers and biomaterials.

References

ADAMSON, M.J., 1980. Thermal expansion and swelling of cured epoxy resin used in graphite/epoxy composite materials. *Journal of Materials Science*, **15**(7), pp. 1736-1745.

AKHTAR, R., MORSE, S. and MUMMERY, P.M., 2005. Nanoindentation of bone in a physiological environment, *Materials Research Society Symposium Proceedings 2005*, Warrendale, Pa.; Materials Research Society; 1999, pp. 15-20.

ALKORTA, J., MARTÍNEZ-ESNAOLA, J.M. and GIL SEVILLANO, J., 2008. Critical examination of strain-rate sensitivity measurement by nanoindentation methods: Application to severely deformed niobium. *Acta Materialia*, **56**(4), pp. 884-893.

ALTAF, K., ASHCROFT, I.A. and HAGUE, R., 2011a. Modelling the effect of moisture on the depth sensing indentation response of a stereolithography polymer. *Computational Materials Science*, In press.

ALTAF, K., ASHCROFT, I.A., SALEH, N. and HAGUE, R., 2011b. Environmental Ageing of Epoxy-Based Stereolithography Parts Part1: Moisture transportation. *Plastics, Rubber and Composites*, In press.

ALTAF, K. and ASHCROFT, I. A. AND HAGUE, R., 2011c. Investigation of the effect of relative humidity on polymers by depth sensing indentation. *Journal of Materials Science*, In press.

ANAND, L. and AMES, N.M., 2006. On modelling the micro-indentation response of an amorphous polymer. *International Journal of Plasticity*, **22**(6), pp. 1123-1170.

ANDERSON, T.L., 2005. *Fracture Mechanics: Fundamentals and Applications*. Third edition, Taylor and Francis, London, UK.

ANTOON, M. and KOENG, J., 2003. Irreversible effects of moisture on the epoxy matrix in glass-reinforced composites. *Journal of Polymer Science: Polymer Physics Edition*, **19**(2), pp. 197-212.

APICELLA, A., NICOLAIS, L., ASTARITA, G. and DRIOLI, E., 1979. Effect of thermal history on water sorption, elastic properties and the glass transition of epoxy resins. *Polymer*, **20**(9), pp. 1143-1148.

ASHCROFT, I.A. and SPINKS, G.M., 1996. A method of monitoring water absorption in polymers using a depth sensing indentation system. *Journal of Materials Research*, **11**(2), pp. 529-536.

ASHCROFT, I.A. and BRISKHAM, G., 2010. Designing adhesive joints for fatigue and creep load conditions, in: D.A. Dillard (Ed.), Woodhead Publishing Limited, Cambridge, UK, pp. 468-511.

ASHCROFT, I.A., ALTAF, K., SALEH, N. and HAGUE, R., 2011. Environmental Ageing of Epoxy-Based Stereolithography Parts_Part2_Effect of absorbed moisture on mechanical properties. *Plastics, Rubber and Composites*, In press.

ASIF, S.A.S. and PETHICA, J.B., 1998. Nano-scale indentation creep testing at non-ambient temperature. *The Journal of Adhesion*, **67**(1), pp. 153-165.

ASIF, S.A.S., WAHL, K.J. and COLTON, R.J., 1999. Nanoindentation and contact stiffness measurement using force modulation with a capacitive load-displacement transducer. *Review of Scientific Instruments*, **70**, pp. 2408-2413.

ASTM D638, 2008. Standard test method for tensile properties of plastics.

ASTM D695, 2008. Standard test method for compressive properties of rigid plastics.

ASTM D2990, 2009. Standard test methods for tensile, compressive, and flexural creep and creep-rupture of plastics.

BALOOCH, G., MARSHALL, G.W., MARSHALL, S.J., WARREN, O.L., ASIF, S.A.S. and BALOOCH, M., 2004. Evaluation of a new modulus mapping technique to investigate microstructural features of human teeth. *Journal of Biomechanics*, **37**(8), pp. 1223-1232.

BARDIA, P. and NARASIMHAN, R., 2006. Characterisation of Pressure-sensitive Yielding in Polymers. *Strain*, **42**(3), pp. 187-196.

BAUWENS, J.C., 1970. Yield condition and propagation of Lüders' lines in tension-torsion experiments on poly (vinyl chloride). *Journal of Polymer Science Part A-2: Polymer Physics*, **8**(6), pp. 893-901.

BEAKE, B.D. and LEGGETT, G.J., 2002. Nanoindentation and nanoscratch testing of uniaxially and biaxially drawn poly (ethylene terephthalate) film. *Polymer*, **43**, pp. 319-327.

BEAKE, B.D. and SMITH, J.F., 2002. High-temperature nanoindentation testing of fused silica and other materials. *Philosophical Magazine A*, **82**(10), pp. 2179-2186.

- BELL, G.A., BIELINSKI, D.M. and BEAKE, B.D., 2008. Influence of water on the nanoindentation creep response of nylon 6. *Journal of Applied Polymer Science*, **107**(1), pp. 577-582.
- BELL, T.J., BENDELI, A., FIELD, J.S., SWAIN, M.V. and THWAITE, E.G., 1991. The determination of surface plastic and elastic properties by ultra micro-indentation. *Metrologia*, **28**, pp. 463-469.
- BERENS, A.R. and HOPFENBERG, H.B., 1978. Diffusion and relaxation in glassy polymer powders: 2. Separation of diffusion and relaxation parameters. *Polymer*, **19**(5), pp. 489-496.
- BERENS, A.R. and HOPFENBERG, H.B., 1979. Induction and measurement of glassy-state relaxations by vapor sorption techniques. *Journal of Polymer Science: Polymer Physics Edition*, **17**(10), pp. 1757-1770.
- BHATTACHARYA, A.K. and NIX, W.D., 1988. Finite element simulation of indentation experiments. *International Journal of Solids and Structures*, **24**(9), pp. 881-891.
- BHUSHAN, B., KULKARNI, A.V., BONIN, W. and WYROBEK, J.T., 1996. Nanoindentation and picondentation measurements using a capacitive transducer system in atomic force microscopy. *Philosophical Magazine-Part A*, **74**(5), pp. 1117-1128.
- BOWDEN, P.B. and JUKES, J.A., 1972. The plastic flow of isotropic polymers. *Journal of Materials Science*, **7**(1), pp. 52-63.
- BOWDITCH, M., 1996. The durability of adhesive joints in the presence of water. *International Journal of Adhesion and Adhesives*, **16**(2), pp. 73-79.
- BREWIS, D.M., COMYN, J. and TEGG, J.L., 1980. The uptake of water vapour by an epoxide adhesive formed from the diglycidyl ether of bisphenol-A and di-(1-aminopropyl-3-ethoxy) ether. *Polymer*, **21**(2), pp. 134-138.
- BRISCOE, B.J., FIORI, L. and PELILLO, E., 1998. Nano-indentation of polymeric surfaces. *Journal of Physics D: Applied Physics*, **31**, pp. 2395-2405.
- BS EN ISO 604, 2002. International Standard, Plastics---Determination of compressive properties.
- BS EN ISO 899, 2003. International Standard, Plastics---Determination of creep behaviour.
- BS EN ISO 62, 2008. International Standard, Plastics – Determination of Water Absorption.

BS EN ISO 527, 2009. International Standard, Plastics---Determination of tensile properties.

BUCAILLE, J.L., STAUSS, S., FELDER, E. and MICHLER, J., 2003. Determination of plastic properties of metals by instrumented indentation using different sharp indenters. *Acta materialia*, **51**(6), pp. 1663-1678.

BURNETT, P.J. and RICKERBY, D.S., 1987. The relationship between hardness and scratch adhesion. *Thin Solid Films*, **154**(1-2), pp. 403-416.

BURNETT, P.J. and RICKERBY, D.S., 1988. The scratch adhesion test: an elastic-plastic indentation analysis. *Thin Solid Films*, **157**(2), pp. 233-254.

BUTKUS, L.M., MATHERN, P.D. and JOHNSON, W.S., 1998. Tensile properties and plane-stress fracture toughness of thin film aerospace adhesives. *The Journal of Adhesion*, **66**(1), pp. 251-273.

CADDELL, R.M., RAGHAVA, R.S. and ATKINS, A.G., 1974. Pressure dependent yield criteria for polymers. *Materials Science and Engineering*, **13**(2), pp. 113-120.

CARE, G. and FISCHER-CRIPPS, A.C., 1997. Elastic-plastic indentation stress fields using the finite-element method. *Journal of Materials Science*, **32**(21), pp. 5653-5659.

CARTER, H.G. and KIBLER, K.G., 1978. Langmuir-type model for anomalous moisture diffusion in composite resins. *Journal of Composite Materials*, **12**(2), pp. 118-131.

CHEN, J., BELL, G.A., DONG, H., SMITH, J.F. and BEAKE, B.D., 2010. A study of low temperature mechanical properties and creep behaviour of polypropylene using a new sub-ambient temperature nanoindentation test platform. *Journal of Physics D: Applied Physics*, **43**(42), pp. 425404-425412.

CHEN, W., LI, M., ZHANG, T., CHENG, Y. and CHENG, C., 2007. Influence of indenter tip roundness on hardness behavior in nanoindentation. *Materials Science and Engineering A*, **445-446**, pp. 323-327.

CHENG, C.M. and CHENG, Y.T., 1997. On the initial unloading slope in indentation of elastic-plastic solids by an indenter with an axisymmetric smooth profile. *Applied Physics Letters*, **71**, pp. 2623-2625.

CHENG, Y.T. and CHENG, C.M., 1998. Relationships between hardness, elastic modulus, and the work of indentation. *Applied Physics Letters*, **73**, pp. 614.

CHENG, Y.T. and CHENG, C.M., 2000. What is indentation hardness? *Surface and Coatings Technology*, **133**, pp. 417-424.

- CHENG, Y.T. and CHENG, C.M., 2005. Relationships between initial unloading slope, contact depth, and mechanical properties for conical indentation in linear viscoelastic solids. *Journal of Materials Research*, **20**(4), pp. 1046-1053.
- CHUDOBA, T. and RICHTER, F., 2001. Investigation of creep behaviour under load during indentation experiments and its influence on hardness and modulus results. *Surface and Coatings Technology*, **148**(2-3), pp. 191-198.
- CORCORAN, S.G., COLTON, R.J., LILLEODDEN, E.T. and GERBERICH, W.W., 1997. Anomalous plastic deformation at surfaces: Nanoindentation of gold single crystals. *Physical Review B*, **55**(24), pp. 16057-16060.
- CRANK, J., 1979. *The mathematics of diffusion*. Second edition, Oxford University Press, London, UK.
- CROCOMBE, A.D., HUA, Y.X., LOH, W.K., WAHAB, M.A. and ASHCROFT, I.A., 2006. Predicting the residual strength for environmentally degraded adhesive lap joints. *International Journal of Adhesion and Adhesives*, **26**(5), pp. 325-336.
- DE WILDE, P.J., 1994. A simple model for moisture sorption in epoxies with sigmoidal and two-stage sorption effects. *Composite Structures*, **27**(3), pp. 243-252.
- DIAMANT, Y., MAROM, G. and BROUTMAN, L.J., 2003. The effect of network structure on moisture absorption of epoxy resins. *Journal of Applied Polymer Science*, **26**(9), pp. 3015-3025.
- DOERNER, M.F. and NIX, W.D., 1986. A method for interpreting the data from depth-sensing indentation instruments. *Journal of Materials Research*, **1**(4), pp. 601-609.
- DUNCAN, B., ROBERTS, S. and URQUHART, J., 2005. *Review of Measurement and Modelling of Permeation and Diffusion in Polymers*. National Physical Laboratory, pp. 2-68.
- FANG, T.H. and CHANG, W.J., 2004. Nanoindentation characteristics on polycarbonate polymer film. *Microelectronics Journal*, **35**(7), pp. 595-599.
- FENG, G. and NGAN, A.H.W., 2002. Effects of creep and thermal drift on modulus measurement using depth-sensing indentation. *Journal of Materials Research*, **17**(3), pp. 660-668.
- FERRY, J.D., 1980. *Viscoelastic Properties of Polymers*. 3rd edition, Wiley, New York, USA.
- FIELD, J.S. and SWAIN, M.V., 1993. A simple predictive model for spherical indentation. *Journal of Materials Research*, **8**(2), pp. 297-306.

FINDLEY, W.N., LAI, J.S. and ONARAN, K., 1989. *Creep and relaxation of nonlinear viscoelastic materials: with an introduction to linear viscoelasticity*. Dover Publications, New York, USA.

FISCHER-CRIPPS, A.C., 2001. Simulation of sub-micron indentation tests with spherical and Berkovich indenters. *Journal of Material Research*, **16**(7), pp. 2149-2157.

FISCHER-CRIPPS, A.C., 2004. A simple phenomenological approach to nanoindentation creep. *Materials Science and Engineering A*, **385**(1-2), pp. 74-82.

FISCHER-CRIPPS, A.C., 2004. *Nanoindentation*. Springer Verlag, New York, USA.

FISCHER-CRIPPS, A.C., 2006. Critical review of analysis and interpretation of nanoindentation test data. *Surface and Coatings Technology*, **200**(14-15), pp. 4153-4165.

GALANOV, B.A., 1982. An approximate method for the solution of some two-body contact problems with creep in the case of an unknown contact area. *International Applied Mechanics*, **18**(8), pp. 711-718.

GAOFEI, Z., YILAN, K., JING, S., QINGHUA, Q., HUAIWEN, W. and DONGHUI, F.U., 2004. Influence of moisture content and time on the mechanical behavior of polymer material. *Science in China Series E-Technological Sciences*, **47**(5), pp. 595-607.

GLEDHILL, R.A., KINLOCH, A.J. and SHAW, S.J., 1980. A model for predicting joint durability. *The Journal of Adhesion*, **11**(1), pp. 3-15.

GOODALL, R.C.T.W. and CLYNE, T.W., 2006. A critical appraisal of the extraction of creep parameters from nanoindentation data obtained at room temperature. *Acta Materialia*, **54**(20), pp. 5489-5500.

GREENWOOD, J.A., 2010. Contact between an axisymmetric indenter and a viscoelastic half-space. *International Journal of Mechanical Sciences*, **52**(6), pp. 829-835.

GRINSTAFF, M.W., 2002. Biodendrimers: New polymeric biomaterials for tissue engineering. *Chemistry - A European Journal*, **8**(13), pp. 2838-2846.

GUPTA, K.M. and PAWAR, S.J., 2005. A nonlinear diffusion model incorporating edge and surface texture effects to predict absorption behaviour of composites. *Materials Science and Engineering: A*, **412**(1-2), pp. 78-82.

GURTIN, M.E. and YATOMI, C., 1979. On a model for two phase diffusion in composite materials. *Journal of Composite Materials*, **13**, pp. 126-130.

- HAGUE, R., CAMPBELL, I. and DICKENS, P., 2003. Implications on design of rapid manufacturing. *Proceedings of the Institution of Mechanical Engineers, Part C: Journal of Mechanical Engineering Science*, **217**(1), pp. 25-30.
- HAGUE, R., MANSOUR, S., SALEH, N. and HARRIS, R., 2004. Materials analysis of stereolithography resins for use in Rapid Manufacturing. *Journal of Materials Science*, **39**(7), pp. 2457-2464.
- HAMID, S.H., 2000. *Handbook of polymer degradation*. Second edition, Marcel Dekker Inc., New York, USA.
- HENGESBERGER, S., KULIK, A. and ZYSSET, P.H., 2002. Nanoindentation discriminates the elastic properties of individual human bone lamellae under dry and physiological conditions. *Bone*, **30**(1), pp. 178-184.
- HOCHSTETTER, G., JIMENEZ, A., CANO, J.P. and FELDER, E., 2003. An attempt to determine the true stress-strain curves of amorphous polymers by nanoindentation. *Tribology International*, **36**(12), pp. 973-985.
- IVANOVA, K., PETHRICK, R. and AFFROSSMAN, S., 2000. Investigation of hydrothermal ageing of a filled rubber toughened epoxy resin using dynamic mechanical thermal analysis and dielectric spectroscopy. *Polymer*, **41**(18), pp. 6787-6796.
- JÄGER, A. and LACKNER, R., 2009. Finer-Scale extraction of viscoelastic properties from nanoindentation characterised by viscoelastic-plastic response. *Strain*, **45**(1), pp. 45-54.
- JOSHI, S. and ASTARITA, G., 1979. Diffusion-relaxation coupling in polymers which show two-stage sorption phenomena. *Polymer*, **20**(4), pp. 455-458.
- KAKANI, S.L. and KAKANI, A., 2004. *Material Science*. New Age International Publishers, New Delhi, India.
- KALPAKJIAN, S. and SCHMID, S.R., 2006. *Manufacturing engineering and technology*. Fifth edition, Reading, Massachusetts, USA.
- KASTURIARACHCHI, K. and PRITCHARD, G., 1985. Scanning electron microscopy of epoxy-glass laminates exposed to humid conditions. *Journal of Materials Science*, **20**(6), pp. 2038-2044.
- KITAGAWA, M., ONODA, T. and MIZUTANI, K., 1992. Stress-strain behaviour at finite strains for various strain paths in polyethylene. *Journal of Materials Science*, **27**(1), pp. 13-23.
- KUMAZAWA, T., OISHI, M. and TODOKI, M., 1994. High-humidity deterioration and internal structure change of epoxyresin for electrical insulation. *IEEE Transactions on Dielectrics and Electrical Insulation*, **1**(1), pp. 133-138.

- LAI, J. and BAKKER, A., 1995. Analysis of the non-linear creep of high-density polyethylene. *Polymer*, **36**(1), pp. 93-99.
- LAU, K., CHEUNG, H., LU, J., YIN, Y., HUI, D. and LI, H., 2008. Carbon nanotubes for space and bio-engineering applications. *Journal of Computational and Theoretical Nanoscience*, **5**(1), pp. 23-35.
- LEE, E.H. and RADOK, J.M.T., 1960. The contact problem for viscoelastic solids. *Journal of Applied Mathematics*, **27**, pp. 438-444.
- LEVY, G.N., SCHINDEL, R. and KRUTH, J.P., 2003. Rapid manufacturing and rapid tooling with layer manufacturing (LM) technologies, state of the art and future perspectives. *CIRP Annals-Manufacturing Technology*, **52**(2), pp. 589-609.
- LI, H. and NGAN, A.H.W., 2004. Size effects of nanoindentation creep. *Journal of Materials Research*, **19**(2), pp. 513-522.
- LI, L., YIN, L. and CHU, P.K., 2008. Finite element analysis of residual stress and interlayer in hard coating/interlayer/soft substrate system during nanoindentation. *Journal of Materials Research*, **23**(5), pp. 1358-1363.
- LICARI, J.J. and HUGHES, L.A., 1990. *Handbook of Polymer Coatings for Electronics: Chemistry, Technology and Applications*. Noyes Publications, New Jersey, USA.
- LILJEDAHN, C.D.M., CROCOMBE, A.D., WAHAB, M.A. and ASHCROFT, I.A., 2005. The effect of residual strains on the progressive damage modelling of environmentally degraded adhesive joints. *Journal of Adhesion Science and Technology*, **19**(7), pp. 525-547.
- LIM, Y.Y. and CHAUDHRI, M.M., 2003. Experimental investigations of the normal loading of elastic spherical and conical indenters on to elastic flats. *Philosophical magazine*, **83**(30), pp. 3427-3462.
- LIN, Y.C. and CHEN, X., 2005. Investigation of moisture diffusion in epoxy system: Experiments and molecular dynamics simulations. *Chemical Physics Letters*, **412**(4-6), pp. 322-326.
- LIU, C.K., LEE, S., SUNG, L.P. and NGUYEN, T., 2006. Load-displacement relations for nanoindentation of viscoelastic materials. *Journal of Applied Physics*, **100**, pp. 033503-033512.
- LOH, W.K., CROCOMBE, A.D., ABDEL WAHAB, M.M. and ASHCROFT, I.A., 2005. Modelling anomalous moisture uptake, swelling and thermal characteristics of a rubber toughened epoxy adhesive. *International Journal of Adhesion and Adhesives*, **25**(1), pp. 1-12.

- LU, Y.C., TANDON, G.P., JONES, D.C. and SCHOEPPNER, G.A., 2009. Elastic and viscoelastic characterization of thermally-oxidized polymer resin using nanoindentation. *Mechanics of Time-Dependent Materials*, **13**(3), pp. 245-260.
- LUCAS, B.N. and OLIVER, W.C., 1999. Indentation power-law creep of high-purity indium. *Metallurgical and Materials Transactions A*, **30**(3), pp. 601-610.
- MARX, V. and BALKE, H., 1997. A critical investigation of the unloading behavior of sharp indentation. *Acta Materialia*, **45**(9), pp. 3791-3800.
- MASARO, L. and ZHU, X.X., 1999. Physical models of diffusion for polymer solutions, gels and solids. *Progress in Polymer Science*, **24**(5), pp. 731-775.
- MATA, M., ANGLADA, M. and ALCALÁ, J., 2002. Contact deformation regimes around sharp indentations and the concept of the characteristic strain. *Journal of Materials Research*, **17**(5), pp. 964-976.
- MATA, M. and ALCALÁ, J., 2004. The role of friction on sharp indentation. *Journal of the Mechanics and Physics of Solids*, **52**(1), pp. 145-165.
- MAY, C.A., 1988. *Epoxy resins: chemistry and technology*. Second edition. Marcel Dekker Inc., New York, USA.
- MAYO, M.J. and NIX, W.D., 1988. A micro-indentation study of superplasticity in Pb, Sn, and Sn-38 wt% Pb. *Acta Metallurgica*, **36**(8), pp. 2183-2192.
- MCKAGUE JR, E.L., REYNOLDS, J.D. and HALKIAS, J.E., 2003. Swelling and glass transition relations for epoxy matrix material in humid environments. *Journal of Applied Polymer Science*, **22**(6), pp. 1643-1654.
- MENCÍK, J. and SWAIN, M.V., 1995. Errors associated with depth-sensing microindentation tests. *Journal of Materials Research*, **10**(6), pp. 1491-1501.
- MENČÍK, J., 2007. Determination of mechanical properties by instrumented indentation. *Meccanica*, **42**(1), pp. 19-29.
- MENCÍK, J., HE, L.H. and SWAIN, M.V., 2009. Determination of viscoelastic-plastic material parameters of biomaterials by instrumented indentation. *Journal of the Mechanical Behavior of Biomedical Materials*, **2**(4), pp. 318-325.
- MENCÍK, J., HE, L.H. and NEMECEK, J., 2011. Characterization of viscoelastic-plastic properties of solid polymers. *Polymer Testing*, **30**, pp. 101-109.
- MOREL, P. and JARDRET, V., 2002. Viscoelastic effects on the scratch resistance of polymers: relationship between mechanical properties and scratch properties at various temperatures, *Materials Research Society Symposium Proceedings*, Warrendale, Pa.; Materials Research Society; 1999, pp. 93-98.

- MORGAN, R.J., O'NEAL, J.E. and FANTER, D.L., 1980. Effect of moisture on the physical and mechanical integrity of epoxies. *Journal of Materials Science*, **15**(3), pp. 751-764.
- MOSTOVOY, S. and RIPLING, E.J., 1971. Fracture toughness stress corrosion cracking characteristics of an anhydride- hardened epoxy adhesive. *Journal of Applied Polymer Science*, **15**(3), pp. 641-659.
- MSC MARC, 2007. *R1, User Manual. A*, pp. 476-477.
- MUBASHAR, A., ASHCROFT, I.A., CRITCHLOW, G.W. and CROCOMBE, A.D., 2009. Moisture absorption-desorption effects in adhesive joints. *International Journal of Adhesion and Adhesives*, **29**(8), pp. 751-760.
- MUBASHAR, A., ASHCROFT, I.A., CRITCHLOW, G.W. and CROCOMBE, A.D., 2010. A method of predicting the stresses in adhesive joints after cyclic moisture conditioning. *Journal of Adhesion*, In press.
- NEWAY, D., WILKINS, M.A. and POLLOCK, H.M., 1982. An ultra-low-load penetration hardness tester. *Journal of Physics E: Scientific Instruments*, **15**, pp. 119-122.
- NGAN, A.H.W. and TANG, B., 2002. Viscoelastic effects during unloading in depth-sensing indentation. *Journal of Materials Research*, **17**(10), pp. 2604-2610.
- OEHR, C., 2003. Plasma surface modification of polymers for biomedical use. *Nuclear Instruments and Methods in Physics Research Section B: Beam Interactions with Materials and Atoms*, **208**, pp. 40-47.
- OLESIAK, S.E., OYEN, M.L. and FERGUSON, V.L., 2009. Viscous behaviour in berkovich nanoindentation of bone, *Proceedings of the SEM Annual Conference, June 1-4, 2009, Society for Experimental Mechanics Inc., New Mexico, USA*.
- OLESIAK, S.E., OYEN, M.L. and FERGUSON, V.L., 2010. Viscous-elastic-plastic behavior of bone using Berkovich nanoindentation. *Mechanics of Time-Dependent Materials*, **14**(2), pp. 111-124.
- OLIVER, W.C. and PHARR, G.M., 1992. Improved technique for determining hardness and elastic modulus using load and displacement sensing indentation experiments. *Journal of Materials Research*, **7**(6), pp. 1564-1583.
- OLIVER, W.C. and PHARR, G.M., 2004. Reviews-Measurement of hardness and elastic modulus by instrumented indentation: Advances in understanding and refinements to methodology. *Journal of Materials Research*, **19**(1), pp. 3-21.

- OVAERT, T.C., KIM, B.R. and WANG, J., 2003. Multi-parameter models of the viscoelastic/plastic mechanical properties of coatings via combined nanoindentation and non-linear finite element modeling. *Progress in Organic Coatings*, **47**(3-4), pp. 312-323.
- OYEN, M.L., 2006. Nanoindentation hardness of mineralized tissues. *Journal of Biomechanics*, **39**(14), pp. 2699-2702.
- OYEN, M.L. and COOK, R.F., 2003. Load-displacement behavior during sharp indentation of viscous-elastic-plastic materials. *Journal of Materials Research*, **18**(1), pp.139-150.
- OYEN, M.L. and COOK, R.F., 2009. A practical guide for analysis of nanoindentation data. *Journal of the Mechanical Behavior of Biomedical Materials*, **2**(4), pp. 396-407.
- OYEN, M.L., COOK, R.F., EMERSON, J.A. and MOODY, N.R., 2004. Indentation responses of time-dependent films on stiff substrates. *Journal of Materials Research*, **19**(8), pp. 2487-2497.
- OYEN, M.L. and KO, C. C., 2007. Examination of local variations in viscous, elastic and plastic indentation responses in healing bones. *Journal of Materials Science: Material Medical*, **18**, pp. 623-628.
- PARK, K., MISHRA, S., LEWIS, G., LOSBY, J., FAN, Z. and PARK, J.B., 2004. Quasi-static and dynamic nanoindentation studies on highly crosslinked ultra-high-molecular-weight polyethylene. *Biomaterials*, **25**(12), pp. 2427-2436.
- PARK, Y., KO, J., AHN, T.K. and CHOE, S., 1997. Moisture effects on the glass transition and the low temperature relaxations in semiaromatic polyamides. *Journal of Polymer Science-B-Polymer Physics Edition*, **35**(5), pp. 807-815.
- PAUL, B., 1968. *Macroscopic criteria of plastic flow and brittle fracture. In: second edition, H. Liebowitz, Editor, Fracture: an Advanced Treatise (Mathematical Fundamentals)*, Academic Press, New York, USA.
- PELEGRI, A.A. and HUANG, X., 2008. Nanoindentation on soft film/hard substrate and hard film/soft substrate material systems with finite element analysis. *Composites Science and Technology*, **68**(1), pp. 147-155.
- PELLETIER, H., KRIER, J., CORNET, A. and MILLE, P., 2000. Limits of using bilinear stress-strain curve for finite element modeling of nanoindentation response on bulk materials. *Thin Solid Films*, **379**(1-2), pp. 147-155.
- PERZYNA, P., 1966. Fundamental problems in viscoplasticity. *Advances in Applied Mechanics*, **9**(2), pp. 244-368.

- PETHICA, J.B., HUTCHINGS, R. and OLIVER, W.C., 1983. Hardness measurement at penetration depths as small as 20 nm. *Philosophical Magazine A*, **48**(4), pp. 593-606.
- PHARR, G.M., HARDING, D.S. and OLIVER, W.C., 1993. In: *Nastasi, M., Parkin, D. M. and Gleiter, H., (ed.); Mechanical properties and deformation behavior of materials having ultra-fine microstructures*. Kluwer Academic Press, Netherland, pp. 449-461.
- PHARR, G.M., BOLSHAKOV, A., TSUI, T.Y. and HAY, J.C., 1998. Nanoindentation of soft films on hard substrates: Experiments and finite element simulations, *Materials Research Society Symposium Proceedings 1998*, Materials Research Society, pp. 109-122.
- RADOK, J.R.M., 1956. Visco-elastic stress analysis. *Quarterly of Applied Mathematics*, **15**, pp. 198-202.
- RANDALL, N.X. and CONSIGLIO, R., 2000. Nanoscratch tester for thin film mechanical properties characterization. *Review of Scientific Instruments*, **71**, pp. 2796-2799.
- RAVVE, A., 2000. *Principles of polymer chemistry*. Second edition, Kluwer Academic/Plenum Publishers, New York, USA.
- RHO, J.Y. and PHARR, G.M., 1999. Effects of drying on the mechanical properties of bovine femur measured by nanoindentation. *Journal of Materials Science: Materials in Medicine*, **10**(8), pp. 485-488.
- RITTER, J.E., FOX, J.R., HUTKO, D.I. and LARDNER, T.J., 1998. Moisture-assisted crack growth at epoxy-glass interfaces. *Journal of Materials Science*, **33**(18), pp. 4581-4588.
- ROSEN, D.W., 2007. Computer-Aided Design for Additive Manufacturing of Cellular Structures. *Computer-Aided Design & Applications*, **4**(5), pp. 585-594.
- ROYLANCE, D., 2001. Engineering viscoelasticity. *Mechanics of Materials*, **3.11**, pp. 14-15.
- SAKAI, M., 1999. The Meyer hardness: a measure for plasticity?. *Journal of Materials Research*, **14**(9), pp. 3630-3639.
- SAKAI, M., SHIMIZU, S. and ITO, S., 2002. Viscoelastic indentation of silicate glasses. *Journal of the American Ceramic Society*, **85**(5), pp. 1210-1216.
- SARDAR, D., RADCLIFFE, S.V. and BAER, E., 1968. Effects of high hydrostatic pressure on the mechanical behavior of a crystalline polymer-polyoxymethylene. *Polymer Engineering and Science*, **8**(4), pp. 290-301.

SCHULTZ, J., 1974. *Polymers Materials Science*. Prentice Hall Inc., New Jersey, USA.

SCHWAIGER, R., MOSER, B., DAO, M., CHOLLACOO, N. and SURESH, S., 2003. Some critical experiments on the strain-rate sensitivity of nanocrystalline nickel. *Acta materialia*, **51**(17), pp. 5159-5172.

SHAMES, I.H. and COZZARELLI, F.A., 1992. *Elastic and inelastic stress analysis*. Prentice Hall Inc., New Jersey, USA.

SHEN, J., CHEN, C.C. and SAUER, J.A., 1985. Effects of sorbed water on properties of low and high molecular weight PMMA: 1. Deformation and fracture behaviour. *Polymer*, **26**(4), pp. 511-518.

SHEN, Y.L. and GUO, Y.L., 2001. Indentation modelling of heterogeneous materials. *Modelling and Simulation in Materials Science and Engineering*, **9**, pp. 391-398.

SHIM, S., OLIVER, W.C. and PHARR, G.M., 2007. A comparison of 3D finite element simulations for Berkovich and conical indentation of fused silica. *International Journal of Surface Science and Engineering*, **1**(2), pp. 259-273.

SHIMIZU, S., YANAGIMOTO, T. and SAKAI, M., 1999. Pyramidal indentation load-depth curve of viscoelastic materials. *Journal of Materials Research*, **14**(10), pp. 4075-4086.

SINGH, S.P., SINGH, R.P. and SMITH, J.F., 2005. Displacement modulation based dynamic nanoindentation for viscoelastic material characterization, *Materials Research Society Symposium Proceedings 2005*, pp. 141–146.

SNEDDON, I.N., 1965. The relation between load and penetration in the axisymmetric Boussinesq problem for a punch of arbitrary profile. *International Journal of Engineering Science*, **3**(1), pp. 47-57.

SPIPKER, R.L., SUH, J.K. and MOW, V.C., 1992. A finite element analysis of the indentation stress-relaxation response of linear biphasic articular cartilage. *Journal of Biomechanical Engineering*, **114**, pp. 191.

ST. LAWRENCE, S., WILLETT, J.L. and CARRIERE, C.J., 2001. Effect of moisture on the tensile properties of poly (hydroxy ester ether). *Polymer*, **42**(13), pp. 5643-5650.

STERNSTEIN, S.S. and ONGCHIN, L., 1969. Yield criteria for deformation of glassy polymers in general stress fields. *ACS Polymer Preprints*, **10**, pp. 1117-1124.

STROJNY, A. and GERBERICH, W.W., 1998. Experimental analysis of viscoelastic behavior in nanoindentation, *In: Fundamentals of nanoindentation and*

nanotribology, *Materials Research Society Symposia Proceedings* 1998, pp-159-164.

SWADDIWUDHIPONG, S., HUA, J., THO, K.K. and LIU, Z.S., 2006. Equivalency of Berkovich and conical load-indentation curves. *Modelling and Simulation in Materials Science and Engineering*, **14**, pp. 71-82.

SWADDIWUDHIPONG, S., POH, L., HUA, J., LIU, Z. and THO, K., 2005. Modeling nano-indentation tests of glassy polymers using finite elements with strain gradient plasticity. *Materials Science and Engineering: A*, **404**(1-2), pp. 179-187.

TAKAHASHI, A., SATO, Y., UNO, S., PEREIRA, P.N.R. and SANO, H., 2002. Effects of mechanical properties of adhesive resins on bond strength to dentin. *Dental Materials*, **18**(3), pp. 263-268.

TALJAT, B., ZACHARIA, T. and PHARR, G.M., 1998. *Fundamentals of Nano-indentation and Nanotribology*. . *Mater. Res. Soc. Symp. Proceedings 1998* , pp. 522-533.

TANG, B., NGAN, A.H.W. and LU, W.W., 2007. An improved method for the measurement of mechanical properties of bone by nanoindentation. *Journal of Materials Science: Materials in Medicine*, **18**(9), pp. 1875-1881.

TEZCAN, J. and HSIAO, K.J., 2008. Nondestructive evaluation of material strength using depth-sensing indentation. *Engineering Structures*, **30**(8), pp. 2206-2210.

TING, T.C.T., 1966. The contact stresses between a rigid indenter and a viscoelastic half space. *Journal of Applied Mechanics – Transactions of the ASME*, **35**, pp. 845-854.

TRANCHIDA, D. and PICCAROLO, S., 2005. Relating morphology to nanoscale mechanical properties: from crystalline to mesomorphic iPP. *Polymer*, **46**(12), pp. 4032-4040.

TRANCHIDA, D., PICCAROLO, S., LOOS, J. and ALEXEEV, A., 2007. Mechanical characterization of polymers on a nanometer scale through nanoindentation. A study on pile-up and viscoelasticity. *Macromolecules*, **40**(4), pp. 1259-1267.

TRESCA, H., 1864. *C. R. Memoire sur l'ecoulement des corps solides soumis a de fortes pressions*. *Academy of Sciences, Paris, France*, **59**, pp. 754-764.

TSAI, C.L., CHENG, M.C. and CHANG, S.L., 2007. Gradient-dependent Model for Moisture Diffusion in a Polymer Matrix Composite Laminate. *Journal of Composite Materials*, **41**(4), pp. 419-434.

TWEEDIE, C.A., CONSTANTINIDES, G., LEHMAN, K.E., BRILL, D.J., BLACKMAN, G.S. and VAN VLIET K.J., 2007. Enhanced stiffness of amorphous

polymer surfaces under confinement of localized contact loads. *Advanced Materials*, **19**, pp. 2540-2546.

ULLETT, J.S., SCHULTZ, J.W. and CHARTOFF, R.P., 2000. Novel liquid crystal resins for stereolithography—processing parameters and mechanical analysis. *Rapid Prototyping Journal*, **6**(1), pp. 8-17.

VANDAMME, M. and ULM, F.J., 2006. Viscoelastic solutions for conical indentation. *International Journal of Solids and Structures*, **43**(10), pp. 3142-3165.

VANLEENE, M., MAZERAN, P.E. and THO, M.C.H.B., 2006. Influence of strain rate on the mechanical behavior of cortical bone interstitial lamellae at the micrometer scale. *Journal of Materials Research*, **21**(8), pp. 2093-2097.

VERDU, J., SALMON, L., THOMINETTE, F. and PAYS, M.F., 1996. Hydrolytic degradation of model networks simulating the interfacial layers in silane-coupled epoxy/glass composites. *Composites Science and Technology*, **57**(8), pp. 1119-1127.

VIETH, W.R. and SLADEK, K.J., 1965. A model for diffusion in a glassy polymer. *Journal of colloid science*, **20**(9), pp. 1014-1033.

VOEVODIN, A.A., BANTLE, R. and MATTHEWS, A., 1995. Dynamic impact wear of TiC_xN_y and Ti-DLC composite coatings. *Wear*, **185**(1-2), pp. 151-157.

VON MISES, R., 1913. Mechanik der Festen Körper im plastisch deformablen Zustand, *Göttin. Nachr. Math. Physics*, **1**, pp. 582-592.

VORA, R.J., ASHCROFT, I.A. and HAGUE, R., 2007. Investigation of stereolithography material by depth sensing indentation and differential scanning calorimetry. *Plastics, Rubber and Composites*, **36**(2), pp. 68-76.

WAHAB, M.M.A., ASHCROFT, I.A., CROCOMBE, A.D. and SHAW, S.J., 2001. Diffusion of moisture in adhesively bonded joints. *The Journal of Adhesion*, **77**(1), pp. 43-80.

WANG, C.L., LAI, Y.H., HUANG, J.C. and NIEH, T.G., 2010. Creep of nanocrystalline nickel: A direct comparison between uniaxial and nanoindentation creep. *Scripta Materialia*, **62**(4), pp. 175-178.

WANG, C.L., MUKAI, T. and NIEH, T.G., 2009. Room temperature creep of fine-grained pure Mg: A direct comparison between nanoindentation and uniaxial tension. *Journal of Materials Research*, **24**(5), pp. 1615-1618.

WANG, S., LU, L. and YASZEMSKI, M.J., 2006. Polymer dynamics and rheology in designing and understanding polymeric biomaterials for tissue engineering

applications, 2006 AIChE Annual Meeting, Nov 12 - 17 2006, American Institute of Chemical Engineers.

WARD, I.M. and SWEENEY, J., 2004. An introduction to the mechanical properties of solid polymers. John Wiley & Sons Inc., New Jersey, USA.

WARNER, M.D., TAYLOR, W.R. and CLIFT, S.E., 2001. Finite element biphasic indentation of cartilage: a comparison of experimental indenter and physiological contact geometries. *Proceedings of the Institution of Mechanical Engineers, Part H: Journal of Engineering in Medicine*, **215**(5), pp. 487-496.

WEPPELMANN, E. and SWAIN, M.V., 1996. Investigation of the stresses and stress intensity factors responsible for fracture of thin protective films during ultra-micro indentation tests with spherical indenters. *Thin Solid Films*, **286**(1-2), pp. 111-121.

WHITE, C.C., VANLANDINGHAM, M.R., DRZAL, P.L., CHANG, N.K. and CHANG, S.H., 2005. Viscoelastic characterization of polymers using instrumented indentation. II. Dynamic testing. *Journal of Polymer Science Part B: Polymer Physics*, **43**(14), pp. 1812-1824.

WHITNEY, W. and ANDREWS, R.D., 1967. Yielding of glassy polymers: volume effect. *Journal of Polymer Science*, **16**, pp. 2290-2981.

WOODWARD, A.E., 1995. *Understanding polymer morphology*. Hanser Publisher, New York, USA.

WRIGHT, W.W., 1981. The effect of diffusion of water into epoxy resins and their carbon-fibre reinforced composites. *Composites*, **12**(3), pp. 201-205.

XIA, L., WEI, Z. and WAN, M., 2010. Conducting polymer nanostructures and their application in biosensors. *Journal of colloid and interface science*, **341**(1), pp. 1-11.

XU, Z.H. and LI, X., 2008. Effects of indenter geometry and material properties on the correction factor of Sneddon's relationship for nanoindentation of elastic and elastic-plastic materials. *Acta Materialia*, **56**(6), pp. 1399-1405.

XU, Z.H. and ROWCLIFFE, D., 2002. Method to determine the plastic properties of bulk materials by nanoindentation. *Philosophical Magazine A*, **82**(10), pp. 1893-1901.

YANG, B., RIESTER, L. and NIEH, T.G., 2006. Strain hardening and recovery in a bulk metallic glass under nanoindentation. *Scripta Materialia*, **54**(7), pp. 1277-1280.

YANG, B., WADSWORTH, J. and NIEH, T.G., 2007. Thermal activation in Au-based bulk metallic glass characterized by high-temperature nanoindentation. *Applied Physics Letters*, **90**, pp. 061911.

YANG, S., ZHANG, Y.W. and ZENG, K., 2004. Analysis of nanoindentation creep for polymeric materials. *Journal of Applied Physics*, **95**, pp. 3655-3666.

YOUNG, R.J. and LOVELL, P.A., 1991. *Introduction to polymers*. Second edition, CRC Press, New York, USA.

ZAIKOV, G.E., (Ed.) 1995. *Degradation & Stabilization of Polymers-Theory & Practice*. Nova Science Publishers, New York, USA.

ZHANG, C.Y., ZHANG, Y.W., ZENG, K.Y. and SHEN, L., 2005. Nanoindentation of polymers with a sharp indenter. *Journal of Materials Research*, **20**(6), pp. 1597-1605.

ZHANG, C.Y., ZHANG, Y.W., ZENG, K.Y. and SHEN, L., 2006. Characterization of mechanical properties of polymers by nanoindentation tests. *Philosophical magazine*, **86**(28), pp. 4487-4506.

Appendix-1

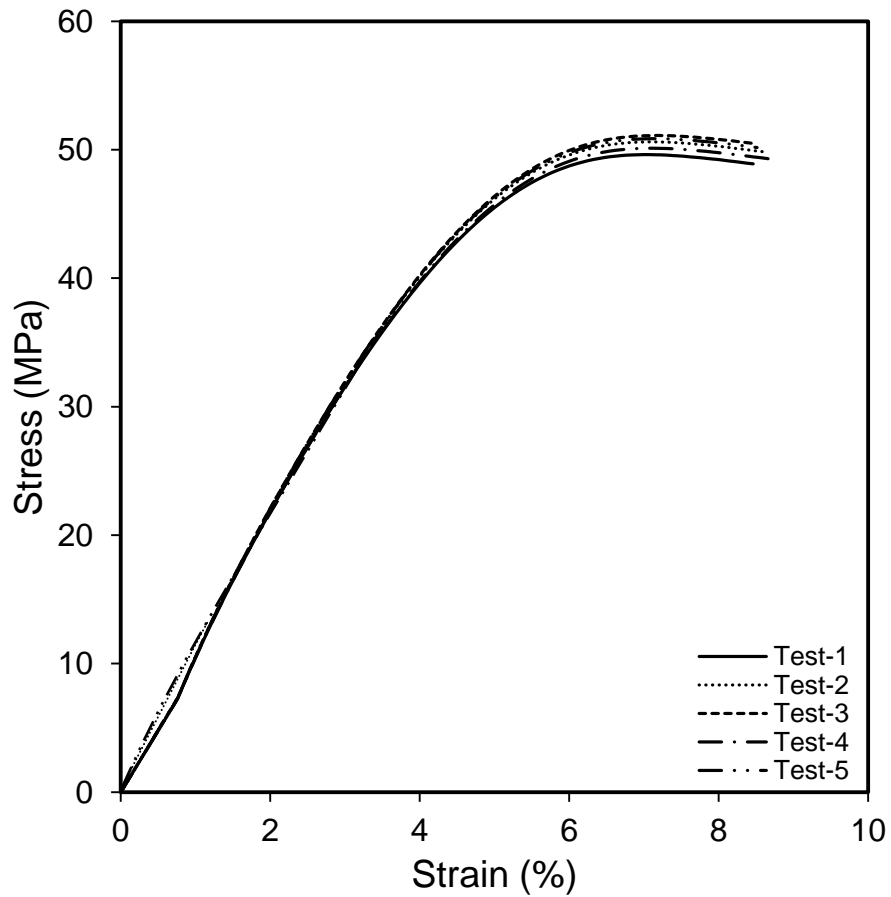


Figure-1: Moisture dependent tensile stress-strain curves for Accura 60 samples after 720 hours conditioning at 33.5 % RH.

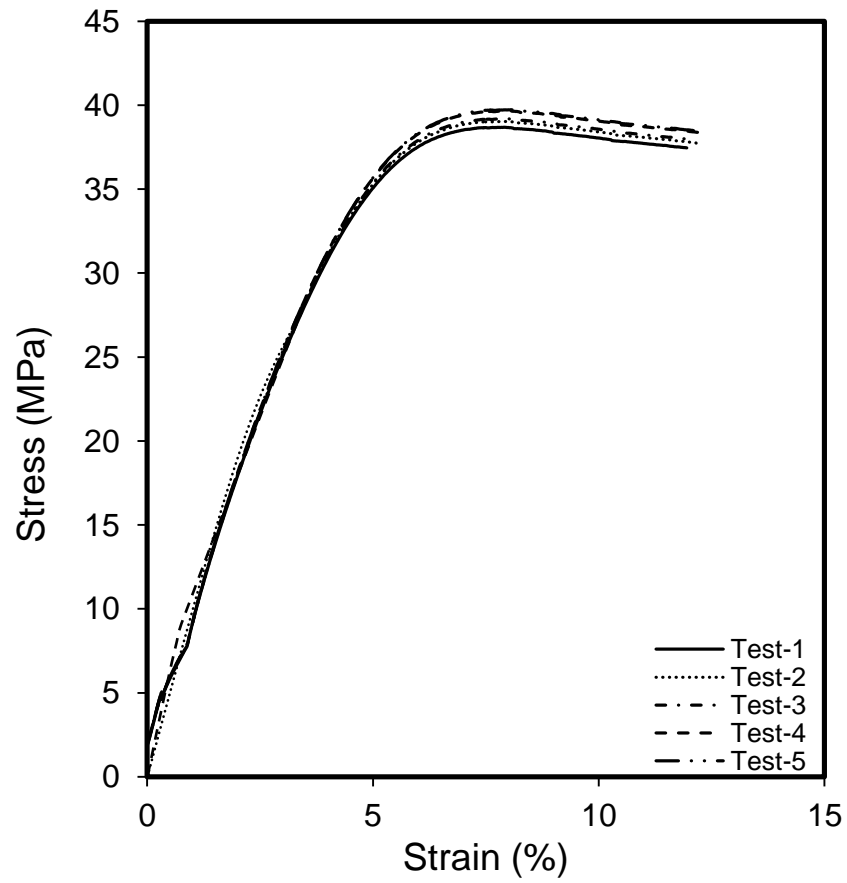


Figure-2: Moisture dependent tensile stress-strain curves for Accura 60 samples after 720 hours conditioning at 53.8 % RH.

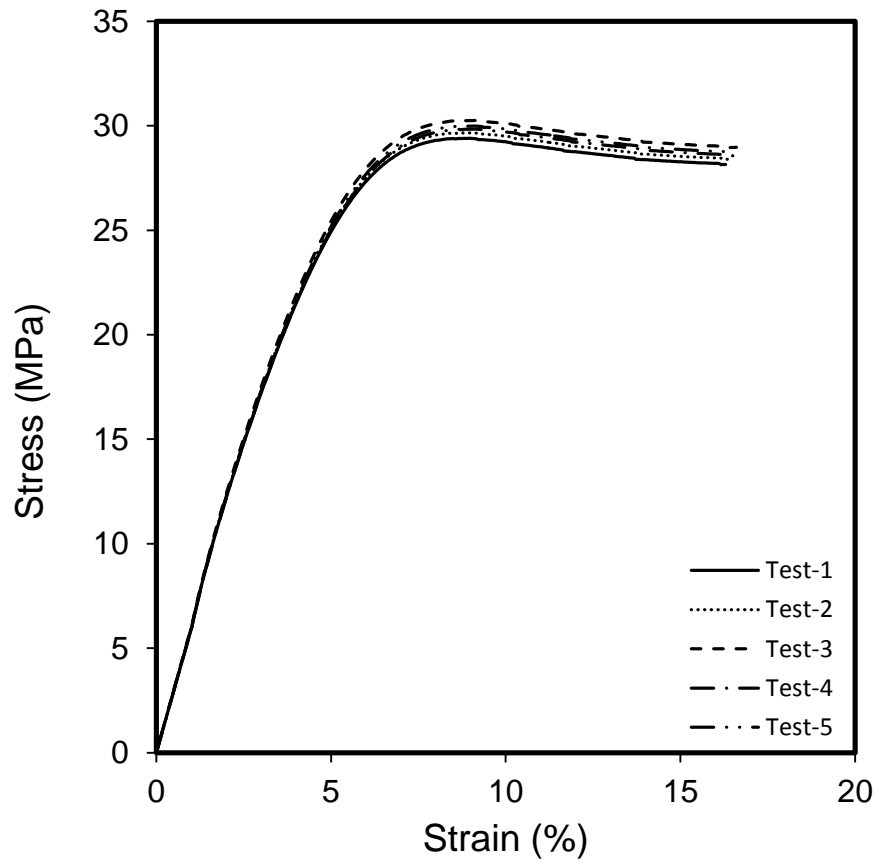


Figure-3: Moisture dependent tensile stress-strain curves for Accura 60 samples after 720 hours conditioning at 75.3 % RH.

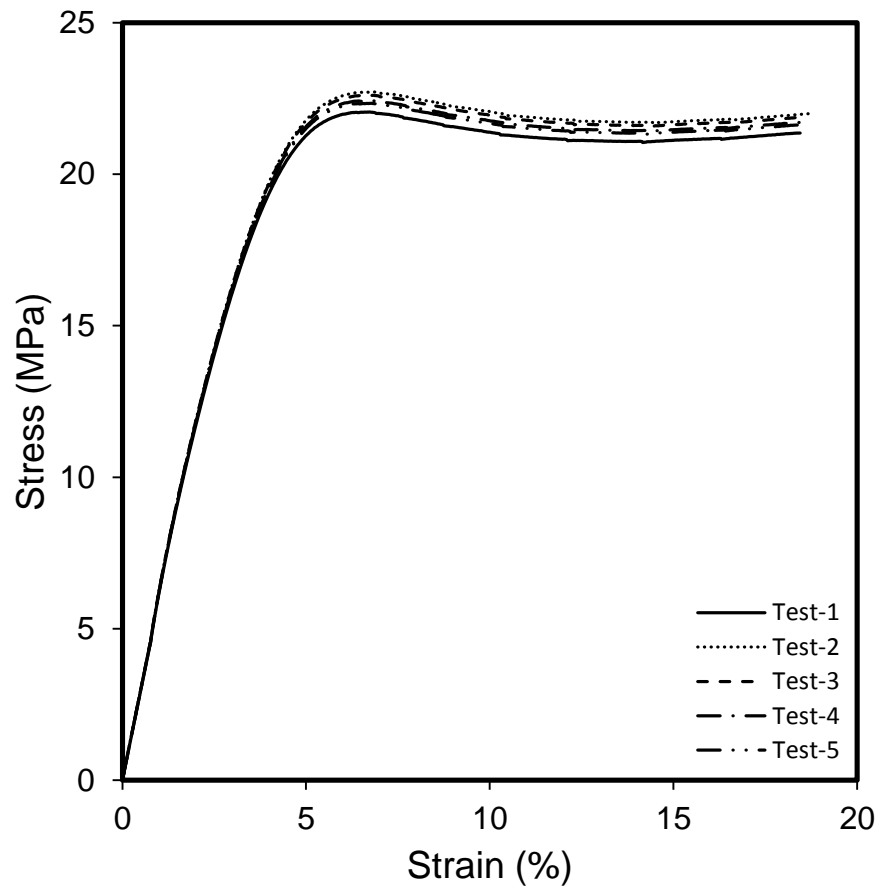


Figure-4: Moisture dependent tensile stress-strain curves for Accura 60 samples after 720 hours conditioning at 84.5 % RH.

Appendix-2

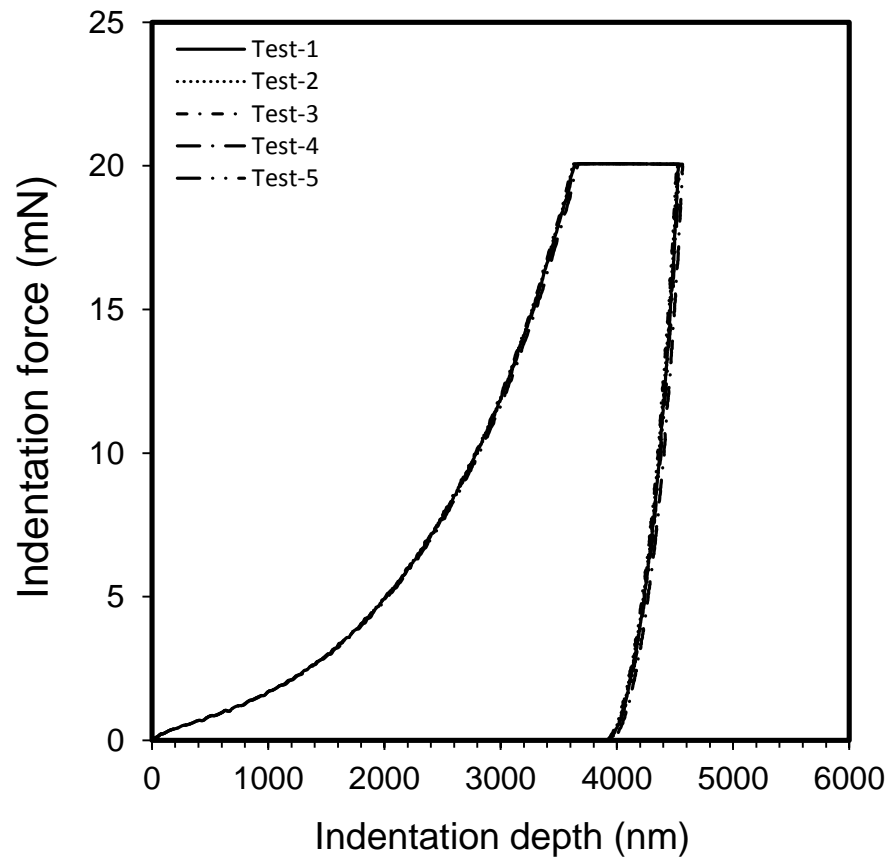


Figure-1: Load-depth plots of samples preconditioned at 33.5 % RH for 24 hours and tested at 33.5 % RH.

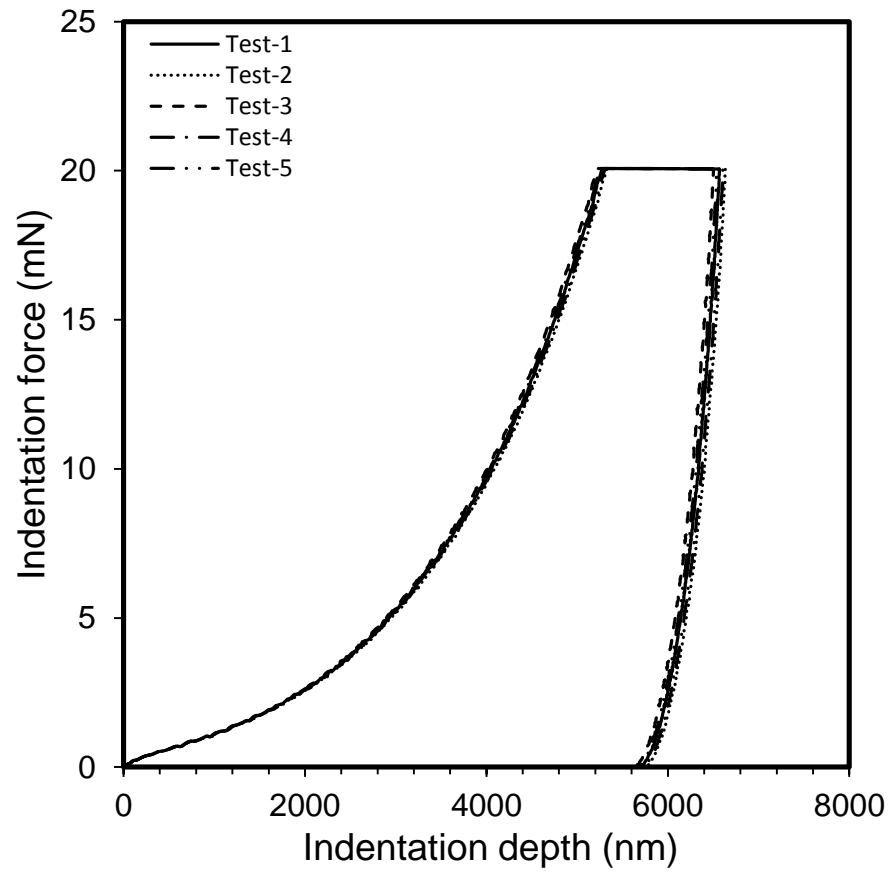


Figure-2: Load-depth plots of samples preconditioned at 53.8 % RH for 24 hours and tested at 33.5 % RH.

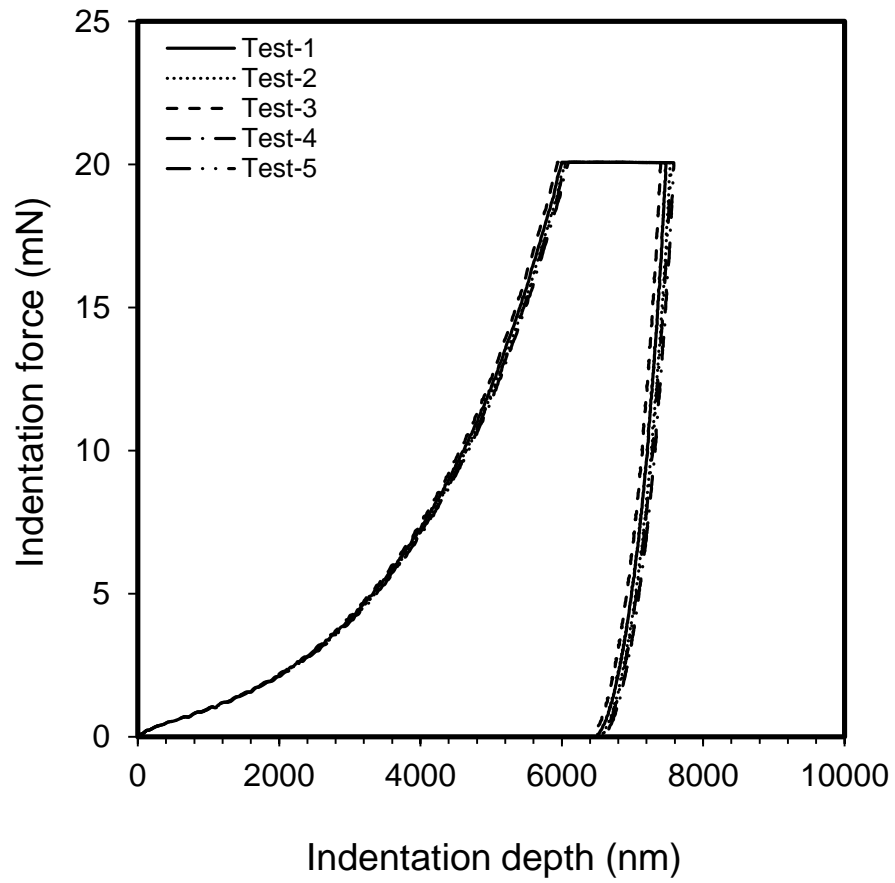


Figure-3: Load-depth plots of samples preconditioned at 75.3 % RH for 24 hours and tested at 33.5 % RH.

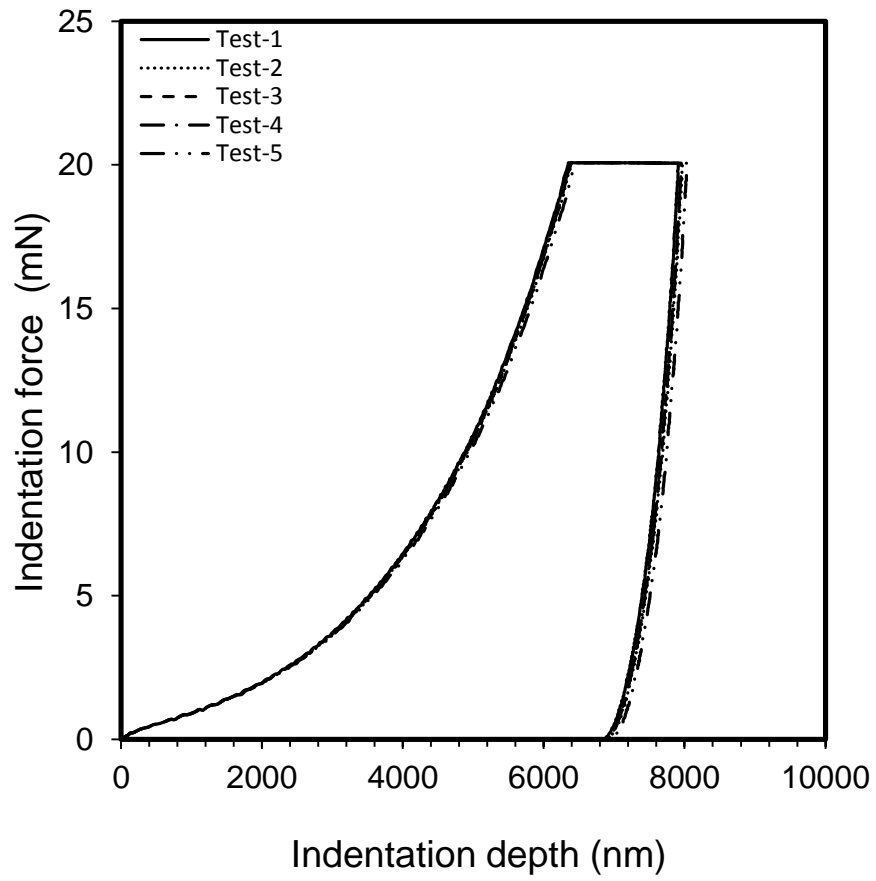


Figure-4: Load-depth plots of samples preconditioned at 84.5 % RH for 24 hours and tested at 33.5 % RH.